UNIVERSITY OF CALIFORNIA, SAN DIEGO

On the Systems Characterization of Metabolic Networks

A dissertation submitted in partial satisfaction of the
requirements for the degree
Doctor of Philosophy

in

Bioengineering

by

Neema Jamshidi

Committee in charge:

Professor Bernhard Ø. Palsson, Chair
Professor Steven P. Briggs
Professor Andrew D. McCulloch
Professor Robert K. Naviaux
Professor Shankar Subramaniam

2009

The dissertation of Neema Jamshidi is approved, and it is acceptable in quality and form for publication on microfilm and electronically:

_____

_____

_____

_____

_____
Chair

University of California, San Diego

2009

DEDICATION

To mom and dad ...

مادر جون،

مرسی که همیشه به من مامان بودید.

پدر جون،

مرسی که همیشه به من بابا بودید.

مامان و بابا،

لغتی نیستش که بتونم تشکر بکنم برایه همهٔ

از کرها که برایه من انجام کردید.

نمونهٔ زندگیی شماها خیلی به من یاد داد.

از نظر کار کردن و پیشرفت کردن، هر ِفتخاری

که برایه من پیش بیاد، از پیشرفت شماها ایجاد

شده و به دستم آمد از زیر نور چشم شماها.

خیلی ممنون هستم.

خیلی دوستتان دارم،

نیما جمشیدی

TABLE OF CONTENTS

LIST OF FIGURES

LIST OF TABLES

ACKNOWLEDGEMENTS

First and foremost I would like to thank Dr. Palsson for being such a fantastic mentor, advisor, and a source of wisdom, with whom I have had the great pleasure of working with for the past [not otherwise specified] years. During my college career(s) I can think of three times when my thinking has changed or evolved in a substantive manner, two of these have occurred under your guidance and supervision.

Dr. Naviaux, thank you for your support and insight. Each time I have met with you, I walked away with a few more deep thoughts and issues to ponder.

Dr. McCulloch, you have been a source of support and encouragement not only during grad school, but prior to that as well. I will never forget that you were the first person who introduced me to a quantitative description of the 'structure determines function' principle when discussing force generation and fiber angles of muscle tissue, back in Biomechanics, BE112A as an undergraduate.

Dr. Briggs, it has been a pleasure working with you (even though the projects didn't get $$ or traction) and I appreciate your candor and genuine advice and look forward to future opportunities to work together.

Dr. Subramaniam, thank you for your support, generosity, and constructive feedback. Additionally, few Professors as busy as yourself would have stepped in to be on my committee given such late notice.

Irene Jacobo, you were my Bioengineering advisor as an undegraduate and later on as a graduate student as well. Unfortunately you left Bioengineering before I finished my PhD, however you have always been a source of support and kindness, and I thank you for this. Jan Lenington, although we had limited interactions, I really appreciate all of your help, support, and hard work during the final steps!

To all the individuals whom I can't list and do justice, thanks for your support. I would like to make mention of one person in particular, Ines Thiele. These last few years I have had the privilege of getting to know you both as a respected colleague and as a dear friend (with whom I often had heated discussions). While our career paths may lead us to live in different parts of the world, I hope we'll be able to stay in touch as friends and colleagues in the coming years.

TW[1] and SAB[2], we shared some great laughs during the good ol' days. I haven't forgotten about our numerous 'business plans' and I look forward to developing a few of these with you both in future years ...

I would like to thank Dr. Joshua Rabinowitz at Princeton and Jie Yuan for allowing me to use their preliminary data; I hope this is a start for a productive collaboration!

The text of Chapter Three in part is reprint of the material as it appears in Molecular Systems Biology and BMC Systems Biology. The dissertation author was the primary researcher and author of this publication, and B.Ø. Palsson directed and supervised the research which formed the basis of the chapter.

While this goes without saying, I would like to my dear family. Mom and dad, thanks for everything that you have done and continue to do. Ramin, Ana, and Mike, thank you for your love and support.

There are a number of individuals from the School of Medicine whom I'd like to thank for their support as well. I'd like to thank Dean Savoia for giving me permission to take a sabbatical from medical school to pursue a PhD following my third year medical clinical clerkships and Dean Kelly for her support when she came to the medical school in 2005. Most of all, I would like to thank Joyce Felder – there aren't enough nice things to say about you, so I won't try. But Joyce, you are a remarkable individual personally and professionally, and it has been a privilege getting to know you.

I have now spent a number of years at UCSD and the faculty, teachers, and research infrastructure at this institution have been remarkable and I look forward to its continued growth at the cutting edge of research.

Lastly, I feel obliged to give a nod to bureaucracies, which while conceived with the intent of creating a procedural, structured, and organized hierarchy for which the division of labor can be transparently observed, more often than not become impediments to progress and development. We all must learn to deal with bureaucracies and at the close of my education at UCSD, I have had a very memorable series of interactions with bureaucracies, notably the Office of Graduate

[1]Natalie TW Duarte Hurlen, PhD, EMT I, Senior Engineer
[2]Scott A Becker, PhD

Studies who have managed to delay the filing of this dissertation by almost exactly 1 year (defense date and committee member signatures received on 7/7/08, filing on approximately 5/09), for reasons that are not rationally viable. These experiences have left me with an even deeper appreciation for the importance of individual character and integrity and call to mind characters from Ayn Rand's 'Atlas Shrugged'. While I found the material in the text to be philosophically compelling, I always thought that there was an exaggeration in the portrayal of some characters (ethically and morally most individuals fell on the black or white side of the spectrum, which was counter to the more typical expectation of people falling within a 'gray area'). I read a series of Ms. Rand's texts the summer before entering UCSD as an undergraduate. 4 degrees later as I close my educational tenure at UCSD, it is interesting that my experiences with the administrative and bureaucratic departments have involved people who have indeed fallen almost strictly into two classes of categories. While some individuals prefer to turn a deaf ear to rational arguments and choose to point fingers rather than take responsibility, others step beyond the call of duty, have a sense of integrity, character, compassion, and most importantly a rational mind. Unfortunately, OGS seems riddled with the former. However, there remains a glimmer of hope in people like Joyce Felder in the School of Medicine and Irene Jacobo in the Department of Chemistry and Biochemistry (formerly in Bioengineering) who admiringly exemplify the latter. It is important to acknowledge this because good science is not just the result of creativity and hard work; ethics, integrity, and rationality are *critical* for quality science. In life almost all of us spend time as both students and teachers, thus at some point we have the opportunity to guide or direct people and we should take these opportunities to foster ethics, integrity, rationality, and pride in all those whom we guide. This is perhaps one of the most important lessons that I have learned at UCSD, a place in which there are remarkable *individuals* but often frustrating and demoralizing bureaucracies. So I thank all of my teachers, inside and outside of the classroom, for imprinting the importance of having a sense of pride, having a sense of integrity, and approaching every new problem, inside or outside of the lab, with a rational frame of mind.

VITA

1998	B. S. Bioengineering, University of California, San Diego
2000	M. S. Bioengineering, University of California, San Diego
2009	Ph. D. Bioengineering, University of California, San Diego

PUBLICATIONS

Jamshidi N, Palsson BØ. Constructing mechanistic kinetic models in a middle out fashion. (in preparation)

Jamshidi N, Palsson BØ. Duality: Dynamics of biological networks. (in preparation)

Jamshidi N, Palsson BØ. Delta networks and analysis: investigations in a mitochondria. (in preparation)

Jamshidi N, Palsson BØ. The Use of In Silico Models to Simulate Dual Perturbation Experiments: Development of procedure and interpretation of outcomes. (in preparation)

Jamshidi N, Palsson BØ. Top-down analysis of temporal hierarchy in biochemical reaction networks. (accepted)

Jamshidi N, Palsson BØ. Formulating genome-scale kinetic models in the post-genome era. Molecular Systems Biology, 2008;4:171.

Jamshidi, N, and Palsson, BØ. Investigating the metabolic capabilities of Mycobacterium tuberculosis H37Rv using the in silico strain iNJ661 and proposing alternative drug targets. BMC systems biology 1, 26.

Mo ML, Jamshidi N, Palsson B. A genome-scale, constraint-based approach to system biology of human metabolism. Molecular BioSystems, 2007 3, 598-603.

Duarte NC, Becker SA, Jamshidi N, Thiele I, Mo ML, Vo TD, Srivas R, Palsson BØ. Global reconstruction of the human metabolic network based on genomic and bibliomic data. Proceedings of the National Academy of Sciences of the United States of America, 2007 104, 1777-1782.

Jamshidi, N and Palsson BØ. Systems biology of SNPs. Molecular Systems Biology, 2006. 2:38.

Jamshidi, N and Palsson BØ. Systems biology of the human red blood cell. Blood Cells Molecules and Disease, 2006. 36(2): p. 239-47.

Overbeek R, Begley T, Butler RM, Choudhuri JV, Chuang HY, Cohoon M, de Crcy-Lagard V, Diaz N, Disz T, Edwards R, Fonstein M, Frank ED, Gerdes S, Glass EM, Goesmann A, Hanson A, Iwata-Reuyl D, Jensen R, Jamshidi N, Krause L, Kubal M, Larsen N, Linke B, McHardy AC, Meyer F, Neuweger H, Olsen G, Olson R, Osterman A, Portnoy V, Pusch GD, Rodionov DA, Rckert C, Steiner J, Stevens R, Thiele I, Vassieva O, Ye Y, Zagnitko O, Vonstein V., The subsystems approach to genome annotation and its use in the project to annotate 1000 genomes. Nucleic Acids Research, 2005. 33(17): p. 5691-702.

Jamshidi N, Wiback SJ, Palsson BØ. In silico model-driven assessment of the effects of single nucleotide polymorphisms (SNPs) on human red blood cell metabolism. Genome Research, 2002. 12(11):1687-92.

Kauffman KJ, Pajerowski JD, Jamshidi N, Palsson BØ, Edwards JS. Description and analysis of metabolic connectivity and dynamics in the human red blood cell. Biophysical Journal, 2002. 83(2):646-62.

Gurtner C, Tu E, Jamshidi N, Haigis RW, Onofrey TJ, Edman CF, Sosnowski R, Wallace B, Heller MJ. Microelectronic array devices and techniques for electric field enhanced DNA hybridization in low-conductance buffers. Electrophoresis. 2002. 23(10):1543-50.

Jamshidi N, Fahland T, Edwards JS, Church GM, Palsson BØ. A Computer Model of Human Red Blood Cell Metabolism. Bioinformatics. 2001. 17: 286-7.

Suzuki H, DeLano FA, Jamshidi N, Katz D, Mori M, Kosaki K, Gottlieb RA, Ishii H, Schimd-Schonbein GW. Enhanced DNA Fragmentation in the Thymus of Spontaneously Hypertensive Rats. American Journal of Physiology. 1999. H2135-H2140.

Suzuki H, DeLano FA, Parks DA, Jamshidi N, Granger DN, Ishii H, Suematsu M, Zweifach. BW, Schmid-Schonbein GW. Xanthine Oxidase Activity Associated with Arterial Blood Pressure in Spontaneously Hypertensive Rats. Proceedings of the National Academy of Sciences of the United States of America, 1998. 95(8): 4754-9.

Lewis NE, Jamshidi N, Thiele I, Palsson BØ. Metabolic Systems Biology: A constraints-based approach. Encyclopedia of Complexity and Systems Science. Springer Publishing.

Jamshidi N, Vo TD, and Palsson BØ. in silico analysis of SNPs and other high throughput data. Methods in Molecular Biology: Cardiac Gene Expression and Regulation. Totowa: Humana Press, Inc.

ABSTRACT OF THE DISSERTATION

On the Systems Characterization of Metabolic Networks

by

Neema Jamshidi
Doctor of Philosophy in Bioengineering
University of California San Diego, 2009
Professor Bernhard Ø. Palsson, Chair

Significant progress has been made in the development of genome-scale models of metabolism in the past 15 years. The majority of the efforts have focused on the analysis of the right null space. While the steady state solution space is very important since homeostatic mechanisms are continuously trying to push the system back to a steady state, there are three other subspaces which also have significance. This dissertation approaches metabolic networks with the goal of investigating all four fundamental subspaces of linear systems, particularly the row and column spaces, which determine the dynamic capabilities of networks. First, the key matrices are defined and their general properties and characteristics are identified. The subspaces are analyzed for a simple metabolic network. Next the right null space is explored in a targeted manner using real networks, the cardiomyocyte mitochondria and a genome-scale model of *Mycobacterium tuberculosis*, focusing on perfectly correlated reaction sets and the biologically interesting implications they may hold. This is followed by the development of analytical methods to define the time scale hierarchy in the column space of the human red cell, human folate metabolism, and yeast glycolysis. These studies are further pursued by investigating various decompositions of the stoichiometric and gradient matrices that are determined by the underlying physico-chemical characteristics. These investigations lead to the identification of key properties of metabolic networks, such as the duality between fluxes and concentrations in dynamic networks.

Having established how to decompose these networks, a middle-out integration approach is described for building or reconstructing kinetic networks using '-omic' data streams that are increasingly available. This approach is applied to construct a dynamic model of human red cell metabolism with and without mechanistic integration of allosteric regulatory functions of enzymes, dynamic models of *E. coli*, as well as a general hepatocyte mitochondria model which can be used for application of these methods, when the appropriate data becomes available. Simulations with the regulated erythrocyte model highlight the importance of active versus inactive states of enzymes and how the binding state of the enzyme exerts control of the flux through competing pathways. The subsequent chapter investigates perturbational analyses and how they can inform functional states and identify pathophysiological conditions. This dissertation culminates in a description of a conceptually new approach to modeling, δ networks, that relaxes data requirements and is focused on identifying the functional differences between different data sets in an effort to understand as much of the four subspaces as possible, not just the right null space. The studies carried out in this dissertation also further support the use of models as data interrogation tools; for data integration, analysis, as well as for the evaluation of data consistency. The developments and advancements made herein take steps towards achieving genome-scale dynamic regulated networks of metabolism, which can in principle be applied to any biological network.

Chapter 1

Introduction

1.1 Systems biology

In the last 10 years the field of Systems Biology has come into its own right. A single unique definition Systems Biology still eludes the field, in part because the field is still growing and maturing, and in part because almost any biological problem can be investigated from a systems view. The nature biological systems almost always involves the interactions between multiple components. Some systems biologists analyze networks of thousands of proteins, trying to understand how they interact. On the other extreme, a systems biologist may focus on the study of a single protein complex, trying to understand in detail how the different sub-units interact. Regardless of the myriad of approaches and philosophies which one may approach Systems Biology, a common feature is to understand how systems will multiple components interact and give rise to complex behavior or phenomenon (see Figure 1.2). Although this field is relatively new, systems analysis of biological systems has been underway for many years. Biology is a technology driven field, thus many of the advancements that have been achieved to date are the result of technological developments and the ability to measure and accumulate various high-throughput data.

From biochemistry to metabolism Biochemistry is a unique biological subdiscipline for a number of a reasons. Almost from the start, biochemistry has

been a quantitative field whose early founders have appreciated importance of the underlying physico-chemical nature of biochemical interactions and their influence on function. Additionally, biochemistry is one of the older of the modern biological disciplines, so it has a relatively long history and a large literature base. The stoichiometric nature of molecular interactions fluidly and naturally lends itself to the construction and analysis of these components as mathematically described networks. Furthermore, the biological phenotype is a quantitative one, described by metabolite and enzyme concentrations, and enzyme reaction rates and fluxes.

The biochemical literature has a rich and deep history, but from its early days there has been a focus and interest on mechanisms of catalysis, regulation, and kinetics. There have been far too many advancements and developments to describe in this brief introduction, but I will touch upon a few landmark findings and developments in the field of biochemistry. Payen and Persoz are credited with the first 'discovery' of an enzyme, amylase, in 1833 [71]. Emil Fisher provided a conceptual breakthrough with the 'lock and key' concept in 1894 [16], which was later revised by Koshland [48]. The first quarter of the 19th Century continued to provide further advancements in the understanding of enzyme catalysis mechanisms along with descriptive quantitative frameworks for their characterization and analysis. These include enzyme-substrate complex by Brown in 1902, the description of substrate concentration on reaction rates by Henri, Michaelis, and Menten in 1903 [27] and 1913 [56], and the introduction of the steady state concept by Briggs and Haldane in 1925 [6]. Developments and revisions progressed consistently over time that altered and revised understanding, to reflect biology more faithfully, for example the 'induced-fit' mechanism for enzyme catalysis introduced by Koshland [48] as a subtle but important departure fom the 'lock and key' conception of catalysis. Monod, Wyman, Changeux described a kinetic model for allosteric enzymes in 1965 [59]. Developments in metabolism have continued at a fast pace and experience significant advancements in the 1960s and 1970s, to the point that the Boehringer Mannheim posters [57] have categorized huge numbers of reactions and databases currently populating the internet. The last quarter of the 20th Century experienced further advancements in biochemistry with the arrival of

molecular biology and '-omics' fields, enabling connections between genotypes and phenotypes to be drawn [54]. Many diseases with Mendelian modes of inheritance involve metabolic enzymes and have been traced down to their molecular [87] and genetic [54, 20] causes.

Systems science Systems analysis of biology has dated back (or at least claimed to date back) almost one century [13]. Physiologists have histoically adopted a systems based approach and made significant advancements through the middle of the 20th Century. Perhaps one of the most identifiable early example of systems analysis has been Guyton's model of cardiovascular physiology [18]. In the area of metabolism, as the scope and appreciation of the size of the networks continued to grow and to become larger and larger, Reich and Selkov laid out foundational concepts for simplifying these complex networks in a biologically meaningful manner [78].

There has been a prolific development of various frameworks and mathematical analysis approaches for describing and analyzing metabolic systems. Rather than try to highlight, summarize, and compare and contrast seemingly innumerable different approaches for building and analyzing networks, I will focus on what I perceive to be the key questions that need to be asked whenever building models. Indeed I believe that failure of some of these earlier approaches have resulted from neglecting some of these points. After defining the question of interest, when building a model, three key questions should always be addressed,

1. What are the governing equations?
2. What are the assumptions that are being made?
3. What are the goals of the model?

A lack of recognition of these minimal requirements can lead to models which may be largely irrelevant. The first question belies the unerlying foundation for any subsequent analysis. Engineering and physical science disciplines place high value on the governing equations, these generally describe fundamental constraints on physical networks, such as conservation of mass, energy, charge and force balances.

The second point is always important to consider, because while no model is expected to be perfect, one can only expect reasonable or relevant models to be derived when the underlying assumptions are consistent with the data that has been collected and the questions that are being investigated. The third question hits upon the need to develop models that do not simply regurgitate the data used to construct them, but models that make new predictions, provide new insights, and help evaluate or propose new hypotheses.

In consideration of some of theses points, the biggest bottlenecks in the development of systems biology as a field has not been a lack of vision or conceptual developments, it has been a lack of the types of data sets that are need to build the models (and then subsequently test them and break them apart to gain insight into their function). Thus one goal of this disseratation is to provide a practical and feasible mathematical framework for building kinetic models, that is a data-driven mathematical framework for the analysis and construction of kinetic networks.

1.2 Biochemical Model Development: Components to systems

Mathematical and subsequently computational descriptions of biochemical interconversions began with the modeling of enzyme catalysis and the interactions with substrates. As experimental knowledge began to expand and fill in pathways, modeling efforts moved from single enzyme to pathway modeling, pursuant to the expanded knowledge. The experimental elucidation of complete pathways promulgated the expansion of models and the construction of models of metabolic networks. For the exception of just one or two models [47], advancements in the size and complexity of kinetic metabolic network models peaked in the late 1980s and early 1990s. This was due in large part to the onerous task of measuring all of the binding constants of substrates and reaction intermediates with the enzyme complex. An added discouraging note was that *in vitro* studies did not always correlate with the realities *in vivo*.

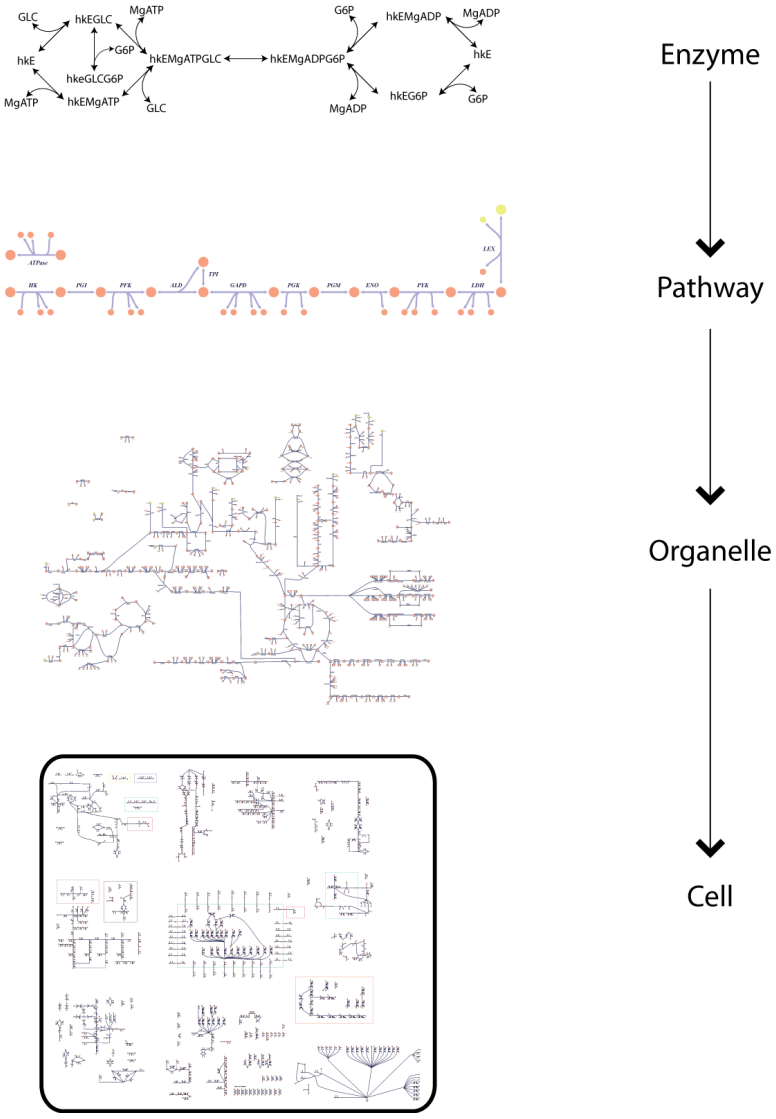

Figure 1.1: Hierarchies of biochemical systems.
Sub-cellular modeling of biochemical interactions can range from focusing on single enzymes to specific cells.

1.2.1 Accounting for individual enzyme rates/activities

The developments at the turn of the 20th Century led to rate law expressions describing enzyme kinetics that have been used extensively throughout the last century. Perhaps the most ubiquitously used has been the Henri-Michaelis-Menten equation (and derivatives thereof for multiple substrate and allosterically regulated enzymes) [88]. While this expression has been very effective for many situations, the assumptions inherent to the equation,

1. The enzyme is saturated by the substrate(s)
2. The formation of the enzyme-substrate complex occurs much more quickly than dissociation of the enzyme-product complex
3. The enzyme-substrate complex achieves steady state

are not always fulfilled *in vivo*. This has been analyzed and pointed out in the literature [67, 65]. Nevertheless, these rate expressions and more complex derivatives of them have been used extensively in the literature [88]. While these approaches have often been successful, they are not uniformly true *in vivo*.

1.2.2 Building kinetic models

The traditional approach for building kinetic models has focused on central metabolism and the processes related to energy and redox equivalent production. Glycolysis is perhaps the most extensively studied and modeled pathway in the literature across a range of organisms. Glycolytic models in yeast and human have been investigated the most and the literature is full of filled with these models [30, 26, 29, 25, 47, 40]. Various phenomena from bifurcations [26] to oscillations [5, 80] have been studies.

These models often require many parameters and experimental measurements in order to construct, thus there are concrete, practical limitations to the scale they can be constructed. Furthermore, the parameters are generally measured *in vitro*, but interest in the analysis lies in the *in vivo* applications. Thus, this approach is neither scaleable nor necessarily relevant for genome-scale applications.

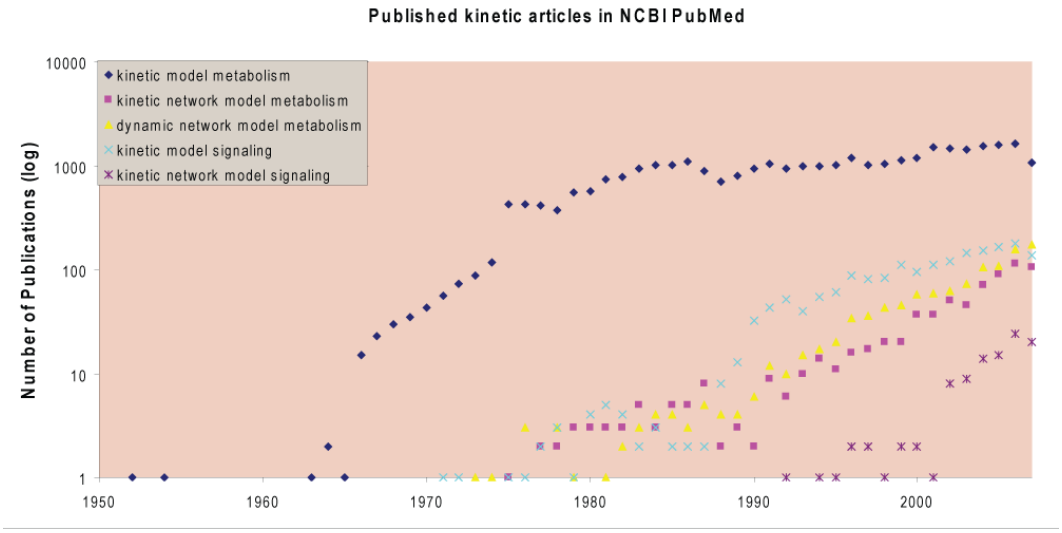

Figure 1.2: Peer-reviewed kinetic publications.
Peer-reviewed articles found in the NCBI PubMed database involving kinetic modeling, metabolism, and/or signaling.

Although the size and complexity of kinetic models has not grown appreciably in the last few decades, there continues to be significant interest in modeling kinetics (dynamics) in metabolism, as noted by the increasing number of published articles in the field (see Figure 1.2).

1.2.3 Genome-scale models

Recognition of some of the problems with building quantitative models in the traditional manner led to the development of Flux Balance Analysis (FBA), which in brief is application of a linear optimization problem to a biochemical network. The constraints to be satisfied are mass conservation and thermodynamic constraints (defining directionality). Framing the problem as a constraints-based optimization circumvented the need for measurement of various parameters *in vitro*. Hence this approach circumvented the problems associated with traditional kinetic modeling of metabolic networks. The key (and the most controversial) assumption in order to carry out FBA is the steady state assumption. For microbial networks the objective function used is often growth , thus since growth occurs

more slowly and many of the metabolic transients occur more quickly than time scales of interest, the steady state assumption becomes a reasonable assumption.

E. coli has been the model organism for development of FBA and constraint based modeling approaches and the scope began with models of relatively modest size [95, 82, 83] to the first genome-scale model [12]. The success of these models in predicting phenotypes and their relative simplicity made FBA and COBRA (Constraints Based Reconstructions and Analysis) very popular in the modeling community. At the turn of the 21st Century the number and size of models began to grow significantly. To date the largest and most complex model is the global reconstruction of the human metabolic network [11]. Methods of analysis have also grown significantly over the past years [73] and even moreso in the past 5 years.

1.2.4 Dynamic Large/Genome-Scale Models

Constraint-based approaches enabled new advancements to be carried out with models, however these models still did not adequately address questions about kinetics or regulation. Biological processes however (particularly in higher order organisms) are inherently dynamic and dynamic interactions are often of great interest, particularly when considering human pathophysiology. The development of the k-cone formalism [14] was the first step towards addressing this problem. This thesis picks up at that point and moves forward. One main topic in this thesis will be to present a data-driven approach for building genome-scale kinetic models. Within this framework, the assumptions built into Michaelis-Menten kinetics (see Section 1.2.1) will be accounted for quantitatively. Hence it will be possible to accept or reject these assumptions.

1.3 Types of Models and Approaches

There are different approaches for modeling. Depending on the type of measurements one can make and the type of predictions they are interested in, different types of models can fit different needs. The two extremes of modeling can be viewed as black-box versus mechanistic, statistical/associative versus causal,

top-down versus bottom-up, and so on. In this dissertation both approaches will be employed, depending on the question of interest and the objective. When building a model, the goal is to incorporate as much mechanistic detail (within practical limitations) as possible, hence the bottom-up approach is appropriate. For analysis however top-down, global assessment may be the most direct route for simplifying or identifying characteristic signatures and motifs. In this thesis a new approach is presented for the feasible construction of large and potentially genome-scale networks which is termed middle-out integration[1]. This approach combines top-down data integration with bottom-up network reconstructions.

1.4 Themes, concepts, and content of the thesis

There are particular themes that tie this dissertation together. Some of these concepts, such as pooled variables that described functional states and the hierarchical structure of metabolic networks have been established decades ago, and still provide a rationale and meaningful framework to describe systems. Other concepts will be relatively novel and still others may reflect lessons and principles once known but perhaps forgotten in the vast scientific literature. Much of the material in this dissertation is conceptual and mathematical. This however does not make it irrelevant to biology. In contrast to many of the previous approaches for mathematical or theoretical biology, in which a theory was developed without consideration of the type of data that may be available. This resulted in 'fundamentally' correct equations, but they were often described in terms of variables that cannot be realistically measured or requiring an impractical number of parameters to be measured experimentally. Hence, a theories were developed, but they were done so without consideration of the type of data that would actually be available. The approach taken here is subtle but important distinctions. The equations, framework and decompositions are motivated by the data types that are becoming increasingly available. There is more of a motivation to build the models and develop the theories around the anticipated data types. Of course this

[1] I would like to credit Sydney Brenner for first coining this term to my knowledge.

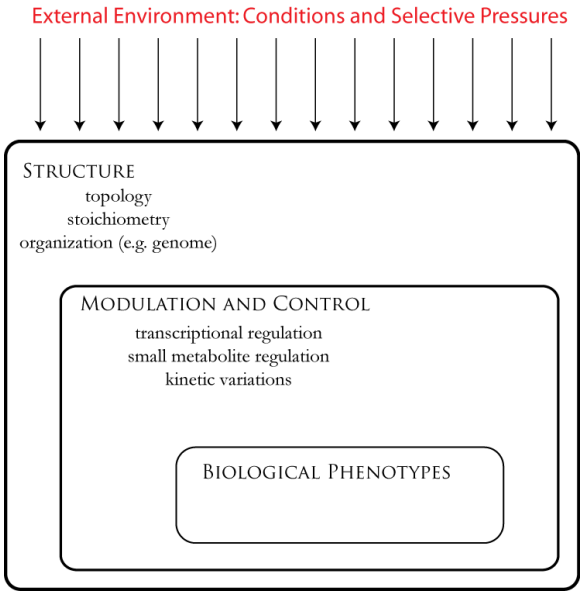

Figure 1.3: A 'high-level' view of biology.

can be done to a certain degree and mathematical rigor must be maintained to a reasonable extent.

Adopting a very 'high-level' view of biology, one might imagine the layering described in Figure 1.3. The external environment provides the cues and pressures which individual organisms must adapt to over small time scales and which species must adapt to over longer time scales. Structural constraints (such as physical topology, stoichiometry, conservation laws, etc) provide the 'hard' constraints that an organism must abide by. At the next level however, there is biological regulation and kinetic variations. These are the biological modulation and control mechanisms that organisms may use to navigate around the hard constraints and environmental cues. A great deal of biological variation occurs in this realm as there are multiple optimal solutions and different definitions of 'optimal' states. Finally these converge onto different biological phenotypes. In the past few decades there has been a focus on understanding the causal genotype-phenotype relationship. In recent years it has become increasingly apparent that it is the environment-genotype-phenotype relationship that must be pursued.

Before closing this brief introduction, it is worth highlighting some of the reasons models are constructed and analyzed (to provide motivation for reading

the dissertation), inspired by Bailey [4],

- Models are not a gospel truth or the end all, be all, they are tools and should be viewed as such; different models have different applications and different strengths, there is no such thing as an all encompassing, comprehensive, perfect model – in any field. When appropriate assumptions are made and the results are interpreted within the context of the assumptions, models can be insightful and relevant. Overinterpretation of results or the application of models to inappropriate areas run the risk of irrelevant results.

- Ideally one would like to build mechanistic, quantitative models in order to describe qualitative changes and behavior in biology.

- Models can be used as tools to test our understanding.

- Models can be used as predictive tools. Once the predictive capabilities are established they can be used to make predictions and drive experimental research.

- The failures of models can be just as informative as the successes; an accurate prediction that is made without an understanding of why the prediction was made is not as useful as an inaccurate prediction accompanied by a detailed understanding of why the model failed, as the latter can form the basis of new hypothesis generation.

A relatively large number of topics will be discussed and various models will be analyzed in this thesis. However all of these seemingly disparate topics are actually tied together and built around the unifying theme of the fundamental subspaces of the stoichiometric matrix. As mentioned earlier, the historical context of this dissertation is to pick up where the k-cone left off. Additionally there is also an effort to tie together the need for steady-state as well as dynamic modeling. In an ideal world one would be able to comprehensively characterize biological networks, however in the real world, with real constraints, this is not always achievable. However sometimes an analysis of the dynamics is not necessary and other times a strictly steady state analysis is not adequate. By focusing

on the different subspaces and the type of information they can provide, I hope to bring some clarity to this area and to highlight how steady state and kinetic analyses complement one another.

Content Overview

The basic foundation for the work will be established in Chapter 2 and in each chapter that follows, a different subspace will be discussed and analyzed, so that by the end of this thesis we will have visited all four subspaces and hopefully the reader will have gained a deeper appreciation for the information to be gained from each subspace and for the challenges associated with attempts to characterize each subspace in metabolic networks. Reading this chapter is requisite for any of the other chapters in this dissertation.

Chapter 3 focuses on correlations within the right null space. So called 'correlated reaction sets' can be used to simplify and modularize large networks and biologically they can be used to help classify diseases on a functional basis or to find alternative drug targets. *in silico* models of the human mitochondria and the pathogen *Mycobacterium tuberculosis* are analyzed in these chapters.

Chapter 4 concerns analysis of the row and column spaces. In analogy to correlations in the steady state solution space (Chapter 3), correlations in dynamics are investigated in a yeast glycolytic model, the human red cell, and the human folate cycle.

Chapter 5 involves topics from a number of different aspects, with the unifying them being mathematics. Biologically the topics of greatest signficance focus on the duality between reaction fluxes and component (metabolite and enzyme) concentrations, which is evinced through analysis of they dynamic relationships in biological networks.

With a bit more mathematics under the belt, the challenge of building kinetic models is tackled in Chapter 6. The approach described in this dissertation is a data driven one, thus it is expected that the data for building such models will become increasingly available (this is very reasonable considering the growth of the field of metabolomics) and metabolomic measurements made *in vivo* will not

suffer from some of the problems associated with the traditional construction of kinetic models. The methods are illustrated by building regulated kinetic models of red cell metabolism and kinetic models of core *E. coli* metabolism. Finally the structure of a hepatocyte mitochondria is constructed in anticipation of the future availability of metabolomic data to create a kinetic model.

With the tools and techniques for model construction having been described, I turn to the topic of functional interrogation of network properties, with the focus on simulation based methods in Chapter 7. Perturbational analysis studies of the red cell further support what every experimental biologist knows: characterizing biological function requires some type of perturbation (genetic and/or environmental).

Finally in Chapter 8 I return to the problem of data completeness. Indeed there will never be enough data to satisfy all of the desires of the modeling community, thus the issue of how to deal with gaps in data and incomplete datasets quickly moves to the front of the field as one of the eminent practical challenges. A new conceptual framework for analyzing models, the Delta Model, is presented with some of the basic (and very simple) underlying mathematics. Tour of the subspaces with a focus on the row and column space characterization. Philosophically have focused on pragmatic and conceivable/realize-able approaches rather than the strictly theoretical. I hope the reader will enjoy flipping through this text as much as I have enjoyed working in this field.

Chapter 2

Fundamental Subspaces and Matrices: Defining the playing fields and the players

This chapter is perhaps the most important for understanding the material in this thesis, as it will set the stage for describing the basis for building and analyzing metabolic networks. By the end of the chapter, hopefully the reader will understand these concepts is core to understanding why a seemingly wide range of topics are actually connected, appreciate why fluxes and concentrations are intimately connected, and hopefully see the common thread tying the chapters of the thesis together.

2.1 The Four Orthogonal Subspaces

The four fundamental subspaces will be introduced in a non-traditional, but hopefully simple and elementary description. If one takes the dot product between two vectors, there can be one of two answers, the result can be zero or it can be some number not equal to zero. If their dot product is equal to zero, then the two vectors are said to be orthogonal (the mathematically trivial situation, for which one of the vectors is the null vector is not considered here). Based on this there are two types of subspaces, those containing the vectors that map a matrix to a

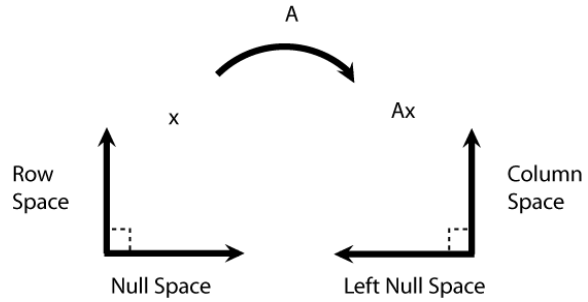

Figure 2.1: Moving from the row to column space.
Multiplication of a vector by a matrix moves from the row to the column space.

null vector and those that don't. Next consider the fact that matrix multiplication does not commute, i.e. $A \cdot B \neq B \cdot A$. This means that when a matrix is multiplied from the left it is mapped onto one space and when a matrix is multiplied from the right it is mapped onto another space. Since one can multiply from the left or the right and vectors may be orthogonal or non-orthogonal to one another, there are four subspaces associated with every matrix. If one multiplies vector of length n by an mxn matrix, $\mathbf{S}$, the resulting vector has length m, so it was mapped from one space to another. If this multiplication resulted in a null vector, then it would be in the null space, since multiplication from the right by a vector takes the linear combinations of the columns. The relationship between the subspaces are visualized conceptually in Figure 2.1.

The Fundamental Theorem of Linear Algebra [91] states that,

- The rank, r, of the column space of a matrix is equal to the rank of the row space of the same matrix
- The size of the null space of a matrix is $n - r$
- The size of the left null space of a matrix is $m - r$
- The nullspace is the orthogonal complement of the row space (both of which are in $\mathbb{R}^n$)
- The left nullspace is the orthogonal complement of the column space (both of which are in $\mathbb{R}^m$)

These statements have significant implications for the stoichiometric matrix, the number of independent rows is equal to the number of independent columns. Note that the actual basis vectors for the two spaces will not be the same, however both will have the same number of independent basis vectors needed to span the space. This fact in addition to the structural constraints of metabolic networks immediately define a way to map between the two dynamic subspaces (the row and column spaces).

The four subspaces of metabolism The study of metabolism involves the characterization and understanding of how cellular components are constructed (anabolism), degraded (catabolism), and interconverted. Key functions of metabolism involve energy production, maintenance of redox capabilities, and satisfying growth demands. Ultimately all cellular processes are reliant on metabolism, hence a firm quantitative understanding of metabolism will contribute broadly to a quantitative understanding of biology. The biochemical phenotype is a quantitative description of an individual's phenotype that also reflects information about the functional state. The phenotype is described in terms of component concentrations and reaction fluxes. The concentrations are the most direct reflection of the phenotype, whereas the fluxes 'tie' the network together and are the means by which the cell responds to pertubations and meets physico-chemical constraints. At the most basic level, systems analysis of metabolism from a physical standpoint must begin with the statement of mass conservation, illustrated in Figure 2.2 and explicitly defined in Equation 2.7,

$$\frac{d\mathbf{x}}{dt} = \mathbf{S} \cdot \mathbf{v} \tag{2.1}$$

A comprehensive understanding of this equation for a particular system or organism, would lead to a complete characterization of it's metabolism, for dynamics and steady states. Draw system boundaries and make the decision of whether one is going to analyze an open or closed system. In closed systems, no transport across the system boundary is permitted, hence the system must always evolve towards state of equilibrium over time. Open systems in contrast permit the transport

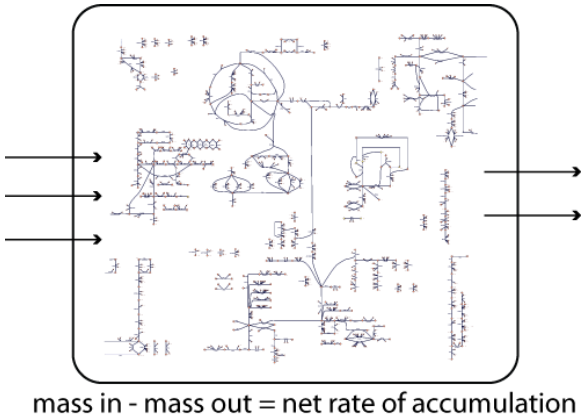

Figure 2.2: Global mass conservation in networks.

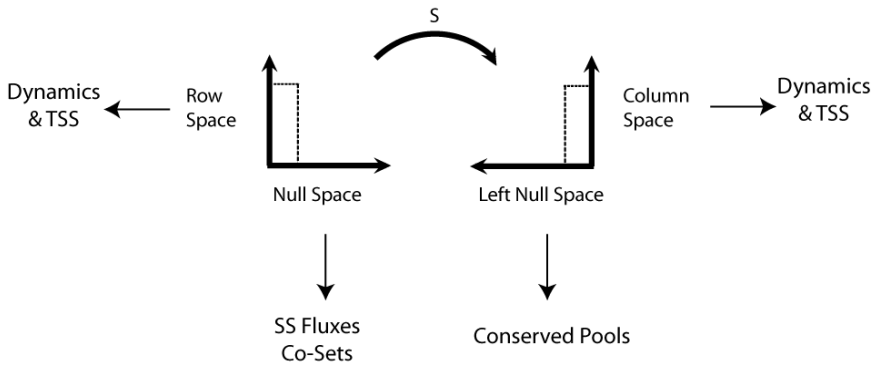

Figure 2.3: Fundamental subspaces of the stoichiometric matrix. Although **S** has started to become synonymous with "steady state", in fact **S** contains information about the dynamic subspaces (the column and row spaces) in addition to the time independent subspaces (the left and right null spaces). TSS: Time scale separation, SS Fluxes: steady state fluxes.

of matter across the system boundaries, hence the system can relax to a steady state. Biologically, a closed metabolic system would result in a dead organism, hence open systems are of interest when studying organisms. Compartmentation occurs extensively in cells, tissues, and organs, hence there may be multiple physical boundaries within a specified system. Note that Equation 2.7 describes a set of time dependent ordinary differential equations, hence spatial gradients of concentrations are explicitly accounted for. This equation assumes that within any compartment, there are not significant metabolite gradients, such that reaction rates are not diffusion limited.

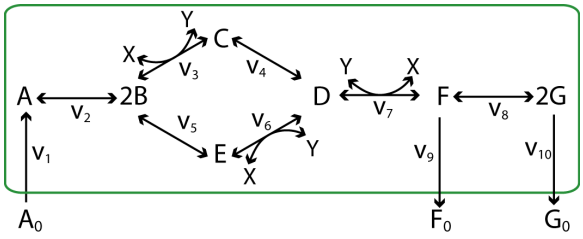

Figure 2.4: Illustrative toy network.
This network will be used throughout this work to provide a simple but realistic and concrete example of the matrices, methods, and analyses developed and described in this thesis.

	v1	v2	v3	v4	v5	v6	v7	v8	v9	v10
A	1	-1	0	0	0	0	0	0	0	0
B	0	2	-1	0	-1	0	0	0	0	0
C	0	0	1	-1	0	0	0	0	0	0
D	0	0	0	1	0	1	-1	0	0	0
E	0	0	0	0	1	-1	0	0	0	0
F	0	0	0	0	0	0	1	-1	-1	0
G	0	0	0	0	0	0	0	2	0	-1
X	0	0	-1	0	0	-1	1	0	0	0
Y	0	0	1	0	0	1	-1	0	0	0

Figure 2.5: The stoichiometric matrix for the system depicted in Figure 2.4.

2.2 Stoichiometric Matrix

2.2.1 Example System

Metabolic maps can be viewed as mathematical graphs, in which the metabolites are nodes and the reactions or biochemical transformations are the links between the nodes. When a metabolic network is described in these terms, one can construct the stoichiometric matrix, whose rows are metabolites and columns correspond to reactions. We will use the following system to exemplify some of these definitions and properties in concrete terms,

This diagram can be depicted mathematically by its stoichiometric matrix,

2.2.2 Right Null Space of S

The right null space of the stoichiometric matrix has special significance. If one is interested in processes that don't change over the time scales of interest, then

a steady state (or quasi steady state) assumption can be made and Equation 2.7 reduces to,

$$\mathbf{S} \cdot \mathbf{v} = \mathbf{0} \tag{2.2}$$

Of course a null $\mathbf{v}$ can satisfy these conditions, but the mathematically trivial case, whose physical interpretation is thermodynamic equilibrium, is not of interest in general. The right null space has been perhaps the most extensively studied subspace in biological networks (followed by the column space) and certainly in genome-scale networks. There has extensive work carried out with the aim of characterizing this space and/or developing a biologically meaningful basis. These methods include extreme pathways [84], elementary modes [86], uniform random sampling [74], flux variability [50] and others. Without delving into a detailed history of the field, suffice it to say that these alternative methods were pursued because although it is easy to calculate a null basis that satisfies Equation 2.2, this basis is not unique and the procedures for calculating the basis [19, 91] use positive or negative combinations of the rows in $\mathbf{S}$, whereas not all reactions are reversible under physiological conditions. Some of these approaches have been conceptually interesting, but impractical for the larger genome-scale models.

One concept which has been successfully implemented and has had interesting biological implications is the calculation of correlated reaction sets, or co-sets. These are groups of reactions (in the right null space) that are always correlated, that is a non-zero flux in one reaction implies a non-zero flux in all of the other reactions that are in the same co-set [70]. This concept can lead to the hierarchical reduction of the network. When co-sets are analyzed in the context of other types of biological information, such as genetic mutations and diseases, there are potentially significant implications that result. For this section I will just specify what is perhaps the most direct and easiest way to determine the perfectly correlated reaction co-sets. Perfect co-sets can be calculated simply by carrying out a Flux Variability Analysis (FVA) [50] and then calculating the correlation matrix for the set of network fluxes. Briefly, FVA is a procedure in which every reaction in a network is minimized and maximized under a specific set of constraints, hence all of the corners of the right null space are identified. Identifying the perfectly

correlated reaction sets in this manner is faster and simpler than other methods, such as flux coupling [7] and sampling [94]. The co-sets for the example system in Figure 2.4 are listed in Figure 2.8. The second and third co-sets are fairly obvious, as is the fourth co-set. The second co-set results from fact that the two branch points in the network split up and then join back together within the same pathway. This 'motif' is observed occasionally in real biological networks, including nitrogen handling pathways and cholesterol metabolism.

Recognizing that there are four perfectly correlated reactions sets (not more and not less) in the network, along with the fact that there size of the right null space is only three 2.2.3 brings to light an interesting conundrum: the co-sets are not completely independent of one another. For example, when one fixes a flux in the first and third co-set, the flux through the second is determined. This is a simple but concrete example of the connected and complex set of relationships between reactions in a network. This also brings into question the utility of defining unique but linearly dependent sets of fluxes. It has been established that there are an astonishing number of basis vectors needed to span a cone in the positive orthant for a genome-scale models [99]. However, even if these were feasible computationally, this size of the right null space still determines the number of independent fluxes needed to shrink the solution to a single point, therefore the convex basis vectors would collapse very quickly as more and more independent reaction fluxes are fixed. Hence a general null basis has not been viewed as particularly relevant. However the mathematics of Equation 2.2 tells us that the null space of a particular network has in effect $n-r$ degrees of freedom. In other words, no matter how one decides to pick a basis, there are at most $n-r$ independently chosen fluxes needed to specify a particular solution within the null space. Thus if one is not necessarily interested in finding a unique basis for the null space, but only to specify the interdependencies of the different fluxes, this can be specified using the row reduced form of $\mathbf{S}$, $\mathbf{S}_r$,

$$\mathbf{C} = sign(\|\mathbf{S}_r^T\| \cdot \|\mathbf{S}_r\|) \tag{2.3}$$

$\mathbf{C}$ is a symmetric nxn matrix describing all of the interdependencies of the fluxes.

As a simple, concrete example, we consider the example system and visualize the **C** in a tree-plot as shown in Figure 2.6. Since the size of the null space is 3, there are at minimum 3 fluxes that need to be specified in order to reduce the solution to a single point. The tree-plot in Figure 2.6 allows one to identify these dependencies and make rational, non-redundant choices. For example specifying reaction 9, 6, and 10 will uniquely determine the null space solution. On the other hand, specifying three reactions that have the same connectivity (reactions 1, 2, and 3 for example) is simply redundant. Nodes are degenerate hence there is not in general a single unique combination of fluxes to uniquely describe the null space.

2.2.3 Left Null Space of S

The left null spaces of the stoichiometric matrix defines the set of time invariant metabolite pools [64]. There have been some investigations into the properties and constituencies of these pools, including the identification of convex bases for these pools [15]. As with the right null space of **S**, there can be a simple approach to identifying the conserved quantities in a network. These steps include,

1. Remove 'pseudo-reactions', such as biomass functions
2. Ensure that all entries in the stoichiometric matrix are integers
3. Calculate a basis for the left null space of **S**
4. Eliminate any negative entries in the basis using elementary row reduction steps

In general it will not always be feasible to remove all of the negative entries for a left null space basis (e.g. see Chapter 6), however this has been achievable with the human red blood cell, the core *E. coli*, the cardiac mitochondria, and the *iJR*904 *E. coli* models. The identification of the conserved pool quantities result in an immediate identification of some of the lumped or pooled variables of interest. For instance, the example system described in Figure 2.4 has two dimensions in the left null space, hence there are two conserved pools of metabolites which are listed in Figure 2.8. The may the network was drawn, it was clearly apparent

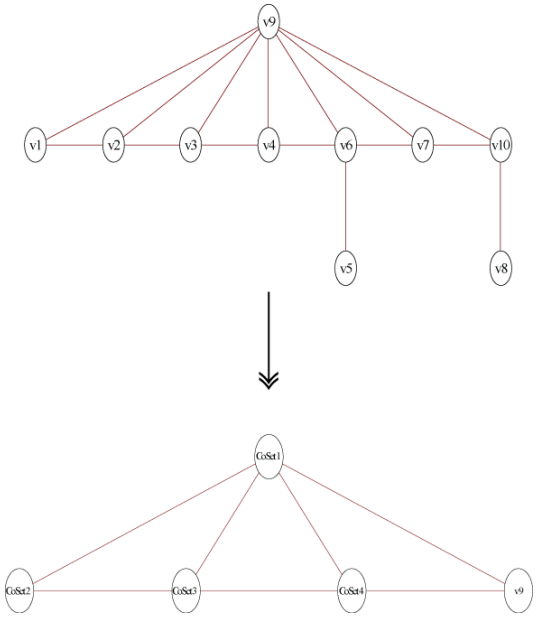

Figure 2.6: Null space flux dependencies for the toy network.
Since the size of the null space is 3, only 3 nodes need to be specified to determine a unique solution in the network. The top figure is for all of the reactions and the bottom is same network after the co-sets are collapsed into single nodes.

that the metabolites X and Y are cofactors, nevertheless, the sum of them have been identified as a conserved pool, that is the quantity $X + Y$ is always constant. The charge ratio $X/(X + Y)$ is the important quantity derived from to the first pool. The charge ratio $(C + D)/(X + C + D)$ is the conserved quantity derived from to the second ratio. While the conservation pool $X + Y$ may be trivial to identify, the other pool may not be as obvious, particularly for a larger network, in which there are a greater number of ways to draw the maps. The conserved pools direct one towards potentially important pooled parameters to investigate, because they involve exchanges of 'biological currencies', such as phosphate bonds, redox potentials, methyl groups, etc. The amount of a particular type of currency reflects how 'rich' the cell is with respect to a particular biological currency.

Strictly speaking, the left null space actually reflects compounds that are transported on extremely slow time scales. Generally it is the ratios of the pools (e.g. the ratio of the reduced form of a compound to the total pool) and changes in these fractions that reflect different functional states.

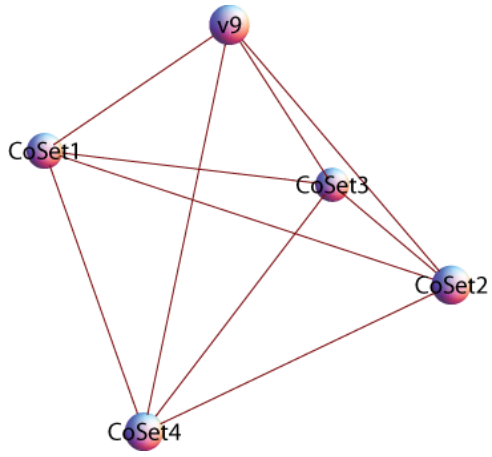

Figure 2.7: Three-dimensional representation of the flux dependencies.
All all of the relationships between the reactions and co-sets can be observed. Any 3 of these 5 nodes (fluxes and/or co-sets) need to be specified in order to identify a unique solution.

Table 2.1: Dimensionality of the toy network.

	Rows	Columns	Rank	Left Null	Right Null
Stoichiometric matrix	9	10	7	2	3
Gradient matrix	10	9	2	1	0

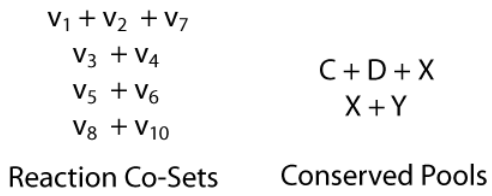

Figure 2.8: Null spaces of the toy network.
The perfectly correlated reaction co-sets and conserved metabolite pools for the network in Figure 2.4.

2.3 The Gradient Matrix

2.3.1 Deriving G, $\mathbf{J}_x$, and $\mathbf{J}_v$

Equation 2.7 generally not lent to analysis, primarily just simulation. However linearization enables analysis in addition to simulations (however simulations need to be restricted to the appropriate regime) [92]. Linearization of Equation 2.7 generally involves carrying out a Taylor series expansion of $\mathbf{S}\cdot\mathbf{v}$ about a particular steady state. However, since the stoichiometric matrix has constant coefficients, I will factor out this quantity and consider the Taylor series expansion about the flux vector, $\mathbf{v}$,

$$\mathbf{v}(\mathbf{x}) = \mathbf{v}(\mathbf{x_{ss}}) + \frac{d\mathbf{v}(\mathbf{x_{ss}})}{d\mathbf{x}} \cdot (\mathbf{x} - \mathbf{x}_{ss}) + \frac{1}{2}\frac{d^2\mathbf{v}(\mathbf{x_{ss}})}{d\mathbf{x}^2} \cdot (\mathbf{x} - \mathbf{x}_{ss})^2 + ... \tag{2.4}$$

in which $\mathbf{x}_{ss}$ refers to a steady state concentration vector. By the definition of linearization, second order and higher terms are neglected, leaving only the first two terms to the right of the equals sign in Equation 2.4. At this point, note that the second term is the product of a matrix and a vector. The entries in this matrix are the derivatives of each flux with respect to each of the metabolites, hence this can be referred as the gradient matrix for the fluxes defined as,

$$\mathbf{G} = \frac{d\mathbf{v}}{d\mathbf{x}} \tag{2.5}$$

so that the linearized flux vector reduces to,

$$\mathbf{v}(\mathbf{x}) = \mathbf{v}(\mathbf{x_{ss}}) + \mathbf{G}_{ss} \cdot (\mathbf{x} - \mathbf{x}_{ss}) \tag{2.6}$$

in which $\mathbf{G}_{ss}$ is the gradient matrix calculated at a steady state. Defining the concentration deviation variable, $\mathbf{x}'$ as the quantity $\mathbf{x} - \mathbf{x}_{ss}$ and substituting Equation 2.4 into Equation 2.7 yields,

$$\frac{d\mathbf{x}'}{dt} = \mathbf{S} \cdot (\mathbf{v}(\mathbf{x_{ss}}) + \mathbf{G}_{ss} \cdot \mathbf{x}') = \mathbf{S} \cdot \mathbf{v}(\mathbf{x_{ss}}) + \mathbf{S} \cdot \mathbf{G}_{ss} \cdot \mathbf{x}' \tag{2.7}$$

Of course at the steady state $\mathbf{S} \cdot \mathbf{v}_{ss} = \mathbf{0}$, so Equation 2.7 becomes,

$$\frac{d\mathbf{x}'}{dt} = \mathbf{S} \cdot \mathbf{G}_{ss} \cdot \mathbf{x}' = \mathbf{J}_x \cdot \mathbf{x}' \tag{2.8}$$

When linearizing a set of equations in systems analysis, the independent variables are generally not specified, as it is implicitly assumed to be unique. However, in this case, I have specified that the Jacobian in Equation 2.8 is defined in terms of the concentrations, $\mathbf{x}$. This has been done because, because through the definition of the gradient matrix has enabled a remarkable transformation between concentrations and fluxes.

If one defines a flux deviation variable, $\mathbf{v}'$, as the quantity, $\mathbf{G}_{ss} \cdot \mathbf{x}'$, then although $\mathbf{J}_x$ will in general be singular for larger networks, by having defined the Jacobian in terms of the stoichiometric and gradient matrices, it is possible to invert Equation 2.8 so that a system of equations in terms of concentration variables can be rewritten as a system of equations in terms of flux variables. First pre-multiply Equation 2.8 by the gradient matrix,

$$\mathbf{G}_{ss} \cdot \frac{d\mathbf{x}'}{dt} = \mathbf{G}_{ss} \cdot \mathbf{S} \cdot \mathbf{G}_{ss} \cdot \mathbf{x}' \tag{2.9}$$

then substitute the definition of the flux deviation variable,

$$\frac{d\mathbf{v}'}{dt} = \mathbf{J}_v \cdot \mathbf{v}' \tag{2.10}$$

where $\mathbf{J}_v$ is the flux Jacobian. The ability to transform a set of dependent variables into independent variables is interesting from a mathematical standpoint, but more significantly it highlights the interrelationship between fluxes and concentrations [38].

The gradient matrix for the example system shown in Figure 2.4 is displayed in Figure 2.10. The 'data' used to construct this matrix are given in Figure 2.11. The explicit method for how this was calculated will be described in Chapter 6. Note that the ratio from between the smallest non-zero entry and the largest magnitude entry is about $1\text{x}10^9$. This large difference determines the time scale

hierarchy in the network (strictly speaking the time scale hierarchy is determined by the condition number of the matrix, which can be approximated by the ratio of the largest to the smallest (non-zero) singular values, which for this network is about $7x10^{10}$).

2.3.2 Properties of G

The derivation above should begin to make it clear to the reader that fundamentally, it is the gradient matrix that determines the dynamics properties of networks. Information about kinetics and thermodynamics and ultimately the dynamic structure and hierarchy are determined by the elements in the gradient matrix. There are a number of interesting implications for the description of a network using the gradient matrix. These properties build upon one another and the most foundational property is that the definition of the gradient matrix is another reflection of how structure determines function. Fundamentally all biochemical reaction mechanisms involve bilinear interactions. The sequence order and complexity of these interactions may vary greatly, however ultimately all of the interactions involve individual steps with two component interactions [88]. Appreciating this fact leads to the observation that the gradient matrix is mathematically similar to the transpose of the stoichiometric matrix,

$$\mathbf{G} \sim \mathbf{S}^T \tag{2.11}$$

Equation 2.11 explicitly, in mathematical reflects the biological principles of 'structure determines function'. The principle of duality between fluxes and concentrations results directly from the relationship between the stoichiometric and gradient matrices and linearization of the equation of reacting systems dynamics, Equations 2.11 and 2.7, respectively. Although the Jacobian is the focus of dynamic systems analysis, the gradient matrix is actually the critical matrix for describing the kinetics and thermodynamics of the interactions between components. The time scale hierarchy in biological networks are also a reflection of the gradient matrix.

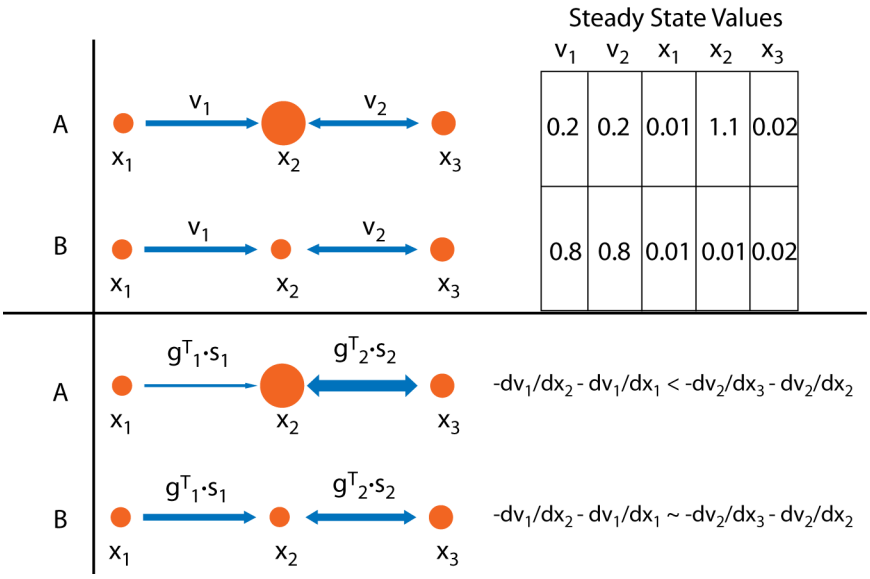

Figure 2.9: Concentrations versus fluxes.
Two scenarios for a 3 flux, 3 metabolite system, A and B. The top panel shows the arrows as fluxes, weighted according to the size of the flux, and the nodes as concentrations, weighted according to the magnitude of the concentration. The table shows the corresponding values (in arbitrary units). The bottom panel shows a similar figure, however the arrows are weighted according to the size of the germ in the gradient matrix. The explicit terms are shown to the right of the figure.

Figure 2.9 provides a graphical description of the relationship between fluxes, concentrations, and terms in the gradient matrix. The magnitude of the concentration of a metabolite is effectively independent of the magnitude of the input and output fluxes. The concentration of a metabolic intermediate is determined by the relative size of the response of the responses of the associated fluxes to a change in the metabolite's concentration. In particular, the response times of the fluxes producing a particular metabolite versus the response times of the fluxes consuming a particular metabolite. These flux and concentration dependencies are described directly by the elements in the gradient matrix.

Specifically, if the response time of an a flux producing a particular metabolite is very large, but the response time of a flux consuming that metabolite is small, then at the steady state, this metabolite will have a relatively large concentration. Conversely, if the response times for a the production and consumption of a par-

ticular metabolite are very fast, then the metabolite will have a low concentration. This basic concept is described in Figure 2.9. It is important to recognize that when metabolites have multiple reactions which can produce them and multiple reactions that can consume them, then the situation becomes 'blurry' and the metabolite will be able to achieve a wide range of steady state concentrations.

The topological interpretation of the products $\widehat{\mathbf{S}} \cdot \widehat{\mathbf{S}^T}$ and $\widehat{\mathbf{S}^T} \cdot \widehat{\mathbf{S}}$ have been described and studied in detail [64] ($\widehat{\cdot}$ indicates the binary from of the matrix). How then does one interpret the corresponding quantities for the gradient matrix. To directly apply the same transformations for the gradient matrices (e.g. the two products of the binary form of the gradient matrices), the result would be the same, i.e. $\widehat{\mathbf{S}^T} \cdot \widehat{\mathbf{S}} = \widehat{\mathbf{G}} \cdot \widehat{\mathbf{G}^T}$ and $\widehat{\mathbf{S}} \cdot \widehat{\mathbf{S}^T} = \widehat{\mathbf{G}^T} \cdot \widehat{\mathbf{G}}$. However, these are not the appropriate analogs for the gradient matrices. The values and signs of the entries in the gradient matrix are all important in this case. The products $\mathbf{G} \cdot \mathbf{G}^T$ and $\mathbf{G}^T \cdot \mathbf{G}$ describe the dynamic connectivity/influence of the reactions on one another and metabolites on one another, respectively. The reaction influence matrix is shown in Figure 2.12. The square root of the diagonal entries are the magnitudes of the rows of the gradient matrix (the square root of the matrix is not taken in order to preserve any negative signs in the off diagonal entries). Large values will reflect 'fast and strong' reactions, whereas smaller values will reflect weaker, less influential reactions. The diagonal entries indicate the 'influence' one reaction has on another (negative entries are inhibitory). Most of these entries are small relative to the corresponding diagonal element, indicating there are not strong interactions. Analogous interpretations follow from the metabolite dynamic connectivity, $\mathbf{G}^T \cdot \mathbf{G}$, shown in Figure 2.13. Some of the off-diagonal entries for ethe metabolites are fairly large, for example the inhibitory effect of Y on F and D. This suggests that when the concentrations of F or D increase, Y will counteract those increases.

2.4 S versus G

A comparison of the characteristics of the stoichiometric matrix and gradient matrix is described in Table 2.4. It is not possible to emphasize the significance

	A	B	C	D	E	F	G	X	Y
v1	-0.03125	0	0	0	0	0	0	0	0
v2	0.774793	-0.123967	0	0	0	0	0	0	0
v3	0	3.73505	-8.78836×10^{-6}	0	0	0	0	0.351535	-0.00219709
v4	0	0	0.664	-0.332	0	0	0	0	0
v5	0	0.02	0	0	-0.04	0	0	0	0
v6	0	0	0	-2.8236×10^{-7}	0.120003	0	0	0.0014118	-0.000014118
v7	0	0	0	20.	0	-17.	0	-2.	1000.
v8	0	0	0	0	0	1.67742	-0.503226	0	0
v9	0	0	0	0	0	1.80851	0	0	0
v10	0	0	0	0	0	0	2.88889	0	0

Figure 2.10: The gradient matrix for the example system.

	Keq	SS flux mM
v1	1	0.15
v2	1	0.15
v3	1000	0.2988
v4	2	0.2988
v5	0.5	0.0012
v6	1000	0.0012
v7	500	0.3
v8	1	0.13
v9	5	0.17
v10	5	0.26

	SS concentration mM
A	0.2
B	0.08
C	0.5
D	0.1
E	0.01
F	0.1
G	0.15
X	0.85
Y	0.002

Figure 2.11: Example network steady state variables and parameters. The steady state fluxes, concentrations, and the equilibrium constants used to construct the gradient matrix for the example network.

	v1	v2	v3	v4	v5	v6	v7	v8	v9	v10
v1	0.00976563	-0.0242123	0.	0.	0.	0.	0.	0.	0.	0.
v2	-0.0242123	0.615673	-0.463023	0.	-0.00247934	0.	0.	0.	0.	0.
v3	0.	-0.463023	14.0742	-5.83547×10^{-6}	0.0747011	0.000496327	-2.90016	0.	0.	0.
v4	0.	0.	-5.83547×10^{-6}	0.55112	0.	9.37434×10^{-8}	-6.64	0.	0.	0.
v5	0.	-0.00247934	0.0747011	0.	0.002	-0.00480011	0.	0.	0.	0.
v6	0.	0.	0.000496327	9.37434×10^{-8}	-0.00480011	0.0144027	-0.0169472	0.	0.	0.
v7	0.	0.	-2.90016	-6.64	0.	-0.0169472	1.00069×10^{6}	-28.5161	-30.7447	0.
v8	0.	0.	0.	0.	0.	0.	-28.5161	3.06697	3.03363	-1.45376
v9	0.	0.	0.	0.	0.	0.	-30.7447	3.03363	3.27071	0.
v10	0.	0.	0.	0.	0.	0.	0.	-1.45376	0.	8.34568

Figure 2.12: The reaction dynamic connectivity for the example system.

	A	B	C	D	E	F	G	X	Y
A	0.601281	-0.0960488	0.	0.	0.	0.	0.	0.	0.
B	-0.0960488	13.9664	-0.000032825	0.	-0.0008	0.	0.	1.313	-0.00820626
C	0.	-0.000032825	0.440896	-0.220448	0.	0.	0.	-3.08941×10^{-6}	1.93088×10^{-8}
D	0.	0.	-0.220448	400.11	-3.38839×10^{-8}	-340.	0.	-40.	20000.
E	0.	-0.0008	0.	-3.38839×10^{-8}	0.0160007	0.	0.	0.00016942	-1.6942×10^{-6}
F	0.	0.	0.	-340.	0.	295.084	-0.844121	34.	-17000.
G	0.	0.	0.	0.	0.	-0.844121	8.59892	0.	0.
X	0.	1.313	-3.08941×10^{-6}	-40.	0.00016942	34.	0.	4.12358	-2000.
Y	0.	-0.00820626	1.93088×10^{-8}	20000.	-1.6942×10^{-6}	-17000.	0.	-2000.	$1.\times10^{6}$

Figure 2.13: The metabolite dynamic connectivity for the example system.

	A	B	C	D	E	F	G	X	Y
0.000962087	0	0	0	-0.02	0	0.02	0	0	-1.
0.200664	-0.37	1.	0	0	0	-0.25	0.12	0.09	-0.16
0.245886	0.48	-1.	0	0	0.01	0	0	-0.09	-0.09
0.425713	-1.	1.	-0.01	0.01	-0.05	0.49	0.16	0.08	0.56
1.0101	1.	-0.12	-0.09	0.04	0.01	0	0	0	-0.04
1.34235	-1.	-0.04	0	0	0	0	0	-0.02	-0.02
6.259	-0.01	-0.01	0	0	-1.	0	0	-0.02	-0.02

Figure 2.14: Example system modal matrix ($\mathbf{J}_x$).
The modal matrix for the metabolite Jacobian, $\mathbf{J}_x$. Each row has been normed (infinity norm) to highlight the dominant interactions on each time scale. The network metabolites appear across the columns and each row corresponds to a different time scale. The time scales (hours) appear in the far lefthand column.

	v1	v2	v3	v4	v5	v6	v7	v8	v9	v10
0.000962087	0	0.01	-0.97	-0.02	0	-0.98	1.	-0.02	-0.02	0
0.200664	-0.16	1.	-0.53	0	-0.42	-0.11	0	0.21	0.11	-0.05
0.245886	0.19	-1.	0.4	0	0.41	0	0	0	0	0
0.425713	-0.33	1.	-0.17	0.01	-0.35	0.18	0	-0.06	-0.16	-0.05
1.0101	-0.81	1.	0.01	-0.1	-0.1	0	0	0	0	0
1.34235	1.	-0.92	-0.04	0	-0.04	0	0	0	0	0
6.259	-0.01	0	0.01	0	-0.99	1.	0	0	0	0

Figure 2.15: Example system modal matrix ($\mathbf{J}_v$).
The modal matrix for the flux Jacobian, $\mathbf{J}_v$. Each row has been normed (infinity norm) to highlight the dominant interactions on each time scale. The network fluxes appear across the columns and each row corresponds to a different time scale. The time scales (hours) appear in the far lefthand column.

Table 2.2: **S** versus **G**.
A comparison of biological and mathematical properties of the stoichiometric and gradient matrices.

Properties	Stoichiometric matrix	Gradient Matrix
Biological	Distal causation	Proximal causation
Genetic	Genomic characteristics of a species	Genetic characteristics of an individual
Informatic	Genomics bibliome	Metabolomics fluxomics kinetic data
Physico-chemical	Chemistry and conservation laws	Kinetics & thermodynamics
Mathematical	Integer entries	Real numbers
Numerical	Sparse and well-conditioned	Sparse and ill-conditioned
Systemic	Steady state pools Network structure	Timescale separation Dynamic structure

of Equation refeq:structfunc; the underlying structure of the two matrices is identical, however the nature of the relationship between the components is vastly different. Mathematically, entries in the stoichiometric matrix are integers and those in the gradient matrix are real values. The physical interpretation of this is that the stoichiometric matrix describes fixed, well-defined chemical interactions. Conversely, the gradient matrix describes dynamic 'influences' of one quantity on another resulting from kinetic properties and thermodynamic constraints. Once these properties are appreciated, then the comparison in Table 2.4 becomes clear, how **S** reflects genomic characteristics of species and is effected by distal causation, and **G** reflects individual genetic characteristics and proximal causation [53].

2.5 Row and Column Spaces: The Jacobian matrices

The analysis of the properties of dynamic systems generally focus on investigating the Jacobian matrix and analysis of its properties [92]. To date this has also implicitly meant that the analysis is focused on the concentration variables. Biochemical systems are best described when one can use both flux and concentration information. Hence it is desirable to be able to describe the dynamics of networks in terms of fluxes or concentrations. For the analysis of biological networks, however I have focused on two other matrices, **S** and **G**. There are two primary reasons for the focus on these matrices,

1. **S** and **G** are directly biologically relevant matrices.

2. Expression of the system in terms of **S** and **G** leads the definition of two, complementary Jacobian matrices, $\mathbf{J}_x$ and $\mathbf{J}_v$, the flux and concentration Jacobians, respectively.

The derivations of Equations 2.8 and 2.10 were not merely mathematical exercises, but were motivated to yield a complementary description of biochemical system dynamics (Figure 2.16) In fact without the definition of the gradient matrix, there did not exist a formal way to explore the row space of the stoichiometric matrix,

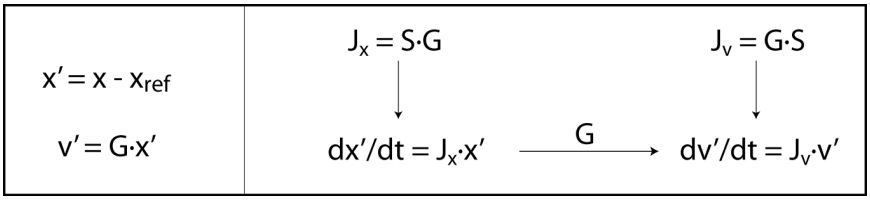

Figure 2.16: **G**, **S** and the Jacobians.
The flux ($\mathbf{v}'$) and concentration ($\mathbf{x}'$) deviation variables are defined on the left hand panel. Mapping between the different Jacobian matrices. These equations all describe the same dynamic interactions, but do so in terms of different variables, this is the basis of duality, all of which is enabled by the gradient matrix.

it was only possible to explore the column space explicitly. Expressing this in another way, the column space of **S**, described by $\mathbf{J}_x$ is the dynamic complement (and orthogonal) to the conserved metabolite pools found in the left null space. Similarly the row space of **S**, described by $\mathbf{J}_v$ is the dynamic complement (and orthogonal) to the steady state flux space. By definition of Equations 2.8 and 2.10, the null spaces of the flux and concentration Jacobians are determined by the stoichiometric and gradient matrices.

2.5.1 Reference Jacobians

There are two basic approaches to defining a 'reference' Jacobian, that is a network that does not exhibit hierarchical dynamics. Both of these approaches involve the manner in with the gradient matrix is defined,

- 'Strictly Analytic Jacobians' are defined by approximating **G** as $-1 \cdot \mathbf{S}^T$. This approach is based solely on the structural relationship between **G** and **S**.

- 'Constraint Consistent Jacobians' are defined by a set of rate constants and solve for a particular flux distribution or solve for steady state concentrations.

The Strictly Analytical Jacobian approximation for the flux Jacobian of the example system is shown in Figure 2.17.

	v1	v2	v3	v4	v5	v6	v7	v8	v9
0.108109	0.21	-0.74	0.28	0.72	-0.27	-0.51	0.24	-1.	1.
0.142112	-0.4	1.	-0.21	0.36	-0.33	-0.32	0.31	-0.15	0.15
0.168815	-0.1	0.2	0	0.21	-0.22	0.46	-1.	-0.22	0.22
0.328809	-0.43	0.22	1.	-0.74	-0.01	0.1	0.1	-0.26	0.26
0.527994	-0.56	-0.03	-0.05	0.08	1.	-0.75	-0.48	-0.03	0.03
0.768874	-0.99	-0.34	-0.27	0.39	0.39	1.	0.54	-0.12	0.12
1.80529	-0.91	-0.66	-0.14	-0.17	-1.	-0.51	-0.23	0.31	-0.31

Figure 2.17: The Strictly Analytical Jacobian.
An approximation for the sample system. There is not evidence of strong time scale separation and the composition of the modes is uniform and fairly unstructured.

	v1	v2	v3	v4	v5	v6	v7	v8	v9	v10
0.0542686	0.16	-0.46	0.56	0.14	0.05	0.65	-0.61	0.09	0.07	-0.01
0.0718448	-0.56	1.18	-0.24	0.17	-0.42	0.34	-0.34	0.15	0.1	-0.02
0.0873476	-0.41	0.7	0.31	0.14	-0.41	0.86	-0.16	-0.73	-0.44	0.15
0.160617	1.21	-1.04	-0.57	0.61	-0.29	0.32	-0.12	-0.02	0	0.01
0.250536	-2.07	1.02	0.24	0.46	1.13	-0.43	-0.19	-0.03	0.02	0.02
0.510739	3.12	-0.49	-0.4	-0.99	-0.78	-0.61	-0.77	-0.08	0.84	0.46
1.19711	4.47	0.12	-0.26	-0.68	-0.29	-0.65	-0.86	-0.08	-0.49	-0.2

Figure 2.18: The Constraint Consistent Jacobian.
An approximation for the example system. Weak time scale separation is observed with an unstructured modal matrix.

The Constraint Consistent Jacobian for the same system shown in Figure 2.18, was calculated by,

1. Solving for the forward rate constants when the reverse rate constants are fixed the same value for all reactions (any value greater than 0 and not equal to 1) and the metabolites are fixed to the same value as well (any value greater than 0 and not equal to 1)

2. Substituting the calculated rate constants into mass action equations and calculating the gradient matrix.

3. Substituting the concentrations used from the first item to fix the gradient matrix at that particular steady state

4. Calculate $\mathbf{J}_x$ or $\mathbf{J}_v$ using $\mathbf{S} \cdot \mathbf{G}$ or $\mathbf{G} \cdot \mathbf{S}$, respectively.

The Constraint Consistent Jacobian has slightly better time scale separation than the Strictly Analytical Jacobian., however both networks have fairly unstructured modal matrices, hence they appear to serve as potential candidates as 'reference' networks or negative controls when evaluating the time scale separation of other networks.

2.6 Adding and removing dimensions

Having defined and investigated the different subspaces for $\mathbf{S}$ and $\mathbf{G}$, it is natural to ask the question: what happens if one adds or removes reactions from a network? More to the point, how does one change the size of the different subspaces. Since the row and column spaces are the same size, increasing the size of one results in an increase in the size of the other. This results from the basic mathematics behind the stoichiometric matrix (see beginning of this Chapter and the Fundamental Theorem of Linear Algebra), again highlighting the tight interconnection between fluxes and concentrations. The row and column spaces of $\mathbf{S}$ can be increased by adding a reaction to the network that is linearly independent of the other reactions. In practical terms, this will be reflected as the addition of

a new (or alternate) pathway in the network. A more interesting question is to investigate what happens with the size of the null spaces are altered?

Figure 2.6 answers this question by considering the example network in three different situations, the normal network, an expanded network in which Y (a member of the conserved pool X+Y) is allowed to enter or leave the cell, and a reduced network in which v_9 is removed. Panel A highlights the interpretation of each of the different subspaces. Panel B describes the dimensions of the network for the normal example, Panel C shows the expanded network, and Panel D shows the results for the reduced network. When a transporter for Y was introduced (Figure 2.6 middle network and Panel C) it resulted in a loss of one dimension from the left null space (i.e. X + Y is no longer a conserved quantity). But where did this quantity go? The rank increased by 1, thus loss of a dimension in the left null space resulted in an increased dimension in the row and column spaces. The result will be a new motion in the dynamics of the network. One can also consider a situation in which a column is removed from the stoichiometric matrix. If the transporter for F_0 shown in the network to the far right and Panel D in Figure 2.6 is removed from the network, the rank is unaffected, so the right null space loses a dimension. These examples highlight how interconnected the subspaces are and a change in one subspace can affect the functional capabilities in another subspace. This is just a reflection of basic linear algebra, but there are non-trivial implications for the interpretation of metabolic netwroks.

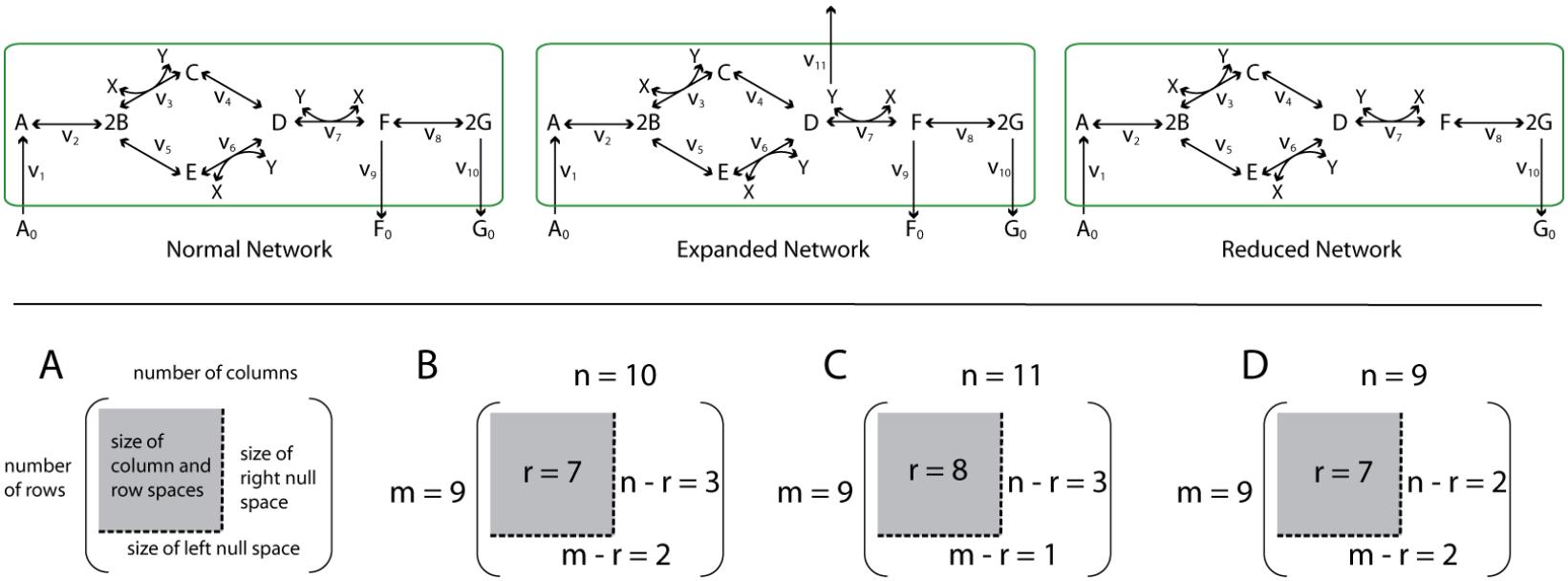

Figure 2.19: The effects of changing the size of the null spaces.
Top panel: Network maps for the 'normal' network, an expanded network, and reduced network. Bottom panel: A. The relationship between the size of a matrix and the size of the different subspaces. B. The size of the network and subspaces for the 'normal' network. C. The size of the network and subspaces for the expanded network. D. The size of the network and subspaces for the reduced network.

Chapter 3

Correlated Reaction Sets: Biochemical correlations in the right null space

3.1 The concepts

High-throughput technologies have enabled the ability to measure thousands of interdependent biological variables and numerous methods are being used to reduce the complexity of HT data sets, to determine dependencies amongst variables, and to correlate them with biological functions [49]. Correlation amongst mRNA levels in expression profiles give rise to co-regulated genes [79]. The HapMap project recently illustrated the power of perfect proxy sets as segments of the human chromosomes and suggested their utility in identifying differences in individual genomes [2].

One of the objectives of Systems Biology is to simplify a complex group of interactions into more palatable organized subgroups or modules. There are different approaches to this end, one is to collect large quantities of data and then to analyze them so that they can be distilled and summarized with a group of key parameters or variables. Another approach is to build a model in a bottom-up or mechanistic fashion and then to analyze the features and capabilities of the model.

Reconstructed metabolic networks present great opportunities for the latter.

3.1.1 Approaches and implications

The study of the functional states of networks has led to the definition of correlated sets of reactions (co-sets): groups of reactions that always [70] or often [7] function together in networks. These co-sets are often non-intuitive as the reactions in a co-set may not be adjacent on a network map. There are two general approaches for the calculations of co-sets: simulation based and topology based methods. Simulation based methods involve actually calculating different functional states in the network (i.e. using FBA or some variant methods that is built upon FBA). Topological methods identify co-sets through the analysis of the structure of the stoichiometric matrix.

The approach for calculating co-sets described in Chapter 2 is perhaps the simplest simulation based method. The primary benefit of simulation based methods over topological based methods is that with the simulation based methods, one is guaranteed that the calculated co-sets will be able to carry a non-zero flux. Simulation based methods may be condition dependent, while topological based methods might select a smaller subset of the co-sets, however they will be generalizable and will be maintained under all growth conditions.

Hard Coupled Reaction Sets

Denoting the binary form of the stoichiometric matrix, $\widehat{S}$, the input/reactant part of the stoichiometric matrix, S_-, and the output/product part of the stoichiometric matrix, S_+, then it is transparent that,

$$S = \widehat{S_-} + \widehat{S_+} \tag{3.1}$$

The input and output connectivities of each metabolite can be calculated for $\widehat{S_-}$ and $\widehat{S_+}$, respectively. The input:output ratio for each metabolite can be determined and all metabolites with 1:1 connectivity will be hard-coupled by the network. Metabolites with 0:2 or 2:0 connectivity reflect metabolites that are hard-coupled

in the event that the corresponding reaction is reversible. Metabolites with 0:1 or 1:0 connectivity are either source/sink transporters or blocked reactions. A general algorithm for calculating hard coupled reaction sets,

1. Identify 1:1, 0:2, and 2:0 metabolites
2. Define $HCRs$
   (a) Identify the sets of reactions corresponding to the metabolites, denote the entire set as HCR_0
   (b) Join any HCR_0 subset that share 1 or more reactions, denote the entire set as HCR_1
   (c) $i \leftarrow 1$
3. while $(HCR_{i-1} \neq HCR_i)$
   (a) Join any HCR_i subset that share 1 or more reactions
   (b) $i \leftarrow i + 1$

Since 0:2 or 2:0 reactions may be irreversible reactions, an intermediate processing step may be needed to verify that there is biological evidence supporting the catalysis of the reaction in the reverse direction. If one does not wish to consider these potential effects and assume that all of the reactions are reversible then step 1 can be simplified by finding all of the 2 metabolites for $\widehat{S}$.

The value of co-sets The principle appeal of co-sets is that they provide a reduction in the size of a network based on hard constraints that must be satisfied (this doesn't mean that the cell always has to be at the steady state, just that it has to be able to satisfy the steady state conditions). This modularization of the network can be used for classification of different functional states, diseases, the identification of alternative but equivalent therapeutic drug targets in humans, or for alternative be equivalent antibiotic drug targets in human pathogens. Some of these will be explored in this chapter.

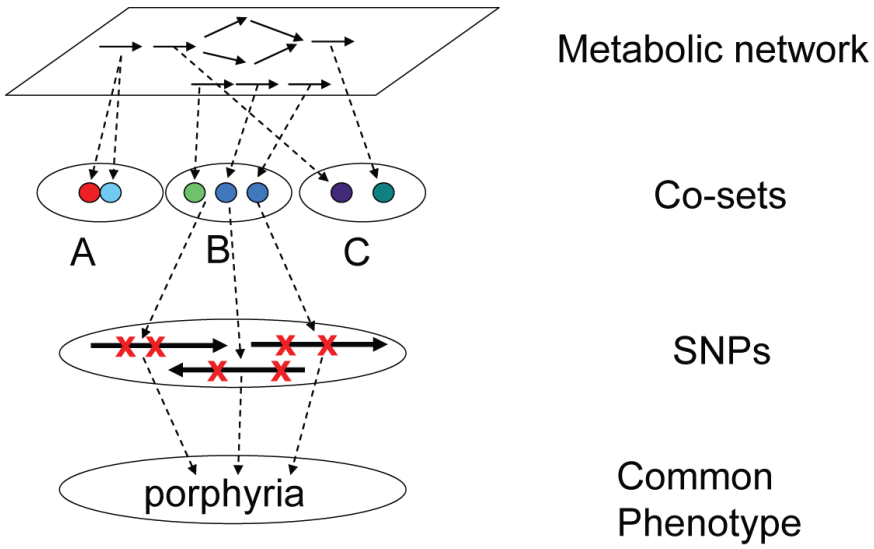

Figure 3.1: Relating SNPs, diseases, and correlated reaction sets. Functional metabolic network analysis results in correlated reaction sets. Causal SNPs in any of the genes encoding proteins in the reaction sets are expected to have similar phenotypic states.

3.2 Human cardiac myocyte mitochondria

Classifying SNPs and co-sets In this study, co-sets are used to seek dependencies amongst single nucleotide polymorphisms (SNPs) with causal implications on metabolic function, by grouping SNPs in proteins that catalyze different reactions, but are shared within the same co-set. Of course, not all SNPs will affect protein function, however since the goal of this systems based analysis is to study functional consequences of causal SNPs, it will be implicit throughout this work that all SNPs considered will only be those with causal implications on enzymatic function. Although the SNPs may affect different proteins with different catalytic activities, if the reactions are in the same co-set, the phenotypic consequences of such SNPs are expected to be similar. One can classify a group of genes that encode members of a co-set into three fundamental types 3.2. SNPs in the gene coding for the protein subunits that catalyze the transformation from one metabolite to another will result in a phenotype that is unable to produce that particular product (Type A co-set). Type B co-sets function in an analogous manner, where

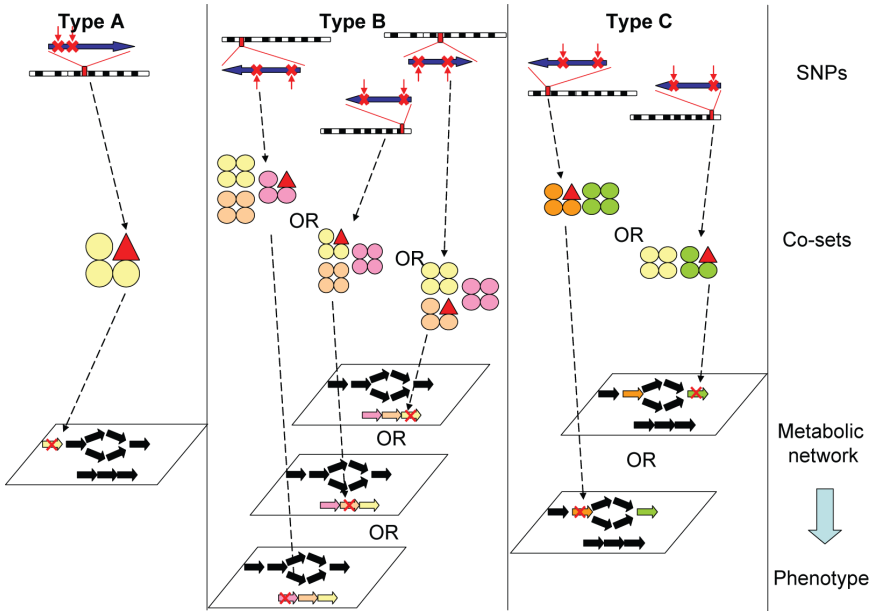

Figure 3.2: Co-set classifications in metabolic networks.
Each sub-panel exemplifies a type of co-set represented by colored arrows and circles (non-black). The circles represent the protein subunits of a particular enzyme. Each enzyme is the same color. Red triangles represent altered protein subunits due to causal SNPs. Each group of colored circles (enzyme) corresponds to the same colored reaction flux in the pathway. Type A describes a multi-meric enzyme, where a SNP in any subunit of the multi-mer can thus result in the same phenotype. Type B represents a co-set of reactions in a contiguous pathway and Type C co-sets are formed by non-contiguous reactions.

causal SNPs affecting a reaction that is part of a correlated reaction set (a linear chain of reactions) will result in a phenotype characterized by an inability to produce the endpoint of the chain. More complex schemes may also occur in which the correlated reaction set is not a linear pathway (Type C co-set).

The NCBI Entrez Gene ID (http://www.ncbi.nlm.nih.gov/entrez/) tags associated with nuclear genes encoding mitochondrial proteins were assembled and all of the genes with diseases associated MIM tags were identified. These sets of genes were then further evaluated for evidence in the literature of causal SNPs related to the corresponding diseases. MIM tags are listed only if causal SNPs have been identified for the particular enzyme deficiency. From the initial 225 unique nuclear encoded mitochondrial proteins in the model, subsequent filtering based on the 33 co-sets described by Thiele et al, resulted in 9 remaining co-sets [35]. Associated diseases due to causal SNPs are described for each enzyme in the co-sets unless otherwise stated. From the 56 genes listed below, all but 4 have been identified/associated with an MIM disease tag. The mitochondrial model and co-sets calculated by Thiele et al used were used [94]. The sampling of the steady state each solution space was performed five times by sampling 500,000 random points with 100 iterations between each point. Co-sets were defined as those sets of enzymatic fluxes which were perfectly correlated (correlation coefficient of 1). The mitochondrial model and co-sets calculated by Thiele et al used were used [94]. The sampling of the steady state each solution space was performed five times by sampling 500,000 random points with 100 iterations between each point. The human mitochondrial metabolic co-sets were then mapped to various diseases in the Online Mendelian Inheritance in Man database [20], followed by identification of cases in which SNPs have been described in the literature. The succinate dehydrogenase (SDH) forms a Type A co-set of genes. A series of SNPs in the different subunits of SDH have been found to have similar phenotypic consequences. The genes that encode the enzymes leading to heme biosynthesis constitute a Type B co-set, Figure 5 3.3. Many SNPs in this set of genes result in various manifestations of porphyria. There is a range of severity and symptoms for a given enzyme and across the different enzymes in this gene set. These variations may be

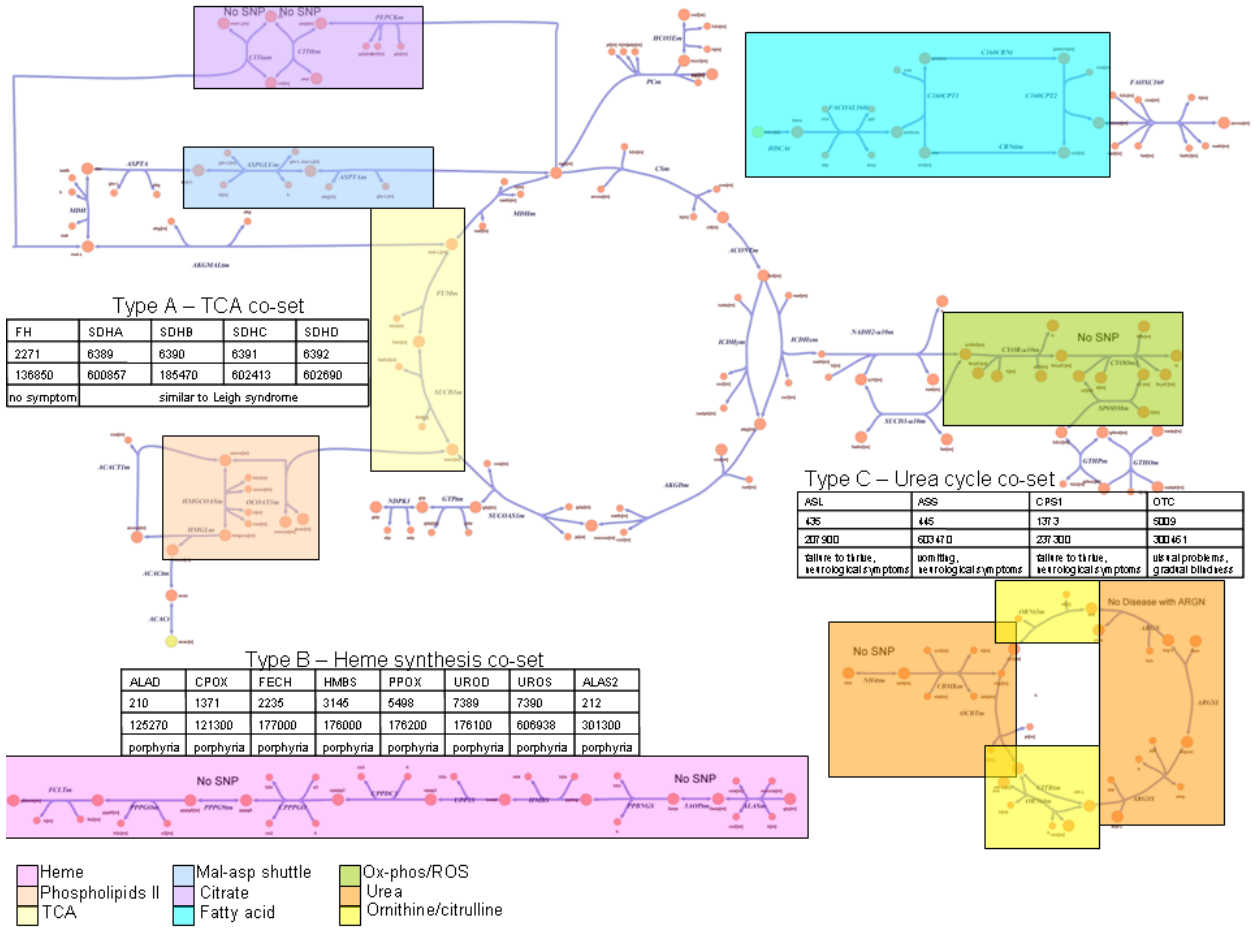

Figure 3.3: Mitochondria SNP-disease co-sets.
Map of mitochondrial metabolism with SNP associated co-sets. An example of each type of co-set is highlighted. The summary charts describe: Gene Abbreviation, Gene-ids, MIMs, and SNP associated signs or symptoms, respectively.

attributable to the specific location of particular SNPs, the presence or absence of other SNPs across the genome, differential tissue expression, the specific metabolic by-products that accumulate or diminish based on the specific reaction, or mitochondrial heteroplasmy. A Type C co-set is found in the urea cycle reffig:mitsnps (although the cardiac mitochondria is not known to have a complete urea cycle from a phenotypic standpoint, the reconstructed network based on proteomic data was the basis for the cardiomyocyte model [96]). There is clinical coherence between SNPs in 3 of the 4 reactions in this set. Type C co-sets are perhaps the most interesting of the three classifications because they are the most non-intuitive, consequently they may have the greatest effect in revising previous views of interactions and classifications of disease. Another particularly interesting case is the citrulline/ornithine co-set. There is only SNP related disease information for one of the two reactions in the co-set, the SLC25A15 transporter, whose deficiency results in the hyperornithinemia, hyperammonemia, and homocitrullinuria syndrome (HHH). Although SNP-diseases have not been described for the other reaction in the co-set, over-expression of SLC25A2 can rescue patients with HHH due to SLC25A15 deficiency [9]. This example presents implications for therapeutic strategies in disease treatment with enzymes capable of binding a range of substrates. If two reactions with overlapping substrate utilization are in the same co-set, then over-expression of one enzyme can compensate for the deficiency or lack of expression of the other. The complete set of SNP associated co-sets identified in the mitochondria The majority of identified co-sets are Type B. While there is a significant amount of overlap between these co-sets there is variability among them. Indeed even for a particular disease type there can be a remarkably broad range of resulting phenotypes. As referred to above, this can be due to a range of factors including differential expression and genomic differences in other regions of the genome. The appropriate manner to resolve many of these issues and to increase the predictive power of these approaches is to incrementally increase the level of detail by accounting for more detailed biological information such as intracellular regulation, intercellular interactions, and different tissue expression states.

Table 3.1: Phospholipids II mitochondrial co-set

Gene Name	HMGCS2	HMGCL	OXCT1
Gene ID	3158	3155	5019
MIM	600234	246450	245050
Symptoms	hypoglycemia, acidosis, seizures	infantile hypoketotic hypoglycemia, acidosis, hepatomegaly, aciduria	acidosis, vomiting, polypnea

Implications of SNP co-set network analysis There are a two points worth highlighting in this conceptual framework and the resulting analysis. First, the tactic of network reconstruction taken is a "bottom-up" approach [75]. In this approach network reconstruction is based on actual and documented physical interactions and biochemical knowledge, rather than inferred interactions form high-throughput data sets. Such reconstructions are a biochemically, genomically and genetically structured (BiGG) data base that represents an integration of all of our knowledge about the network being analyzed [75]. Consequently, the co-set predictions made are a direct result of a network-wide analysis reflecting fundamental properties of the reconstructed biochemical network. The use of co-sets to detect functionally related reactions is but approach to analyzing reconstructed biological networks [70] and a number of others are emerging [73]. Second, the ability to map similarly causal SNPs to co-sets represents a new dimension in SNP analysis that is enabled by systems biology. Like 'perfect-proxy sets' in the HapMap [2], co-sets take a step beyond trying to track individual components independently, towards appreciating how a number of cellular components interact to produce biological functionality and thus how their malfunction to result in patho-physiological states can correlate. Therefore, by adopting a systems approach one can begin to define some of the general underlying principles of biological functions, and in doing so, can impact the classification of diseases, the mechanistic understanding of the genotype-phenotype relationship, and the potential identification of therapeutic targets and strategies for disease treatment.

Table 3.2: Properties of the *in silico* strain of *M. tb*.
The confidence level for each reaction is based on a scale from 0 to 4, 4 being the highest level of confidence (experimental biochemical evidence supporting the inclusion of a reaction) and 1 being the lowest level of confidence (inclusion of a reaction solely on modeling functionality). Sequence based annotations have a confidence level of 2.

Network Properties of *iNJ*661	
Genes	661
Proteins	543
Reactions (intra-system)	939
Reactions (exchange)	88
Gene Associated Reactions	77%
Metabolites	828
Average Confidence Level	2.31

3.3 *Mycobacterium tuberculosis*

Tuberculosis continues to be a devastating pathogen throughout the world, particularly in developing nations. In 2001, the World Health Organization (WHO) estimated 8.5 million new cases of tuberculosis (based on 3.8 million new reported cases) and an estimated 1.8 million deaths from tuberculosis in 2000 [43]. Within the United States, the number of reported cases of tuberculosis has been decreasing with the exception of a period when the trend reversed in 1986 and peaked in 1992 [85]. This reversal has been attributed principally to HIV/AIDs, immigration from countries with high prevalence of tuberculosis, poverty, homelessness, and multi-drug resistant (MDR) tuberculosis [**?**, 43, 85]. MDR tuberculosis is generally defined as strains that are resistant to treatment with isoniazid and rifampin [89], two of the key first line antituberculosis drugs [43]. MDR strains of tuberculosis emerged in the early 1990s and have now been found all over the world [89].

Many of the properties to unique to tuberculosis are attributable to the organisms metabolic capabilities, particularly the complex fatty acid anabolism and catabolism. These mycolic acids, phenolic glycolipids, and mycoceric acids confer many of the properties such as its acid-fastness and are believed to contribute to the resilience of the organism. *Mycobacterium tuberculosis* can survive in a wide range of environments (many different tissues) and fairly extreme pHs [97]. One

of the most confounding factors with these bacteria is their ability to survive for long periods of time in a dormant stage. The slow doubling time of tuberculosis has further limited the amount of experimental data that can be generated. Many of the first and second line drugs used to treat tuberculosis have metabolic targets, so developing systems level models of metabolism are anticipated to be of great use in the future.

DNA sequencing of the $\approx$ 4.4 Mbp genome of *Mycobacterium tuberculosis* H37Rv (*M. tb*) in 1998 [10] enabled the ability the pursuit of genome-scale analyses of this microorganism. The remarkable relevance to world health and disease control and the need to understand the metabolic function of the organism all evoke the need of a genome-scale metabolic model. Long-term anticipated goals and applications of such models are to understand the growth of mycobacteria under different conditions, identifying strategies to improve growth in vitro (for experimental and diagnostic purposes), and identifying new drug targets for treatment.

M. tb in silico In order to gain understanding about the unique characteristics of this important pathogen, the metabolic network of *M. tb in silico* (*iNJ*661)was manually reconstructed, from which a model was developed to compute perform computational analyses and interpret experimental data. These bottom-up reconstructions have been described in the past as, biochemically, genetically and genomically structured (BiGG) databases. Constraint-based reconstruction and analysis (COBRA) of this BiGG reconstruction was employed to learn about its normal metabolic function and to infer new potential targets for drugs.

The reconstruction process has been described previously [75]. The network statistics for *iNJ*661, which has 661 genes and 939 intra-system reactions, are summarized in Table 1 3.3. A biomass objective function was defined using available measurements of *M. tb* H37Rv and other mycobacteria strains if information was lacking. Flux Balance Analysis (FBA) was used to grow *iNJ*661 *in silico* maximizing the biomass function [37]. *iNJ*661 was grown in silico on three different types of media, Middlebrook 7H9 (supplemented with glucose and glycerol) [58], Youmans [100], and the chemically defined rich culture media (CAMR) [32]. The

doubling times are within the range described in the literature [32], and as expected, the growth rates are higher with the richer media. The minimum doubling time of 14.7/hr described by [32] are within the capabilities of maximum growth of $iNJ661$.

3.3.1 Equivalent but alternative drug targets

Biomass functions can help improve predictions under well-defined conditions by constraining the steady state solution space. However, different growth conditions can appreciably alter the composition and the objectives of bacteria. Significant changes in fatty acid composition have been observed even while growing *M. tb* in culture over the span of weeks. These changes would be reflected as changes in the composition and the coefficients of the biomass function, consequently altering the predictions made by the model. Not all COBRA methods require the definition of objective functions [73] and identifying groups of reactions that operate together can help simplify a network and provide insight into its functionality. Correlated reaction sets have been calculated using sampling [34] and flux coupling [35] and implications for classifying diseases and identifying pathway specific drug targets have been discussed [36].

Applying the same systems view of metabolic networks to pathogens such as *M. tb* causes one to adopt the view that single enzyme drug targets actually knock out complete pathways. As a result, terminating the activity of any other enzyme in that pathway should have the same effect. Similar to the correlated reaction sets calculated by sampling or flux coupling, HCR sets are defined by mass balance constraints. The definition of HCRs is stricter in the sense that it is based on metabolites with one-to-one connectivity. However in contrast to the other approaches, it is independent of the exchange reactions with the environment and any requirements for demand functions. Consequently, the sets can be calculated directly from the stoichiometric matrix. There is a significant degree of overlap between HCRs and the Enzyme Subsets (ES) described by Pfeiffer et al [72]. Since ESs are not constrained by 1:1 connectivity, in principle they may include additional reactions. On the same token, when the same reaction is carried

out by multiple co-factors and the reactions are reversible, which is not uncommon in metabolic networks, ESs may add reactions which form loops, similar to Type III Extreme Pathways [64]. Additionally, intermediate steps in the calculation of HCRs allow the consideration of inclusion or removal of potentially reversible reactions. Biomass functions were removed from the stoichiometric matrix before calculating the HCR sets.

The HCRs calculated for *iNJ661* had 94 0:2/2:0 reactions (See Appendix Table .1). Of these, 24 overlapped with the core set of 147 1:1 HCRs. Since the set of 0:2/2:0 reactions did not have additional gene associations (that werent already in the 1:1 set) and since they had many irreversible reactions throughout, the 1:1 set and the 0:2/2:0 set were not combined (step 1 in the above algorithm outline would involve only identifying the 1:1 metabolites).

147 HCR sets (1:1 only, additional reversible reactions, 0:2/2:0, were not included) were calculated for the network, the average size of each set was 2.93, with median and modes both equal to 2. The largest set, HCR 40, consisted of 13 reactions involved in Cofactor Metabolism and Porphyrin Metabolism. Using the Gene-Protein-Reaction relationships, the HCRs were mapped back to the gene loci. The HCR set was compared to various datasets which grew *M. tb* under different conditions and was found to share 8 HCR sets (HCR 2, 3, 11, 12, 43, 57, 69, and 122) [37]. The intersection of these datasets identifies a subset of reactions that are consistently expressed under different conditions and also required for optimal growth in vitro. These HCR sets may reflect underlying core sets of reactions vital to growth and survival in vitro. Many of the tuberculosis treatment drugs have metabolic targets and a use of this metabolic based reconstruction can be to assist in identifying new and alternative chemotherapy targets for tuberculosis. Mdluli and Spigelman recently discussed the drug targets in M. tb reasonably comprehensively [55]. The drug targets discussed by Mdluli and Spigelman, absent the DNA synthesis and Regulatory Protein targets, were mapped them to the 147 HCR sets (Figure 3.5). The final column lists the number of different reactions in the HCR. Other reactions that are shared within a particular HCR which contains a known drug target, have the potential to be alternative but metabolically

Drug Target	Gene Locus	HCR	HCR size
EmbA	Rv3794	43	10
EmbB	Rv3795	43	10
EmbC	Rv3793	43	10
AftA	Rv3792	43	10
decaprenyl phosphoryltransferase	Rv3806c	62	3
udp galatofuraosyltransferase	Rv3808c	43	10
dTDP-deoxy-hexulose reductase	Rv3809c	43	10
RmlA	Rv0334	69	4
RmlB	Rv3464	69	4
RmlC	Rv3465	69	4
RmbD	Rv3266c	69	4
InhA	Rv1484	57	3
MabA	Rv1483	90	5
KasA	Rv2245	90	5
KasB	Rv2246	90	5
MmaA4	Rv0642c	93	4
Pks13	Rv3800c	86	4
FadD32	Rv3801c	86	4
AccD5	Rv3280	78	2
LeuD	Rv2987c	14	2
TrpD	Rv2192c	10	4
DapB	Rv2773c	2	3
AroA	Rv3227	20	3
AroC	Rv2540c	20	3
AroE	Rv2537c	11	4
AroG	Rv2178c	11	4
AroQ	Rv2537c	11	4
ilvG (acetolactate synthase)	Rv1820	3	3
ilvX (acetolactate synthase)	Rv3509c	3	3
ilvN (acetolactate synthase)	Rv3002c	3	3
ilvB (acetolactate synthase)	Rv3003c	3	3
ilvB2 (acetolactate synthase)	Rv3470c	3	3
branchd chain aminotransferase	Rv2210c	84	2
dihyropteroate synthase	Rv3608c	9	3
dihyropteroate synthase	Rv1207	9	3
PanB	Rv2225	12	4
PanC	Rv3602c	12	4
riboflavin synthase	Rv1416	56	3
riboflavin synthase	Rv1412	56	3
sulfotransferase	Rv1373	131	2
MshA	Rv0486	80	2
MshB	Rv1170	80	2
MshC	Rv2130c	50	2
MshD	Rv0819	50	2
IspD	Rv3582c	16	5
IspE	Rv1011	16	5
IspF	Rv3581c	16	5
MenA	Rv0534c	13	2
MenB	Rv0548c	122	3
MenD	Rv0555	125	2
MenE	Rv0542c	122	3

Figure 3.4: Mapping the HCR sets to the drug targets described by Mdluli and Spigelman [55].

equivalent targets. The drug targets mapped to 25 of the HCR sets. A selected set of these are depicted in Figure 3.5 and a full image of the large map can be found at systemsbiology.ucsd.edu. These 25 HCR sets contain all of the 8 HCR sets identified by the overlap between the different experimental data sets. The

Interpreting large, complex networks in a functionally meaningful manner is enabled by adopting a hierarchical view of the network, where one identifies groups of reactions that respond in unison to changes in media conditions. Groups of reactions strictly bound together based on mass conservation and stoichiometry constraints can lead to the definition of hierarchical sets of reactions [70]. This principle was applied to causal SNP associated diseases in the human mitochondria, and it was found that reactions in the same co-set had similar disease phenotypes. This same concept was applied to *iNJ*661, in search of alternative drug targets.

Unbiased analysis methods, methods that calculate properties of the network independent of objective functions, can provide interesting and valuable insights into network capabilities. The definition of HCR sets, in a similar vein to correlated reaction sets from sampling and flux-coupling, can confer a hierarchical structure to metabolic networks, and may assist in the identification of alternative drug targets. Using these models in conjunction with experimental data can assist in screening and identifying new and alternative drug targets.

Taken together, this study adds another high resolution reconstruction of microbial metabolism. There now exist a growing number of such reconstructions that have been particularly useful for basic studies of network properties and for bioprocessing applications [42-44]. As the number of reconstructions of human pathogens grows, it should become feasible to expand their uses towards improved understanding pathogenic mechanisms, and design of interventions and treatment. Large-scale rigorous experimental validation studies should now be performed to further these goals.

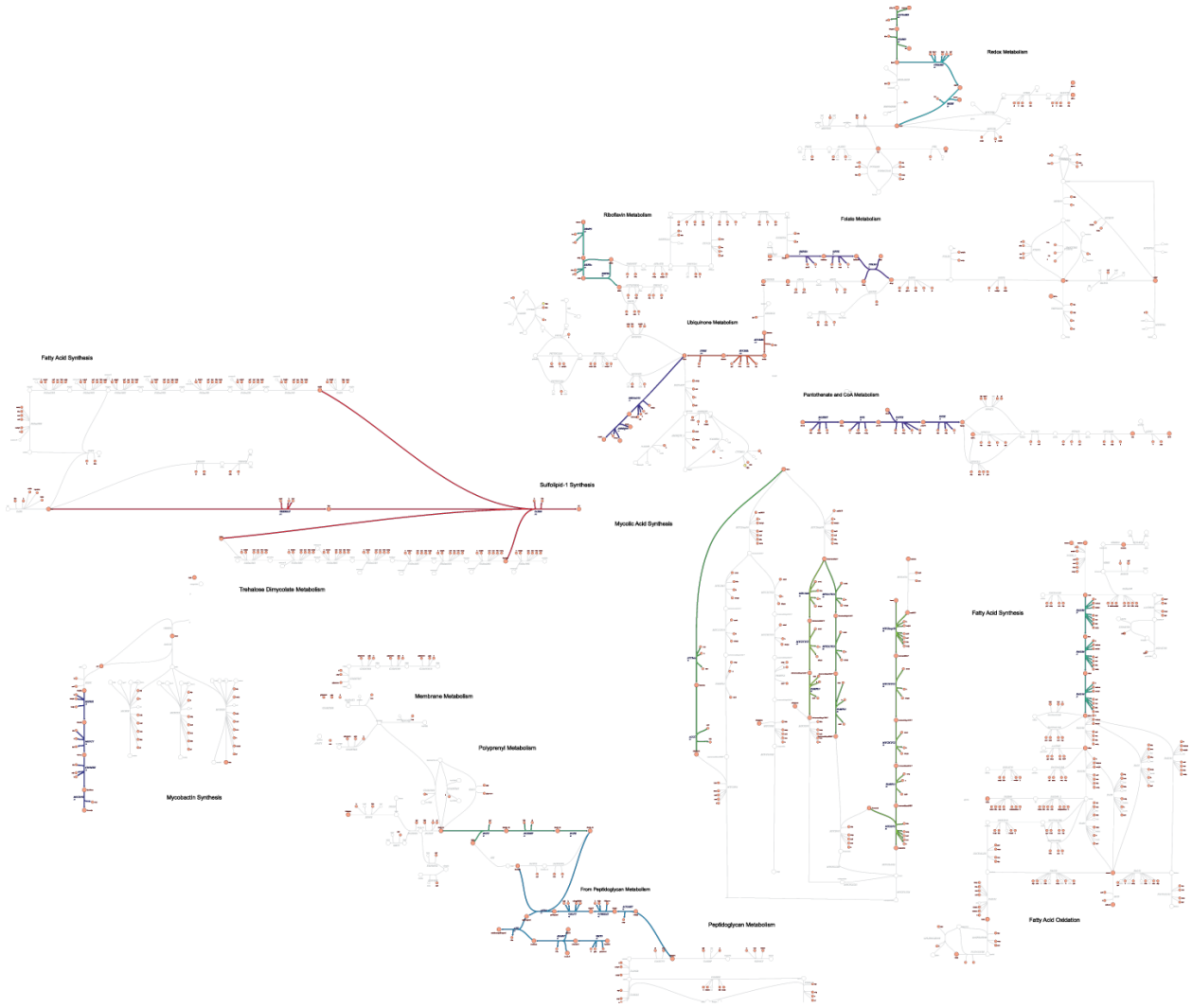

Figure 3.5: A highly abbreviated map of the drug target co-sets in *iNJ661*. Colored reactions indicate HCRs.

3.4 Summary

This chapter focused on the use of co-sets to categorize different diseases associated with causal SNP mutations and to propose alternative candidate drug targets in a pathogen of significant relevance in the third world. There were encouraging lines of evidence in both cases to suggest that there is a causal connection between the reactions within co-sets. The simulation based sampling approach was used for the identification of co-sets for the mitochondria. In contrast the topology based HCRs were used for the analysis of the *in silico M. tb* model, since the organism can survive in a wide range of environments and the interest was to find the most generalizable set of reaction co-sets. A similar concept but with very different endpoints, different applications, and different algorithmic approaches was explored in this chapter. Over time and with iterative improvements, metabolic network reconstructions have achieved the stage of hypothesis generation and model-driven biological discovery in systems biology [75]. There is an additional applicaiton which uses the co-set concept that can help simplify and gain insight into biological networks and that is the problem of regulation. The existence of co-sets yield two implications regarding regulation of these reactions,

1. Within each co-set there should only be one enzyme that is actively regulated
2. There are two classes of regulated or regulatory enzymes with regards to co-sets: Some regulatory enzymes will appear within co-sets and others will appear outside of co-sets

Looking at the co-sets in the human red blood cell (see Chapter 6), it appears that these statements are consistent, as HK, PFK, and PK all appear in different co-sets. The experimental investigations to test the hypotheses put forth by co-sets will hopefully lead to validation, rejection, or revision of this concept.

The text of Chapter Three in part is reprint of the material as it appears in Molecular Systems Biology and BMC Systems Biology. The dissertation author was the primary researcher and author of this publication, and B.Ø. Palsson directed and supervised the research which forms the basis of this chapter.

Chapter 4

Hierarchical Pooling: Biochemical correlations in the column space

The network of interactions that occur between biological components on a range of various spatial and temporal scales confer hierarchical functionality in living cells. In order to determine how molecular events organize themselves into coherent physiological functions, *in silico* approaches are needed to analyze how physiological functions emerge from the evolved temporal structure of networks. Time scale decomposition is a well-established, classical approach to dissecting network dynamics and there is a notable history of analyzing the time scale hierarchy in metabolic networks and matching the events that unfold on each time scale with a physiological function [44, 66, 24]. This approach enables the identification of the independent, characteristic time scales for a dynamic system. In particular it has been possible to decompose a cell-scale kinetic model of the human red blood cell in time to show how its key metabolic demands are met through a dynamic structure-function relationship. The underlying principle is one of aggregation of concentration variables into pools of concentrations that move in tandem on slower time scales [66, 78].

The dynamics of biological networks characteristically span large time scales (8 to 10 orders of magnitude), which contributes to the challenge of analyzing and interpreting related models. However, there is structure in this dynamic hierarchy of events, particularly in biochemical networks in which the fastest motions gen-

erally correspond to the chemical equilibria between metabolites, and the slower motions reflect more physiologically relevant transformations. Appreciation of this observation can result in elucidating structure from the network and simplifying the interactions. The reduction in dynamic dimensionality is based on such pooling and the analysis of pooling is focused in the underlying time scale hierarchy and its determinants. Understanding the time scale hierarchy and pooling structure of these networks is critical to understanding network behavior and simplifying it down to the core interactions.

Top-down studies of dynamic characteristics of networks begin with fully developed kinetic models that are formal representations of large amounts of data about the chemistry and kinetics component interactions. Network properties can be studied by numerical simulations (that are condition-specific) or by analysis (that often yield general model properties) of the model equations. Since comprehensive numerical simulation studies become intractable for larger networks and the identification of general model properties are needed for the judicious simplification of models, there is a need for analysis based methods in order to characterize properties of dynamic networks. In this study we present an *in silico* analysis method to determine pooling of variables in complex dynamic models of biochemical reaction networks. This method is used to study metabolic network models and allows us to identify and analyze pool formation resulting from the underlying stoichiometric, thermodynamic, and kinetic properties.

Hierarchical pooling has been introduced in Chapter 2. For simple networks this process is fairly uncomplicated, however for larger networks, this becomes a more complex and taxing endeavor. Simulation based methods have been successful for elucidating the pooling structure [44], however doing this required significant knowledge about the system *a priori*, such as the relevant set of initial conditions to consider and the time scales of interest. An algorithmic approach for identification of the pooling structure has been lacking to date. An analytical approach for identifying the pooling structure of networks is described and subsequently applied to three different experimentally validated, kinetic models of metabolism, the human red blood cell, the human folate cycle, and the yeast glycolytic pathway.

4.1 The approach

Dynamic description of networks: Linearizing the mass conservation equations for a chemical reacting system around the steady state yields the linear form of the dynamic mass balances,

$$\frac{dx'(t)}{dt} = Jx'(t) \tag{4.1}$$

where J is the nxn (metabolite) Jacobian matrix, and x' (= x - x_{ss}) is the deviation vector of the concentration variables from the steady state (x_{ss}). J describes the dynamical characteristics of the network near the steady state. The properties of J can be analyzed using matrix decomposition methods, and it is important for these methods to capture the interactions between components across all of the time scales of the network.

Temporal decomposition can be carried out by applying a similarity transformation,

$$J = M^{*}\Lambda M^{*-1} \tag{4.2}$$

where Λ is a diagonal matrix with the eigenvalues, that are the negative reciprocal time constants [91]. The superscript star indicates the possible presence of imaginary components in the matrices. Complex conjugate pairs can be removed by pre-multiplying by a modified identity matrix with block diagonal ones at the rows and columns in which the matrix has imaginary components. The complex conjugate pairs arise in situations in which the motions of these modes cannot be decomposed in time. The modal matrix, M^{-1}, can then be used to define the modes, m, such that,

$$m = M^{-1}x \tag{4.3}$$

which combined with Equation refeq:lineardxdt yields,

$$\frac{dm}{dt} = \Lambda m \tag{4.4}$$

as described previously [68]. The rows in the modal matrix define dynamically independent 'aggregates', or pooling of metabolites into independent dynamic vari-

ables. Time scale decomposition can be successfully performed only if the eigenvalues are well separated. When J is rank deficient, it implies the presence of dynamically invariant pools reflecting chemically conserved moieties in the network, whose sum total is constant. These vectors are not included in the modal matrix. The modal matrix separates the dynamics of the network into a series of dynamically independent motions, moving from the fastest (top) modes to the slowest (bottom) modes as the time scales lengthen 4.1. Here we present an approach to the analysis of the modal matrix that simplifies the elucidation of notable pools without the need for intensive calculations of dynamic phase portraits and autocorrelations functions in order to identify biologically relevant interpretations of these modes as pools of metabolites being created and consumed on different time scales [44]. An illustrative toy example of time scale decomposition is described in the supplementary material.

Table 4.1 summarizes some of the trade-offs between the characterization of dynamics using the Jacobian matrix and carrying out large numbers of dynamic simulations directly. Although carrying out dynamic simulations are not restricted to a particular steady state, they are condition dependent (e.g. initial conditions) and resource intensive. Hence for larger networks, dynamic simulations are not a viable option. In contrast, characterization of the pooling structure of networks via analysis of the Jacobian requires only a single set of calculations to characterize a particular steady state and this approach can be applied to large and small networks alike. Furthermore, different steady states can be characterized as well, by recalculating the Jacobian at the alternate steady states. Defining pools from modes: A column of the modal matrix describes the participation of a concentration in each of the linearly independent modes. When two concentrations (x_i and x_j) become dynamically correlated beyond a particular time scale (say after the k^{th} time constant), the entries of the modal matrix in the two corresponding columns are correlated with one another on the subsequent time scales (Figure 2). This characteristic enables the identification of the time scales that two concentrations would pool together.

Employing a geometric interpretation for this determination, one can ex-

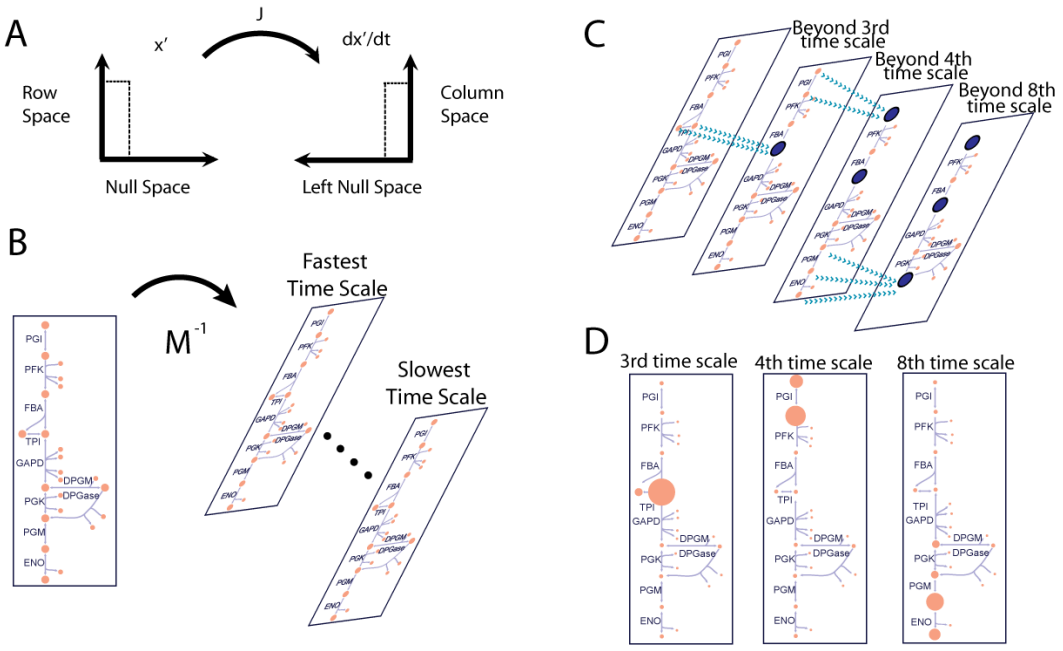

Figure 4.1: Hierarchical decomposition in network analysis.

A. The Jacobian acts as a linear operator mapping the dynamics onto the deviation variable. B. The modal matrix maps network dynamics onto independent time scales. Panels C and D illustrate two approaches to understanding the interactions between metabolites on the different time scales. C. Beginning from the fastest time scale and moving forward, components that move together on subsequent time scales are lumped into an aggregate pool variable. The pooling pictorially for three different time scales in glycolysis and the Rapoport-Leubering shunt in the red cell. The large blue dots indicate pool formation between two metabolites, signifying that these two metabolites become coupled or correlated on slower times scales. In this case, glyceraldehyde 3-phosphate and dihydroxyacetone phosphate pool together after the first time scale, the hexose phosphates pool together after the fourth time scale, and the triose phosphates pool together after the eighth time scale. D. Each time scale is analyzed independently and the interactions are defined in terms of the coefficients in the model and their contribution to the cumulative sum of the modal coefficients. Analyzing all of the modes in this manner allows the identification of variables that are dominant across multiple modes and identifying the time scales across which they are most active. Four fundamental subspaces are associated with J and its mapping onto its time derivative. The key to temporal decomposition is the time-ordered removal of dynamic motions that lead to the step-by-step increase in the null and left null spaces of J.

Table 4.1: Analysis versus simulations.
A comparison between the trade-offs for analyzing the Jacobian around a particular steady state versus carrying out dynamic simulations. The approach presented here for analysis of the Jacobian in order to characterize network dynamics allows generalized, comprehensive elucidation of dynamics around a particular steady state directly and in a scaleable manner. In contrast, although the approach using dynamic simulations is not restricted to a particular steady state, it is resource intensive and for larger networks it is infeasible to characterize all of the different possible initial conditions, due to combinatorial growth of the possible combinations.

Jacobian Analysis	Dynamic Simulations
Generalized results	Condition specific results
Scaleable	Intractable for large systems
A single set of calculations to characterize a particular steady state	Resource intensive, many simulations in order to characterize network pooling
Linear regime near a steady state	May move from one steady to another

plicitly identify pool formation by calculating the angle between columns $(\mathbf{M}_x^{-1})_i$ of the modal matrix,

$$\mathbf{\Theta} = cos(\theta_{ij}) = \frac{(\mathbf{M}_x^{-1})_i^T \cdot (\mathbf{M}_x^{-1})_j}{\|(\mathbf{M}_x^{-1})_i^T\| \|(\mathbf{M}_x^{-1})_j\|} \tag{4.5}$$

in which $(\mathbf{M}_x^{-1})_i$ refers to the magnitude of the i^{th} column of the modal matrix and θ_{ij} refers to the angle between the i^{th} and j^{th} columns of the modal matrix. However, if one were to simply calculate the correlations between metabolites across all time scales, in general no pooling would be observed among the metabolites, even though there may be physiologically relevant pooling between metabolites, that characteristically occur on slower time scales. A simple illustration of this is depicted in by the modal matrix in Figure 4.2, which highlights the need to characterize aggregate pool formation of variables in the context of progressively slower time scales. Hence this approach analyzes progressive pooling across all of the networks independent time scales, in contrast to simulation based methods which are dependent on a priori specification of the time scales of interest for identifying correlations between metabolites. In order to identify the time scales at which pool formation occurs, we compute the angle between two columns as a function of an index k that runs from 1 to n time scales. As each row of the modal matrix is removed (k increases by one) the angle is recomputed to form a series of angles as a function of k; i.e., (k), k =1, 2, , n. If the angle (k) is close to zero, the two columns are correlated at and above that k value and the two corresponding concentrations will move in tandem for the subsequent time scales, thus forming an aggregate variable or a pool. The practical issue is to determine when the angle is close enough to zero to make a call on the formation of a pool.

The pools can be described as a sum of matrix products over the time scales of the network,

$$\mathbf{F}_i^{ts} \cdot \mathbf{M}_x^{-1} \cdot \mathbf{F}_i^m \tag{4.6}$$

$\mathbf{F}_i^{ts}$ is a binary diagonal matrix, with $n - i$ non-zero elements on the diagonal. $\mathbf{F}_i^m$ is a binary matrix with off-diagonal elements whenever two columns meet a specific cutoff and can be combined into an aggregate pool. $\mathbf{F}_i^{ts}$ and $\mathbf{F}_i^m$ act on

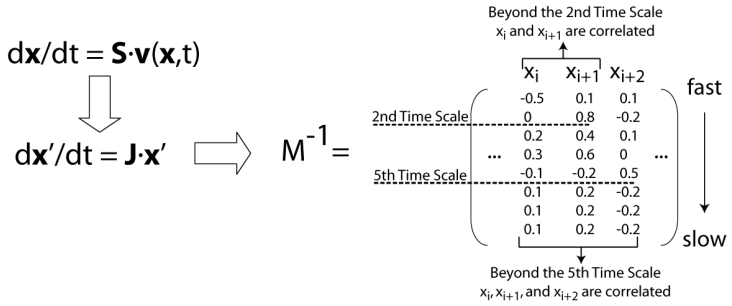

Figure 4.2: Correlations across time-scales.

Illustration of the progression correlation between two variables as fast time scales are removed. The set of dynamic equations are linearized about a particular steady state. Applying a similarity transformation to the Jacobian, enables the calculation of the modal matrix (depicted to the right). The rows of the matrix correspond to different time scales. When the ratios between two entries are constant, the two metabolites pool together. After the second time scale, metabolites x_i and x_{i+1} form an aggregate pool and after the fifth time scale, x_{i+2} joins the pool. If the variables were compared across all time scales, no significant correlations would be observed. Hence, this simple example highlights the need for a method to analyze correlations between metabolites with consideration of the characteristic time scales of the network.

the modal matrix, by filtering out modes or combining variables, respectively. For a network with m metabolites, in which no aggregate pools form, there will be m sets of pooling matrices. Conversely, for the extreme case in which all of the metabolites form a single aggregate pool on a single time scale there will only be a single pooling matrix.

Defining dominant interactions for each mode One can quantitatively ascertain the contribution of each metabolite to each mode by rank ordering the normalized mode and keeping only the largest weights that add up to the specified cutoff percentage. At low cut-off ranges, all metabolites with small contributions to the mode will be zeroed out. The interactions across the modes can be mapped on top of the interactions defined by the stoichiometric matrix in order to compare and contrast the topological connectivity versus the dynamic connectivity at time scales of interest.

4.2 Human red blood cell

Once the modal matrix, $\mathbf{M}^{-1}$, was calculated, all pairwise angles between the metabolites (columns of the modal matrix) were calculated (see Equation 4.5). The modal matrix is rank ordered from the fastest (k = 1) to the slowest (k = n) modes. The angles between the columns of the modal matrix were recalculated n-1 more times, in which an additional row of the modal matrix is zeroed out at each iteration. For example at the third iteration (k = 2), the first two rows of the modal matrix have been zeroed out. The spectrum of correlation cut-off values for pooling were considered from 10% to 99%. Cut-off values in the range 85% to 95% resulted in pooling of variables most consistent with the known pooling structures of the human red cell [66, 44]. A value of 90% was used as the correlation cutoff for the red cell, folate, and yeast glycolysis models. The angle between two zero vectors was classified as undefined and the angle between any zero vector and another vector with at least one non-zero element was defined as $90\,^{\circ}$. Fragmentation of the pooling structure, in the strictest sense, was identified by any 0 entry (or less than $\sim 10^{-13}$) in the final row of the metabolite modal matrix.

The results of the hierarchical correlations can be presented in a symmetric correlation tiled array, where each entry can be used to represent k for a pair of concentrations. Figure 4.3 shows the result of such an array for the human red cell. Since the array is symmetric we can display both k and the modal coefficient ratio in the pool (x_i/x_j) for each pair of concentrations; thus

- The lower left triangle of the tiled array indicates the time scale k beyond which pooling occurs in the network. So for example, G6P and F6P pool together after the fourth mode in the red cell metabolic model. For the highly interconnected metabolic network in the red cell, eventually, all of the metabolites pool together.

- The upper right triangle of the tiled array contains plots show the ratios of the modal coefficients (x_i/x_j) for each of the concentration pairs at all of the time scales above k for that pair. For many of the concentration pairs, the ratio remains fairly constant (glycolytic pools, pentose phosphate pools, etc)

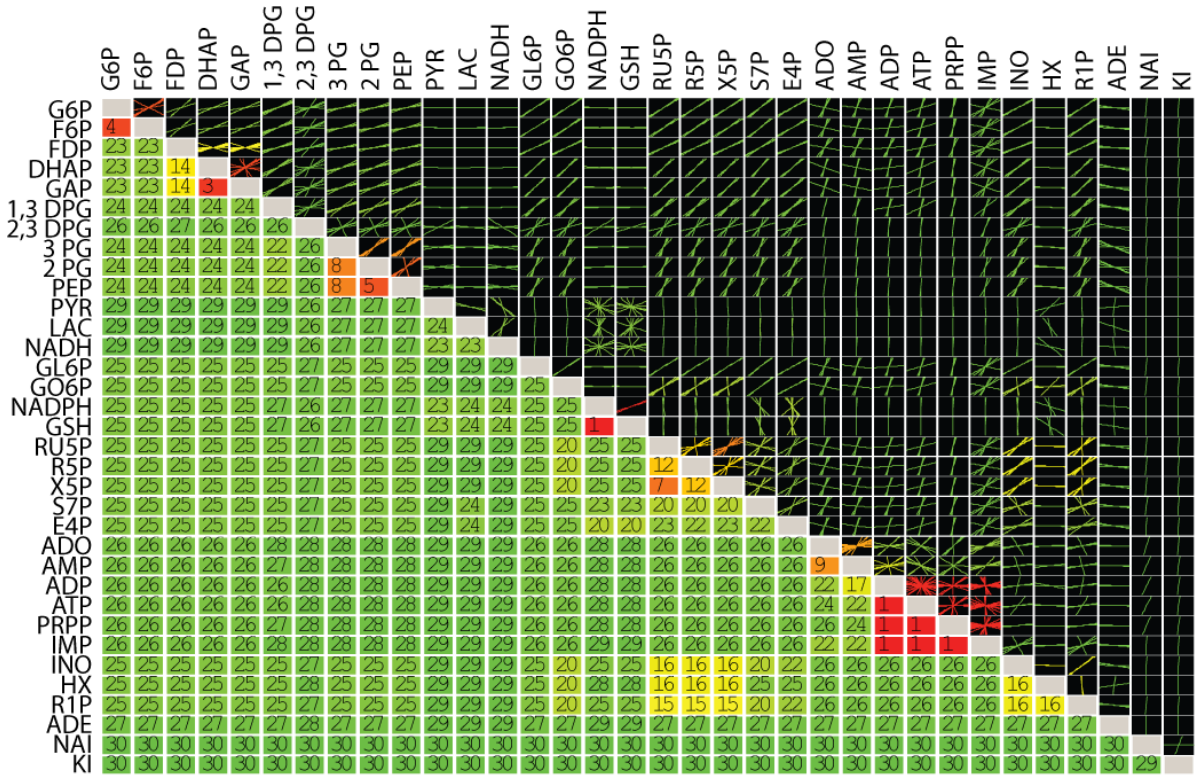

Figure 4.3: Hierarchical pool formation in the human red blood cell.

The lower left triangle indicates the modes after which pooling occurs between the corresponding metabolites (1 being the fastest time scale). The upper right triangle plots slopes between the two metabolites for the remaining time scales after pool formation (through the origin), color coded according to the time scale at which pooling occurs. Some metabolites (e.g. phosphoglycerates) have fairly constant ratios once they join aggregate pools. Others, such as ATP and ADP have varying ratios. These ratios change when interactions with other pathways dominate on subsequent time scales, for example when glycolytic intermediates dominate on one time scale and nucleotide salvage metabolites dominate on another, the respective interactions between ATP and ADP are affected differently. The cutoff value for $cos(\theta)$ was 0.9.

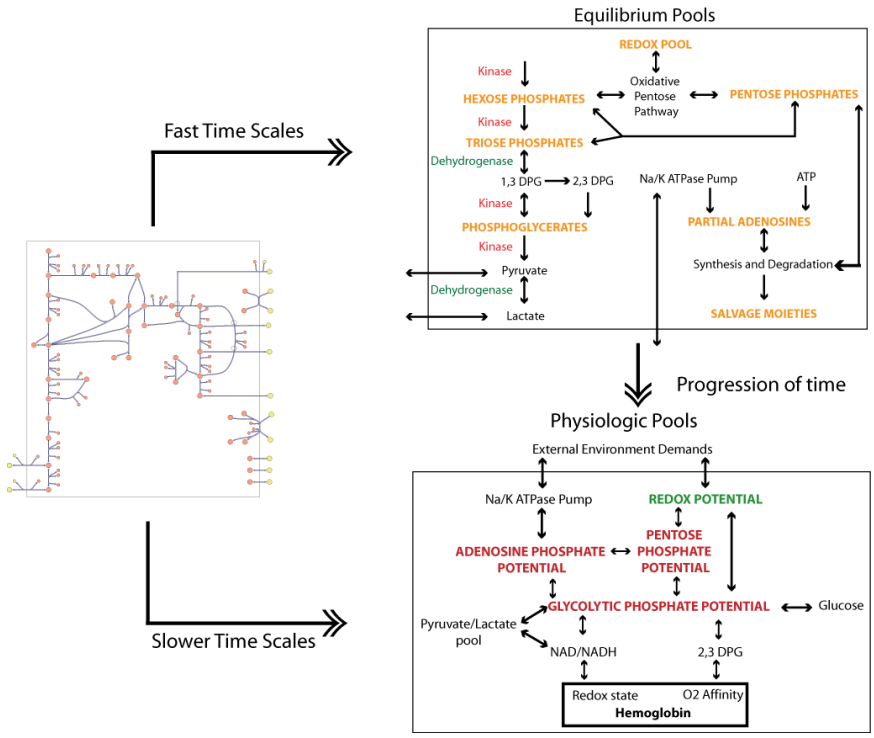

Figure 4.4: Dynamics driven network simplification.

Converting human red cell metabolic network map into lumped pools according to time scale decomposition (adapted from [33]). Pooling on fast time scales define the chemical equilibrium pools and on slower time scales the physiological pools.

past a certain time scale showing the relative contribution of the compounds to a pool.

- The pooling structure observed in Figure 4.3 is consistent with the previous descriptions [44] and enable the simplification of the network into equilibrium pools on fast time scales and physiological ones on slower time scales (Figure 4.4).

The time scale (k) for the formation of pools and the ratio between a pair of concentrations are functions of three factors: network stoichiometry (or topology), thermodynamics, and kinetic properties of the transformations in the network. Viewing the dynamics of the network in terms of the modal matrix and the pairwise concentration correlations on progressing time scales enables one to consider the questions of A) the thermodynamic versus kinetic control of concentrations within the whole network, and B) the delineation of kinetic versus topological decoupling in networks.

A) Steady state kinetic vs. thermodynamic equilibrium effects: The thermodynamic equilibrium pools of the network can be seen in Figure 4.5. Comparison of these pools with those in Figure reffig:rbcpool distinguishes between the equilibrium state and the kinetically driven steady state. In many cases such comparisons show a thermodynamic basis for pool formation, such as the hexose phosphates, the pentose phosphates, and the triose phosphates. For metabolite pairs that are thermodynamically close (with regards to the Gibbs free energy of formation), the kinetics presumably have been adjusted to be fast, making such thermodynamically neutral events lead to reduction in effective dynamic dimensionality. Deviations from such behavior are however observed, such as with 1,3 DPG and 2,3 DPG. Although the free energy of formation of these two must are close (as approximated by the group contribution method [52]), 2,3DPG does not pool together with 1,3DPG until the 31st mode (Figure 4.3). Hence the kinetic and allosteric regulatory 'control' dominates. This 'control' has physiological significance because 2,3DPG can regulate the binding affinity of hemoglobin for oxygen and is maintained at a higher concentration than the glycolytic intermediates. Other examples in which kinetic control dominates include ATP and NADPH,

ADP and NADH, and G6P and ADP.

B) Kinetic and topological decoupling: Two striking features of the tiled array are 1) the pooling between the majority of the compounds occurs on the slowest time scales and 2) the slopes for many of these are horizontal or vertical lines, implying dynamically independent behavior. This dynamically independent behavior may result from a lack of connectivity (topological decoupling) or from independent kinetics (e.g. kinetic decoupling resulting from a zero order rate law). Thus, if compounds are detected to be topologically decoupled in the tiling array they are expected to dominate a particular mode.

A kinetic or topologically decoupled compound will undergo the largest changes in concentration and interactions with other compounds during those time scales on which it plays a dominant role the modes. After these time scales have been passed, concentration changes are likely to be less significant and the compounds could be viewed as joining an aggregate pool, but may not be in a fixed ratio as would be dictated through strictly thermodynamic or kinetic coupling.

Networks that are tightly connected in terms of stoichiometry and kinetics will result in complete pooling of all metabolites on the slowest time scales, which is seen in large part in the red cell (Figure 4.3). There are examples of effectively uncoupled metabolites in this model however. Sodium and potassium for example are uncoupled from all metabolites except for the adenosine phosphates, which results from topological decoupling, since the only metabolites these ions interact with in the model are ATP and ADP via the Na/K ATPase. In contrast, pyruvate and lactate are decoupled from the rest of glycolysis, in spite of topological connections, thus the decoupling is driven by kinetic effects. The tiled arrays can be used to define the effective dynamic dimensionality of the models by counting the number of different time scales during which two or more variables form an aggregate pool. For the networks considered, the effective dynamic dimensionality reduced the dimension by one-third to one-half (see Table 4.2).

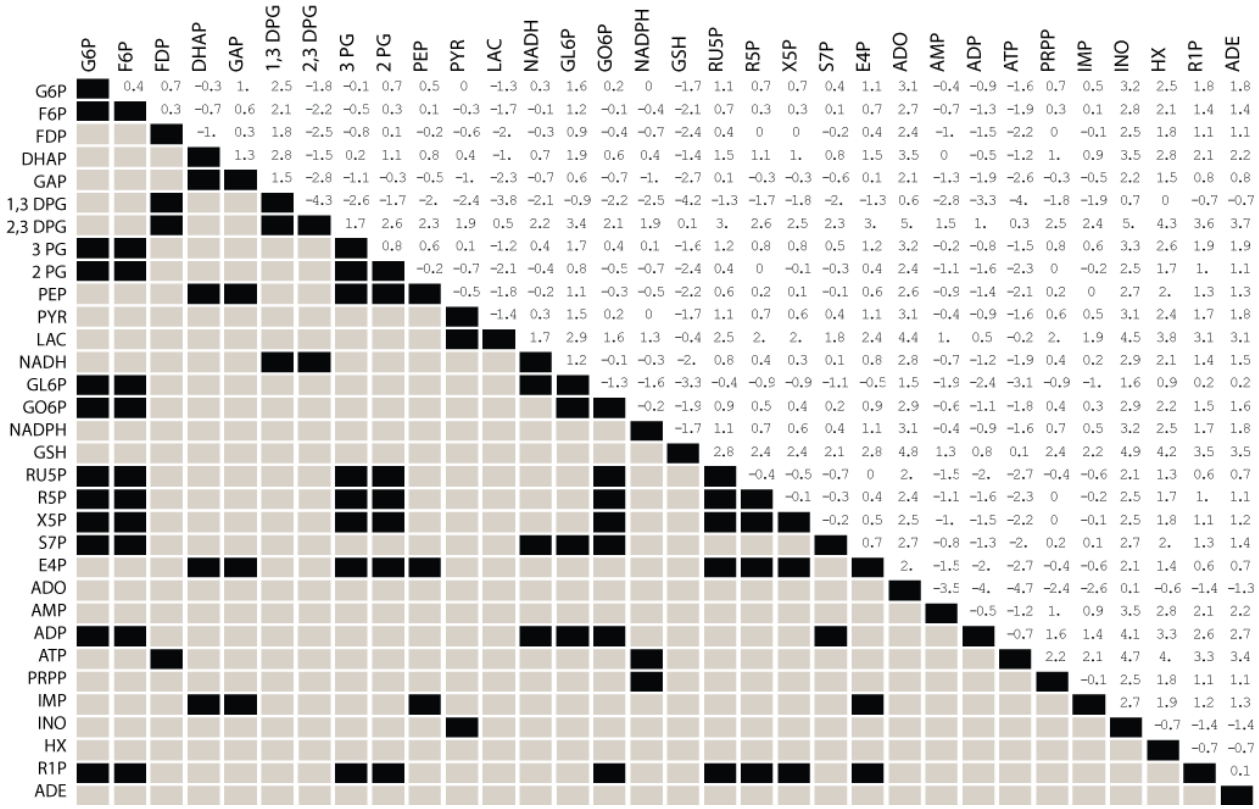

Figure 4.5: Metabolite free energy ratios for the red cell.

The lower left triangle of the tiled array depicts a matrix with the ratios of the Gibbs free energy of formation between the metabolites in the red blood cell metabolic network. Ratios below 0.85 or above 1.15 were filtered out and not shown. The remaining entries (blackened entries) indicate expected pools if thermodynamic considerations alone determined the behavior of the network in a closed system. Values for the Gibbs standard free energies of formation for the metabolites in the human red cell model were used from [28].

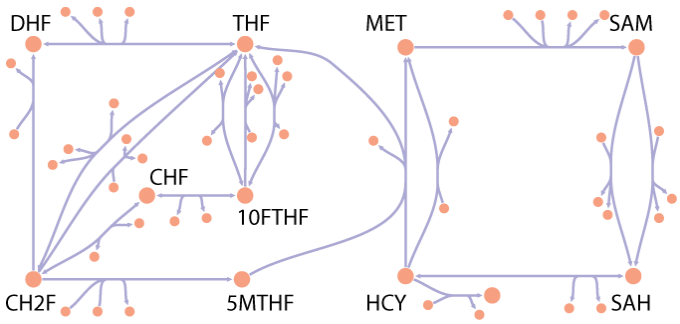

Figure 4.6: A map of the folate network.

4.3 Human folate metabolism

The tiled pooling array for a model of folate metabolism [77] depicted in Figure 4.6 was computed (Figure 4.7). There were 7 independent time scales in the modal matrix and one conserved folate moiety pool from the left null space. From the array it is observed that the folate carrier branch (5MTHF, THF, DHF, CH2F, CHF, 10FTHF) of the network and the methionine metabolism branch (MET, SAM, SAH, HCY) of the network act fairly independently dynamically. S-adenosylmethionine (SAM) is the primary metabolite which joins the interactions between the two branches. In order to identify if these interactions are topologically driven, kinetically driven, or combinations of both, one can plot the modes in which these interactions are most significant. Figure 4.8 depicts the primary interactions on the slowest mode in the network. It can be seen that SAM is not directly topologically coupled to the folate branch, so the interactions between the two branches, mediated by SAM is driven by kinetic effects. Additionally, note that although they pool together, SAM moves in opposition to the folate carriers. Combining Figures 4.6 and 4.7, the progression of pooling of the folate network can be depicted, Figure 4.9. On time scales slower than the minute time scales (the sixth mode corresponds to $\approx$ 6 minutes) the network boils down to interactions between the folate pool and the methionine pool. So on physiologically relevant time scales, the various possible interactions depicted in Figure 4.6 simplify to shifting between two carrier pools.

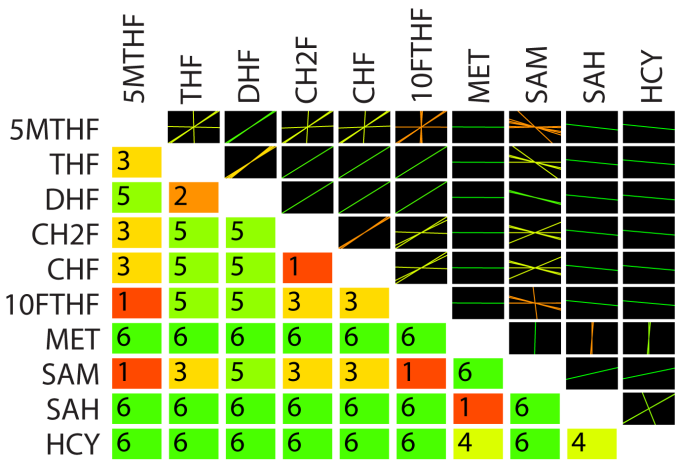

Figure 4.7: Hierarchical pool formation in human folate metabolism.

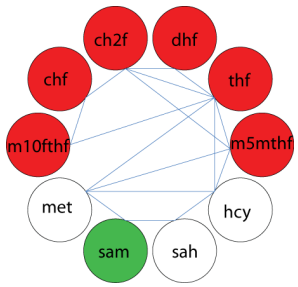

Figure 4.8: Topological versus kinetic interactions.

An example of a graphical overlay of topological and kinetic data for the dominant interacting metabolites for a particular mode. The slowest mode in the folate network ($\sim$ 30 minute time scale) is shown. The green and red shaded elements reflect the dynamic interactions between the metabolites on the 30 minute time scale (the colors reflect positive and negative entries, respectively). The blue lines indicate topological connectivity (i.e. from the stoichiometric matrix).

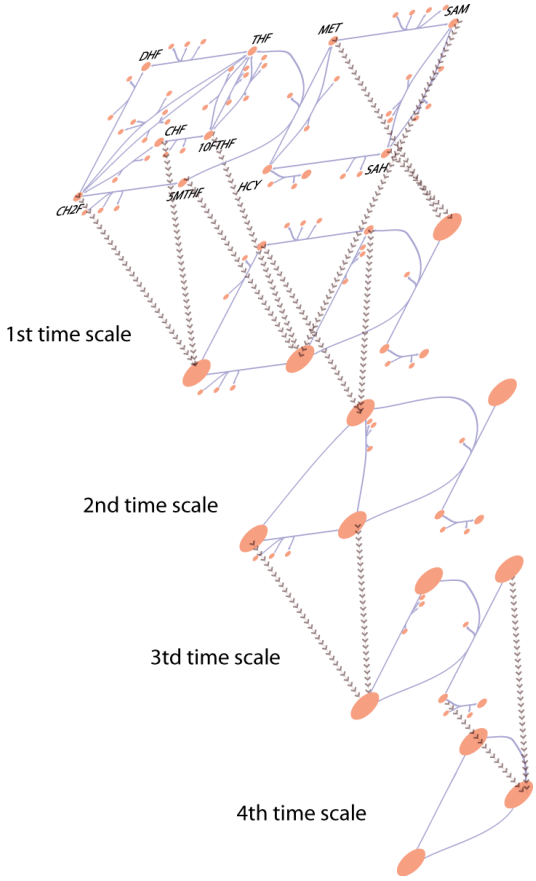

Figure 4.9: Metabolite pool formation in folate metabolism.

Pool An illustration of progressive pool formation across the first 4 time scales for the folate network based on the results from Figure 4.7. Beyond the first time scale pools form between CHF and CH2F; and 5MTHF, 10FTHF, SAM; and MET and SAH. DHF and THF form a pool beyond the second time scale. Beyond the third time scale CH2F/CHF join the 5MTHF/10FTHF/SAM pool. Beyond the fourth time scale HCY joins the MET/SAH pool. Ultimately, on time scales on the order of a minute and slower, interactions between the pools of folate carriers and methionine metabolites interact.

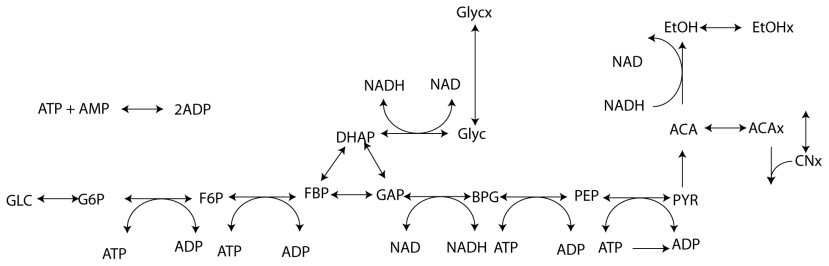

Figure 4.10: A diagram of the yeast glycolytic pathway.

4.4 Yeast glycolytic pathway

A similar analysis was carried out for the yeast glycolytic pathway shown in Figure 4.10 and originally described by [93]. The tiled pooling array for the yeast glycolytic pathway was computed (Figure 4.11). The pooling structure of the glycolytic pathway is very similar to pool formation in the red cell, with glycolytic intermediates aggregating together on the faster time scales. The adenosine phosphates also pool together very quickly. A feature of the tiled array not observed with the other models considered is fragmentation of the pooling structure. This implies that unlike the other two models considered, all of the metabolites do not eventually move together in fixed ratios on the slowest time scales. These effects can be driven by topological properties or kinetic properties of the network as well. Comparing the topological versus kinetic interactions in a graphical format (not shown) illustrates that the lack of interactions by acetate (ACA) and cyanide (CNX) with the other components in the network are due to topological constraints. The fragmented pooling reflects the fact that interactions between ACA and CNX and the rest of the network can only occur during particular time scales. These constraints however dictate much of the overall behavior of the network. The fragmented pooling observed in Figure 4.11 result in a simplified view of the network built around the transporters, as seen in Figure 4.12.

Taken together, this chapter has resulted in: 1) the development of top-down approaches for the computationally driven delineation of pools, 2) illustration of how to distinguish between topological, kinetic and thermodynamic basis for pool formation and 3) application of the methods to analyze the dynamic struc-

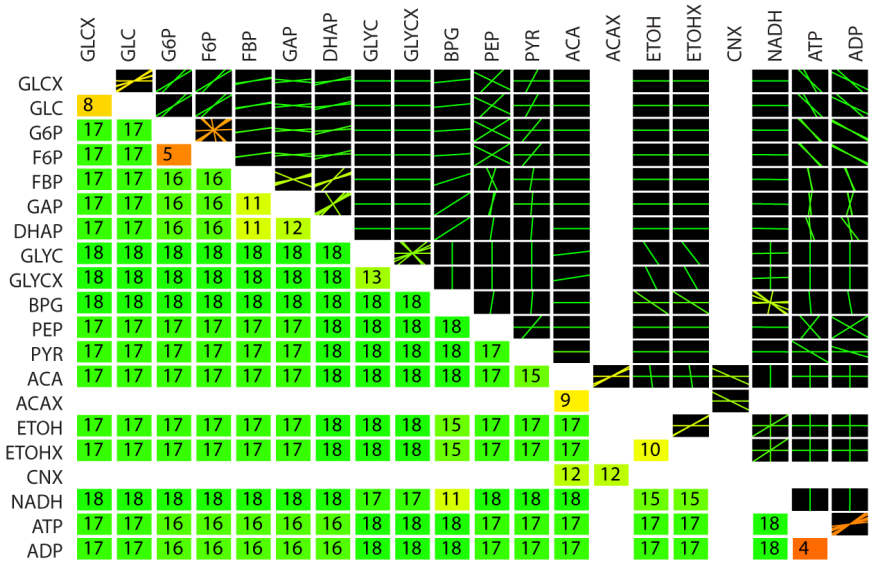

Figure 4.11: Hierarchical pool formation in yeast glycolysis.

Tiled array of the hierarchical pool formation for the yeast glycolytic pathway. Glycolytic intermediates and adenosine phosphates pool together on fast time scales. Fragmented pooling is also observed (i.e. there were 0 entries in the slowest mode, indicating that on the slowest time scale, all of the components in the network do not move together in a lumped pool).

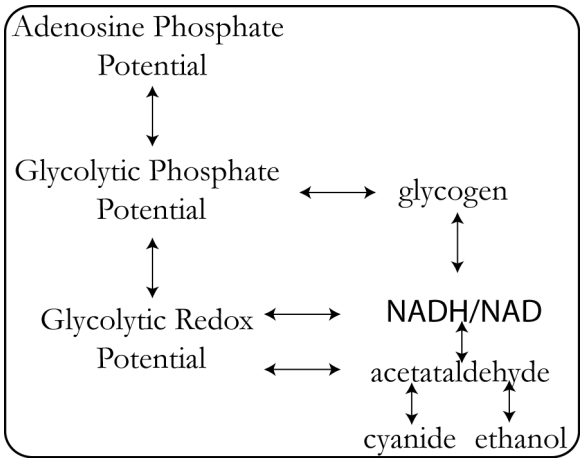

Figure 4.12: Dynamics driven simplification of yeast glycolysis.

Simplified model of the yeast glycolytic pathway dictated by the fragmented pooling of the network. The glycolytic and redox potentials are similar to those in the red cell. The adenosine phosphate potential is only composed of ATP and ADP. The NADH/NAD ratio determines the redox interactions with glycolysis, glycogen, and conversion between acetaldehyde and ethanol.

ture of metabolic network models in yeast and humans. The application of these methods enabled the simplification of the networks based on the dynamic pooling of metabolites on progressive time scales and the identification of the key metabolic interactions on the slower time scales.

There were some observations in the results worth pointing to suggest further areas worthy of investigation. The pooling ratios between metabolites are not always constant and metabolites that pool early on are more likely to have changing ratios on subsequent time scales. Furthermore, metabolites that are connected to multiple pathways are likely to have change ratios even after they begin pooling, as observed for ATP and ADP in the human red blood cell (Figure 4.3). These metabolites interact with glycolysis, the pentose phosphates, and the nucleotide salvage pathway and these interactions vary as the time scales are dominated by the different pathways. Conversely, the ATP/ADP ratio is fairly fixed and uniform in the yeast glycolytic model. This appears to be a result of the fact that there is only one major pathway that interacts with ATP and ADP. Further investigations into when and why pooling ratios change may lead to a richer appreciation of the integrated dynamic structure of metabolic networks. Additionally it was observed that the pooling structure may changes about different steady states. For example, in the human red cell changing the magnitude of the energy load will shift the time scale of the ATPase and hence alter the pooling of the network (not shown). This is also an area in which further investigation will yield an appreciation of altered dynamics corresponding to different steady state conditions.

Increasing numbers of large-scale kinetic models of biochemical reaction networks are arising (e.g. http://www.siliconcell.net/, http://www.cellml.org/). There are also growing compilations of information regarding enzyme kinetics (e.g. BRENDA, SABIORK), which portend the development and availability of more kinetic models. Since dynamics simulations are not a viable approach for the comprehensive characterization of pool formation for larger models, there is a need for analysis based approaches to identify these general characteristics in metabolic networks.

Table 4.2: Descriptive characteristics of network dynamics.
Summary of properties of the various kinetic models, particularly the Jacobian matrices of the networks. Pooling of the tiled modal arrays can be classified as complete (in which all elements pools together eventually) or fragmented. The number of conservation pools is equal to the size of the left null space of the stoichiometric matrix. The effective dynamic dimensionality (Eff Dim) is the number of different time scales at which pooling occurs. The time scale span is the ratio of the largest to smallest eigenvalue for each of the networks.

	Dimension	Rank	Pooling	Left Null	Eff Dim	Time Scale Span
RBC	34	34	complete	0	17	$1.3\text{x}10^{10}$
Folate	10	9	complete	1	6	$4.88\text{x}10^{4}$
Yeast	20	20	fragmented	0	13	$7.5\text{x}10^{6}$

4.5 Summary

The pooling approaches developed here were based on identifying the dynamically independent times scales and their corresponding modes. The principle pooling approach considered here was based on a particular calculation given by,

$$(\mathbf{M}_x^{-1})^T \cdot \mathbf{M}_x^{-1} \tag{4.7}$$

This matrix product reflects the dynamic connectivity of the network. These collective analyses of the modal matrix allowed the subsequent identification of pools, effective dimensionality reduction, differentiation between kinetic and topological properties, and characterizing the component condition numbers and strength of interactions between components in the network.

There has been an increased interest in the analysis of the intrinsic characteristics of the growing number of available large-scale kinetic biological network models [30, 14, 47, 90]. The systematic, algorithmic approach described herein demonstrated a general approach to pool identification, thus demonstrating how top-down analyses can be used to identify the hierarchical interactions between components over the span of time scales and assist in the simplification, analysis, and interpretation of network capabilities. This type of an analysis thus helps to link the component interactions to the overall physiological functions and how

such functions can be affected by genetic parameters and how they respond to environmental conditions.

Chapter 5

Math interlude

Just as understanding the four subspaces was important for understanding the biological interpretation of different aspects of networks, the approaches considered here are motivated by a desire to understand the underlying structure and properties leading to the hierarchical decomposition of metabolic networks. Hence, certain approximations are often made, with biological rather than mathematical motivations in the process of identifying and simplifying the structure of networks. Many of the core concepts and principles of network analysis and characterization of the dynamics of biological networks have been presented at this point. A number of real examples have been discussed as well. Topics discussed in this chapter include, specific approaches concerning the decomposition of the Jacobian matrices, 'cleaning' the structure of the modal matrices, and briefly touch up the a key property of the gradient matrix. Since mathematics is an important aspect of the material described in this dissertation, a number of topics that are mathematical but ultimately of interest for the analysis and characterization of metabolic networks are addressed here. In a manner of speaking, in this chapter takes a look at the nuts, bolts, and inner workings of these matrices.

5.1 Decompositions

The understanding of how a complex system produces certain behavior is one of goals of systems analysis. To successfully carry out an analysis of a

particular system, it is important to dissect a complex system into its constituent components in a manner that preserves the relevant relationships. Analysis of the Jacobian matrices is core to the appreciation and characterization of dynamic networks, hence the topics in this chapter are devoted in one way or another to characterize, elucidate, and simplify the Jacobian matrices and the constituent matrices, particularly the gradient matrix. This section will focus on different factorizations of the Jacobian matrices, $\mathbf{J}_x$ (Figure 5.1) and $\mathbf{J}_v$ (Figure 5.2).

The slowest mode is driven by the potassium leak channel and the fastest modes include NADPH charging by glutathione. The fluxes through the Rapoport-Leubering shunt are most active on the approximately 10-20 hour time scales. Although the values in the matrix had to be truncated for visualization purposes, the structural differences between $\mathbf{J}_x$ and $\mathbf{J}_v$ can still be identified, particularly the 'pooling' of the metabolites in $\mathbf{J}_x$, and the lack of any 'pooling' of fluxes in $\mathbf{J}_v$.

Matrix multiplication does not commute, hence $\mathbf{S}\cdot\mathbf{G} \neq \mathbf{G}\cdot\mathbf{S}$, however as we have seen, these two matrices share the same eigenvectors and eigenvalues. Thus they both describe the same dynamics, but in terms of different variables (namely concentration variables or flux variables, respectively). Depending the whether $\mathbf{\Gamma}$ is factored from the left or the right, the interpretation of the constituent matrices may vary (Figure 5.3).

5.1.1 $\mathbf{S}\cdot\kappa\cdot\mathbf{\Gamma}$: Factorization of G from the left

Some approaches for decomposing networks are mathematically convenient, such as similarity transformations and singular value decompositions [91]. Such methods have been very successful for the analysis of a variety of systems. For biological networks however, problems are introduced with such decompositions, because the underlying stoichiometric relationships between metabolites and reactions are often lost. $\mathbf{G}$ can be factored from the left, such that the metabolite Jacobian, $\mathbf{J}_x$ can be expressed as,

$$\mathbf{J}_x = \mathbf{S}\cdot\mathbf{G} = \mathbf{S}\cdot\kappa\cdot\mathbf{\Gamma} \tag{5.1}$$

	G6P	F6P	FDP	DHAP	GAP	DPG13	DPG23	PG3	PG2	PEP	PYR	LAC	NADH	GL6P	GO6P	NADPH	GSH	RU5P	R5P	X5P	S7P	E4P	ADO	AMP	ADP	ATP	PRPP	IMP	INO	HX	R1P	ADE	NAI	KI
1.33962×10^{-8}	0	0	0	0	0	0	0	0	0	0	0	0	0	0	0	-1.	0.16	0	0	0	0	0	0	0	0	0	0	0	0	0	0	0	0	0
2.24584×10^{-7}	0	0	0	0	0	-1.	0	0	0	0	0	0	0	0	0	0	0	0	0	0	0	0	0	0	0	0	0	0	0	0	0	0	0	0
1.3812×10^{-6}	0	0	0	0.04	-1.	-0.06	0	0	0	0	0	0	0	0	0	0	0	0	0	0	0	0	0	0	0	0	0	0	0	0	0	0	0	0
4.78546×10^{-6}	-0.41	1.	0	0	0	0	0	0	0	0	0	0	0	0	0	0	0	0	0	0	0	0	0	0	0	0	0	0	0	0	0	0	0	0
9.27721×10^{-6}	0	0	0	0	0	0.05	0	0.05	-1.	0.39	0	0	0	0	0	0	0	0	0	0	0	0	0	0	0	0	0	0	0	0	0	0	0	0
0.0000245481	0	0	0	0.01	0	0.03	0	-0.02	0	0.01	-0.31	0.01	-1.	0	0	0	0	0	0	0	0	0	0	0	0	0	0	0	0	0	0	0	0	0
0.0000302197	0	0	0	0	0	0	0	0	0	0	0	0	0	0	0	0	0	-1.	0.03	0.31	0	0	0	0	0	0	0	0	0	0	0	0	0	0
0.0000728205	0	0	-0.01	-0.01	0	0.33	0	0.34	-0.55	-1.	-0.02	0	-0.01	0	0	0	0	0	0	0	0	0	0	0	0	0	0	0	0	0	0	0	0	0
0.000205508	0	0	0	0	0	0	0	0	0	0	0	0	0	0	0	0	0	0	0	0	0	0	1.	0	0	0	0	0	0	0	0	0	0	0
0.000345655	0	0	0	0	0	0	0	0	0	0	0	0	0	0	0	0	0	0	0	0	0	0	0.2	0	0	0	0	0	1.	-0.01	0	0	0	0	0
0.000620365	-0.01	-0.01	1.	-0.48	-0.46	0.45	0	0.4	0.46	0.48	-0.65	0.03	0.57	0.01	0	0.01	0	0	0.01	0	-0.01	0.04	-0.16	0	-0.11	0.02	0	0	-0.01	0	-0.01	0	0	0	0
0.000744573	0	0	0	0	0	0	0	0	0	0	0	0	0	-0.07	0	-0.17	-0.09	-0.53	1.	-0.64	0	-0.01	-0.08	0	0	0	0	0	-0.75	0.01	-0.48	0	0	0	0
0.000999516	-0.01	-0.01	0	0	0	0	0	0	0	0	0	0	0	0.69	-0.01	1.	0.5	0	0	0	0	0	0	0	0	0	0	0	0	0	0	0	0	0	0
0.00121876	-0.03	-0.03	1.	-0.1	-0.1	-0.13	0	-0.11	-0.12	-0.12	0.17	-0.01	-0.16	-0.05	0	-0.08	-0.04	0	0	0	0	0.02	-0.02	-0.05	0.03	0	0	0	0	0	0	0	0	0	0
0.00226677	0	0	0	0	0	0	0	0	0	0	0	0	0	0.01	0	0	0	-0.05	-0.01	-0.05	0	0	0.09	0	0	0	0	0	1.	0.02	0.99	0	0	0	0
0.00234305	0	0	0	0	0	0	0	0	0	0	0	0	0	0	0	0	0	0	0	0	0	0	-0.09	0	0	0	0	0	-0.98	-1.	0.01	0	0	0	0
0.00498523	-0.05	-0.05	-0.21	0.1	0.1	-0.21	0	0.35	0.35	0.35	-0.4	0.01	0.41	0.01	0	-0.06	-0.03	-0.03	-0.03	-0.02	0.07	-0.33	-0.38	-1.	0.52	-0.04	0	0	-0.04	0	-0.05	0.04	0	0	0
0.00646139	0.05	0.05	-0.06	-0.02	-0.02	-0.02	0	0	0	0	0	0	0	-0.21	-0.01	0.24	0.12	0.06	0.06	0.06	-0.21	1.	0.02	0	0.01	-0.01	0	0	0.09	0	0.1	0	0	0	0
0.00733185	0	0	0	0	0	0	0	0	0	0	0	0	0	-1.	-0.05	0.95	0.47	0.01	0.01	0.01	0.01	-0.04	0	0	0	0	0	0	0.01	0	0.02	0	0	0	0
0.0207413	0	0	-0.08	-0.04	-0.04	-0.02	0	0	0	0	0.02	0	-0.02	0.59	-0.03	-0.72	-0.36	0.91	0.89	0.91	-0.34	-0.8	0.1	0.02	0.01	-0.01	0	0	0.84	-0.01	1.	-0.02	0	0	0
0.0245323	0	0	0	0	0	0	0	0	0	0	0	0	0	0	0	0	0	0	0	0	0	0	0	0	0	0	-0.01	0	0	0	0	-1.	0	0	0
0.0303075	0.88	0.88	-0.53	-0.17	-0.18	-0.46	0	0.07	0.06	0.06	-0.26	0.02	0.28	0.47	-0.01	0.28	0.14	0.17	0.16	0.17	-0.04	-0.75	1.	0.67	0.2	-0.33	0	0	0.15	0	0.18	0.07	0	0	0
0.0402444	-0.59	-0.59	0.13	0.02	0.02	-0.78	0	-1.	-1.	-1.	-0.9	-0.13	0.77	-0.2	0.08	-0.3	-0.15	0.07	0.07	0.06	0.16	0.62	-0.31	-0.17	-0.06	0.16	0	0	0.06	0	0.07	-0.07	0	0	0
0.0806219	0.8	0.8	0.41	0.21	0.21	-0.61	0.01	-0.37	-0.37	-0.37	-0.19	0.62	0.81	0.16	-0.23	0.51	0.25	-0.28	-0.29	-0.28	-0.85	-1.	0.46	0.34	0.1	-0.13	-0.01	0	-0.24	0	-0.29	0.08	0	0	0
0.274512	-0.36	-0.36	-0.49	-0.25	-0.25	-0.17	0	-0.09	-0.09	-0.09	0.06	-0.03	-0.08	0.06	0.29	-0.34	-0.17	0.35	0.36	0.35	1.	0.74	0.17	0.1	0.02	-0.06	0	0	0.3	0	0.37	0.02	0	0	0
1.52981	-0.74	-0.74	-1.	-0.5	-0.5	-0.44	0.02	-0.19	-0.19	-0.19	0.04	-0.01	-0.05	-0.75	-0.82	-0.02	-0.01	-0.71	-0.71	-0.71	-0.93	-0.66	0.37	0.25	0	-0.26	-0.26	0.1	-0.59	0.01	-0.71	0.08	0	0	0
2.90482	-0.06	-0.06	-0.08	-0.04	-0.04	-0.03	0	-0.01	-0.01	-0.01	0	0	0	-0.06	-0.07	0	0	-0.07	-0.07	-0.07	-0.08	-0.06	0.02	0.01	-0.01	-0.03	-1.	0.02	-0.05	0	-0.07	0.15	0	0	0
21.7782	0.23	0.23	0.31	0.16	0.16	0.2	0.54	0.12	0.12	0.12	0.03	-0.01	-0.04	0.22	0.22	0.01	0	0.22	0.22	0.22	0.27	0.19	0.56	0.74	0.81	0.88	1.	0.26	0.18	0	0.22	-0.04	0.02	0	
14.5319	-0.12	-0.12	-0.16	-0.08	-0.08	-0.08	-0.08	-0.04	-0.04	-0.04	0	0	0	-0.12	-0.12	0	0	-0.12	-0.12	-0.12	-0.15	-0.1	-0.64	-0.81	-0.85	-0.89	-1.	-0.39	-0.1	0	-0.12	0.03	-0.84	0	
17.0043	0.13	0.13	0.18	0.09	0.09	0.09	0.07	0.04	0.04	0.04	0	0	0	0.13	0.13	0	0	0.13	0.13	0.13	0.16	0.11	0.66	0.84	0.88	0.93	1.	0.29	0.11	0	0.13	-0.02	-0.04	0	
174.512	0.01	0.01	0.02	0.01	0.01	0.01	0	0	0	0	0	0	0	0.01	0.01	0	0	0.01	0.01	0.01	0.02	0.01	0.05	0.07	0.07	0.08	0.07	0.01	0.01	0	0.01	0	0.24	1.	

Figure 5.1: Kinetic red cell metabolite modal matrix.

The modal matrix for $\mathbf{J}_x$ is shown. Due to font limitations, only two digits of precision are shown. Entries for metabolites such as PG3, PG2, etc on the 174 hour time scale that appear to be zero actually have non-zero entries, they are very small however. The left most column lists the time scales (hours).

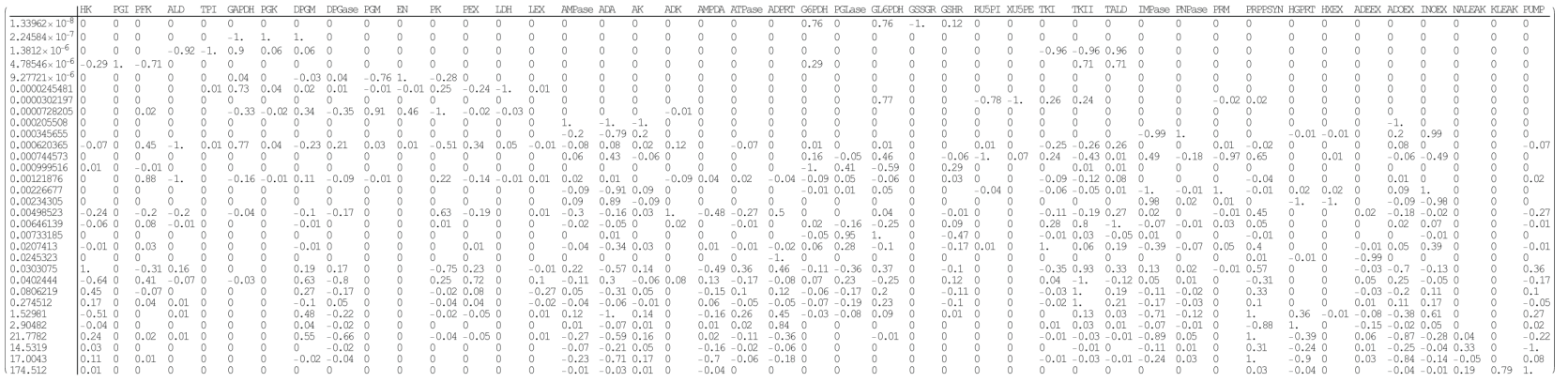

	HK	PGI	PFK	ALD	TPI	GAPDH	PGK	DPGM	DPGase	PGM	EN	PK	PEX	LDH	LEX	AMPase	ADA	AK	ADK	AMPDA	ATPase	ADPRT	G6PDH	PGLase	GL6PDH	GSSGR	GSHR	RU5PI	XU5PE	TKI	TKII	TALD	IMPase	PNPase	PRM	PRPPSYN	HGPRT	HXEX	ADEEX	ADOEX	INOEX	NALEAK	KLEAK	PUMP
1.33962×10^{-8}	0	0	0	0	0	0	0	0	0	0	0	0	0	0	0	0	0	0	0	0	0	0	0.76	0	0.76	-1.	0.12	0	0	0	0	0	0	0	0	0	0	0	0	0	0	0	0	0
2.24584×10^{-7}	0	0	0	0	0	-1.	1.	1.	0	0	0	0	0	0	0	0	0	0	0	0	0	0	0	0	0	0	0	0	0	0	0	0	0	0	0	0	0	0	0	0	0	0	0	0
1.3812×10^{-6}	0	0	0	-0.92	-1.	0.9	0.06	0.06	0	0	0	0	0	0	0	0	0	0	0	0	0	0	0	0	0	0	0	0	0	-0.96	-0.96	0.96	0	0	0	0	0	0	0	0	0	0	0	0
4.78546×10^{-6}	-0.29	1.	-0.71	0	0	0	0	0	0	0	0	0	0	0	0	0	0	0	0	0	0	0	0.29	0	0	0	0	0	0	0	0.71	0.71	0	0	0	0	0	0	0	0	0	0	0	0
9.27721×10^{-6}	0	0	0	0	0	0.04	0	-0.03	0.04	-0.76	1.	-0.28	0	0	0	0	0	0	0	0	0	0	0	0	0	0	0	0	0	0	0	0	0	0	0	0	0	0	0	0	0	0	0	0
0.0000245481	0	0	0	0	0.01	0.73	0.04	0.02	0.01	-0.01	-0.01	0.25	-0.24	-1.	0.01	0	0	0	0	0	0	0	0	0	0	0	0	0	0	0	0	0	0	0	0	0	0	0	0	0	0	0	0	0
0.0000302197	0	0	0	0	0	0	0	0	0	0	0	0	0	0	0	0	0	0	0	0	0	0	0	0	0.77	0	0	-0.78	-1.	0.26	0.24	0	0	0	0	-0.02	0.02	0	0	0	0	0	0	0	0
0.0000728205	0	0	0.02	0	0	-0.33	-0.02	0.34	-0.35	0.91	0.46	-1.	-0.02	-0.03	0	0	0	0	-0.01	0	0	0	0	0	0	0	0	0	0	0	0	0	0	0	0	0	0	0	0	0	0	0	0	0
0.000205508	0	0	0	0	0	0	0	0	0	0	0	0	0	0	0	1.	-1.	-1.	0	0	0	0	0	0	0	0	0	0	0	0	0	0	0	0	0	0	0	0	-1.	0	0	0	0	0
0.000345655	0	0	0	0	0	0	0	0	0	0	0	0	0	0	0	-0.2	-0.79	0.2	0	0	0	0	0	0	0	0	0	0	0	0	0	0	-0.99	1.	0	0	-0.01	-0.01	0	0.2	0.99	0	0	0
0.000620365	-0.07	0	0.45	-1.	0.01	0.77	0.04	-0.23	0.21	0.03	0.01	-0.51	0.34	0.05	-0.01	-0.08	0.08	0.02	0.12	0	-0.07	0	0.01	0	0.01	0	0	0.01	0	-0.25	-0.26	0.26	0	0	0.01	-0.02	0	0	0	0.08	0	0	0	-0.07
0.000744573	0	0	0	0	0	0	0	0	0	0	0	0	0	0	0	0.06	0.43	-0.06	0	0	0	0	0.16	-0.05	0.46	0	-0.06	-1.	0.07	0.24	-0.43	0.01	0.49	-0.18	-0.97	0.65	0	0.01	0	-0.06	-0.49	0	0	0
0.000999516	0.01	0	-0.01	0	0	0	0	0	0	0	0	0	0	0	0	0	0	0	0	0	0	0	-1.	0.41	-0.59	0	0.29	0	0	0	0.01	0.01	0	0	0	0	0	0	0	0	0	0	0	0
0.00121876	0	0	0.88	-1.	0	-0.16	-0.01	0.11	-0.09	-0.01	0	0.22	-0.14	-0.01	0.01	0.02	0.01	0	-0.09	0.04	0.02	-0.04	-0.09	0.05	-0.06	0	0.03	0	0	-0.09	-0.12	0.08	0	0	0	-0.04	0	0	0	0.01	0	0	0	0.02
0.00226677	0	0	0	0	0	0	0	0	0	0	0	0	0	0	0	-0.09	-0.91	0.09	0	0	0	0	-0.01	0.01	0.05	0	0	-0.04	0	-0.06	-0.05	0.01	-1.	-0.01	1.	-0.01	0.02	0.02	0	0.09	1.	0	0	0
0.00234305	0	0	0	0	0	0	0	0	0	0	0	0	0	0	0	0.09	0.89	-0.09	0	0	0	0	0	0	0	0	0	0	0	0	0	0	0.98	0.02	0.01	0	-1.	-1.	0	-0.09	-0.98	0	0	0
0.00498523	-0.24	0	-0.2	-0.2	0	-0.04	0	-0.1	-0.17	0	0	0.63	-0.19	0	0.01	-0.3	-0.16	0.03	1.	-0.48	-0.27	0.5	0	0	0.04	0	-0.01	0	0	-0.11	-0.19	0.27	0.02	0	-0.01	0.45	0	0	0.02	-0.18	-0.02	0	0	-0.27
0.00646139	-0.06	0	0.08	-0.01	0	0	0	-0.01	0	0	0	0.01	0	0	0	-0.02	-0.05	0	0.02	0	-0.01	0	0.02	-0.16	-0.25	0	0.09	0	0	0.28	0.8	-1.	-0.07	-0.01	0.03	0.05	0	0	0	0.02	0.07	0	0	-0.01
0.00733185	0	0	0	0	0	0	0	0	0	0	0	0	0	0	0	0	0.01	0	0	0	0	0	-0.05	0.95	1.	0	-0.47	0	0	-0.01	0.03	-0.05	0.01	0	0	-0.01	0	0	0	0	-0.01	0	0	0
0.0207413	-0.01	0	0.03	0	0	0	0	-0.01	0	0	0	0	0.01	0	0	-0.04	-0.34	0.03	0	0.01	-0.01	-0.02	0.06	0.28	-0.1	0	-0.17	0.01	0	1.	0.06	0.19	-0.39	-0.07	0.05	0.4	0	0	-0.01	0.05	0.39	0	0	-0.01
0.0245323	0	0	0	0	0	0	0	0	0	0	0	0	0	0	0	0	0	0	0	0	0	-1.	0	0	0	0	0	0	0	0	0	0	0	0	0	0.01	-0.01	0	-0.99	0	0	0	0	0
0.0303075	1.	0	-0.31	0.16	0	0	0	0.19	0.17	0	0	-0.75	0.23	0	-0.01	0.22	-0.57	0.14	0	-0.49	0.36	0.46	-0.11	-0.36	0.37	0	-0.1	0	0	-0.35	0.93	0.33	0.13	0.02	-0.01	0.57	0	0	-0.03	-0.7	-0.13	0	0	0.36
0.0402444	-0.64	0	0.41	-0.07	0	-0.03	0	0.63	-0.8	0	0	0.25	0.72	0	0.1	-0.11	0.3	-0.06	0.08	0.13	-0.17	-0.08	0.07	0.23	-0.25	0	0.12	0	0	0.04	-1.	-0.12	0.05	0.01	0	-0.31	0	0	0.05	0.25	-0.05	0	0	-0.17
0.0806219	0.45	0	-0.07	0	0	0	0	0.27	-0.17	0	0	-0.02	0.08	0	-0.27	0.05	-0.31	0.05	0	-0.15	0.1	0.12	-0.06	-0.17	0.2	0	-0.11	0	0	-0.03	1.	0.19	-0.11	-0.02	0	0.33	0	0	-0.03	-0.2	0.11	0	0	0.1
0.274512	0.17	0	0.04	0.01	0	0	0	-0.1	0.05	0	0	-0.04	0.04	0	-0.02	-0.04	-0.06	-0.01	0	0.06	-0.05	-0.05	-0.07	-0.19	0.23	0	-0.1	0	0	-0.02	1.	0.21	-0.17	-0.03	0	0.1	0	0	0.01	0.11	0.17	0	0	-0.05
1.52981	-0.51	0	0	0.01	0	0	0	0.48	-0.22	0	0	-0.02	-0.05	0	0.01	0.12	-1.	0.14	0	-0.16	0.26	0.45	-0.03	-0.08	0.09	0	0.01	0	0	0	0.13	0.03	-0.71	-0.12	0	1.	0.36	-0.01	-0.08	-0.38	0.61	0	0	0.27
2.90482	-0.04	0	0	0	0	0	0	0.04	-0.02	0	0	0	0	0	0	0.01	-0.07	0.01	0	0.01	0.02	0.84	0	0	0	0	0	0	0	0.01	0.03	0.01	-0.07	-0.01	0	-0.88	1.	0	-0.15	-0.02	0.05	0	0	0.02
21.7782	0.24	0	0.02	0.01	0	0	0	0.55	-0.66	0	0	-0.04	-0.05	0	0.01	-0.27	-0.59	0.16	0	0.02	-0.11	-0.36	0	0	-0.01	0	0	0	0	-0.01	-0.03	-0.01	-0.89	0.05	0	1.	-0.39	0	0.06	-0.87	-0.28	0.04	0	-0.22
14.5319	0.03	0	0	0	0	0	0	0	-0.02	0	0	0	0	0	0	-0.07	-0.21	0.05	0	-0.16	-0.02	-0.06	0	0	0	0	0	0	0	0	-0.01	0	-0.11	0.01	0	0.31	-0.24	0	0.01	-0.25	-0.04	0.33	0	-1.	
17.0043	0.11	0	0.01	0	0	0	0	-0.02	-0.04	0	0	0	0	0	0	-0.23	-0.71	0.17	0	-0.7	-0.06	-0.18	0	0	0	0	0	0	0	-0.01	-0.03	-0.01	-0.24	0.03	0	1.	-0.9	0	0.03	-0.84	-0.14	-0.05	0	0.08	
174.512	0.01	0	0	0	0	0	0	0	0	0	0	0	0	0	0	-0.01	-0.03	0.01	0	-0.04	0	0	0	0	0	0	0	0	0	0	0	0	0	0	0	0.03	-0.04	0	0	-0.04	-0.01	0.19	0.79	1.	

Figure 5.2: Kinetic red cell metabolite modal matrix($\mathbf{J}_v$).

Decomposition of the flux Jacobian for the same network in Figure 5.1. The left most column lists the time scales (hours).

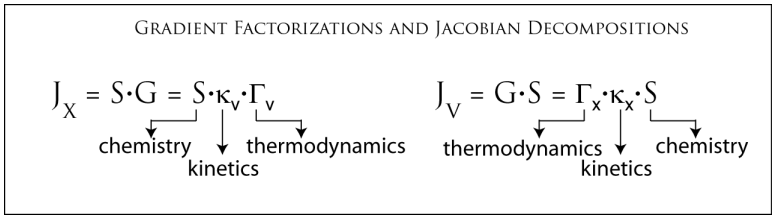

Figure 5.3: Gradient and Jacobian factorizations.

Non-orthogonal decompositions for the concentration and flux Jacobians. $\kappa_{\mathbf{x}}$ and $\kappa_{\mathbf{v}}$ are diagonal matrices resulting from the factorization of $\mathbf{G}$.

in which κ is a diagonal matrix containing the norms of the rows of $\mathbf{G}$ and $\mathbf{\Gamma}$ is a matrix that is mathematically similar to $\mathbf{S}^T$ (when not otherwise specified κ refers to the nxn κ matrix). Although this decomposition looks similar to mathematically driven decompositions such as the singular value decomposition and the similarity transform, it lacks the often convenient features such as invertibility ($\mathbf{S}$, and $\mathbf{\Gamma}$ are singular matrices) and orthonormality. The trade-off for the properties underlying SVD and similarity transforms is balanced by the fact that there is biological and thermodynamic significance to the factorization in Equation 5.1. The physical interpretation of κ are the rate constants corresponding to the reactions and the $\mathbf{\Gamma}$ specifies the directions of the reactions. If the approximate time scales of each reaction are known, then the entries in can be filled in. Similarly if the thermodynamics of the reactions can be approximated (e.g. irreversible versus reversible under a specified set of physiological conditions), then the values in $\mathbf{\Gamma}$ can be approximated. Note that due to the similarity to the transpose of the stoichiometric matrix, the locations of the non-zero entries in $\mathbf{\Gamma}$ are known. Such approximations would yield rough estimates of the dynamics of the network, but could be useful in establishing fine-grained approximation to the dynamic hierarchy of a system. In order to understand the effects and influences of κ on the Jacobian matrices, one can reconstruct a gross approximation to the gradient matrix as, $-1 \cdot \kappa \cdot \mathbf{S}^T$, such that $\mathbf{J}_x \approx -1 \cdot \mathbf{S} \cdot \kappa \cdot \mathbf{S}^T$. Note that this equation implicitly assumes that all of the reactions in the network are reversible. The resulting concentration modal matrix is depicted in Figure 5.4 The condition number of the approximated modal matrix is about the same order of magnitude as the real modal matrix, although the

	G6P	F6P	FDP	DHAP	GAP	DPG13	DPG23	PG3	PG2	PEP	PYR	LAC	NADH	GL6P	GO6P	NADPH	GSH	RU5P	R5P	X5P	S7P	E4P	ADO	AMP	ADP	ATP	PRPP	IMP	INO	HX	R1P	ADE	NAI	KI
3.04038×10^{-9}	0	0	0	0	0	0	0	0	0	0	0	0	0	0	0	0.5	-1.	0	0	0	0	0	0	0	0	0	0	0	0	0	0	0	0	0
5.89335×10^{-8}	0	0	0	0	-0.02	1.	0	-0.99	0	0	0	0	0.01	0	0	0	0	0	0	0	0	0	0	0	0.99	-0.99	0	0	0	0	0	0	0	0
6.21095×10^{-7}	0	0	0	0.8	-1.	0.15	0	0.06	0	0	0.01	-0.01	0.21	0	0	0	0	0	0	0	0	0	0	0	-0.06	0.06	0	0	0	0	0	0	0	0
2.00362×10^{-6}	0	0	0	0.7	0.21	-0.68	0	-0.25	0.03	0	-0.09	0.09	-1.	0	0	0	0	0	0	0	0	0	0	0	0.23	-0.23	0	0	0	0	0	0	0	0
2.38536×10^{-6}	-1.	0.99	0	0	0	0	0	0	0	0	0	0	0	0.01	0	0	0	0	0	0	0	0	0	0	0	0	0	0	0	0	0	0	0	0
5.26043×10^{-6}	0	0	0	0.02	0.01	0.04	0	0.18	-1.	0.76	-0.02	0.02	-0.05	0	0	0	0	0	0	0	0	0	0	0	0.07	-0.07	0	0	0	0	0	0	0	0
0.0000104159	0	0	0.01	-0.3	-0.26	0.42	-0.01	0.18	0.02	-0.08	-1.	1.	-0.47	0	0	0	0	0	0	0	0	0	0.01	-0.01	-0.12	0.12	0	0	0	0	0	0	0	0
0.0000154272	0	0	0	0	0	0	0	0	0	0	0	0	0	0.01	-0.01	0	-1.	0.05	0.94	0	0	0	0	0	0	0	0	0	0	0	0	0	0	0
0.0000233946	0	0	-0.01	0.1	0.1	0.15	-0.01	1.	-0.43	-0.89	0.09	-0.09	-0.09	0	0	0	0	0	0	0	0	0	-0.1	0.09	0.43	-0.42	0	0	0	0	0	0	0	0
0.0000912494	0	0	-0.16	0.3	0.3	0.48	-0.12	-0.12	-0.27	-0.3	0.13	-0.1	-0.2	0	0	0	0	0	-0.01	0	0.01	-0.01	1.	-0.92	-0.3	0.3	0	0	-0.07	0.03	0.03	0	0	0
0.000126877	0	0	0.02	-0.03	-0.03	-0.04	0.02	0.01	0.02	0.02	-0.01	0	0.01	0	0	0	0	0.02	-0.12	0.03	0	0	-0.01	0.06	0.02	-0.02	0	0	-1.	0.94	0.95	0	0	0
0.000166844	0.5	0.51	-0.01	-0.01	-0.01	0	0	0	0	0	0	0	-0.01	-1.	0.15	-0.88	-0.44	-0.12	0.14	-0.14	-0.02	0.02	0	0	0	0	0	0	-0.02	0.01	0	0	0	0
0.000183506	0	0	-1.	0.73	0.73	0.39	-0.26	0.11	0.15	0.16	-0.19	0.19	0.35	-0.01	0	-0.01	0	0	-0.05	0.01	0.05	-0.04	-0.38	0.34	-0.15	0.13	0	0	0	0.03	0.03	0	0	0
0.000207498	0.07	0.07	0.02	-0.01	-0.01	-0.01	0	0	0	0	0.01	0	-0.01	-0.14	-0.06	-0.06	-0.03	0.43	-1.	0.51	0.01	0.01	0	-0.01	0	0	0	0	0.09	-0.08	0.02	0	0	0
0.000350954	0	0	0.31	-0.05	-0.05	0.31	-1.	0.03	0.04	0.05	0.21	-0.16	-0.36	0	0	0	0	0	0	0	-0.01	0.01	-0.2	0.17	-0.15	0.12	0	0	0.02	0.02	0.02	0	0	0
0.000763604	0.27	0.28	-0.09	-0.03	-0.03	-0.01	-0.02	0	0	0	0.01	-0.01	-0.02	-0.36	-1.	0.41	0.21	0.43	0.5	0.45	-0.19	0.11	0.04	0.04	0	-0.01	0	0	-0.17	0.07	-0.21	0	0	0
0.00105661	-0.11	-0.11	0.03	0.03	0.03	-0.3	-0.52	0.53	0.54	0.54	-0.5	-0.18	0.33	0.01	0.19	-0.1	-0.05	0.06	-0.03	0.06	0.07	-0.06	0.91	0.16	0.51	-0.32	0	0	-1.	-0.55	-0.57	0	0	0
0.0013154	0.01	0.01	-0.09	-0.05	-0.05	0.26	0.4	-0.49	-0.5	-0.49	0.57	0.26	-0.31	0.14	0.28	-0.08	-0.04	0.07	-0.02	0.07	-0.09	0.08	0.15	1.	-0.61	0.14	-0.01	0	-0.95	-0.49	-0.53	-0.01	0	0
0.00160359	0.25	0.25	-0.39	-0.15	-0.15	-0.08	-0.11	0.04	0.04	0.04	-0.01	-0.08	-0.07	0.35	0.35	0	0	0.03	-0.01	0.02	-1.	0.86	0.02	-0.1	0.1	-0.02	0	0	0.05	0.01	0.04	0	0	0
0.00199341	-0.18	-0.18	0.01	0.01	0.01	0.01	0.01	0	0	0	0	0.01	0	0.04	0.5	-0.19	-0.09	0.4	0.23	0.4	0.01	-0.1	-0.2	-0.21	0.03	0.04	0	0	-0.01	1.	-0.98	0	0	0
0.00264924	-0.03	-0.03	-0.02	-0.01	-0.01	0.01	0.01	-0.04	-0.04	-0.04	0.1	0.08	-0.02	-0.01	0.07	-0.02	-0.01	0.07	0.05	0.07	0.02	-0.04	-1.	-1.	0.21	0.26	0.01	0	-0.75	-0.65	-0.08	0.02	0	0
0.00501246	0.63	0.63	0.03	0	0	0	0	0	0	0	-0.01	-0.01	0	0.98	-1.	-0.37	-0.19	-0.69	-0.69	-0.69	0.47	0.25	-0.14	-0.14	0.08	0.08	0.01	0	-0.25	0.49	-0.79	0.01	0	0
0.00768133	0.04	0.04	0.29	0.13	0.13	0.24	0.26	-0.05	-0.05	-0.06	-0.89	-1.	-0.11	0.21	-0.04	-0.18	-0.09	0.1	0.09	0.1	-0.14	-0.05	-0.26	-0.01	-0.74	-0.45	0	0	-0.1	-0.11	0.03	0	0	0
0.00800378	-0.13	-0.13	-0.14	-0.06	-0.06	-0.07	-0.07	0.01	0.01	0.01	0.2	0.2	0	0.85	-0.43	-1.	-0.5	0.41	0.38	0.41	-0.35	-0.63	0.12	0.05	0.14	0.07	-0.01	0	0.14	-0.19	0.35	0	0	0
0.0121112	0.58	0.58	-0.59	-0.31	-0.31	-0.06	-0.06	-0.04	-0.04	-0.04	-0.09	-0.34	-0.25	0.18	0.44	0.42	0.21	0.01	0	0.01	0.04	-1.	0.04	0.02	0.16	0.14	0	0	0.02	0.01	0.01	0	0	0
0.0212872	-0.17	-0.17	-0.73	-0.37	-0.37	-0.07	-0.07	-0.07	-0.07	-0.07	-0.1	-0.41	-0.3	0.06	-0.01	-0.22	-0.11	0.2	0.21	0.2	1.	0.68	0.04	0.05	0.11	0.11	-0.03	0	0.06	-0.08	0.15	-0.08	0	0
0.0236261	0	0	0.03	0.02	0.02	0.01	0.01	0	0	0	-0.01	0	0.01	0	0	0.01	0	-0.01	-0.01	-0.01	-0.03	-0.01	-0.01	0	0.02	0.03	-0.19	0	0	0	-0.01	-1.	0	0
0.0784667	0.33	0.33	-0.01	0	0	0.43	0.43	0.71	0.71	0.71	0.85	0.42	-0.43	0.26	0.26	0.08	0.04	0.18	0.17	0.18	0.44	0.12	-0.01	-0.3	-0.72	-1.	0.29	-0.01	0.03	-0.07	0.11	-0.14	0	0
0.107107	-0.85	-0.85	-1.	-0.5	-0.5	0.13	0.13	0.22	0.22	0.22	0.26	-0.37	-0.63	-0.7	-0.7	-0.16	-0.08	-0.54	-0.52	-0.54	-0.8	-0.52	-0.06	-0.15	-0.27	-0.36	0.54	-0.06	-0.12	0.2	-0.35	-0.14	0	0
0.148238	-0.05	-0.05	-0.04	-0.02	-0.02	0.12	0.12	0.11	0.11	0.11	0.09	-0.06	-0.14	-0.04	-0.04	-0.01	0	-0.03	-0.03	-0.03	-0.06	-0.03	-0.01	0	0.01	0.02	-1.	0.11	-0.01	0.01	-0.02	0.19	0	0
0.870644	0	0	-0.35	-0.17	-0.17	-0.7	-0.7	-0.38	-0.38	-0.38	-0.06	0.47	0.53	-0.02	-0.02	0.02	0.01	-0.03	-0.03	-0.03	0.09	-0.09	-0.01	-0.33	-0.67	-1.	-0.33	0.62	-0.01	0.01	-0.02	0	-0.01	0.01
1.49295	0	0	0.05	0.03	0.03	0.11	0.11	0.05	0.05	0.05	0	-0.07	-0.08	0	0	0	0	0	0	0	-0.01	0.01	0	0.05	0.11	0.16	0.17	1.	0	0	0	-0.02	0	0
4.61809	0	0	0	0	0	0	0	0	0	0	0	0	0	0	0	0	0	0	0	0	0	0	0	0	0	0.01	0	0	0	0	0	0	-1.	0.54
61.516	0	0	0	0	0	0	0	0	0	0	0	0	0	0	0	0	0	0	0	0	0	0	0	0	0	0	0	0	0	0	0	0	0.54	1.

Figure 5.4: Modal matrix approximation for kinetic red cell.

The modal matrix for the kinetic red blood cell network constructed using only $\mathbf{S}$ and κ. As with Figure 5.1, the entries had to be truncated after the second decimal place, on there are small, but non-zero entries in the slowest modes.

slowest time scale is about one-third that of the full kinetic model. The most noticeable difference between the two is that the last two modes of the approximated modal matrix is really only driven by sodium and potassium. Qualitatively this is similar to the real modal matrix, although quantitatively, the 'weightings' of the metabolites are very small. There are a number of striking similarities between the two matrices, including the composition of the 1st and 2nd modes. Additionally the equilibration between G6P and F6P is noted on the 5th mode. Furthermore the 1.5 hour time scale, the slowest 'metabolite driven' mode is largely driven by the 1,3DPG and 2,3DPG, consistent with physiological expectations. Overall the structure is similar as well, with more individualized interactions on the faster time scales (metabolites achieving equilibrium with one another) and aggregate pools forming on the slower time scales. These qualitatively important features are the result of the preservation of the underlying stoichiometric interactions between components and the time scale separation provided by the κ matrix. Something that is noticeably lacking in the modal matrix is the relative ratio between the elements within each mode. For example, the ratio between G6P and F6P in the 5th mode is approximately one, whereas in reality is should be approximately 0.41. The reason for this will become clear in the following section. Nevertheless, given the relevant physical interpretation of the decomposition and the ability to reproduce important qualitative features of the matrix, this approximation for the modal structure may be useful when detailed knowledge about rate constants, fluxes, and concentrations are lacking.

5.1.2 Factorization of G from the right

There are two approaches for factorization of **G** from the right and the difference lies in the interpretation of the resulting matrices. Following analogy to 5.1.1, **G** can be factored from the right hand side, such that,

$$\mathbf{J}_v = \mathbf{G} \cdot \mathbf{S} = \mathbf{\Gamma}_\mathbf{x} \cdot \kappa_\mathbf{x} \cdot \mathbf{S} \tag{5.2}$$

$\kappa_\mathbf{x}$ is an mxm diagonal matrix and $\mathbf{\Gamma}_\mathbf{x}$ is an nxm matrix.

Alternatively, one can choose to factor $\mathbf{G}$ from the right, so that the columns are normalized and flux Jacobian, $\mathbf{J}_v$ becomes,

$$\mathbf{J}_v = \mathbf{G} \cdot \mathbf{S} = \mathbf{\Omega} \cdot \mu \cdot \mathbf{S} \tag{5.3}$$

In symmetrical analogy with Equation 5.1, this is a product of three matrices with the middle being diagonal. $\mathbf{\Omega}$ is similar to $\mathbf{\Gamma}$ and to $\mathbf{S}^T$. The physical interpretation of the entries μ is $1/\mathbf{x}$, that is the reciprocal concentration vector corresponding to the metabolites in the columns of $\mathbf{G}$. In contrast to $\mathbf{\Gamma}$ which was a matrix describing the thermodynamic driving forces, $\mathbf{\Omega}$ is a matrix describing the kinetic driving forces for each of the reactions. Following suit to the previous section if one were to build a rough approximation of the kinetic structure of a network, but lacked information about the turnover rates of the enzymes or their approximate time scales, Equation 5.3 presents an alternative. Approximating the structure of the gradient matrix by, $1 \cdot \mathbf{\Omega} \cdot \mu$, and carrying out modal decomposition on $\mathbf{J}_v$, yields Figure 5.5. The timescale separation is almost identical to the full kinetic network. Many encouraging similarities are observed, such as the slowest modes driven by the potassium leak channel and 2,3DPG moving primarily along the 10-20 hour time scales. Furthermore, the ratio between G6P and F6P (reflected in the 5th mode as the interaction between HK, PGI, and PFK) is closer to the physiological values of -0.29, 1, and -0.71, respectively (which correspond to the -0.41 to 1 ratio between G6P and F6P). Taking the approximation one step further and approximating μ as $1/\mathbf{x}$, yields Figure 5.6 after modal decomposition. Although the time scale separation is still fairly good and much of the structure of the modal matrix is preserved (the 1st mode and the last three modes), other information is lost, such as the equilibrium ratio between the hexose phosphates. If the approximate pool sizes of the different metabolites in the network are known, then the elements in μ can be estimated.

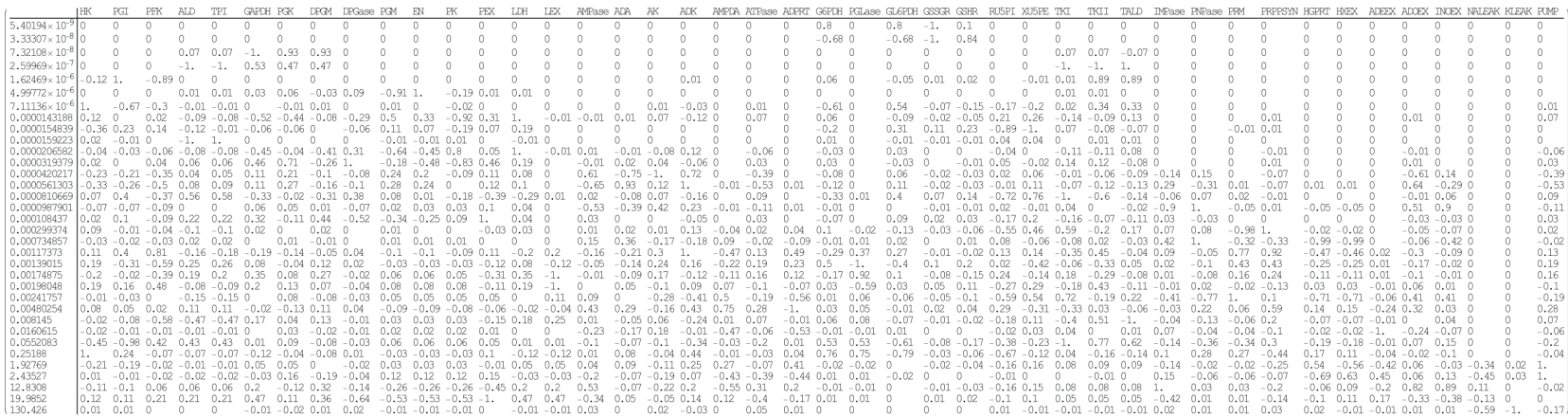

	HK	PGI	PFK	ALD	TPI	GAPDH	PGK	DPGM	DPGase	PGM	EN	PK	PEX	LDH	LEX	AMPase	ADA	AK	ADK	AMPDA	ATPase	ADPRT	G6PDH	PGLase	GL6PDH	GSSGR	GSHR	RU5PI	XU5PE	TKI	TKII	TALD	IMPase	PNPase	PRM	PRPPSYN	HGPRT	HXEX	ADSEX	ADCEX	INOEX	NALEAK	KLEAK	PUMP
5.40194×10^{-9}	0	0	0	0	0	0	0	0	0	0	0	0	0	0	0	0	0	0	0	0	0	0	0.8	0	0.8	-1.	0.1	0	0	0	0	0	0	0	0	0	0	0	0	0	0	0	0
3.33307×10^{-8}	0	0	0	0	0	0	0	0	0	0	0	0	0	0	0	0	0	0	0	0	0	0	-0.68	0	-0.68	-1.	0.84	0	0	0	0	0	0	0	0	0	0	0	0	0	0	0	0
7.32108×10^{-8}	0	0	0	0.07	0.07	-1.	0.93	0.93	0	0	0	0	0	0	0	0	0	0	0	0	0	0	0	0	0	0	0	0	0	0.07	0.07	-0.07	0	0	0	0	0	0	0	0	0	0	0
2.59969×10^{-7}	0	0	0	-1.	-1.	0.53	0.47	0.47	0	0	0	0	0	0	0	0	0	0	0	0	0	0	0	0	0	0	0	0	0	-1.	-1.	1.	0	0	0	0	0	0	0	0	0	0	0
1.62469×10^{-6}	-0.12	1.	-0.89	0	0	0	0	0	0	0	0	0	0	0	0	0	0	0	0.01	0	0	0	0.06	0	-0.05	0.01	0.02	0	-0.01	0.01	0.89	0.89	0	0	0	0	0	0	0	0	0	0	0
4.99772×10^{-6}	0	0	0	0.01	0.01	0.03	0.06	-0.03	0.09	-0.91	1.	-0.19	0.01	0.01	0	0	0	0	0	0	0	0	0	0	0	0	0	0	0.01	0.01	0	0	0	0	0	0	0	0	0	0	0	0	0
7.11136×10^{-6}	1.	-0.67	-0.3	-0.01	-0.01	0	-0.01	0.01	0	0.01	0	-0.02	0	0	0	0	0	0.01	-0.03	0	0.01	0	-0.61	0	0.54	-0.07	-0.15	-0.17	-0.2	0.02	0.34	0.33	0	0	0	0	0	0	0	0	0	0	0	0.01
0.0000143188	0.12	0	0.02	-0.09	-0.08	-0.52	-0.44	-0.08	-0.29	0.5	0.33	-0.92	0.31	1.	-0.01	-0.01	0.01	0.07	-0.12	0	0.07	0	0.06	0	-0.09	-0.02	-0.05	0.21	0.26	-0.14	-0.09	0.13	0	0	0	0.01	0	0	0	0.01	0	0	0	0.07
0.0000154839	-0.36	0.23	0.14	-0.12	-0.01	-0.06	-0.06	0	-0.06	0.11	0.07	-0.19	0.07	0.19	0	0	0	0	0	0	0	0	-0.2	0	0.31	0.11	0.23	-0.89	-1.	0.07	-0.08	-0.07	0	0	-0.01	0.01	0	0	0	0	0	0	0	0
0.0000159223	0.02	-0.01	0	-1.	1.	0	0	0	0	-0.01	-0.01	0.01	0	-0.01	0	0	0	0	0	0	0	0	0.01	0	-0.01	-0.01	-0.01	0.04	0.04	0	0.01	0.01	0	0	0	0	0	0	0	0	0	0	0
0.0000206582	-0.04	-0.03	-0.06	-0.08	-0.08	-0.45	-0.04	-0.41	0.31	-0.64	-0.45	0.8	0.05	1.	-0.01	0.01	-0.01	-0.08	0.12	0	-0.06	0	-0.03	0	0.03	0	0	-0.04	0	-0.11	-0.11	0.08	0	0	0	-0.01	0	0	0	-0.01	0	0	0	-0.06
0.0000319379	0.02	0	0.04	0.06	0.06	0.46	0.71	-0.26	1.	-0.18	-0.48	-0.83	0.46	0.19	0	-0.01	0.02	0.04	-0.06	0	0.03	0	0.03	0	-0.03	0	-0.01	0.05	-0.02	0.14	0.12	-0.08	0	0	0	0.01	0	0	0	0.01	0	0	0	0.03
0.0000420217	-0.23	-0.21	-0.35	0.04	0.05	0.11	0.21	-0.1	-0.08	0.24	0.2	-0.09	0.11	0.08	0	0.61	-0.75	-1.	0.72	0	-0.39	0	-0.08	0	0.06	-0.02	-0.03	0.02	0.06	-0.01	-0.06	-0.09	-0.14	0.15	0	-0.07	0	0	0	-0.61	0.14	0	0	-0.39
0.0000561303	-0.33	-0.26	-0.5	0.08	0.09	0.11	0.27	-0.16	-0.1	0.28	0.24	0	0.12	0.1	0	-0.65	0.93	0.12	1.	-0.01	-0.53	0.01	-0.12	0	0.11	-0.02	-0.03	-0.01	0.11	-0.07	-0.12	-0.13	0.29	-0.31	0.01	-0.07	0.01	0.01	0	0.64	-0.29	0	0	-0.53
0.0000810669	0.07	0.4	-0.37	0.56	0.58	-0.33	-0.02	-0.31	0.38	0.08	0.01	-0.18	-0.39	-0.29	0.01	0.02	-0.08	0.07	-0.16	0	0.09	0	-0.33	0.01	0.4	0.07	0.14	-0.72	0.76	-1.	-0.6	-0.14	-0.06	0.07	0.02	-0.01	0	0	0	-0.01	0.06	0	0	0.09
0.0000987901	-0.07	-0.07	-0.09	0	0	0.06	0.05	0.01	-0.07	0.02	0.03	0.03	0.1	0.04	0	-0.53	-0.39	0.42	0.23	-0.01	-0.11	0.01	-0.01	0	0	-0.01	-0.01	0.02	-0.01	0.04	0	-0.02	-0.9	1.	-0.05	0.01	-0.05	-0.05	0	0.51	0.9	0	0	-0.11
0.000108437	0.02	0.1	-0.09	0.22	0.22	0.32	-0.11	0.44	-0.52	-0.34	-0.25	0.09	1.	0.04	0	0.03	0	0	-0.05	0	0.03	0	-0.07	0	0.09	0.02	0.03	-0.17	0.2	-0.16	-0.07	-0.11	0.03	-0.03	0	0	0	0	0	-0.03	-0.03	0	0	0.03
0.000299374	0.09	-0.01	-0.04	-0.1	-0.1	0.02	0	0.02	0	0.01	0	0	-0.03	0.03	0	0.01	0.02	0.01	0.13	-0.04	0.02	0.04	0.1	-0.02	-0.13	-0.03	-0.06	-0.55	0.46	0.59	-0.2	0.17	0.07	0.08	-0.98	1.	-0.02	-0.02	0	-0.05	-0.07	0	0	0.02
0.000734857	-0.03	-0.02	-0.03	0.02	0.02	0	0.01	-0.01	0	0.01	0.01	0.01	0	0	0	0.15	0.36	-0.17	-0.18	0.09	-0.02	-0.09	-0.01	0.01	0.02	0	0.01	0.08	-0.06	-0.08	0.02	-0.03	0.42	1.	-0.32	-0.33	-0.99	-0.99	0	-0.06	-0.42	0	0	-0.02
0.00117373	0.11	0.4	0.81	-0.16	-0.18	-0.19	-0.14	-0.05	0.04	-0.1	-0.1	-0.09	0.11	-0.2	0.2	-0.16	-0.21	0.3	1.	-0.47	0.13	0.49	-0.29	0.37	0.27	-0.01	-0.02	0.13	0.14	-0.35	0.45	-0.04	0.09	-0.05	0.77	0.92	-0.47	-0.46	0.02	-0.3	-0.09	0	0	0.13
0.00139015	0.19	-0.31	-0.59	0.25	0.26	0.08	-0.04	0.12	0.02	-0.03	-0.03	-0.03	-0.12	0.08	-0.12	-0.05	-0.14	0.24	0.16	-0.22	0.19	0.23	0.5	-1.	-0.4	0.1	0.2	0.02	-0.42	-0.06	-0.33	0.05	0.02	-0.1	0.43	0.43	-0.25	-0.25	0.01	-0.17	-0.02	0	0	0.19
0.00174875	-0.2	-0.02	-0.39	0.19	0.2	0.35	0.08	0.27	-0.02	0.06	0.06	0.05	-0.31	0.35	-1.	-0.01	-0.09	0.17	-0.12	-0.11	0.16	0.12	-0.17	0.92	0.1	-0.08	-0.15	0.24	-0.14	0.18	-0.29	-0.08	0.01	-0.08	0.16	0.24	-0.11	-0.11	0.01	-0.1	-0.01	0	0	0.16
0.00198048	0.19	0.16	0.48	-0.08	-0.09	0.2	0.13	0.07	-0.04	0.08	0.08	0.08	-0.11	0.19	-1.	0	0.05	-0.1	0.09	0.07	-0.1	-0.07	0.03	-0.59	0.03	0.05	0.11	-0.27	0.29	-0.18	0.43	-0.11	-0.01	0.02	-0.02	-0.13	0.03	0.03	-0.01	0.06	0.01	0	0	-0.1
0.00241757	-0.01	-0.03	0	-0.15	-0.15	0	0.08	-0.08	-0.03	0.05	0.05	0.05	0.05	0	0.11	0.09	0	-0.28	-0.41	0.5	-0.19	-0.56	0.01	0.06	-0.06	-0.05	-0.1	-0.59	0.54	0.72	-0.19	0.22	-0.41	-0.77	1.	0.1	-0.71	-0.71	-0.06	0.41	0.41	0	0	-0.19
0.00480254	0.08	0.05	0.02	0.11	0.11	-0.02	-0.13	0.11	0.04	-0.09	-0.09	-0.08	-0.06	-0.02	-0.04	0.43	0.29	-0.16	0.43	0.75	0.28	-1.	0.03	0.05	-0.01	0.02	0.04	0.29	-0.31	-0.33	0.03	-0.06	-0.03	0.22	0.06	0.59	0.14	0.15	-0.24	0.32	0.03	0	0	0.28
0.008145	-0.02	-0.08	-0.58	-0.47	-0.47	0.17	0.04	0.13	-0.01	0.03	0.03	0.03	-0.15	0.18	0.25	0.01	-0.05	0.06	-0.24	0.01	0.07	-0.01	0.06	0.08	-0.07	-0.01	-0.02	-0.18	0.11	-0.4	0.51	-1.	-0.04	-0.13	-0.06	0.2	-0.07	-0.07	-0.01	0	0.04	0	0	0.07
0.0160615	-0.02	-0.01	-0.01	-0.01	-0.01	0	0.03	-0.02	-0.01	0.02	0.02	0.02	0.01	0	0	-0.23	-0.17	0.18	-0.01	-0.47	-0.06	-0.53	-0.01	-0.01	0.01	0	0	-0.02	0.03	0.04	0	0.01	0.07	-0.04	-0.04	-0.1	-0.02	-0.02	-1.	-0.24	-0.07	0	0	-0.06
0.0552083	-0.45	-0.98	0.42	0.43	0.43	0.01	0.09	-0.08	-0.03	0.06	0.06	0.06	0.05	0.01	0.01	-0.1	-0.07	-0.1	-0.34	-0.03	-0.2	0.01	0.53	0.53	-0.61	-0.08	-0.17	-0.38	-0.23	-1.	0.77	0.62	-0.14	-0.36	-0.34	0.3	-0.19	-0.18	-0.01	0.07	0.15	0	0	-0.2
0.25188	1.	0.24	-0.07	-0.07	-0.07	-0.12	-0.04	-0.08	0.01	-0.03	-0.03	-0.03	0.1	-0.12	-0.12	0.01	0.08	-0.04	0.44	-0.01	-0.03	0.04	0.76	0.75	-0.79	-0.03	-0.06	-0.67	-0.12	0.04	-0.16	-0.14	0.1	0.28	0.27	-0.44	0.17	0.11	-0.04	-0.02	-0.1	0	0	-0.04
1.92769	-0.21	-0.19	-0.02	-0.01	-0.01	0.05	0.05	0	-0.02	0.03	0.03	0.03	-0.01	0.05	0.05	0.04	0.09	-0.11	0.25	0.27	-0.07	0.41	-0.02	-0.02	0	-0.02	-0.04	-0.16	0.16	0.08	0.09	0.09	-0.14	-0.02	-0.02	-0.25	0.54	-0.56	-0.42	0.06	-0.03	-0.34	0.02	1.
2.43527	0.01	-0.01	-0.02	-0.02	-0.02	-0.03	0.16	-0.19	-0.04	0.12	0.12	0.12	0.15	-0.03	-0.03	-0.2	-0.07	-0.19	0.07	-0.43	-0.39	-0.44	0.01	0.01	-0.02	0	0	-0.01	0	0	-0.01	0	0.15	-0.06	-0.06	-0.07	-0.69	0.63	0.45	0.06	0.13	-0.45	0.03	1.
12.8308	-0.11	-0.1	0.06	0.06	0.06	0.2	-0.12	0.32	-0.14	-0.26	-0.26	-0.26	-0.45	0.2	0.2	0.53	-0.07	-0.22	0.2	-0.55	0.31	0.2	-0.01	-0.01	0	-0.01	-0.03	-0.16	0.15	0.08	0.08	0.08	1.	0.03	0.03	-0.2	-0.06	0.09	-0.2	0.82	0.89	0.11	0	-0.02
19.9852	0.12	0.11	0.21	0.21	0.21	0.47	0.11	0.36	-0.64	-0.53	-0.53	-0.53	-1.	0.47	0.47	-0.34	0.05	-0.05	0.14	0.12	-0.4	-0.17	0.01	0.01	0	0.01	0.02	-0.1	0.1	0.05	0.05	0.05	-0.42	0.01	0.01	-0.14	-0.1	0.11	0.17	-0.33	-0.38	-0.13	0	0
130.426	0.01	0.01	0	0	0	-0.01	-0.02	0.01	0.02	-0.01	-0.01	-0.01	0	-0.01	-0.01	0.03	0	0.02	-0.03	0	0.05	0.01	0	0	0	0	0	0	0.01	-0.01	-0.01	-0.01	-0.01	0.02	0.01	0.01	0.03	0.02	-0.01	-0.01	0.01	0.01	-0.59	-1.	-0.17

Figure 5.5: Modal matrix approximation for the kinetic red cell (alternate approach).

The modal matrix for the kinetic red blood cell network constructed using only $\mathbf{S}$ and μ.

	HK	PGI	PFK	ALD	TPI	GAPDH	PGK	DPGM	DPGase	PGM	EN	PK	PEX	LDH	LEX	AMPase	ADA	AK	ADK	AMPDA	ATPase	ADPRT	G6PDH	PGLase	GL6PDH	GSSGR	GSHR	RU5PI	XU5PE	TKI	TKII	TALD	IMPase	PNPase	PRM	PRPPSYN	HGPRT	HXEX	ADEEX	ADOEX	INOEX	NALEAK	KLEAK	PUMP
9.1784×10^{-6}	0	0	0	0	0	0	0	0	0	0	0	0	0	0	0	-0.38	1.	0.38	0	0	0	0	0	0	0	0	0	0	0	0	0	0	0.62	-0.66	0.01	0	0.03	0.03	0	0.38	-0.62	0	0	0
0.0000158018	0	0	0	0	0	0	0	0	0	0	0	0	0	0	0	1.	-0.29	-1.	0	0	0	0	0	0	0	0	0	0	0	0	0	0	0.71	-0.79	0.01	0	0.06	0.06	0	-1.	-0.71	0	0	0
0.0000759083	0	0	0	-0.01	-0.01	1.	-0.99	-0.99	0	0	0	0	0	0	0	0	0	0	0	0	0	0	0	0	0	0	0	0	0	0	-0.01	-0.01	0.01	0	0	0	0	0	0	0	0	0	0	0
0.0000825685	0	0	0	0	0	0	0	0	0	0	0	0	0	0	0	0.1	0.23	-0.1	0	-0.01	0	-0.01	0	0	0	0	0	0	0	0	0	0	0.33	0.72	-0.05	0.01	-1.	-0.99	0	-0.1	-0.33	0	0	0
0.000506082	0	0	0	0	0	0	0	0	0	0	0	0	0	0	0	0	0	0	0	0	0	-1.	0	0	0	0	0	0	0	0	0	0	-0.01	-0.02	0.01	0.04	-0.03	0.01	-0.96	0	0.01	0	0	0
0.000735094	0	0	0	-0.05	-0.05	0.03	0.02	0.02	0	0	0	0	0	0	0	-0.05	-0.13	0.05	0	0	0	0.01	0	0	-0.03	0	0	0.1	0.04	-0.14	-0.08	0.08	-0.17	-0.47	1.	-0.06	-0.29	-0.27	0.02	0.05	0.18	0	0	0
0.000854694	-0.01	0.01	0	0.02	0.02	-0.01	-0.01	-0.01	0	0	0	0	0	0	0	0	0	0	0	0	0	0	1.	-1.	0.05	-0.01	0	-0.02	-0.02	0.03	0.03	-0.03	0	-0.01	0.01	0	0	0	0	0	0	0	0	0
0.00087246	0	0	-0.04	0.59	0.55	-0.36	-0.21	-0.2	0	0	0	0	0	0.01	0	-0.01	-0.04	0.01	0	0	0	0	-0.06	0.06	0.06	0	0	-0.11	-0.18	0.78	1.	-0.94	-0.05	-0.14	0.23	0.06	-0.09	-0.08	0.01	0.01	0.05	0	0	0
0.00147434	0	0.01	0.01	-0.13	-0.11	0.08	0.04	0.04	0	0	0	0	0	0	0	-0.01	-0.03	0.01	0	-0.01	0	-0.01	-0.05	0.03	0.91	-0.02	0	-1.	-0.95	0.12	-0.1	0.22	-0.04	-0.11	0.04	0.18	-0.07	-0.04	0.02	0.01	0.04	0	0	0
0.00339393	0	0	0.07	-0.22	-0.15	0.11	0.06	0.05	0	0	0	0	0	-0.01	0	0.05	0.12	-0.05	-0.02	0.1	0	0.15	-0.02	0	0.39	-0.02	0	0.26	-0.36	-0.76	0.51	-0.44	0.07	0.33	0.19	-1.	0.39	-0.07	-0.21	-0.02	-0.14	0	0	0
0.00417411	-0.03	0.31	-0.86	1.	0.41	-0.31	-0.16	-0.16	-0.01	0.03	-0.03	0.01	0	0.05	0	0.02	0.07	-0.03	0	0.08	-0.01	0.11	0	0.01	0.15	-0.01	0	0.12	-0.11	0.02	-0.17	0.89	0.01	0.15	0.11	-0.52	0.24	-0.1	-0.14	-0.01	-0.07	0	0	-0.01
0.00485436	0	0.02	-0.02	0.01	0	0.01	0.03	-0.02	0.05	-0.73	1.	-0.35	0.03	0.04	0	0	0	0	-0.01	0	0	0	0	0	0	0	0	0	-0.01	0	0.02	0.02	0	0	0	0	0	0	0	0	0	0	0	0
0.00506282	-0.06	0.53	-0.6	-0.3	-0.42	0.33	0.18	0.16	0.01	0	-0.03	0.04	-0.01	-0.08	0	-0.02	-0.04	0.01	0.03	-0.09	-0.01	-0.09	0.04	0.03	-0.26	0.02	0	0.12	-0.19	-0.05	1.	0.45	0.02	-0.07	-0.07	0.31	-0.18	0.11	0.11	0.01	0.05	0	0	-0.01
0.0068296	0	-0.06	-0.48	0.57	0	-0.02	-0.01	-0.01	0	-0.01	0.01	0.01	0	0.01	0	-0.07	-0.15	0.06	0.05	-0.52	-0.01	-0.25	-0.03	-0.01	0.47	-0.05	0	-0.09	0.32	-1.	-0.09	-0.52	0.3	-0.03	-0.08	0.38	-0.54	0.53	0.3	0.03	0.18	0	0	-0.01
0.00882609	-0.03	0.01	-0.58	0.29	-0.34	0.32	0.19	0.13	0.03	-0.1	-0.01	0.16	-0.07	-0.23	0	0.09	0.25	-0.12	-0.01	1.	-0.02	-0.02	0	0	0.03	0	0	-0.46	0.48	-0.27	-0.08	-0.49	-0.66	-0.12	-0.07	0.38	0.42	-0.55	0.02	-0.04	-0.29	0	0	-0.02
0.0107183	-0.02	-0.19	-0.15	0.19	-0.12	0.42	0.3	0.12	0.13	-0.62	-0.07	1.	-0.4	-0.86	0.01	-0.06	-0.1	0.01	0.13	-0.41	-0.05	0.17	-0.01	-0.02	-0.12	0.03	0	0.02	-0.12	0.36	-0.22	-0.15	0.25	0.02	0.03	-0.25	-0.01	0.03	-0.19	0.02	0.12	0	0	-0.05
0.012852	-0.07	0.26	0.66	-0.27	0.77	-0.53	-0.23	-0.31	0.08	-0.65	-0.1	1.	-0.32	-0.17	0	0.1	0.21	-0.1	-0.09	0.68	0	-0.52	0.01	0.03	0.38	-0.1	0	0.37	-0.05	-0.5	0.32	0.5	-0.36	0.06	0.02	0.36	-0.17	0.24	0.57	0	-0.22	0	0	0
0.0152605	-0.39	0.91	0.07	-0.53	0.31	-0.36	-0.15	-0.22	0.03	-0.28	-0.08	0.38	-0.01	0.35	0	-0.12	-0.19	0.09	0.21	-0.52	-0.03	0.56	0.25	0.28	0.16	-0.13	0	-0.87	1.	-0.2	0.15	0	0.21	-0.14	-0.09	-0.1	0.25	-0.4	-0.6	-0.02	0.16	0	0	-0.03
0.0188918	0.12	-0.31	-0.21	0.03	-0.41	-0.19	0	-0.19	0.16	-0.53	-0.29	0.45	0.25	1.	-0.01	-0.02	0	-0.02	0.08	-0.01	-0.04	0.02	-0.11	-0.13	-0.22	0.14	0	0.02	-0.23	0.02	-0.04	-0.09	-0.01	0	0	0.01	0.01	-0.01	-0.02	0	0	0	0	-0.04
0.0225885	0.94	-0.6	0.07	-0.07	0.27	-0.14	-0.16	0.01	-0.08	0.07	0.08	0.02	-0.17	-0.26	0	-0.04	-0.1	0.13	-0.06	-0.16	0.09	0.27	-0.97	-1.	-0.04	0.55	-0.01	-0.39	0.36	-0.35	0.53	0.45	0.03	-0.1	-0.08	0.14	0.14	-0.25	-0.28	-0.07	0.03	0	0	0.09
0.0291089	-0.17	-0.12	0.22	0.28	0.1	-0.19	-0.19	0	-0.17	0.12	0.14	0.07	-0.19	-0.13	0	0	-0.01	0.02	-0.04	-0.01	0.02	0.01	0.39	0.34	-1.	0.52	-0.01	-0.58	-0.51	-0.58	0.05	0	0	-0.01	-0.01	0.01	0.01	-0.01	-0.01	0	0	0	0	0.02
0.0372846	-0.04	0.15	0.23	0.14	0.63	0.52	0.74	-0.22	1.	-0.49	-0.66	-0.57	0.68	-0.16	0	0.07	0.02	-0.03	-0.24	0.05	0.05	-0.08	-0.03	-0.04	-0.19	0.33	-0.01	-0.27	0.04	-0.13	0.05	0.08	0.04	0	0	-0.14	-0.06	0.06	0.09	0.08	0.06	0	0	0.05
0.0385669	0.05	-0.63	0.24	0.24	0.2	0.11	0.23	-0.12	0.19	0.01	-0.05	-0.13	0.15	-0.05	0	-0.31	-0.09	0.15	1.	-0.21	-0.16	0.36	0.32	0.32	0.07	-0.62	0.01	0.3	-0.19	-0.31	0.29	0.28	-0.19	0	0	0.6	0.26	-0.25	-0.37	-0.37	-0.28	0	0	-0.17
0.0400067	-0.78	0.41	-0.16	-0.24	0.28	0.02	0.17	-0.15	-0.07	0.24	0.19	0	0.02	0.01	0	-0.2	0.08	-0.18	1.	0	-0.38	-0.04	-0.53	-0.53	0.02	0.92	-0.02	0.2	-0.22	0.05	-0.3	-0.26	-0.12	0.12	0.11	0.11	0.02	0.11	0.04	-0.09	-0.17	0	0	-0.39
0.0699701	-0.54	1.	0.98	1.	-0.99	-0.07	-0.38	0.31	0.08	-0.4	-0.35	-0.15	0.04	-0.15	0.01	-0.14	-0.27	0.91	-0.49	-0.27	0.77	0.39	-0.29	-0.27	0.39	0.7	-0.03	0.65	-0.24	-0.07	-0.08	-0.06	-0.14	0.09	0.08	0.72	0.31	-0.22	-0.4	-0.78	-0.5	-0.01	0	0.81
0.0819056	0.04	0	-0.05	-0.04	0.4	0.33	-0.27	0.6	-0.86	-0.28	-0.11	0.2	1.	-0.07	0	-0.02	-0.01	0.04	0.03	-0.01	0.02	0	0.03	0.02	-0.02	0.03	0	0	-0.03	-0.02	-0.02	-0.02	-0.01	0.02	0.02	0.02	0.01	0.01	0	-0.05	-0.04	0	0	0.02
0.0973978	-0.99	-0.36	1.	0.92	-0.79	0.11	0.14	-0.03	-0.29	0.09	0.12	0.13	0.4	-0.02	0	0.15	0.11	-0.61	0.02	0.14	-0.45	-0.06	-0.26	-0.25	0.21	-0.14	0.01	-0.19	0.45	-0.02	0.57	0.54	0.13	-0.3	-0.29	-0.29	-0.14	-0.16	0.06	0.65	0.54	0.01	0	-0.49
0.277904	-1.	-0.58	-0.37	-0.25	0.6	0.24	0.03	0.21	0.02	0.04	0.04	0.03	-0.34	0.3	-0.07	0.1	-0.11	0.1	-0.62	-0.04	0.2	0.22	-0.13	-0.12	0.08	-0.06	0.01	0.32	-0.22	-0.16	0.03	0.01	0.04	-0.28	-0.28	0.25	0.06	-0.34	-0.22	0.11	0.22	-0.01	0	0.25
1.12857	0.18	-0.03	0.1	0.1	0.08	0.25	0.11	0.14	-0.04	0.07	0.06	0.06	-0.19	0.24	-1.	0	0	-0.01	0.03	0	-0.01	-0.01	0.2	0.2	0.2	0.37	-0.39	0.05	0.15	0.07	0.07	0.07	0	0.01	0.01	-0.01	0	0.01	0.01	0	-0.01	0.01	0	0	-0.05
1.18693	0.08	-0.4	-0.16	-0.16	-0.13	-0.18	-0.07	-0.11	0.03	-0.04	-0.04	-0.04	0.13	-0.16	0.92	0.02	-0.01	-0.04	-0.08	0	-0.02	0.06	0.48	0.48	0.48	0.9	-1.	0.27	0.22	0.11	0.12	0.11	0.01	-0.1	-0.1	0.07	0.01	-0.11	-0.06	0.08	0.09	0.03	0	-0.12
1.55907	-0.04	-0.06	-0.01	-0.01	-0.02	0	0.07	-0.07	-0.02	0.05	0.05	0.05	0.05	0	0	0.01	0.05	-0.17	0.3	0.04	-0.16	-0.04	0.02	0.02	0.02	0.03	-0.05	-0.04	0.06	0.03	0.03	0.03	0.02	0.01	0.01	-0.06	-0.02	0.03	0.04	0.12	0.07	-0.37	0.02	1.	
8.6538	0.22	0.21	0.09	0.09	0.1	0.12	-0.36	0.48	-0.03	-0.4	-0.4	-0.4	-0.53	0.13	0.15	1.	0.23	-0.19	0.91	0.39	0.81	0.09	0.01	0.01	0.01	0.02	0.06	0.14	-0.13	-0.06	-0.06	-0.06	0.84	0.34	0.34	0.54	0.45	-0.11	-0.09	0.96	0.73	0.28	-0.01	-0.06	
17.0677	-0.05	-0.05	-0.2	-0.2	-0.2	-0.48	-0.13	-0.35	0.62	0.51	0.52	0.52	1.	-0.48	-0.52	0.32	0.01	0.08	-0.06	0.08	0.4	0.11	0	0	0	0	0	0.16	-0.16	-0.08	-0.08	-0.08	0.25	0.03	0.03	0.27	0.16	-0.13	-0.11	0.23	0.22	0.13	0	0.01	
104.317	0.01	0.01	0	0	0	-0.01	-0.02	0.01	0.02	-0.01	-0.01	-0.01	0	-0.01	-0.01	0.03	0	0.02	-0.03	0.01	0.05	0.01	0	0	0	0	0	0.01	-0.01	-0.01	-0.01	-0.01	0.02	0.01	0.01	0.03	0.02	-0.01	-0.01	0.01	0.01	-0.59	-1.	-0.17	

Figure 5.6: The modal matrix for the kinetic red blood cell network constructed using only $\mathbf{S}$ and $1/\mathbf{x}$

5.1.3 Two way factorizations

In an attempt to achieve 'the best of both worlds', one can reconstruct the gradient matrix using both κ and μ, such that

$$\mathbf{G} \approx -1 \cdot \kappa \cdot \mathbf{S}^T \cdot \mu \tag{5.4}$$

Carrying this out an calculating the modal matrix results in Figure 5.7. This result has encouraging as well as discouraging aspects. To begin with it should be noted that while all 34 modes are shown, the first 2 and the last mode are really 0 (the next few are debateable) This would reflected an invariant modal pools. All of the modes are shown because, 1) the manner in which the network was constructed was through gross approximations and so approximating very large and very small numbers can leading to numerically unstable areas and 2) the actual composition of the modes are *very* close to the actual modal matrix.

The main point to recognize here is that time scale separation and dynamic hierarchy result from the order of magnitude differences between kinetics of the various enzymes *and* the order of magnitude differences between concentrations metabolites; these differences are largely inseparable and actually joined in each element of the gradient matrix. Combing approximations for κ and μ may actually be useful approaches to obtaining an order of magnitude of the structure of the modal matrix and the range of time scales.

5.2 Flux-concentration duality

The duality between fluxes and concentrations was described earlier, in this section the general, underlying relationships between fluxes ($\mathbf{v}$) and concentrations ($\mathbf{x}$) through the use of net elementary reaction rates and the formulation of the gradient matrix $\mathbf{G}$ ($= d\mathbf{v}/d\mathbf{x}$) will be further explored. Analysis of metabolic networks in terms of the gradient matrix results in characterization of the underlying relationship between fluxes and concentrations as dual variables, also enabling decomposition of the system into constituent direction-driver relationships resulting

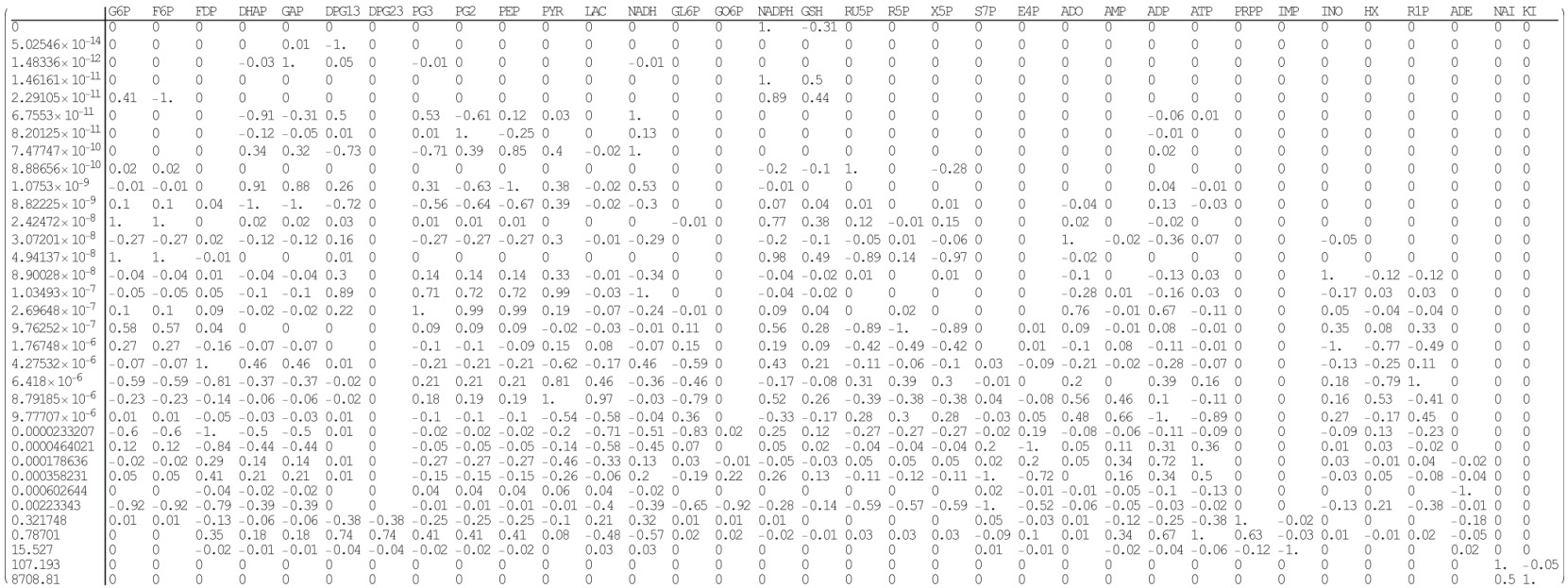

	G6P	F6P	FDP	DHAP	GAP	DPG13	DPG23	PG3	PG2	PEP	PYR	LAC	NADH	GL6P	GO6P	NADPH	GSH	RU5P	R5P	X5P	S7P	E4P	ADO	AMP	ADP	ATP	PRPP	IMP	INO	HX	R1P	ADE	NAI	KI
0	0	0	0	0	0	0	0	0	0	0	0	0	0	0	0	1.	-0.31	0	0	0	0	0	0	0	0	0	0	0	0	0	0	0	0	0
5.02546×10^{-14}	0	0	0	0	0.01	-1.	0	0	0	0	0	0	0	0	0	0	0	0	0	0	0	0	0	0	0	0	0	0	0	0	0	0	0	0
1.48336×10^{-12}	0	0	0	-0.03	1.	0.05	0	-0.01	0	0	0	0	-0.01	0	0	0	0	0	0	0	0	0	0	0	0	0	0	0	0	0	0	0	0	0
1.46161×10^{-11}	0	0	0	0	0	0	0	0	0	0	0	0	0	0	0	1.	0.5	0	0	0	0	0	0	0	0	0	0	0	0	0	0	0	0	0
2.29105×10^{-11}	0.41	-1.	0	0	0	0	0	0	0	0	0	0	0	0	0	0.89	0.44	0	0	0	0	0	0	0	0	0	0	0	0	0	0	0	0	0
6.7553×10^{-11}	0	0	0	-0.91	-0.31	0.5	0	0.53	-0.61	0.12	0.03	0	1.	0	0	0	0	0	0	0	0	0	0	0	-0.06	0.01	0	0	0	0	0	0	0	0
8.20125×10^{-11}	0	0	0	-0.12	-0.05	0.01	0	0.01	1.	-0.25	0	0	0.13	0	0	0	0	0	0	0	0	0	0	0	-0.01	0	0	0	0	0	0	0	0	0
7.47747×10^{-10}	0	0	0	0.34	0.32	-0.73	0	-0.71	0.39	0.85	0.4	-0.02	1.	0	0	0	0	0	0	0	0	0	0	0	0.02	0	0	0	0	0	0	0	0	0
8.88656×10^{-10}	0.02	0.02	0	0	0	0	0	0	0	0	0	0	0	0	0	-0.2	-0.1	1.	0	-0.28	0	0	0	0	0	0	0	0	0	0	0	0	0	0
1.0753×10^{-9}	-0.01	-0.01	0	0.91	0.88	0.26	0	0.31	-0.63	-1.	0.38	-0.02	0.53	0	0	-0.01	0	0	0	0	0	0	0	0	0.04	-0.01	0	0	0	0	0	0	0	0
8.82225×10^{-9}	0.1	0.1	0.04	-1.	-1.	-0.72	0	-0.56	-0.64	-0.67	0.39	-0.02	-0.3	0	0	0.07	0.04	0.01	0	0.01	0	0	-0.04	0	0.13	-0.03	0	0	0	0	0	0	0	0
2.42472×10^{-8}	1.	1.	0	0.02	0.02	0.03	0	0.01	0.01	0.01	0	0	0	-0.01	0	0.77	0.38	0.12	-0.01	0.15	0	0	0.02	0	-0.02	0	0	0	0	0	0	0	0	0
3.07201×10^{-8}	-0.27	-0.27	0.02	-0.12	-0.12	0.16	0	-0.27	-0.27	-0.27	0.3	-0.01	-0.29	0	0	-0.2	-0.1	-0.05	0.01	-0.06	0	0	1.	-0.02	-0.36	0.07	0	0	-0.05	0	0	0	0	0
4.94137×10^{-8}	1.	1.	-0.01	0	0	0.01	0	0	0	0	0	0	0	0	0	0.98	0.49	-0.89	0.14	-0.97	0	0	-0.02	0	0	0	0	0	0	0	0	0	0	0
8.90028×10^{-8}	-0.04	-0.04	0.01	-0.04	-0.04	0.3	0	0.14	0.14	0.14	0.33	-0.01	-0.34	0	0	-0.04	-0.02	0.01	0	0.01	0	0	-0.1	0	-0.13	0.03	0	0	1.	-0.12	-0.12	0	0	0
1.03493×10^{-7}	-0.05	-0.05	0.05	-0.1	-0.1	0.89	0	0.71	0.72	0.72	0.99	-0.03	-1.	0	0	-0.04	-0.02	0	0	0	0	0	-0.28	0.01	-0.16	0.03	0	0	-0.17	0.03	0.03	0	0	0
2.69648×10^{-7}	0.1	0.1	0.09	-0.02	-0.02	0.22	0	1.	0.99	0.99	0.19	-0.07	-0.24	-0.01	0	0.09	0.04	0	0.02	0	0	0	0.76	-0.01	0.67	-0.11	0	0	0.05	-0.04	-0.04	0	0	0
9.76252×10^{-7}	0.58	0.57	0.04	0	0	0	0	0.09	0.09	0.09	-0.02	-0.03	-0.01	0.11	0	0.56	0.28	-0.89	-1.	-0.89	0	0.01	0.09	-0.01	0.08	-0.01	0	0	0.35	0.08	0.33	0	0	0
1.76748×10^{-6}	0.27	0.27	-0.16	-0.07	-0.07	0	0	-0.1	-0.1	-0.09	0.15	0.08	-0.07	0.15	0	0.19	0.09	-0.42	-0.49	-0.42	0	0.01	-0.1	0.08	-0.11	-0.01	0	0	-1.	-0.77	-0.49	0	0	0
4.27532×10^{-6}	-0.07	-0.07	1.	0.46	0.46	0.01	0	-0.21	-0.21	-0.21	-0.62	-0.17	0.46	-0.59	0	0.43	0.21	-0.11	-0.06	-0.1	0.03	-0.09	-0.21	-0.02	-0.28	-0.07	0	0	-0.13	-0.25	0.11	0	0	0
6.418×10^{-6}	-0.59	-0.59	-0.81	-0.37	-0.37	-0.02	0	0.21	0.21	0.21	0.81	0.46	-0.36	-0.46	0	-0.17	-0.08	0.31	0.39	0.3	-0.01	0	0.2	0	0.39	0.16	0	0	0.18	-0.79	1.	0	0	0
8.79185×10^{-6}	-0.23	-0.23	-0.14	-0.06	-0.06	-0.02	0	0.18	0.19	0.19	1.	0.97	-0.03	-0.79	0	0.52	0.26	-0.39	-0.38	-0.38	0.04	-0.08	0.56	0.46	0.1	-0.11	0	0	0.16	0.53	-0.41	0	0	0
9.77707×10^{-6}	0.01	0.01	-0.05	-0.03	-0.03	0.01	0	-0.1	-0.1	-0.1	-0.54	-0.58	-0.04	0.36	0	-0.33	-0.17	0.28	0.3	0.28	-0.03	0.05	0.48	0.66	-1.	-0.89	0	0	0.27	-0.17	0.45	0	0	0
0.0000233207	-0.6	-0.6	-1.	-0.5	-0.5	0.01	0	-0.02	-0.02	-0.02	-0.2	-0.71	-0.51	-0.83	0.02	0.25	0.12	-0.27	-0.27	-0.27	-0.02	0.19	-0.08	-0.06	-0.11	-0.09	0	0	-0.09	0.13	-0.23	0	0	0
0.0000464021	0.12	0.12	-0.84	-0.44	-0.44	0	0	-0.05	-0.05	-0.05	-0.14	-0.58	-0.45	0.07	0	0.05	0.02	-0.04	-0.04	-0.04	0.2	-1.	0.05	0.11	0.31	0.36	0	0	0.01	0.03	-0.02	0	0	0
0.000178636	-0.02	-0.02	0.29	0.14	0.14	0.01	0	-0.27	-0.27	-0.27	-0.46	-0.33	0.13	0.03	-0.01	-0.05	-0.03	0.05	0.05	0.05	0.02	0.2	0.05	0.34	0.72	1.	0	0	0.03	-0.01	0.04	-0.02	0	0
0.000358231	0.05	0.05	0.41	0.21	0.21	0.01	0	-0.15	-0.15	-0.15	-0.26	-0.06	0.2	-0.19	0.22	0.26	0.13	-0.11	-0.12	-0.11	-1.	-0.72	0	0.16	0.34	0.5	0	0	-0.03	0.05	-0.08	-0.04	0	0
0.000602644	0	0	-0.04	-0.02	-0.02	0	0	0.04	0.04	0.04	0.06	0.04	-0.02	0	0	0	0	0	0	0	0.02	-0.01	-0.01	-0.05	-0.1	-0.13	0	0	0	0	0	-1.	0	0
0.00223343	-0.92	-0.92	-0.79	-0.39	-0.39	0	0	-0.01	-0.01	-0.01	-0.01	-0.4	-0.39	-0.65	-0.92	-0.28	-0.14	-0.59	-0.57	-0.59	-1.	-0.52	-0.06	-0.05	-0.03	-0.02	0	0	-0.13	0.21	-0.38	-0.01	0	0
0.321748	0.01	0.01	-0.13	-0.06	-0.06	-0.38	-0.38	-0.25	-0.25	-0.25	-0.1	0.21	0.32	0.01	0.01	0.01	0	0	0	0	0.05	-0.03	0.01	-0.12	-0.25	-0.38	1.	-0.02	0	0	0	-0.18	0	0
0.78701	0	0	0.35	0.18	0.18	0.74	0.74	0.41	0.41	0.41	0.08	-0.48	-0.57	0.02	0.02	-0.02	-0.01	0.03	0.03	0.03	-0.09	0.1	0.01	0.34	0.67	1.	0.63	-0.03	0.01	-0.01	0.02	-0.05	0	0
15.527	0	0	-0.02	-0.01	-0.01	-0.04	-0.04	-0.02	-0.02	-0.02	0	0.03	0.03	0	0	0	0	0	0	0	0.01	-0.01	0	-0.02	-0.04	-0.06	-0.12	-1.	0	0	0	0.02	0	0
107.193	0	0	0	0	0	0	0	0	0	0	0	0	0	0	0	0	0	0	0	0	0	0	0	0	0	0	0	0	0	0	0	0	1.	-0.05
8708.81	0	0	0	0	0	0	0	0	0	0	0	0	0	0	0	0	0	0	0	0	0	0	0	0	0	0	0	0	0	0	0	0	0.5	1.

Figure 5.7: The modal matrix for the kinetic red blood cell network constructed using only κ and μ

from the thermodynamic and kinetic influences in the network.

As described in Chapter 2, a complete study of the system properties of Equation 2.7 would result in the characterization of all four subspaces of $\mathbf{S}$ [91]. The null and left null spaces of $\mathbf{S}$ have been thoroughly studied [64], containing steady state pathways and time-invariant pools [15], respectively. Conversely, the focus of dynamic analysis is in the row and column spaces of $\mathbf{S}$, as the driving forces are in the row space and the thermodynamically determined direction of motion is in the column space. The drivers for change result from the inner product of a row in the stoichiometric matrix ($\mathbf{s}_i^v$) and the flux vector $\mathbf{v}$. If their inner product, $\langle \mathbf{s}_i^v, \mathbf{v} \rangle$, is non-zero then a time derivative of concentration $\mathbf{x}$ changes. If the inner product, $\langle \mathbf{s}_i^v, \mathbf{v} \rangle$, is zero, then the flux vector is orthogonal to the row space vector and the time derivative of concentrations is equal to the null vector. The vector of the time derivatives of concentration variables is simply a linear combination of the columns of $\mathbf{S}$ (see Equation 2.7) and hence is in the column space of $\mathbf{S}$.

Dynamic analysis of complex systems is normally carried out with the linearization of the right hand side of Equation 2.7. Noting that $\mathbf{S}$ is a matrix with constant coefficients, linearization of equation (1) comes down to the linearization of the reaction rates , $\mathbf{v}(\mathbf{x})$, following Taylor series expansion:

$$\mathbf{v}(\mathbf{x}) = \mathbf{v}(\mathbf{x}_0) + \frac{d\mathbf{v}}{d\mathbf{x}}|_{\mathbf{x}_0} \cdot (\mathbf{x} - \mathbf{x}_0) + \frac{1}{2}\frac{d^2\mathbf{v}}{d\mathbf{x}^2}|_{\mathbf{x}_0} \cdot (\mathbf{x} - \mathbf{x}_0)^2 + ... \tag{5.5}$$

$$\mathbf{v}(\mathbf{x}) = \mathbf{v}(\mathbf{x}_0) + \mathbf{G}|_{\mathbf{x}_0} \cdot (\mathbf{x} - \mathbf{x}_0) + ... \tag{5.6}$$

The gradient matrix is a data matrix [38], and it has three notable properties.

1. Bilinear kinetics: The interactions that occur in biological networks, including macromolecular interactions and enzymatic catalysis are all fundamentally bilinear interactions. That is, most reactions involve two molecules combining to form a third. The general rate law for any of these steps is given by, $v = kx_1x_2$, in which k is a bilinear rate constant, and x_1 and x_2 are the concentrations of the interacting components.

2. Structural similarity: When the reaction rates in the flux vector are

written as net elementary reaction rates then it follows that, $\mathbf{S}$ and $\mathbf{G}^T$ have a similar structure [38] in the sense that the same elements in corresponding row and column entries have zero or non-zero entries. The key difference between the matrices is that the entries in $\mathbf{S}$ are integers, whereas the entries in $\mathbf{G}^T$ are real valued and have the opposite sign to the corresponding elements in $\mathbf{S}$.

3. Elementary features: The gradient matrix arises naturally from the linearization of the flux vector comprised of net elementary reaction rates. $\mathbf{G}$ is a matrix of reciprocal time constants representing the response times of the reaction rates to changes in concentrations. Different elements in the network typically have a wide range of response times, hence the gradient matrix gives rise to the characteristically wide ranging hierarchical dynamics in biological systems in addition to the wide range of concentrations in biological systems (from nanomolar to millimolar) at steady states.

5.2.1 The Jacobian Matrix for Concentrations

Specifying a steady state, $\mathbf{x}_0$, Equation 2.7 becomes:

$$\frac{d\mathbf{x}'}{dt} = \mathbf{S} \cdot \mathbf{G} \cdot \mathbf{x}' \tag{5.7}$$

in which $\mathbf{x}'$ is the deviation variable, $(\mathbf{x} - \mathbf{x}_0)$. $\mathbf{J}_x = \mathbf{S} \cdot \mathbf{G}$, is the Jacobian for the system of equations describing the concentration variables. The metabolite Jacobian can be analyzed, decomposed, and reconstructed in terms of topological, thermodynamic, and kinetic terms.

Note that this factorization separates the chemistry that specifies network topology (through $\mathbf{S}$) and the kinetics and thermodynamics that give the driving forces and their time scale of action (residing in $\mathbf{G}$). Kinetic and thermodynamic effects can be effectively separated by scaling the rows of $\mathbf{G}$ to unity as $\mathbf{G} = \kappa_v \cdot \mathbf{\Gamma}_v$ [38]. The rows (γ_i^v) in $\mathbf{\Gamma}_v$ (a row-normalized gradient matrix with each row corresponding to a reaction) represent the direction of the driving forces (the thermodynamics) in the row space. The elements of the diagonal matrix κ_v represent the time scales on which the thermodynamic driver of a reaction acts.

Equation 5.7 can be written as [1]:

$$\frac{d\mathbf{x}'}{dt} = \sum_{i=1}^{m} \mathbf{s}_i^v \langle \mathbf{g}_i^v, \mathbf{x}' \rangle = \sum_{i=1}^{m} \kappa_i^v \mathbf{s}_i^v \langle \gamma_i^v, \mathbf{x}' \rangle \tag{5.8}$$

in which the reaction vectors $\mathbf{s}_i^v$ are fixed and determine the direction of motion, while the inner product $\langle \gamma_i^v, \mathbf{x}' \rangle$ is a time dependent driving force along this direction, and κ_i^v sets the motion's time scale. Thus, the rows of the gradient matrix represent drivers whereas the columns of the stoichiometric matrix give the directions of motion.

5.2.2 The Jacobian Matrix for Fluxes

The gradient matrix enables the change of the system of equations from the concentration variables to a system of equations in terms of flux variables. Defining the flux deviation variable, $\mathbf{v}' = \mathbf{G} \cdot \mathbf{x}' = \mathbf{v} - \mathbf{v}_0$, and pre-multiplying Equation 5.7 by the gradient matrix yields,

$$\frac{d\mathbf{v}'}{dt} = \mathbf{G} \cdot \mathbf{S} \cdot \mathbf{v}' \tag{5.9}$$

Thus the Jacobian matrix when treating the fluxes as the independent variables is: $\mathbf{J}_v = \mathbf{G} \cdot \mathbf{S}$. In a complementary manner, the flux Jacobian can also be investigated in terms of the topological, thermodynamic, and kinetic influences in this 'node view' of networks.

$\mathbf{G}$ can be factored as $\mathbf{G} = \mathbf{\Gamma}_x \cdot \kappa_x$, where $\mathbf{\Gamma}_x$ has the columns of $\mathbf{G}$ (i.e., the columns, $\mathbf{g}_i^x$, corresponding to the compounds that influence the directions of the reactions) normalized and the diagonal matrix κ_x contains the length of these columns. κ_i represent the 'kinetic potential' of compound or node, i, and γ_i^x represent the distribution of this potential amongst the links to the node and $\mathbf{J}_v = \mathbf{\Gamma}_x \cdot \kappa_x \cdot \mathbf{S}$.

[1] A column in $\mathbf{S}$ corresponds to a reaction and we use the superscript v to designate this by $\mathbf{s}_i^v$. Similarly, a row in $\mathbf{S}$ corresponds to a compound, and we designate a row as $\mathbf{s}_i^x$. For the matrix $\mathbf{G}$ the opposite is the case, thus $\mathbf{g}_i^v$ designates a row in $\mathbf{G}$ and $\mathbf{g}_i^x$ designates a column.

Equation 5.9 can be written as,

$$\frac{d\mathbf{v}'}{dt} = \sum_{i=1}^{n} \mathbf{g}_i^x \langle \mathbf{s}_i^x, \mathbf{v}' \rangle = \sum_{i=1}^{m} {\kappa_i}^x \gamma_i^x \langle \mathbf{s}_i^x, \mathbf{v}' \rangle \tag{5.10}$$

The scaled kinetic connectivity vectors γ_i^x are fixed and determine the direction of motion of the flux vector, reflecting the kinetically balanced outflow of a compound from a node if the concentration of the compound in that node is perturbed from steady state. The κ_i^x sets the strength for this motion on the network flux state. The inner product $\langle \mathbf{s}_i^x, \mathbf{v}' \rangle$ is a time dependent driving force along this direction. This driving force is simply a non-steady state mass balance on a node. Thus, the rows of the stoichiometric matrix represent drivers for flux whereas the columns of the gradient matrix give the directions of the flux distribution from a node.

5.2.3 Duality of Fluxes and Concentrations

Thus, there are two Jacobian matrices describing the same network, $\mathbf{J}_x = \mathbf{S} \cdot \mathbf{G}$ and $\mathbf{J}_v = \mathbf{G} \cdot \mathbf{S}$, depending on which variables, concentrations or fluxes, are used as state variables. The former gives a link (reaction)-centric view of the dynamics, while the latter gives a node (compound)-centric view. These are complementary views of the same system. The $\mathbf{J}_v$ and $\mathbf{J}_x$ are structurally similar to the reaction adjacency matrix ($\mathbf{A}_v = \widehat{\mathbf{S}}^T\widehat{\mathbf{S}}$) [2] and the compound adjacency matrix ($\mathbf{A}_x = \widehat{\mathbf{S}}\widehat{\mathbf{S}}^T$), respectively (see Chapter 7 in [64]), demonstrating that network topology has an overarching effect on the dynamics. One can view $\mathbf{J}_x$ as a weighted version of $\mathbf{A}_x$ and $\mathbf{J}_v$ as a weighted version of $\mathbf{A}_v$.

Modal decomposition of the Jacobian has previously been applied in biological network analysis [67, 65]. We note that the two Jacobian matrices share the same eigenvalues. The eigenvectors/rows of $\mathbf{J}_x$, relate to pool formation on various time scales [66, 63], while the eigenvectors/rows of $\mathbf{J}_v$, relate the formation of groups of fluxes that move these pools.

The driving forces for the flux motions are non-flux balance variables ($\mathbf{S} \cdot \mathbf{v} \neq \mathbf{0}$) on the nodes. The direction of motion for the flux vector are the columns, $\mathbf{g}^x$,

[2] $\widehat{\mathbf{S}}$ refers to the binary from of the stoichiometric matrix.

which we view as 'kinetic' connectivity of the metabolites. The driving forces on the concentration are dis-equilibrium type thermodynamic variables. The direction of motion for the concentrations are the reaction vectors ($\mathbf{s^v}$).

Forming the dual Jacobian matrices The dual Jacobian matrices can be decomposed into a summation of rank one matrices. The reaction based decomposition of $\mathbf{J}_x = \mathbf{S} \cdot \mathbf{G}$ has the logical scaling factors $\kappa_i^v = -\langle \mathbf{g}_i^v, \mathbf{s}_i^v \rangle$, whose inner products are the absolute lengths of the reaction row ($\mathbf{g}^v$), corresponding to the time scale of the corresponding reaction. When the scaling factors differ significantly, then each rank one component matrix in $\mathbf{J}_x$ will contribute very differently to the Jacobian matrix, determined by the response time of a reaction and its equilibrium constant.

Analogously, decomposition of $\mathbf{J}_v = \mathbf{G} \cdot \mathbf{S}$ in terms of the compounds (nodes) with logical scaling factors $\kappa_i{}^x = -\langle \mathbf{s}_i^x, \mathbf{g}_i{}^x \rangle$, whose inner products are the absolute lengths of the connectivity column ($\mathbf{g}^x$), correspond to the kinetic potential of the corresponding compound (node). The relative contribution of each node to $\mathbf{J}_v$ is determined by the response time of the fastest reaction connected to the node.

In order to develop predictive models which also advance the understanding of biological processes, it is vital to move towards describing and decomposing systems in terms of the underlying physico-chemical processes and subsequently analyzing the interactions among the components.

Herein we showed how the gradient matrix underlies the relationship between the fluxes and concentrations. Using the gradient matrix enables dynamic states of a biochemical reaction network to be described by dual Jacobian matrices, $\mathbf{S} \cdot \mathbf{G}$ and $\mathbf{G} \cdot \mathbf{S}$. The ability to convert from one set of variables into another is not just of mathematical interest, but highlights the underlying root of the physical relationship between fluxes and concentrations and how they determine dynamic states via thermodynamic and kinetic influences.

The thermodynamic and kinetic influences can be decomposed into direction-driver relationships that illustrate the link or node view point of the dynamic states of a network. These relationships can be used to formulate timescale hierar-

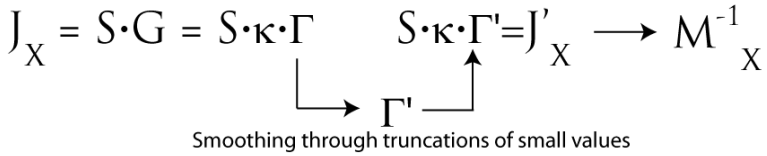

Figure 5.8: Adjusting the entries in $\mathbf{\Gamma}$ in order to clean the structure of the modal matrix.

chy through scaling of $\mathbf{G}$ that enables a decomposition into reaction (link based) physico-chemical properties on one hand and in terms of network level (node based) physico-chemical properties on the other. This dual representation can be used for any biochemical reaction network that is represented in terms of net elementary reactions. Analysis of networks in this context can bring the 'natural' time scale hierarchy into focus and enable investigation of the (dynamic) structure - (physiological) structure relationship.

5.3 Smoothing gamma

Another approach to 'cleaning' or clarifying the structure of the modal matrices is to adjust the values in the matrix $\mathbf{\Gamma}$. Recall that $\mathbf{\Gamma}$ matrix resulting from left factorization of $\mathbf{G}$ and contains information about the directions of the reactions (i.e. the steady state thermodynamics of the reactions). Thermodynamically, under a specified set of conditions, reactions are often classified as being reversible or irreversible. Thus the entries in the magnitude of the rows in $\mathbf{\Gamma}$ tend to be close to one (reflecting reversibility) or much larger/smaller than one (irreversible). In recognition of this, the Jacobian can be decomposed as, $\mathbf{S} \cdot \kappa \cdot \mathbf{\Gamma}$, the entries in $\mathbf{\Gamma}$ can be rounded and $\mathbf{J_x}$ and $\mathbf{J_v}$ can be reconstructed. The process is schematically outlined in Figure 5.8.

Figure 5.9 shows the results of modal decomposition of the flux Jacobian, when $\mathbf{\Gamma}$ is rounded to the tenths digit. The fast modes do not appear to change significantly, however in the slower modes, some interesting differences are immediately observed, in particular, the slowest mode is *much* slower, on the order of 10 days. This motion is driven almost solely by the Rapoport-Leubering shunt. The

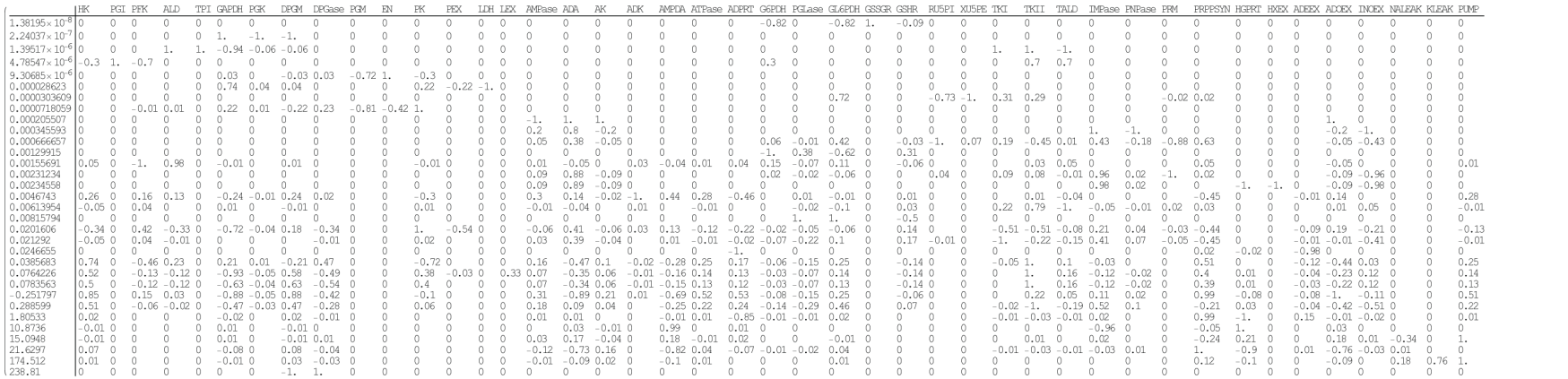

Figure 5.9: The smoothing of the flux modal matrix for the kinetic red blood cell network, with $\mathbf{\Gamma}$ rounded to tenths digit.

overall structure of the matrix is very similar to Figure 5.2, with the 'smoothed' $\mathbf{\Gamma}$ modal matrix having a slightly cleaner structure and a fewer number of elements that are very small (e.g. PGM and EN).

5.4 Rotating modes

As noted earlier, the analysis of modal matrices has been made difficult due to the non-integer and often difficult to interpret ratios in the entries. The tendency of metabolites to pool together in metabolic networks has provided the motivation to develop methods for identification and characterization of the formation of pools, as described in Chapter 4. This is effective for the analysis of the concentration Jacobian, $\mathbf{J}_x$, however since fluxes do not pool together, such approaches are not relevant for the analysis of the flux Jacobian, $\mathbf{J}_v$. An approach for clarifying the structure of the matrix is to construct the modal matrix for the flux Jacobian, and then apply an oblique rotation [21]. Briefly, oblique rotation methods rotate a given matrix by maximizing particular terms in a matrix and minimizing others. In carrying out such a transformation, a 'target loadings' matrix needs to be specified in order to identify which entries in the matrix need to be maximized or minimized. The natural choice for defining target matrices for the rotation of modal matrices is the modal matrix, rounded to the nearest integer.

The analysis will focus on the modal matrix of the full kinetic red blood cell model [34]. The trivial approach of just rounding the digits in the row-normalized modal matrix will be used as the basis for comparison to the oblique rotation approach. The obliquely rotated flux modal matrix rounded to the nearest tenths after the rotation can be seen in Figure 5.10, and to the flux modal matrix rounded to the nearest tenths is shown in Figure 5.10. Interestingly, both have vary similar structures, although the obliquely rotated matrix has slightly fewer entries than the rounded matrix. The slowest modes are approximately identical for the two matrices, although some of the slower modes become more transparent when they are rotated. For example the exchange between the oxidative and non-oxidative branch in the 7th mode becomes clear for the rotated matrix, but less so for

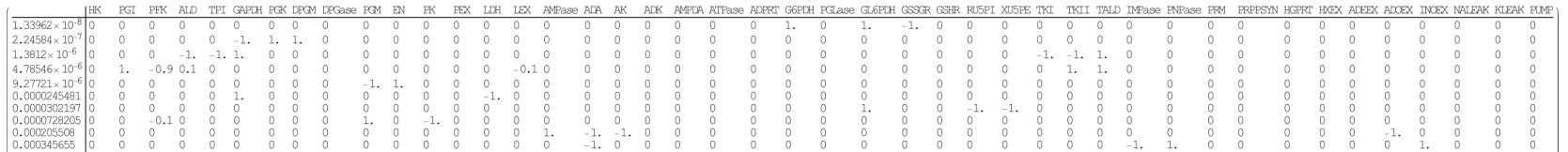

	HK	PGI	PFK	ALD	TPI	GAPDH	PGK	DPGM	DPGase	PGM	EN	PK	PEX	LDH	LEX	AMPase	ADA	AK	ADK	AMPDA	AIPase	ADPRT	G6PDH	PGLase	GL6PDH	GSSGR	GSHR	RU5PI	XU5PE	TKI	TKII	TALD	IMPase	PNPase	PRM	PRPPSYN	HGPRT	HXEX	ADEEX	ADOEX	INOEX	NALEAK	KLEAK	PUMP
1.33962×10^{-8}	0	0	0	0	0	0	0	0	0	0	0	0	0	0	0	0	0	0	0	0	0	0	1.	0	1.	-1.	0	0	0	0	0	0	0	0	0	0	0	0	0	0	0	0	0
2.24584×10^{-7}	0	0	0	0	0	-1.	1.	1.	0	0	0	0	0	0	0	0	0	0	0	0	0	0	0	0	0	0	0	0	0	0	0	0	0	0	0	0	0	0	0	0	0	0	0
1.3812×10^{-6}	0	0	0	-1.	-1.	1.	0	0	0	0	0	0	0	0	0	0	0	0	0	0	0	0	0	0	0	0	0	0	0	-1.	-1.	1.	0	0	0	0	0	0	0	0	0	0	0
4.78546×10^{-6}	0	1.	-0.9	0.1	0	0	0	0	0	0	0	0	0	0	-0.1	0	0	0	0	0	0	0	0	0	0	0	0	0	0	1.	1.	0	0	0	0	0	0	0	0	0	0	0	0
9.27721×10^{-6}	0	0	0	0	0	0	0	0	0	-1.	1.	0	0	0	0	0	0	0	0	0	0	0	0	0	0	0	0	0	0	0	0	0	0	0	0	0	0	0	0	0	0	0	0
0.0000245481	0	0	0	0	1.	0	0	0	0	0	0	0	-1.	0	0	0	0	0	0	0	0	0	0	0	0	0	0	0	0	0	0	0	0	0	0	0	0	0	0	0	0	0	0
0.0000302197	0	0	0	0	0	0	0	0	0	0	0	0	0	0	0	0	0	0	0	0	0	0	0	0	1.	0	0	-1.	-1.	0	0	0	0	0	0	0	0	0	0	0	0	0	0
0.0000728205	0	0	-0.1	0	0	0	0	0	0	1.	0	-1.	0	0	0	0	0	0	0	0	0	0	0	0	0	0	0	0	0	0	0	0	0	0	0	0	0	0	0	0	0	0	0
0.00020508	0	0	0	0	0	0	0	0	0	0	0	0	0	0	0	1.	-1.	-1.	0	0	0	0	0	0	0	0	0	0	0	0	0	0	0	0	0	0	0	-1.	0	0	0	0	0
0.000345655	0	0	0	0	0	0	0	0	0	0	0	0	0	0	0	0	-1.	0	0	0	0	0	0	0	0	0	0	0	0	0	0	-1.	1.	0	0	0	0	0	1.	0	0	0	0
0.000620365	0	0	0.6	-1.	0	0.6	0	0	0	0	0	-0.5	0.5	0	0	0	0	0	0	0	0	0	0	0	0	0	0	0	0	0	0	0	0	0	0	0	0	0	0	0	0	0	0
0.000744573	0	0	0	0	0	0	0	0	0	0	0	0	0	0	0	0	0.8	0	0.1	0	0.1	0	0	0	0.8	0	-0.1	-0.8	-0.1	-0.1	-0.1	0	0	0.8	-0.2	-1.	0.7	-0.1	-0.1	0	0	-0.8	0	0	0
0.000999516	0	0	0	0	0	0	0	0	0	0	0	0	0	0	0	0	0	0	0	0	0	0	-1.	0.1	-1.	0.2	0.4	0	0.1	0	0	0	0	0	0	0	0	0	0	0	0	0	0
0.00121876	0	0	0.9	-1.	0	0	0	0	0	0	0	0	0	0	0	0	0	0	0	0	0	0	0	0	0	0	0	0	0	0	0	0	0	0	0	0	0	0	0	0	0	0	0
0.00226677	0	0	0	0	0	0	0	0	0	0	0	0	0	0	0	0	-1.	0	0	0	0	0	0	0	0	0	0	0	0	0	0	-1.	0	1.	0	0	0	0	1.	0	0	0	0
0.00234305	0	0	0	0	0	0	0	0	0	0	0	0	0	0	0	0	1.	0	0	0	0	0	0	0	0	0	0	0	0	0	0	1.	0	0	0	-1.	-1.	0	0	-1.	0	0	0
0.00498523	0	-0.1	-0.1	-0.1	0	-0.1	0	-0.1	-0.2	-0.2	-0.2	1.	-0.1	-0.1	0	-0.1	0	-0.2	1.	-0.1	-0.3	0.1	0	0	0	0	0	0	0	0	0	0	0.1	0.1	0.1	0.1	0	-0.1	0.1	0.1	-0.1	0	0
0.00646139	0	0	0	0	0	0	0	0	0	0	0	0	0	0	0	0	0	0	0	0	0	0	0	0	0	0	0	0	0	0.5	-1.	0	0	0	0	0	0	0	0	0	0	0	0
0.00733185	0	0	0	0	0	0	0	0	0	0	0	0	0	0	0	0	0	0	0	0	0	0	-0.1	1.	1.	-0.2	-0.4	0	0	0	0	0	0	0	0	0	0	0	0	0	0	0	0
0.0207413	-0.1	-0.1	0	0	0	0	0	0	0	0	0	0	0	0	0	0	-1.	0.1	0	0	0.1	0	0.1	0.1	-0.1	0	-0.1	-0.1	0	1.	0.1	0.1	-1.	0.1	0.1	1.	0	0.1	0	0	1.	0	0	0
0.0245323	0	0	0	0	0	0	0	0	0	0	0	0	0	0	0	0	0	0	0	0	0	-1.	0	0	0	0	0	0	0	0	0	0	0	0	0	0	0	-1.	0	0	0	0	0
0.0303075	1.	0	-0.3	0.2	0	0	0	0.2	0.2	0	0	-0.8	0.3	0	0	0.2	-0.6	0.2	0	-0.5	0.3	0.5	-0.1	-0.3	0.3	0	-0.1	0	0	-0.2	0.8	0.2	0	0	0	0.5	0	0	0	-0.7	-0.1	0	0	0.3
0.0402444	-0.9	-0.1	0.8	-0.1	0.1	0	0	0.9	-1.	0	0	0.1	1.	0	0.1	0	0	0	-0.1	0	0	0	0.1	0.1	0	0	0.1	0	-0.1	-0.1	-0.9	0	0	-0.1	-0.1	0	0	-0.1	0	0	0.1	0	0	0
0.0806219	0.5	0	0	0	0	0	0	0.2	-0.2	0	0	0	0.1	0	-0.3	0	-0.2	0	0	-0.2	0	0	0	-0.2	0.2	0	-0.1	0	0	0	1.	0.2	0	0	0	0.2	-0.1	0	0	-0.3	0	0	0	0
0.274512	0.1	0	0	0	0	0	0	-0.1	0	0	0	0	0	0	0	0	0	0	0	0	0	0	0	-0.1	0.3	0	-0.1	0	0	0	1.	0.1	-0.1	0	0	0.1	0	0	0	0.1	0.2	0	0	0
1.52981	-0.5	0	0	0	0	0	0	0.5	-0.2	0	0	0	0	0	0	0.1	-1.	0.1	0	-0.2	0.3	0.5	0	0	0	0	0	0	0	0	0.2	0	-0.7	-0.2	0	0.9	0.4	0.1	0	-0.4	0.6	0	0	0.2
2.90482	0	0	0	0	0	0	0	0	0	0	0	0	0	0	0	0	0	0	0	0	0	0.8	0	0	0	0	0	0	0	0	0	0	0	0	0	-1.	1.	0.1	-0.1	0	0	0	0	0
21.7782	0.3	0	0	0	0	0	0	0.6	-0.7	0	0	0	0	0	0	-0.3	-0.6	0.2	0	0	-0.2	-0.4	0	0	0	0	0	0	0	0	0	0	-0.9	0	0	1.	-0.4	0	0	-0.9	-0.3	0	0	-0.3
14.5319	0	0	0	0	0	0	0	0	0	0	0	0	0	0	0	0	-0.2	0	0	-0.1	0	0	0	0	0	0	0	0	0	0	0	0	-0.1	0	0	0.4	-0.2	0	0	-0.2	0	0.4	0	-1.
17.0043	0.1	0	0	0	0	0	0	0	0	0	0	0	0	0	0	-0.2	-0.7	0.2	0	-0.7	-0.1	-0.2	0	0	0	0	0	0	0	0	0	0	-0.2	0	0	1.	-0.9	0	0	-0.8	-0.1	0	0	0.1
174.512	0	0	0	0	0	0	0	0	0	0	0	0	0	0	0	0	0	0	0	0	0	0	0	0	0	0	0	0	0	0	0	0	0	0	0	0	0	0	0	0	0	0.2	0.8	1.

Figure 5.10: Oblique rotation of flux model matrix.

The flux modal matrix for the kinetic red blood cell network constructed obliquely rotated to minimize the number of non-zero entries and rounded to a single digit.

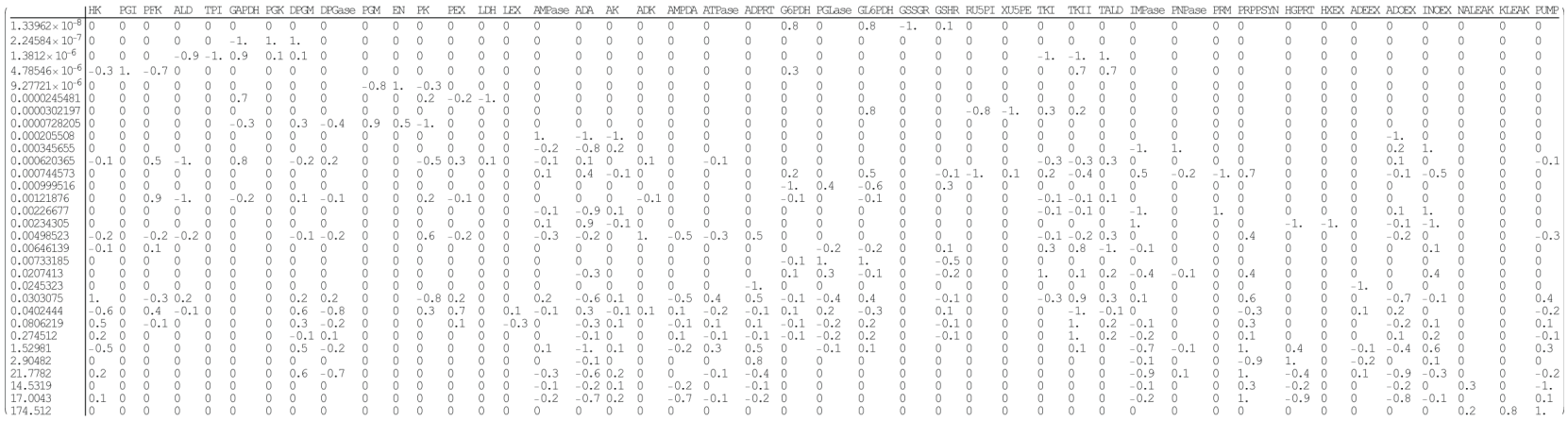

	HK	PGI	PFK	ALD	TPI	GAPDH	PGK	DPGM	DPGase	PGM	EN	PK	PEX	LDH	LEX	AMPase	ADA	AK	ADK	AMPDA	ATPase	ADPRT	G6PDH	PGLase	GL6PDH	GSSGR	GSHR	RU5PI	XU5PE	TKI	TKII	TALD	IMPase	PNPase	PRM	PRPPSYN	HGPRT	HXEX	ADEEX	ADOEX	INOEX	NALEAK	KLEAK	PUMP
1.33962×10^{-8}	0	0	0	0	0	0	0	0	0	0	0	0	0	0	0	0	0	0	0	0	0	0	0.8	0	0.8	-1.	0.1	0	0	0	0	0	0	0	0	0	0	0	0	0	0	0	0
2.24584×10^{-7}	0	0	0	0	0	-1.	1.	1.	0	0	0	0	0	0	0	0	0	0	0	0	0	0	0	0	0	0	0	0	0	0	0	0	0	0	0	0	0	0	0	0	0	0	0
1.3812×10^{-6}	0	0	0	-0.9	-1.	0.9	0.1	0.1	0	0	0	0	0	0	0	0	0	0	0	0	0	0	0	0	0	0	0	0	0	-1.	-1.	1.	0	0	0	0	0	0	0	0	0	0	0
4.78546×10^{-6}	-0.3	1.	-0.7	0	0	0	0	0	0	0	0	0	0	0	0	0	0	0	0	0	0	0	0.3	0	0	0	0	0	0	0	0.7	0.7	0	0	0	0	0	0	0	0	0	0	0
9.27721×10^{-6}	0	0	0	0	0	0	0	0	0	-0.8	1.	-0.3	0	0	0	0	0	0	0	0	0	0	0	0	0	0	0	0	0	0	0	0	0	0	0	0	0	0	0	0	0	0	0
0.0000245481	0	0	0	0	0	0.7	0	0	0	0	0	0.2	-0.2	-1.	0	0	0	0	0	0	0	0	0	0	0	0	0	0	0	0	0	0	0	0	0	0	0	0	0	0	0	0	0
0.0000302197	0	0	0	0	0	0	0	0	0	0	0	0	0	0	0	0	0	0	0	0	0	0	0	0	0.8	0	0	-0.8	-1.	0.3	0.2	0	0	0	0	0	0	0	0	0	0	0	0	0
0.0000728205	0	0	0	0	0	-0.3	0	0.3	-0.4	0.9	0.5	-1.	0	0	0	0	0	0	0	0	0	0	0	0	0	0	0	0	0	0	0	0	0	0	0	0	0	0	0	0	0	0	0
0.000205508	0	0	0	0	0	0	0	0	0	0	0	0	0	0	0	1.	-1.	-1.	0	0	0	0	0	0	0	0	0	0	0	0	0	0	0	0	0	0	0	0	0	-1.	0	0	0
0.000345655	0	0	0	0	0	0	0	0	0	0	0	0	0	0	0	-0.2	-0.8	0.2	0	0	0	0	0	0	0	0	0	0	0	0	0	0	-1.	1.	0	0	0	0	0	0.2	1.	0	0
0.000620365	-0.1	0	0.5	-1.	0	0.8	0	-0.2	0.2	0	0	-0.5	0.3	0.1	0	-0.1	0.1	0	0.1	0	-0.1	0	0	0	0	0	0	0	0	-0.3	-0.3	0.3	0	0	0	0	0	0	0	0.1	0	0	0	-0.1
0.000744573	0	0	0	0	0	0	0	0	0	0	0	0	0	0	0	0.1	0.4	-0.1	0	0	0	0	0.2	0	0.5	0	-0.1	-1.	0.1	0.2	-0.4	0	0.5	-0.2	-1.	0.7	0	0	0	-0.1	-0.5	0	0	0
0.000999516	0	0	0	0	0	0	0	0	0	0	0	0	0	0	0	0	0	0	0	0	0	0	-1.	0.4	-0.6	0	0.3	0	0	0	0	0	0	0	0	0	0	0	0	0	0	0	0
0.00121876	0	0	0.9	-1.	0	-0.2	0	0.1	-0.1	0	0	0.2	-0.1	0	0	0	0	0	-0.1	0	0	0	-0.1	0	-0.1	0	0	0	0	-0.1	-0.1	0.1	0	0	0	0	0	0	0	0	0	0	0
0.00226677	0	0	0	0	0	0	0	0	0	0	0	0	0	0	0	-0.1	-0.9	0.1	0	0	0	0	0	0	0	0	0	0	0	-0.1	-0.1	0	-1.	0	1.	0	0	0	0	0.1	1.	0	0	0
0.00234305	0	0	0	0	0	0	0	0	0	0	0	0	0	0	0	0.1	0.9	-0.1	0	0	0	0	0	0	0	0	0	0	0	0	0	0	1.	0	0	0	-1.	-1.	0	-0.1	-1.	0	0	0
0.00498523	-0.2	0	-0.2	-0.2	0	0	0	-0.1	-0.2	0	0	0.6	-0.2	0	0	-0.3	-0.2	0	1.	-0.5	-0.3	0.5	0	0	0	0	0	0	0	-0.1	-0.2	0.3	0	0	0	0.4	0	0	0	-0.2	0	0	0	-0.3
0.00646139	-0.1	0	0.1	0	0	0	0	0	0	0	0	0	0	0	0	0	0	0	0	0	0	0	0	-0.2	-0.2	0	0.1	0	0	0.3	0.8	-1.	-0.1	0	0	0	0	0	0	0	0.1	0	0	0
0.00733185	0	0	0	0	0	0	0	0	0	0	0	0	0	0	0	0	0	0	0	0	0	0	-0.1	1.	1.	0	-0.5	0	0	0	0	0	0	0	0	0	0	0	0	0	0	0	0	0
0.0207413	0	0	0	0	0	0	0	0	0	0	0	0	0	0	0	0	-0.3	0	0	0	0	0	0.1	0.3	-0.1	0	-0.2	0	0	1.	0.1	0.2	-0.4	-0.1	0	0.4	0	0	0	0	0.4	0	0	0
0.0245323	0	0	0	0	0	0	0	0	0	0	0	0	0	0	0	0	0	0	0	0	-1.	0	0	0	0	0	0	0	0	0	0	0	0	0	0	0	0	0	-1.	0	0	0	0	0
0.0303075	1.	0	-0.3	0.2	0	0	0	0.2	0.2	0	0	-0.8	0.2	0	0	0.2	-0.6	0.1	0	-0.5	0.4	0.5	-0.1	-0.4	0.4	0	-0.1	0	0	-0.3	0.9	0.3	0.1	0	0	0.6	0	0	0	-0.7	-0.1	0	0	0.4
0.0402444	-0.6	0	0.4	-0.1	0	0	0	0.6	-0.8	0	0	0.3	0.7	0	0.1	-0.1	0.3	-0.1	0.1	0.1	-0.2	-0.1	0.1	0.2	-0.3	0	0.1	0	0	0	-1.	-0.1	0	0	0	-0.3	0	0	0.1	0.2	0	0	0	-0.2
0.0806219	0.5	0	-0.1	0	0	0	0	0.3	-0.2	0	0	0	0.1	0	-0.3	0	-0.3	0.1	0	-0.1	0.1	0.1	-0.1	-0.2	0.2	0	-0.1	0	0	0	1.	0.2	-0.1	0	0	0.3	0	0	0	-0.2	0.1	0	0	0.1
0.274512	0.2	0	0	0	0	0	0	-0.1	0.1	0	0	0	0	0	0	0	-0.1	0	0	0.1	-0.1	-0.1	-0.1	-0.2	0.2	0	-0.1	0	0	0	1.	0.2	-0.2	0	0	0.1	0	0	0	0.1	0.2	0	0	-0.1
1.52981	-0.5	0	0	0	0	0	0	0.5	-0.2	0	0	0	0	0	0	0.1	-1.	0.1	0	-0.2	0.3	0.5	0	-0.1	0.1	0	0	0	0	0	0.1	0	-0.7	-0.1	0	1.	0.4	0	-0.1	-0.4	0.6	0	0	0.3
2.90482	0	0	0	0	0	0	0	0	0	0	0	0	0	0	0	0	-0.1	0	0	0	0	0.8	0	0	0	0	0	0	0	0	0	0	-0.1	0	0	-0.9	1.	0	-0.2	0	0.1	0	0	0
21.7782	0.2	0	0	0	0	0	0	0.6	-0.7	0	0	0	0	0	0	-0.3	-0.6	0.2	0	0	-0.1	-0.4	0	0	0	0	0	0	0	0	0	0	-0.9	0.1	0	1.	-0.4	0	0.1	-0.9	-0.3	0	0	-0.2
14.5319	0	0	0	0	0	0	0	0	0	0	0	0	0	0	0	-0.1	-0.2	0.1	0	-0.2	0	-0.1	0	0	0	0	0	0	0	0	0	0	-0.1	0	0	0.3	-0.2	0	0	-0.2	0	0.3	0	-1.
17.0043	0.1	0	0	0	0	0	0	0	0	0	0	0	0	0	0	-0.2	-0.7	0.2	0	-0.7	-0.1	-0.2	0	0	0	0	0	0	0	0	0	0	-0.2	0	0	1.	-0.9	0	0	-0.8	-0.1	0	0	0.1
174.512	0	0	0	0	0	0	0	0	0	0	0	0	0	0	0	0	0	0	0	0	0	0	0	0	0	0	0	0	0	0	0	0	0	0	0	0	0	0	0	0	0	0.2	0.8	1.

Figure 5.11: The flux modal matrix for the kinetic red blood cell network rounded to a single digit.

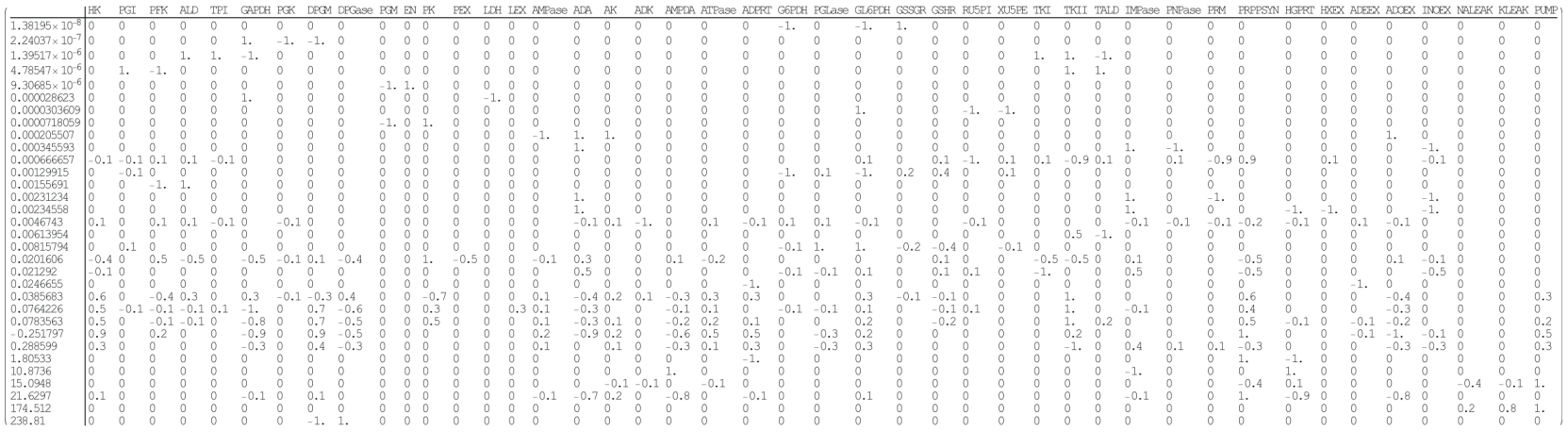

	HK	PGI	PFK	ALD	TPI	GAPDH	PGK	DPGM	DPGase	PGM	EN	PK	PEX	LDH	LEX	AMPase	ADA	AK	ADK	AMPDA	ATPase	ADPRT	G6PDH	PGLase	GL6PDH	GSSGR	GSHR	RU5PI	XU5PE	TKI	TKII	TALD	IMPase	PNPase	PRM	PRPPSYN	HGPRT	HXEX	ADEEX	ADOEX	INOEX	NALEAK	KLEAK	PUMP
1.38195×10^{-8}	0	0	0	0	0	0	0	0	0	0	0	0	0	0	0	0	0	0	0	0	0	0	-1.	0	-1.	1.	0	0	0	0	0	0	0	0	0	0	0	0	0	0	0	0	0
2.24037×10^{-7}	0	0	0	0	0	1.	-1.	-1.	0	0	0	0	0	0	0	0	0	0	0	0	0	0	0	0	0	0	0	0	0	0	0	0	0	0	0	0	0	0	0	0	0	0	0
1.39517×10^{-6}	0	0	0	1.	1.	-1.	0	0	0	0	0	0	0	0	0	0	0	0	0	0	0	0	0	0	0	0	0	0	0	1.	1.	-1.	0	0	0	0	0	0	0	0	0	0	0
4.78547×10^{-6}	0	1.	-1.	0	0	0	0	0	0	0	0	0	0	0	0	0	0	0	0	0	0	0	0	0	0	0	0	0	0	1.	1.	0	0	0	0	0	0	0	0	0	0	0	0
9.30685×10^{-6}	0	0	0	0	0	0	0	0	0	-1.	1.	0	0	0	0	0	0	0	0	0	0	0	0	0	0	0	0	0	0	0	0	0	0	0	0	0	0	0	0	0	0	0	0
0.000028623	0	0	0	0	0	1.	0	0	0	0	0	0	-1.	0	0	0	0	0	0	0	0	0	0	0	0	0	0	0	0	0	0	0	0	0	0	0	0	0	0	0	0	0	0
0.0000303609	0	0	0	0	0	0	0	0	0	0	0	0	0	0	0	0	0	0	0	0	0	0	0	0	0	1.	0	0	-1.	-1.	0	0	0	0	0	0	0	0	0	0	0	0	0
0.0000718059	0	0	0	0	0	0	0	0	0	-1.	0	1.	0	0	0	0	0	0	0	0	0	0	0	0	0	0	0	0	0	0	0	0	0	0	0	0	0	0	0	0	0	0	0
0.000205507	0	0	0	0	0	0	0	0	0	0	0	0	0	0	0	-1.	1.	1.	0	0	0	0	0	0	0	0	0	0	0	0	0	0	0	0	0	0	0	0	1.	0	0	0	0
0.000345593	0	0	0	0	0	0	0	0	0	0	0	0	0	0	0	0	1.	0	0	0	0	0	0	0	0	0	0	0	0	0	0	1.	-1.	0	0	0	0	0	0	-1.	0	0	0
0.000666657	-0.1	-0.1	0.1	0.1	-0.1	0	0	0	0	0	0	0	0	0	0	0	0	0	0	0	0	0	0	0	0.1	0	0.1	-1.	0.1	0.1	-0.9	0.1	0	0.1	-0.9	0.9	0	0.1	0	0	-0.1	0	0
0.00129915	0	-0.1	0	0	0	0	0	0	0	0	0	0	0	0	0	0	0	0	0	0	0	0	-1.	0.1	-1.	0.2	0.4	0	0.1	0	0	0	0	0	0	0	0	0	0	0	0	0	0
0.00155691	0	0	-1.	1.	0	0	0	0	0	0	0	0	0	0	0	0	0	0	0	0	0	0	0	0	0	0	0	0	0	0	0	0	0	0	0	0	0	0	0	0	0	0	0
0.00231234	0	0	0	0	0	0	0	0	0	0	0	0	0	0	0	0	1.	0	0	0	0	0	0	0	0	0	0	0	0	0	0	0	1.	0	-1.	0	0	0	0	0	-1.	0	0
0.00234558	0	0	0	0	0	0	0	0	0	0	0	0	0	0	0	0	1.	0	0	0	0	0	0	0	0	0	0	0	0	0	0	0	1.	0	0	0	-1.	-1.	0	0	-1.	0	0
0.0046743	0.1	0	0.1	0.1	-0.1	0	-0.1	0	0	0	0	0	0	0	0	0	-0.1	0.1	-1.	0	0.1	-0.1	0.1	0.1	-0.1	0	0	-0.1	0	0	0	0	-0.1	-0.1	-0.1	-0.2	-0.1	0	0.1	-0.1	0	0	0	0
0.00613954	0	0	0	0	0	0	0	0	0	0	0	0	0	0	0	0	0	0	0	0	0	0	0	0	0	0	0	0	0	0	0.5	-1.	0	0	0	0	0	0	0	0	0	0	0
0.00815794	0	0.1	0	0	0	0	0	0	0	0	0	0	0	0	0	0	0	0	0	0	0	0	-0.1	1.	1.	-0.2	-0.4	0	-0.1	0	0	0	0	0	0	0	0	0	0	0	0	0	0
0.0201606	-0.4	0	0.5	-0.5	0	-0.5	-0.1	0.1	-0.4	0	0	1.	-0.5	0	0	-0.1	0.3	0	0	0.1	-0.2	0	0	0	0	0	0.1	0	0	-0.5	-0.5	0	0.1	0	0	-0.5	0	0	0	0.1	-0.1	0	0
0.021292	-0.1	0	0	0	0	0	0	0	0	0	0	0	0	0	0	0	0.5	0	0	0	0	0	-0.1	-0.1	0.1	0	0.1	0.1	0	-1.	0	0	0.5	0	0	-0.5	0	0	0	0	-0.5	0	0	0
0.0246655	0	0	0	0	0	0	0	0	0	0	0	0	0	0	0	0	0	0	0	0	0	-1.	0	0	0	0	0	0	0	0	0	0	0	0	0	0	0	0	-1.	0	0	0	0
0.0385683	0.6	0	-0.4	0.3	0	0.3	-0.1	-0.3	0.4	0	0	-0.7	0	0	0	0.1	-0.4	0.2	0.1	-0.3	0.3	0.3	0	0	0.3	-0.1	-0.1	0	0	0	1.	0	0	0	0.6	0	0	0	-0.4	0	0	0	0.3
0.0764226	0.5	-0.1	-0.1	-0.1	0.1	-1.	0	0.7	-0.6	0	0	0.3	0	0	0.3	0.1	-0.3	0	0	-0.1	0.1	0	-0.1	-0.1	0.1	0	-0.1	0.1	0	0	1.	0	-0.1	0	0	0.4	0	0	0	-0.3	0	0	0	0
0.0783563	0.5	0	-0.1	-0.1	0	-0.8	0	0.7	-0.5	0	0	0.5	0	0	0	0.1	-0.3	0.1	0	-0.2	0.2	0.1	0	0	0.2	0	-0.2	0	0	0	1.	0.2	0	0	0.5	-0.1	0	-0.1	-0.2	0	0	0	0.2
-0.251797	0.9	0	0.2	0	0	-0.9	0	0.9	-0.5	0	0	0	0	0	0	0.2	-0.9	0.2	0	-0.6	0.5	0.5	0	-0.3	0.2	0	0	0	0	0	0.2	0	0	0	0	1.	0	0	-0.1	-1.	-0.1	0	0	0.5
0.288599	0.3	0	0	0	0	-0.3	0	0.4	-0.3	0	0	0	0	0	0	0.1	0	0.1	0	-0.3	0.1	0.3	0	-0.3	0.3	0	0	0	0	0	-1.	0	0.4	0.1	0.1	-0.3	0	0	0	-0.3	-0.3	0	0	0.3
1.80533	0	0	0	0	0	0	0	0	0	0	0	0	0	0	0	0	0	0	0	0	0	-1.	0	0	0	0	0	0	0	0	0	0	0	0	1.	-1.	0	0	0	0	0	0	0
10.8736	0	0	0	0	0	0	0	0	0	0	0	0	0	0	0	0	0	0	0	1.	0	0	0	0	0	0	0	0	0	0	0	-1.	0	0	0	1.	0	0	0	0	0	0	0
15.0948	0	0	0	0	0	0	0	0	0	0	0	0	0	0	0	0	0	-0.1	-0.1	0	-0.1	0	0	0	0	0	0	0	0	0	0	0	0	0	-0.4	0.1	0	0	0	0	-0.4	-0.1	1.
21.6297	0.1	0	0	0	0	-0.1	0	0.1	0	0	0	0	0	0	0	-0.1	-0.7	0.2	0	-0.8	0	-0.1	0	0	0.1	0	0	0	0	0	0	-0.1	0	0	1.	-0.9	0	0	-0.8	0	0	0	0	0
174.512	0	0	0	0	0	0	0	0	0	0	0	0	0	0	0	0	0	0	0	0	0	0	0	0	0	0	0	0	0	0	0	0	0	0	0	0	0	0	0	0	0	0.2	0.8	1.
238.81	0	0	0	0	0	0	0	-1.	1.	0	0	0	0	0	0	0	0	0	0	0	0	0	0	0	0	0	0	0	0	0	0	0	0	0	0	0	0	0	0	0	0	0	0	0

Figure 5.12: The flux modal matrix for the kinetic red blood cell network rounded with the 'smoothed' rotated obliquely to minimize zero entries.

the strictly rounded matrix. An oblique rotation was applied to the $\mathbf{\Gamma}$ smoothed modal matrix (Figure 5.9) and a cleaner modal structure was observed there as well, shown in Figure 5.12. Conceptually, applying a rotation is more appealing, as it 'relaxes' the independence of the modes, by forcing some modes to become dependent on others. By doing this however, no information is 'lost', whereas strictly rounding the elements effectively discards information. Having made this point, it is important to recognize that even with the obliquely rotated matrix, many entries (to the hundreths digit) are still non-zero, hence rounding is still required to clean up the matrix. Furthermore, as the size of the network increases, the highly connected nature of the network and the non-integer entries of the gradient matrix make it unlikely to derive stoichiometric ratios between elements in the flux modal matrices, without knowing or specifying the structure of those networks *a priori*.

5.5 Complex modes

Discussing with pooling, need to remove complex conjugate values. Reference Strogatz, well known that eigenvalues determine the stability of a particular steady state. Pure imaginary eigenvalues reflect pure oscillatory behavior (i.e. spinning in circles). Real valued positive eigenvalues are unstable and reflect motion *away* from the steady state over time. Real valued negative eigenvalues are stable and converge to the steady state over time. Complex eigenvalues can be interpreted through the appropriate combinations of the above 3 classifications. Thus a complex eigenvalue with a positive real component spirals away from a steady state, whereas a complex eigenvalues with a negative real component spirals toward a steady state. Complex conjugate eigenvalues occur occasionally in metabolic networks, however one can add the two modes together in order to eliminate the oscillatory component. The most relevant conditions in general for the analysis of metabolism *in vivo* are steady states with negative eigenvalues. Complex conjugate eigenvalues are also acceptable in conditions which the non-oscillatory component is dominant. For example, given a complex number

M_x^{-1}

	G6P	FGP	FDP	DHAP	GAP	DPG13	PG3	PG2	PEP	PYR	LAC	NADH	ADP	ATP
7.43519×10^{-3}	0	0	0	0	0	-1.	0	0	0	0	0	0	0	0
1.50372×10^{-6}	0.41	-1.	0	0	0	0	0	0	0	0	0	0	0	0
0.000128383	0	0	-0.46	0.04	1.	0	0	0	0	0	0	0	0	0
0.000683629	0.01	0.01	-0.41	0.04	-0.2	0.01	0	0.12	-0.16	0.52	-0.02	1.	-0.01	0
0.00160209	0.01	0.01	-0.29	0.03	-0.25	0.17	0.17	-1.	0.01	-0.01	0	0	0	0
$0.0025979 + 0.000105735\,i$	$-0.06 + 0.06\,i$	$-0.06 + 0.06\,i$	$0.03 + 1.\,i$	$-0.16 + 0.02\,i$	$0.02 + 1.\,i$	$-0.04 + 0.06\,i$	$-0.04 + 0.06\,i$	$0.13 - 0.27\,i$	$0.06 - 0.1\,i$	$0.02\,i$	0	0	0	$-0.01\,i$
$0.0025979 - 0.000105735\,i$	$0.06 + 0.06\,i$	$0.06 + 0.06\,i$	$0.03 - 1.\,i$	$0.16\,i$	$0.02 - 1.\,i$	$-0.04 - 0.06\,i$	$-0.04 - 0.06\,i$	$0.13 + 0.27\,i$	$0.06 + 0.1\,i$	$-0.02\,i$	0	0	0	$0.01\,i$
0.0114311	0.2	0.2	-0.56	0.46	-1.	-0.85	-0.87	-0.01	0.01	-0.01	0	0.01	0	0.01
0.0341432	1.	1.	-0.26	-0.35	0.09	0.1	0.06	0.04	0.04	0	0	0	0	0.04
0.0541434	1.	1.	0.19	0.16	0.03	0.02	0.01	0.01	0.01	0	0	0	0	0.01
0.194446	-0.59	-0.59	0.05	0.03	0.02	0.68	0.17	0.16	0.16	-0.35	-1.	-0.66	0.01	0.51
433.679	0.75	0.75	1.	0.5	0.5	0.51	0.26	0.26	0.26	0.01	0	-0.01	-0.24	0.01

M_v^{-1}

	HK	PGI	PFK	ALD	TPI	GAPDH	PGK	PGM	EN	PK	LDH	LEX	ATPase	PUMP
7.43519×10^{-3}	0	0	0	0	0	-1.	1.	0	0	0	0	0	0	0
1.50372×10^{-6}	0.29	-1.	0.71	0	0	0	0	0	0	0	0	0	0	0
0.000128383	0	0	0.31	-1.	-0.64	0.67	0	0	0	0	0	0	0	0
0.000683629	0	0	0.27	-0.16	0.15	-0.78	0	-0.08	0.18	-0.45	1.	-0.01	0	0
0.00160209	0.01	0	-0.25	0.06	-0.24	0.36	0	-1.	0.86	-0.01	0.01	0	0	0
$0.0025979 + 0.000105735\,i$	$0.01 - 0.05\,i$	0	$-0.02 + 0.92\,i$	$-0.14\,i$	$-0.04 + 1.\,i$	$-0.01 - 0.82\,i$	0	$0.16 - 0.27\,i$	$-0.07 + 0.14\,i$	$-0.06 + 0.1\,i$	$-0.01\,i$	0	0	0
$0.0025979 - 0.000105735\,i$	$0.01 + 0.05\,i$	0	$-0.02 - 0.92\,i$	$0.14\,i$	$-0.04 - 1.\,i$	$-0.01 + 0.82\,i$	0	$0.16 + 0.27\,i$	$-0.07 - 0.14\,i$	$-0.06 - 0.1\,i$	$0.01\,i$	0	0	0
0.0114311	0.13	0	-0.53	0.01	-1.	0.11	0	0.59	0.01	0	0	0	-0.01	-0.01
0.0341432	-0.74	0	1.	0	-0.34	-0.01	0	0.02	0	0	0	0	0.03	0.03
0.0541434	-1.	0	0.83	0	0.13	0.01	0	0	0	0	0	0	0.01	0.01
0.194446	-1.	0	0.12	0	-0.01	0	0	-0.01	0	0	0	0.91	-0.46	-0.46
433.677	-1.	0	0	0	0	0	0	0	0	0	0	0	0.5	0.5

The culprit:

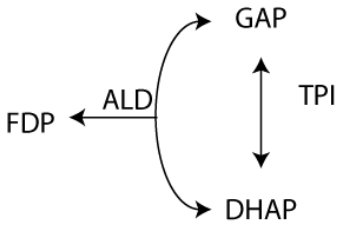

Basic pattern for Jacobian yielding complex conjugate eigenvalues:

$$\begin{pmatrix} 0 & 0 & \alpha \\ \beta & 0 & 0 \\ 0 & \gamma & 0 \end{pmatrix}$$

Figure 5.13: The 'root' of complex eigenvalues.

Identifying causes of complex eigenvalues in metabolic networks. Top panel: The modal matrices for a model of glycolysis showing the first 12 modes, without removal of complex conjugate eigenvalue pairs. Bottom panel: The reaction scheme between aldolase and triose phosphate isomerase can result in complex conjugate pairs. When the stoichiometric motif found at the bottom appears in Jacobian matrices, complex conjugated pairs arise.

$z = a - ib$, conditions which satisfy, $|Re(z)|/|z| > 1/\sqrt{2}$.

The appearance of complex conjugate pairs of eigenvalues in metabolic networks following a similarity transformation reflects an interaction between metabolites that cannot be separated, i.e. a reaction(s) that cannot be split apart. Complex conjugate eigenvalue pairs can appear even in a seemingly simple glycolytic pathway [38] shown in Figure 5.13. α, β, and γ are non-zero entities that may or may not all share the same sign.

5.6 Generalized duality

The gradient matrix has been defined,

$$G_{ij} = \frac{\partial v_i}{\partial x_j} \tag{5.11}$$

By definition of the total derivative, Equation 5.11 can be rewritten as

$$d\mathbf{v} = \mathbf{G} \cdot d\mathbf{x} \tag{5.12}$$

Integration of 5.12 between two states, s1 and s2 yields,

$$\int_{s1}^{s2} d\mathbf{v} = \mathbf{v}_{s2} - \mathbf{v}_{s2} = \int_{s1}^{s2} \mathbf{G} \cdot d\mathbf{x} \tag{5.13}$$

in which $\mathbf{v}_{s1}$ and $\mathbf{v}_{s2}$ are the fluxes at state s1 and s2, respectively. There are at least key points to recognize about this relationship,

1. This is a general relationship and is independent of linearization
2. Equation 5.12 is not dependent on a particular steady state and analysis of fluxes and concentrations in the context of this relationship allows relaxation of the steady state or quasi-steady state assumptions
3. This will allow 'random' sampling of measurements to be taken and to be analyzed in the context of a network without intensive parameterization

It is beyond the scope of this current work to delve into this generalization of duality (in addition to the lack of proper data at this point to test this relationship in a substantive manner). However, this relationship is central to the dual relationship between fluxes and concentrations and the implication that the steady state constraints may be relaxed, in conjunction with the delta model concept (Chapter 8), may have a very large impact on the uses and applications of stoichiometrically constructed biological networks.

5.7 Simulateable networks

As discussed in Chapter 4 and Table 4.1, systems analysis can be carried out using analytical approaches or simulation based approaches. Each have associated pros and cons and the decision to use one versus the other of these complementary techniques is based on the type of question one wants answered, as well as the practical challenges (e.g. feasibility of numerical challenges versus analytical methods). Results based on simulations, such as those that will be seen in Chapter 6 and 7 are more directly testable in the experimental laboratory and often more directly interpretable as well.

Approaches focused on reconstructing the Jacobian matrices ($\mathbf{J}_x$ and $\mathbf{J}_v$) do so with the intent of the subsequent application of analytical methods. While these results are often valuable for characterization and modularization of networks, the results are often difficult to test or evaluate experimentally. Results from simulations however are often directly testable in the laboratory and allow the support (or refutation) of a particular hypothesis. The primary quality control criteria for analysis based methods for the Jacobian is the evaluation of the signs of the eigenvalues. Quality control issues for simulation based networks, or for networks with the intent to carry out simulations are more complex. The stability issues associated with the Jacobian are present here as well (e.g. stability of the steady state), however there are additional challenges. Notably the need to have positive rate constants and the reconciliation of simulation results with existing data (e.g. equilibrium constant). Depending on the type of analysis that one

wants to carry out, then different quality control/quality assurance measures need to be taken. Testing simulateable networks is fairly easy, one just integrates the differential equations until a steady state is reached. Trouble-shooting when errors appear however is not always trivial and this is an area which will need attention as more data is published and more kinetic models are constructed.

5.8 Summary

While the topics in this chapter have varied, the focus has been to investigate approaches for clarifying the structure of the Jacobian matrices by appreciating the underlying structure of the dynamic network matrices,

- Understanding the components and underlying structure of the gradient (and by extension the Jacobian matrices) can enable approaches to approximate the entries when detailed information is lacking. This may be useful in the process of building kinetic networks.

- There are different ways to factor the gradient matrix. Factorization from the left yields the κ matrix, whose entries are the corresponding 'rate constants' for the reactions. Factorization from the right can be done in two ways. One approach yields the reciprocal concentrations, the μ matrix.

- As a consequence of duality, there are two approaches for decomposing the Jacobians (one approach for each Jacobian). Using the row and column factors of the gradient matrix, one can recreate the structure of the Jacobian to an approximation.

- Using oblique rotations to clean the structure of modal matrices are slightly better than strictly rounding the entries, however there is not a significant substantive improvement. The approach for using oblique rotations may become more useful if a methodology to develop biological driven target matrices is developed.

- Complex conjugate eigenvalues appear when the reactions are not decomposable. Patterns within the Jacobian can be identified to pick out these non-decomposable groups of reactions.

- The gradient matrix is not dependent on linearization of Equation 2.7. The integral form of the definition has implications that can result in the relaxation of steady state assumptions and potentially have applications for the analysis of patient measurements and *in vivo* data.

- The decision to carry out analytical based computations versus simulations is dependent on the type of question that the investigator is asking. Constructing simulation-worthy models however is not a trivial process and quality control measures need to be in place to ensure that non-sensical parameters are not used and mis-interpretation of the results does not occur.

Chapter 6

Building Kinetic Networks

The increasing availability of metabolomic data in conjunction with the increasing number of stoichiometric metabolite network reconstructions has made genome-scale kinetic model reconstructions a feasible goal, given the underlying equations described in Chapter 2. Figure 6.1 outlines a practical approach for building large-scale kinetic models. Stoichiometric network reconstructions serve as the 'bottom-up' framework on which to build the model. The increasing availability of metabolomic data [98, 31] have created data streams which can feed into the model and be used for constructing kinetic networks. An additional set of data, the equilibrium constants (K_{eq}) for each reaction are also needed for this framework. Integrating these data with the network and then solving for the rate constants that satisfy the steady state conditions results in a dynamic description of the network which can then be interrogated through analytical and simulation based methods.

A basic approach for building approximations for the kinetic structure of networks is outline in Figure 6.2. This basic stepwise procedure will characterize the dynamics of a network about a particular steady state. The first step involves specifying a particular steady state flux distribution. Next, the concentrations (generally there will need to be some approximations of these) of the metabolites at this steady state need to be identified. Third, the equilibrium constant approximations need to be determined and the steady state fluxes and concentrations will be incorporated into mass action rate laws. Finally, the forward rate constants can

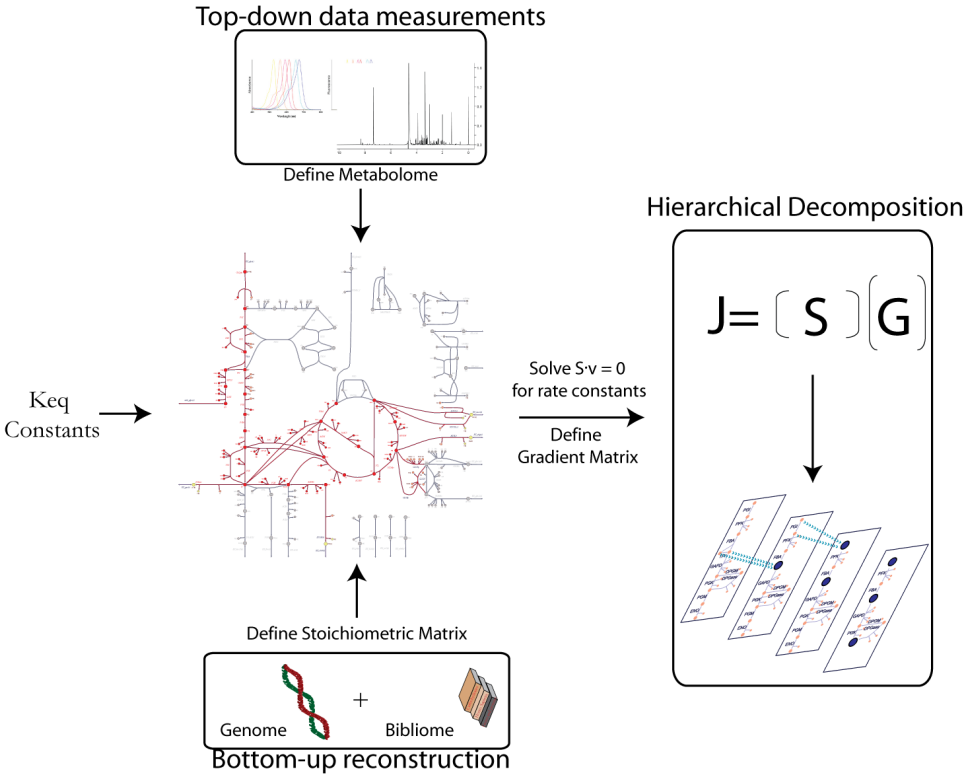

Figure 6.1: Kinetic networks through middle-out integration.

An overall strategy for the integration of existing metabolic networks with metabolomic data in order to build kinetic models.

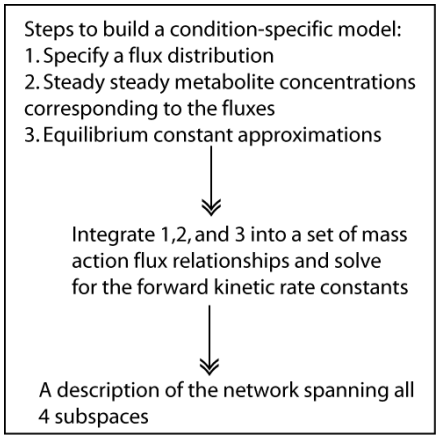

Figure 6.2: The process of kinetic network cosntruction.

Explicit procedure to build a kinetic network beginning with a curated stoichiometric, mass-balanced model.

be solved by solving n linear equations for forward rate constants. For situations in which all of the concentrations are not known or if one whats to trace the effects of particular metabolites in multiple rate constants, rather than n linear equations, one can solve m equations by solving the steady state mass conservation relationship (Equation 2.2). Note that in general since $m < n$, the alternative approach will result in an underdetermined solution set.

6.1 Mass Action Model of Glycolysis

The process outlined in Figure 6.2 was carried out for the glycolytic pathway of the human red blood cell. Steady state fluxes and concentrations from the kinetic model of red cell metabolism [34] were used to construct the model. Equilibrium constant approximations from [41] were used. Using mass action rate law formulations, the steady state equations were solved for the forward rate laws. These were then substituted back into the rate laws, so that the gradient matrix could be calculated. Table 6.1 shows the dimensions of the matrix and the size of the subspaces.

Figure 6.3 shows the network along with the Jacobian matrices, decomposed through left and right factorizations of the $\mathbf{\Gamma}$ matrices. The structural similarity

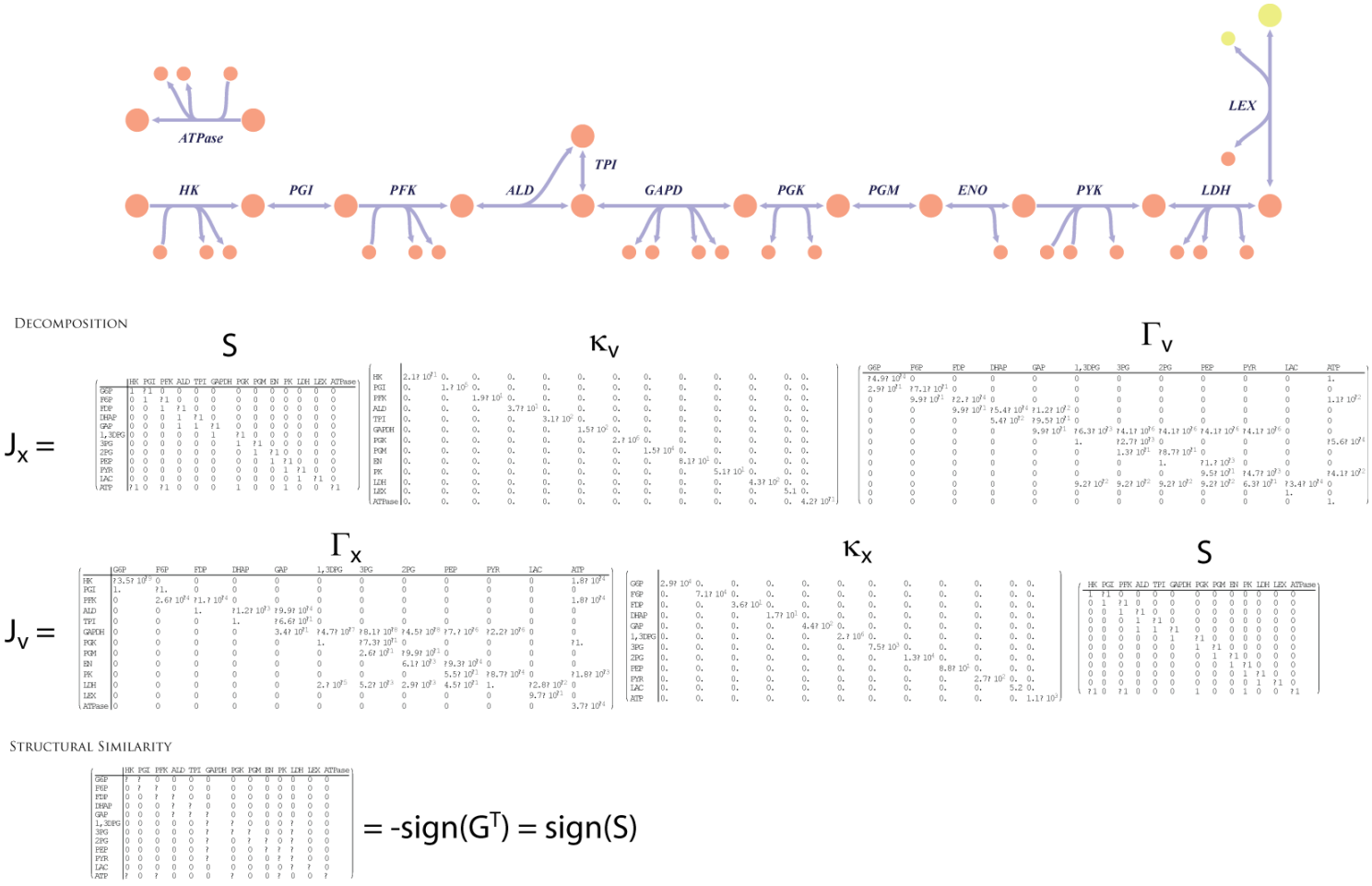

Figure 6.3: Mass action model of glycolysis.

The pathway with its corresponding metabolite and flux Jacobians decomposed into their constituent matrices. The bottom panel explicitly highlights the structural similarity between $\mathbf{S}^T$ and $\mathbf{G}$.

DUALITY

THE JACOBIAN IN TERMS OF METABOLITES: J_X

	G6P	F6P	FDP	DHAP	GAP	1,3DPG	3PG	2PG	PEP	PYR	LAC	ATP
G6P	-2.9×10^{4}	7.1×10^{4}	0.	0.	0.	0.	0.	0.	0.	0.	0.	2.1×10^{-1}
F6P	2.9×10^{4}	-7.1×10^{4}	3.7×10^{-3}	0.	0.	0.	0.	0.	0.	0.	0.	-2.1×10^{-1}
FDP	0.	1.8×10^{1}	-3.6×10^{1}	$2.\times10^{-2}$	4.3×10^{-1}	0.	0.	0.	0.	0.	0.	2.1×10^{-1}
DHAP	0.	0.	3.6×10^{1}	-1.7×10^{1}	2.9×10^{2}	0.	0.	0.	0.	0.	0.	0.
GAP	0.	0.	3.6×10^{1}	1.6×10^{1}	-4.4×10^{2}	9.4×10^{-1}	6.1×10^{-4}	6.1×10^{-4}	6.1×10^{-4}	6.1×10^{-4}	0.	0.
1,3DPG	0.	0.	0.	0.	1.5×10^{2}	$-2.\times10^{6}$	5.5×10^{3}	-6.1×10^{-4}	-6.1×10^{-4}	-6.1×10^{-4}	0.	1.1×10^{3}
3PG	0.	0.	0.	0.	0.	$2.\times10^{6}$	-7.4×10^{3}	1.3×10^{4}	0.	0.	0.	-1.1×10^{3}
2PG	0.	0.	0.	0.	0.	0.	$2.\times10^{3}$	-1.3×10^{4}	8.1×10^{-2}	0.	0.	0.
PEP	0.	0.	0.	0.	0.	0.	0.	8.1×10^{1}	-4.8×10^{1}	2.4×10^{-1}	0.	2.1
PYR	0.	0.	0.	0.	0.	-3.9×10^{1}	-3.9×10^{1}	-3.9×10^{1}	9.	-2.7×10^{2}	1.5×10^{-1}	-2.1
LAC	0.	0.	0.	0.	0.	3.9×10^{1}	3.9×10^{1}	3.9×10^{1}	3.9×10^{1}	2.7×10^{2}	-5.2	0.
ATP	$1.\times10^{-4}$	-1.8×10^{1}	3.7×10^{-3}	0.	0.	$2.\times10^{6}$	-5.5×10^{3}	0.	4.8×10^{1}	-2.4×10^{-1}	0.	-1.1×10^{3}

G

THE JACOBIAN IN TERMS OF FLUXES: J_V

	HK	PGI	PFK	ALD	TPI	GAPDH	PGK	PGM	EN	PK	LDH	LEX	ATPase
HK	-2.1×10^{-1}	$1.\times10^{-4}$	-2.1×10^{-1}	0.	0.	0.	2.1×10^{-1}	0.	0.	2.1×10^{-1}	0.	0.	-2.1×10^{-1}
PGI	2.9×10^{4}	$-1.\times10^{5}$	7.1×10^{4}	0.	0.	0.	0.	0.	0.	0.	0.	0.	0.
PFK	-2.1×10^{-1}	1.8×10^{1}	-1.9×10^{1}	3.7×10^{-3}	0.	0.	2.1×10^{-1}	0.	0.	2.1×10^{-1}	0.	0.	-2.1×10^{-1}
ALD	0.	0.	3.6×10^{1}	-3.7×10^{1}	-4.1×10^{-1}	4.3×10^{-1}	0.	0.	0.	0.	0.	0.	0.
TPI	0.	0.	0.	-2.7×10^{2}	-3.1×10^{2}	2.9×10^{2}	0.	0.	0.	0.	0.	0.	0.
GAPDH	0.	0.	0.	1.5×10^{2}	1.5×10^{2}	-1.5×10^{2}	9.4×10^{-3}	0.	0.	0.	6.1×10^{-4}	0.	0.
PGK	1.1×10^{3}	0.	1.1×10^{3}	0.	0.	$2.\times10^{6}$	$-2.\times10^{6}$	5.5×10^{3}	0.	-1.1×10^{3}	0.	0.	1.1×10^{3}
PGM	0.	0.	0.	0.	0.	0.	$2.\times10^{3}$	-1.5×10^{4}	1.3×10^{4}	0.	0.	0.	0.
EN	0.	0.	0.	0.	0.	0.	0.	8.1×10^{1}	-8.1×10^{1}	8.1×10^{-2}	0.	0.	0.
PK	2.1	0.	2.1	0.	0.	0.	-2.1	0.	4.8×10^{1}	-5.1×10^{1}	2.4×10^{-1}	0.	2.1
LDH	0.	0.	0.	0.	0.	3.9×10^{1}	0.	0.	0.	2.3×10^{2}	-2.7×10^{2}	1.5×10^{-1}	0.
LEX	0.	0.	0.	0.	0.	0.	0.	0.	0.	0.	5.1	-5.1	0.
ATPase	-4.2×10^{-1}	0.	-4.2×10^{-1}	0.	0.	0.	4.2×10^{-1}	0.	0.	4.2×10^{-1}	0.	0.	-4.2×10^{-1}

TIME SCALE HIERARCHY

FROM J_X

Time Scales (hrs)	G6P	F6P	FDP	DHAP	GAP	DPG13	PG3	PG2	PEP	PYR	LAC	ATP
4.95978×10^{-7}	0	0	0	0	0	-1.	0	0	0	0	0	0
9.9213×10^{-6}	-0.41	1.	0	0	0	0	0	0	0	0	0	0
0.0000651335	0	0	0	0	0	0.15	0.15	-1.	0	0	0	0
0.00222678	0	0	0.08	0.04	-1.	0	0	0	0	0	0	0
0.00368113	0	0	0.02	0.01	-0.13	-0.16	-0.15	-0.15	0.04	-1.	0	-0.01
0.0198252	-0.02	-0.02	0.11	0.04	-0.09	-0.3	-0.26	-0.25	1.	0	0	-0.04
0.0276334	0.17	0.17	-1.	0	0	0	-0.01	-0.01	0.02	0	0	0.01
0.104852	-1.	-1.	0.78	0.4	0.17	-0.29	-0.28	-0.27	-0.02	0	0	-0.02
0.141642	1.	1.	-0.32	-0.16	-0.09	0.05	0.04	0.04	0.01	0	0	0.01
0.188046	-1.	-1.	0	0	0	0	0	0	0	0	0	0
0.197903	1.	1.	0.05	0.02	0.02	0	0	0	0	0	0	0
2668.44	0.75	0.75	1.	0.5	0.5	0.5	0.25	0.25	0.25	0	0	0.25

S

FROM J_V

Time Scales (hrs)	HK	PGI	PFK	ALD	TPI	GAPDH	PGK	PGM	EN	PK	LDH	LEX	ATPase
4.95978×10^{-7}	-0.001	0	-0.001	0	0	-0.997	1.	-0.003	0	0.001	0	0	-0.001
9.9213×10^{-6}	-0.291	1.	-0.709	0	0	0	0	0	0	0	0	0	0
0.0000651335	0	0	0	-0.001	-0.001	0.129	-0.001	-1.	0.873	0	0	0	0
0.00222678	-0.001	0	0.081	-1.	-0.992	0.956	0	0	0	0	0	0	0
0.00368113	0.007	0	0.026	-0.132	-0.13	-0.03	0	0.001	0.184	-1.	0.953	-0.001	0.008
0.0198252	0.02	0	0.138	-0.123	-0.101	-0.173	0	0.005	1.	-0.833	-0.001	0	0.035
0.0276334	0.143	0	-1.	0.85	-0.002	-0.002	0	0	0.024	-0.013	0	0	-0.004
0.104852	-0.548	0	1.	-0.114	-0.13	-0.258	0	0.001	0.141	0.003	0	0	0.01
0.141642	0.746	0	-1.	0.047	0.052	0.105	0	0	-0.019	-0.001	0	0	-0.008
0.188046	-1.	0	0.999	0	0	0	0	0	0	0	0	0	0
0.197903	1.	0	-0.947	-0.007	-0.007	-0.015	0	0	-0.002	0	0	-0.005	0.002
2668.44	1.	0	0	0	0	0	0	0	0	0	0	0	-0.5

Figure 6.4: The Jacobian and modal matrices for the mass action description of glycolysis.

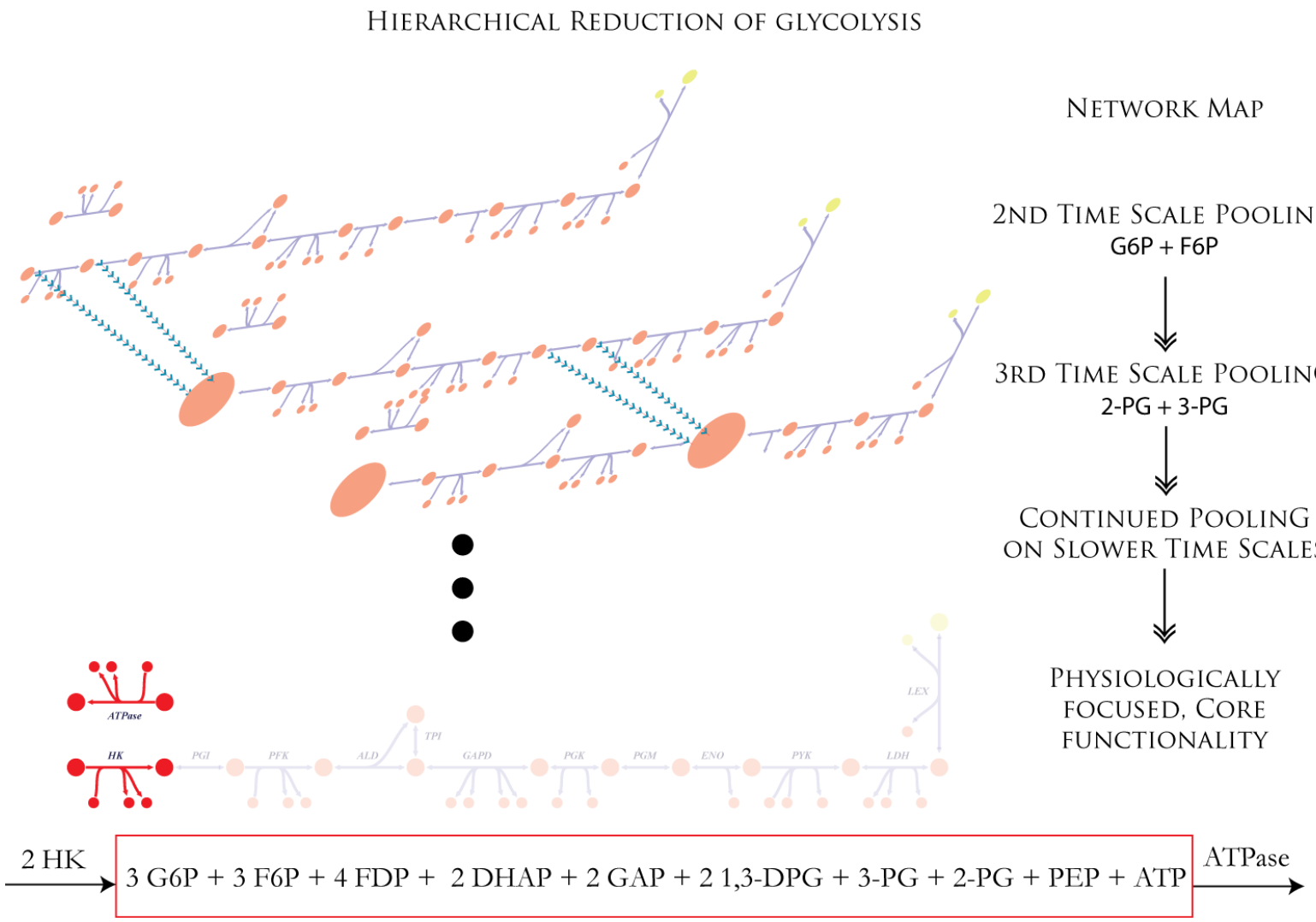

Figure 6.5: Hierarchical decomposition of the mass action glycolytic network.

Table 6.1: Dimensions of mass action glycolysis.
The dimensions of the stoichiometric and gradient matrices, along with their ranks and sizes of their null spaces for the regulated mass action glycolytic model.

	Rows	Columns	Rank	Left Null	Right Null
Stoichiometric matrix	12	13	12	0	1
Gradient matrix	13	12	12	1	0

is also highlighted for this particular network, explicitly showing how the mathematical similarity between the stoichiometric and gradient matrices is immediately apparent through inspection of the structures alone.

Figure 6.4 explicitly shows the Jacobian matrices and how one maps from the flux to the concentration Jacobians. The modal structure for this network is exceedingly clear and visually illustrated in Figure 6.5. Moving from the very fast time scales to the slower ones, one observes the well-known examples of pool formation between hexose phosphates (HP) and phosphoglycerates (PG). With successive removal of time scales (modes), more and more of the metabolites begin to form aggregate variables and move together in a concerted fashion at fixed ratios. For glycolysis alone the successive aggregation of chemical moieties (i.e. HP, PG) culminates in, on the slowest time scale, the formation of a physiologically meaningful pool that represents the sum of high-energy phosphate bonds found in the glycolytic intermediates (i.e. their ATP equivalents). The last row of $\mathbf{M}^{-1}$ for $\mathbf{J}_v$ shows that this pool is moved by hexokinase as the input and ATPase as the output The modal matrices investigated in Chapter 5 were much more difficult to interpret and were dependent on involved algorithmic approaches (Chapter 4) to elucidate the structure. As alluded to earlier, this is because as the size of networks increase and the non-integer entries in $\mathbf{G}$ which tends to be an ill-conditioned matrix, interactions become ore tightly tied together.

Table 6.2: Dimensions of mass action red blood cell.
The dimensions of the stoichiometric and gradient matrices, along with their ranks and sizes of their null spaces for the regulated mass action red blood cell model.

	Rows	Columns	Rank	Left Null	Right Null
Stoichiometric matrix	36	42	33	3	9
Gradient matrix	42	36	36	6	0

6.2 Mass Action Model of the Human Red Blood Cell

The approach described in Figure 6.2 was applied to a full model of human red blood cell metabolism (See Appendix Figure .2 and Table .1). Steady state concentrations fluxes and concentrations [42] reported in the literature were used in conjunction with equilibrium constants reported in the literature [41, 78]. A map of the network is shown in Figure 6.6 and the dimensions of the network along with the size of the subspaces are shown in Table 6.2. As expected from the size of the left null space, there are three conserved pools of metabolites, the sum of the phosphates, the NAD moiety, and the NADP moiety 6.7. The amount of glutathione in the network is also conserved, however since the dimeric form is not included as a dynamic variable in the network, it does not appear in the left null space. This network has nine co-sets, which coincidentally is the same size as the right null space. However as discussed in Chapter 2, these co-sets are not independent of one another, and reactions outside of the co-set need to be specified in order to converge to a unique solution. The tree-plot for the reaction dependencies in the network is shown in Figure 6.8.

The gradient matrix for the network has similar characteristics to the other gradient matrices described thus far (Figure 6.9). The Jacobian matrices are shown in Figures 6.10 and 6.11. In order to further clean the structure of the network, the flux Jacobian was rotated obliquely, as described in Chapter 5. There is good time scale separation (about 20 milliseconds to 5 hours), although the high and low end are not as large as the full red cell model. Part of the reason for this is that sodium and potassium were not included in this model and it was the potassium

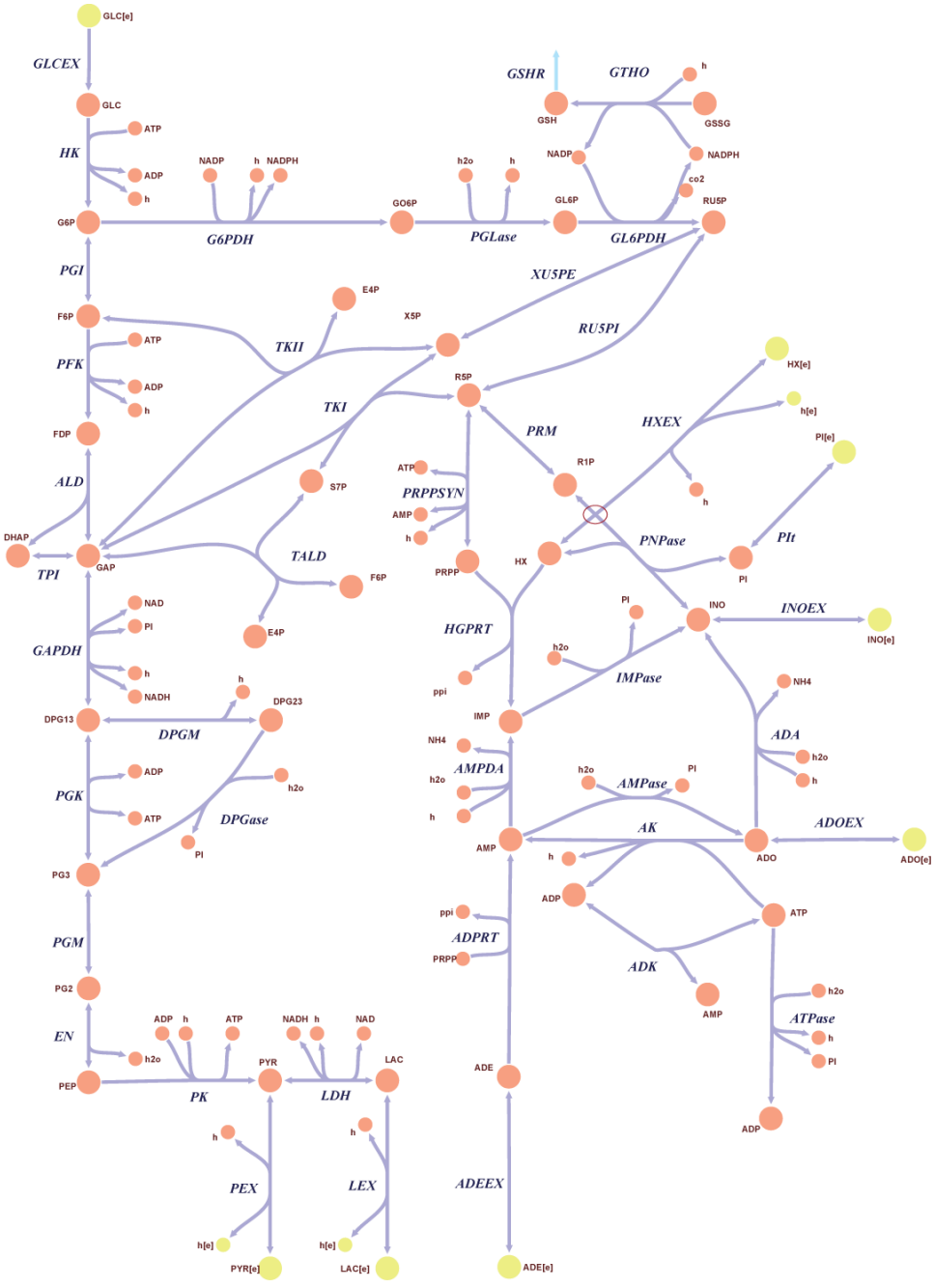

Figure 6.6: Network map of a model of red cell metabolism.

	HK	PGI	PFK	ALD	TPI	GAPDH	PGK	DPGM	DPGase	PGM	EN	PK	LDH	AMPase	ADA	AK	ADK	AMPDA	ATPase	ADPRT	G6PDH	PGLase	GL6PDH	GSSGR	GSHR	RU5PI	XU5PE	TKI	TKII	TALD	IMPase	PNPase	PRM	PRPPSYN	HGPRT	GLCEX	PEX	LEX	HXEX	ADEEX	ADOEX	INOEX
GLC	-1	0	0	0	0	0	0	0	0	0	0	0	0	0	0	0	0	0	0	0	0	0	0	0	0	0	0	0	0	0	0	0	0	0	1	0	0	0	0	0	0
G6P	1	-1	0	0	0	0	0	0	0	0	0	0	0	0	0	0	0	0	0	0	-1	0	0	0	0	0	0	0	0	0	0	0	0	0	0	0	0	0	0	0	0
F6P	0	1	-1	0	0	0	0	0	0	0	0	0	0	0	0	0	0	0	0	0	0	0	0	0	0	0	0	0	1	1	0	0	0	0	0	0	0	0	0	0	0
FDP	0	0	1	-1	0	0	0	0	0	0	0	0	0	0	0	0	0	0	0	0	0	0	0	0	0	0	0	0	0	0	0	0	0	0	0	0	0	0	0	0	0
DHAP	0	0	0	1	-1	0	0	0	0	0	0	0	0	0	0	0	0	0	0	0	0	0	0	0	0	0	0	0	0	0	0	0	0	0	0	0	0	0	0	0	0
GAP	0	0	0	1	1	-1	0	0	0	0	0	0	0	0	0	0	0	0	0	0	0	0	0	0	0	0	0	1	1	-1	0	0	0	0	0	0	0	0	0	0	0
DPG13	0	0	0	0	0	1	-1	-1	0	0	0	0	0	0	0	0	0	0	0	0	0	0	0	0	0	0	0	0	0	0	0	0	0	0	0	0	0	0	0	0	0
DPG23	0	0	0	0	0	0	0	1	-1	0	0	0	0	0	0	0	0	0	0	0	0	0	0	0	0	0	0	0	0	0	0	0	0	0	0	0	0	0	0	0	0
PG3	0	0	0	0	0	0	1	0	1	-1	0	0	0	0	0	0	0	0	0	0	0	0	0	0	0	0	0	0	0	0	0	0	0	0	0	0	0	0	0	0	0
PG2	0	0	0	0	0	0	0	0	0	1	-1	0	0	0	0	0	0	0	0	0	0	0	0	0	0	0	0	0	0	0	0	0	0	0	0	0	0	0	0	0	0
PEP	0	0	0	0	0	0	0	0	0	0	1	-1	0	0	0	0	0	0	0	0	0	0	0	0	0	0	0	0	0	0	0	0	0	0	0	0	0	0	0	0	0
NAD	0	0	0	0	0	-1	0	0	0	0	0	0	1	0	0	0	0	0	0	0	0	0	0	0	0	0	0	0	0	0	0	0	0	0	0	0	0	0	0	0	0
PYR	0	0	0	0	0	0	0	0	0	0	0	1	-1	0	0	0	0	0	0	0	0	0	0	0	0	0	0	0	0	0	0	0	0	0	0	0	-1	0	0	0	0
LAC	0	0	0	0	0	0	0	0	0	0	0	0	1	0	0	0	0	0	0	0	0	0	0	0	0	0	0	0	0	0	0	0	0	0	0	0	0	-1	0	0	0
NADH	0	0	0	0	0	1	0	0	0	0	0	0	-1	0	0	0	0	0	0	0	0	0	0	0	0	0	0	0	0	0	0	0	0	0	0	0	0	0	0	0	0
NADP	0	0	0	0	0	0	0	0	0	0	0	0	0	0	0	0	0	0	0	0	-1	0	-1	1	0	0	0	0	0	0	0	0	0	0	0	0	0	0	0	0	0
GL6P	0	0	0	0	0	0	0	0	0	0	0	0	0	0	0	0	0	0	0	0	1	-1	0	0	0	0	0	0	0	0	0	0	0	0	0	0	0	0	0	0	0
GO6P	0	0	0	0	0	0	0	0	0	0	0	0	0	0	0	0	0	0	0	0	0	1	-1	0	0	0	0	0	0	0	0	0	0	0	0	0	0	0	0	0	0
NADPH	0	0	0	0	0	0	0	0	0	0	0	0	0	0	0	0	0	0	0	0	1	0	1	-1	0	0	0	0	0	0	0	0	0	0	0	0	0	0	0	0	0
GSH	0	0	0	0	0	0	0	0	0	0	0	0	0	0	0	0	0	0	0	0	0	0	2	-1	0	0	0	0	0	0	0	0	0	0	0	0	0	0	0	0	0
RU5P	0	0	0	0	0	0	0	0	0	0	0	0	0	0	0	0	0	0	0	0	0	0	1	0	0	-1	-1	0	0	0	0	0	0	0	0	0	0	0	0	0	0
R5P	0	0	0	0	0	0	0	0	0	0	0	0	0	0	0	0	0	0	0	0	0	0	0	1	0	-1	0	0	0	0	1	-1	0	0	0	0	0	0	0	0	0
X5P	0	0	0	0	0	0	0	0	0	0	0	0	0	0	0	0	0	0	0	0	0	0	0	0	1	-1	-1	0	0	0	0	0	0	0	0	0	0	0	0	0	0
S7P	0	0	0	0	0	0	0	0	0	0	0	0	0	0	0	0	0	0	0	0	0	0	0	0	0	1	0	-1	0	0	0	0	0	0	0	0	0	0	0	0	0
E4P	0	0	0	0	0	0	0	0	0	0	0	0	0	0	0	0	0	0	0	0	0	0	0	0	0	0	-1	1	0	0	0	0	0	0	0	0	0	0	0	0	0
ADO	0	0	0	0	0	0	0	0	0	0	0	0	0	1	-1	-1	0	0	0	0	0	0	0	0	0	0	0	0	0	0	0	0	0	0	0	0	0	0	0	0	-1	0
Phosi	0	0	0	0	0	-1	0	0	1	0	0	0	0	1	0	0	0	0	1	2	0	0	0	0	0	0	0	0	0	0	1	-1	0	0	2	0	0	0	0	0	0
AMP	0	0	0	0	0	0	0	0	0	0	0	0	0	-1	0	1	1	-1	0	1	0	0	0	0	0	0	0	0	0	0	0	0	0	1	0	0	0	0	0	0	0
ADP	1	0	1	0	0	0	-1	0	0	0	0	-1	0	0	0	1	-2	0	1	0	0	0	0	0	0	0	0	0	0	0	0	0	0	0	0	0	0	0	0	0	0
ATP	-1	0	-1	0	0	0	1	0	0	0	0	1	0	0	0	-1	1	0	-1	0	0	0	0	0	0	0	0	0	0	0	0	0	0	0	0	-1	0	0	0	0	0
PRPP	0	0	0	0	0	0	0	0	0	0	0	0	0	0	0	0	0	0	0	-1	0	0	0	0	0	0	0	0	0	0	0	0	0	1	-1	0	0	0	0	0	0
IMP	0	0	0	0	0	0	0	0	0	0	0	0	0	0	0	0	0	1	0	0	0	0	0	0	0	0	0	0	0	0	0	-1	0	0	1	0	0	0	0	0	0
INO	0	0	0	0	0	0	0	0	0	0	0	0	0	0	1	0	0	0	0	0	0	0	0	0	0	0	0	0	0	1	-1	0	0	0	0	0	0	0	0	0	-1
HX	0	0	0	0	0	0	0	0	0	0	0	0	0	0	0	0	0	0	0	0	0	0	0	0	0	0	0	0	0	0	1	0	0	-1	0	0	0	-1	0	0	0
R1P	0	0	0	0	0	0	0	0	0	0	0	0	0	0	0	0	0	0	0	0	0	0	0	0	0	0	0	0	0	0	1	-1	0	0	0	0	0	0	0	0	0
ADE	0	0	0	0	0	0	0	0	0	0	0	0	0	0	0	0	0	0	0	-1	0	0	0	0	0	0	0	0	0	0	0	0	0	0	0	0	0	0	0	-1	0	0

Left Null Space Pools

2 ADP + AMP + 3 ATP + DHAP + 2 DPG13 + 2 DPG23 + E4P + F6P + 2 FDP + G6P + GAP + GL6P + GO6P + IMP + PEP + PG2 + PG3 + Phosi + 3 PRPP + R1P + R5P + RU5P + S7P + X5P

NAD + NADH

NADP + NADPH

Co-sets

GLCEX + HK

ALD + PFK + TPI

EN + GAPDH + LDH + LEX + PGM + PK

DPGase + DPGM

ADK + PRPPSYN

ADEEX + ADPRT

G6PDH + GL6PDH + GSHR + GSSGR + PGLase

TALD + TKI + TKII + XU5PE

PNPase + PRM

Figure 6.7: Stoichiometric matrix, left null space pools, and co-sets for the mass action model of the human red blood cell.

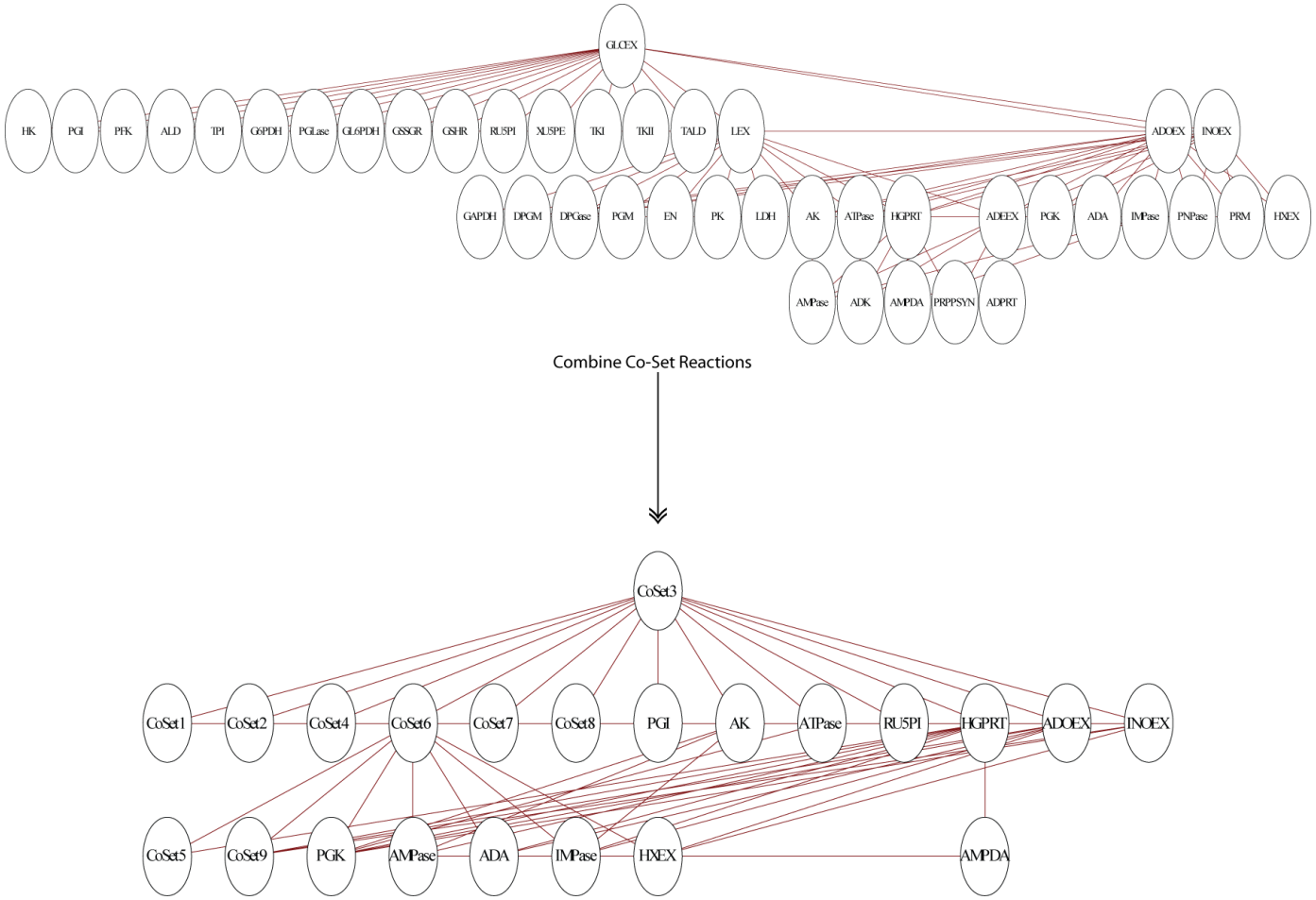

Figure 6.8: Red blood cell null space tree plots.

The tree-plots showing the null space dependence of the reactions for the mass action model of the red blood cell. The lower figure condenses the network according to the co-sets (numbered according to Figure 6.7.

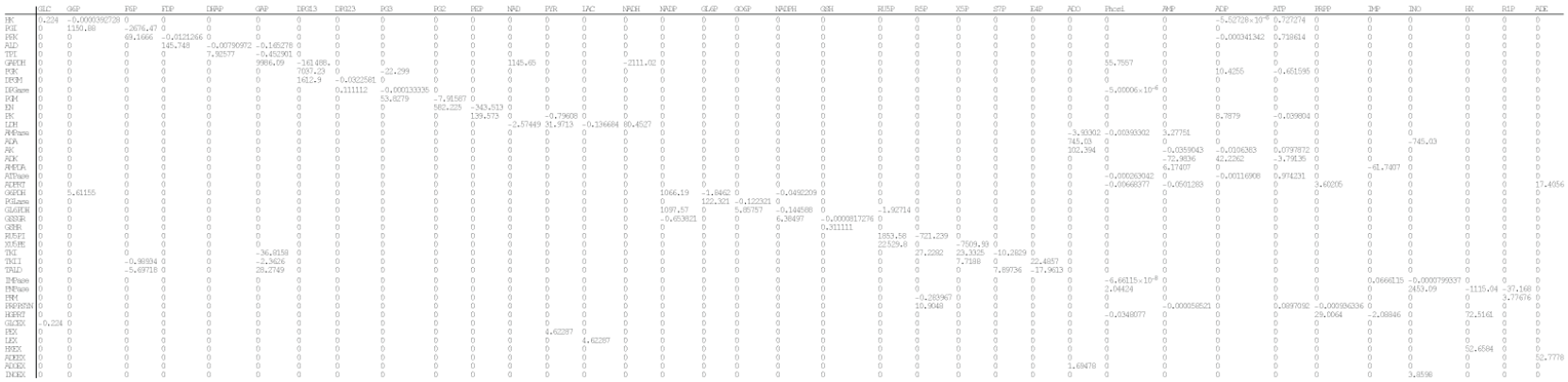

	GLC	G6P	F6P	F1P	DHAP	GAP	DPG13	DPG23	PG3	PG2	PEP	NAD	PYR	LAC	NADH	NADP	GL6P	GO6P	NADPH	G3H	RL5P	R5P	X5P	S7P	E4P	ADO	Phcel	AMP	ADP	ATP	PRPP	IMP	INO	HX	R1P	ADE
HK	0.224	-0.0000392728	0	0	0	0	0	0	0	0	0	0	0	0	0	0	0	0	0	0	0	0	0	0	0	0	0	0	-5.52728×10^{-6}	0.727274	0	0	0	0	0	0
PGI	0	1150.88	-2676.47	0	0	0	0	0	0	0	0	0	0	0	0	0	0	0	0	0	0	0	0	0	0	0	0	0	0	0	0	0	0	0	0	0
PFK	0	0	69.1666	-0.0121266	0	0	0	0	0	0	0	0	0	0	0	0	0	0	0	0	0	0	0	0	0	0	0	0	-0.000341342	0.719614	0	0	0	0	0	0
ALD	0	0	0	145.748	-0.00790972	-0.165278	0	0	0	0	0	0	0	0	0	0	0	0	0	0	0	0	0	0	0	0	0	0	0	0	0	0	0	0	0	0
TPI	0	0	0	0	7.92577	-5.45290	0	0	0	0	0	0	0	0	0	0	0	0	0	0	0	0	0	0	0	0	0	0	0	0	0	0	0	0	0	0
GAPDH	0	0	0	0	0	9986.09	-161486.	0	0	0	0	1145.65	0	0	-2111.02	0	0	0	0	0	0	0	0	0	0	0	55.7557	0	0	0	0	0	0	0	0	0
PGK	0	0	0	0	0	0	7037.23	0	-22.299	0	0	0	0	0	0	0	0	0	0	0	0	0	0	0	0	0	0	0	10.4255	-0.651595	0	0	0	0	0	0
PGDH	0	0	0	0	0	0	1612.9	-0.0322581	0	0	0	0	0	0	0	0	0	0	0	0	0	0	0	0	0	0	0	0	0	0	0	0	0	0	0	0
DPGase	0	0	0	0	0	0	0	0.111112	-0.000133035	0	0	0	0	0	0	0	0	0	0	0	0	0	0	0	0	0	0	-5.80006×10^{-6}	0	0	0	0	0	0	0	0
PGM	0	0	0	0	0	0	0	0	53.8279	-7.91587	0	0	0	0	0	0	0	0	0	0	0	0	0	0	0	0	0	0	0	0	0	0	0	0	0	0
EN	0	0	0	0	0	0	0	0	0	585.225	-343.513	0	0	0	0	0	0	0	0	0	0	0	0	0	0	0	0	0	0	0	0	0	0	0	0	0
PK	0	0	0	0	0	0	0	0	0	0	139.573	0	-0.79608	0	0	0	0	0	0	0	0	0	0	0	0	0	0	0	8.7879	-0.039804	0	0	0	0	0	0
LDH	0	0	0	0	0	0	0	0	0	0	0	-2.57449	31.9713	-0.136684	80.4527	0	0	0	0	0	0	0	0	0	0	0	0	0	0	0	0	0	0	0	0	0
AK6ase	0	0	0	0	0	0	0	0	0	0	0	0	0	0	0	0	0	0	0	0	0	0	0	0	0	0	-3.93302	-0.00393302	3.27751	0	0	0	0	0	0	0
ADA	0	0	0	0	0	0	0	0	0	0	0	0	0	0	0	0	0	0	0	0	0	0	0	0	0	0	745.03	0	0	0	0	0	-745.03	0	0	0
AK	0	0	0	0	0	0	0	0	0	0	0	0	0	0	0	0	0	0	0	0	0	0	0	0	0	0	102.394	0	-0.0369043	-0.0106383	0.0797872	0	0	0	0	0
ADK	0	0	0	0	0	0	0	0	0	0	0	0	0	0	0	0	0	0	0	0	0	0	0	0	0	0	0	0	-72.9836	42.2262	-3.79135	0	0	0	0	0
AMPDA	0	0	0	0	0	0	0	0	0	0	0	0	0	0	0	0	0	0	0	0	0	0	0	0	0	0	0	0	6.17407	0	0	0	-61.7407	0	0	0
ATPase	0	0	0	0	0	0	0	0	0	0	0	0	0	0	0	0	0	0	0	0	0	0	0	0	0	0	0	-0.0050939042	0	-0.0011698	0.974231	0	0	0	0	0
ADPRT	0	0	0	0	0	0	0	0	0	0	0	0	0	0	0	0	0	0	0	0	0	0	0	0	0	0	0	-0.00668377	-0.0501283	0	0	3.60205	0	0	0	17.4656
G6PDH	0	5.61155	0	0	0	0	0	0	0	0	0	0	0	0	0	1066.19	-1.8462	0	-0.0492209	0	0	0	0	0	0	0	0	0	0	0	0	0	0	0	0	0
PGLase	0	0	0	0	0	0	0	0	0	0	0	0	0	0	0	0	122.321	-0.122321	0	0	0	0	0	0	0	0	0	0	0	0	0	0	0	0	0	0
GLUDH	0	0	0	0	0	0	0	0	0	0	0	0	0	0	0	1097.57	0	5.85757	-0.144588	0	-1.92714	0	0	0	0	0	0	0	0	0	0	0	0	0	0	0
GSSGR	0	0	0	0	0	0	0	0	0	0	0	0	0	0	0	-0.653821	0	0	6.38497	-0.0000817276	0	0	0	0	0	0	0	0	0	0	0	0	0	0	0	0
GSHS	0	0	0	0	0	0	0	0	0	0	0	0	0	0	0	0	0	0	0	0.311111	0	0	0	0	0	0	0	0	0	0	0	0	0	0	0	0
R5PI	0	0	0	0	0	0	0	0	0	0	0	0	0	0	0	0	0	0	0	0	1853.58	-721.239	0	0	0	0	0	0	0	0	0	0	0	0	0	0
X5PE	0	0	0	0	0	0	0	0	0	0	0	0	0	0	0	0	0	0	0	0	22529.8	0	-7509.93	0	0	0	0	0	0	0	0	0	0	0	0	0
TKT	0	0	0	0	0	-36.8158	0	0	0	0	0	0	0	0	0	0	0	0	0	0	0	27.2282	23.3025	-10.2829	0	0	0	0	0	0	0	0	0	0	0	0
TKT1	0	0	-0.98934	0	0	-2.3626	0	0	0	0	0	0	0	0	0	0	0	0	0	0	0	0	7.7188	0	22.4857	0	0	0	0	0	0	0	0	0	0	0
TALD	0	0	-5.69718	0	0	28.2749	0	0	0	0	0	0	0	0	0	0	0	0	0	0	0	0	0	7.89736	-17.9613	0	0	0	0	0	0	0	0	0	0	0
IMPase	0	0	0	0	0	0	0	0	0	0	0	0	0	0	0	0	0	0	0	0	0	0	0	0	0	0	-6.66115×10^{-8}	0	0	0	0	0.0666115	-0.0000799337	0	0	0
PMPase	0	0	0	0	0	0	0	0	0	0	0	0	0	0	0	0	0	0	0	0	0	0	0	0	0	0	2.04424	0	0	0	2453.09	-1135.04	-37.168	0	0	0
PRM	0	0	0	0	0	0	0	0	0	0	0	0	0	0	0	0	0	0	0	0	0	-0.283967	0	0	0	0	0	0	0	0	0	0	0	3.77676	0	0
PRPPSN	0	0	0	0	0	0	0	0	0	0	0	0	0	0	0	0	0	0	0	0	0	10.9048	0	0	0	0	0	-0.000058521	0	0.0897092	-0.000956336	0	0	0	0	0
HGPRT	0	0	0	0	0	0	0	0	0	0	0	0	0	0	0	0	0	0	0	0	0	0	0	0	0	0	-0.0348077	0	0	0	29.0064	-2.08846	0	72.5161	0	0
GLCDC	-0.224	0	0	0	0	0	0	0	0	0	0	0	0	0	0	0	0	0	0	0	0	0	0	0	0	0	0	0	0	0	0	0	0	0	0	0
PDC	0	0	0	0	0	0	0	0	0	0	0	0	4.62287	0	0	0	0	0	0	0	0	0	0	0	0	0	0	0	0	0	0	0	0	0	0	0
LDX	0	0	0	0	0	0	0	0	0	0	0	0	0	4.62287	0	0	0	0	0	0	0	0	0	0	0	0	0	0	0	0	0	0	0	0	0	0
HXGX	0	0	0	0	0	0	0	0	0	0	0	0	0	0	0	0	0	0	0	0	0	0	0	0	0	0	0	0	0	0	0	0	0	52.6584	0	0
AUXDC	0	0	0	0	0	0	0	0	0	0	0	0	0	0	0	0	0	0	0	0	0	0	0	0	0	0	0	0	0	0	0	0	0	0	52.7778	0
ADDEX	0	0	0	0	0	0	0	0	0	0	0	0	0	0	0	0	0	0	0	0	0	0	0	0	0	1.69478	0	0	0	0	0	0	0	0	0	0
INDEX	0	0	0	0	0	0	0	0	0	0	0	0	0	0	0	0	0	0	0	0	0	0	0	0	0	0	0	0	0	0	0	0	3.8598	0	0	0

Figure 6.9: Gradient matrix for the mass action model of the human red blood cell.

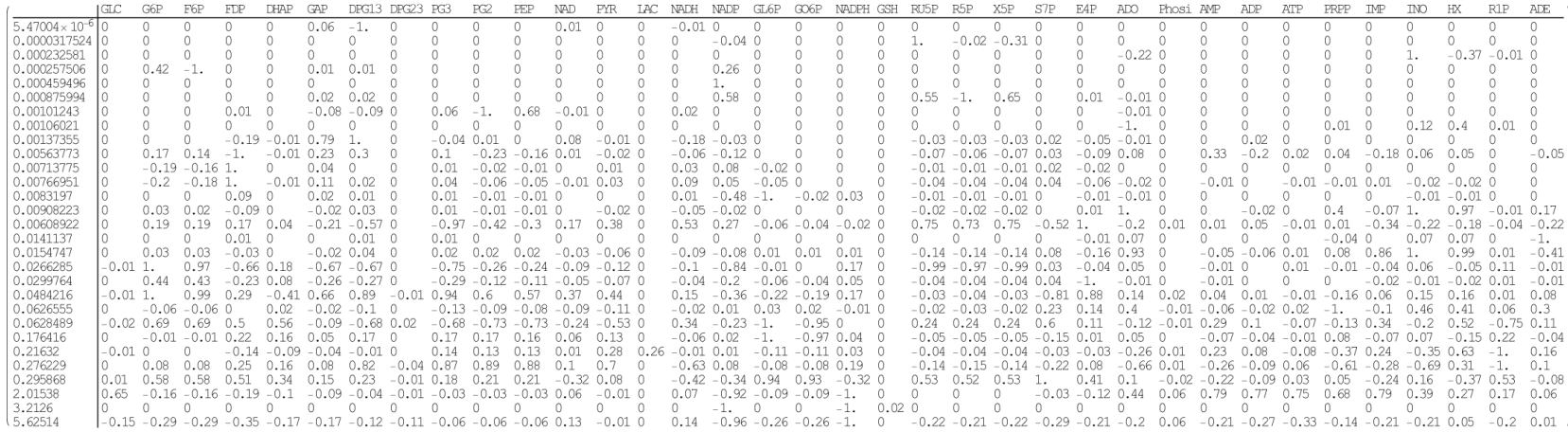

	GLC	G6P	F6P	FDP	DHAP	GAP	DPG13	DPG23	PG3	PG2	PEP	NAD	PYR	LAC	NADH	NADP	GL6P	GO6P	NADPH	GSH	RU5P	R5P	X5P	S7P	E4P	ADO	Phosi	AMP	ADP	ATP	PRPP	IMP	INO	HX	R1P	ADE
5.47004×10^{-6}	0	0	0	0	0	0.06	-1.	0	0	0	0	0.01	0	0	-0.01	0	0	0	0	0	0	0	0	0	0	0	0	0	0	0	0	0	0	0	0	0
0.0000317524	0	0	0	0	0	0	0	0	0	0	0	0	0	0	0	-0.04	0	0	0	0	1.	-0.02	-0.31	0	0	0	0	0	0	0	0	0	0	0	0	0
0.000232581	0	0	0	0	0	0	0	0	0	0	0	0	0	0	0	0	0	0	0	0	0	0	0	0	0	-0.22	0	0	0	0	0	0	1.	-0.37	-0.01	0
0.000257506	0	0.42	-1.	0	0	0.01	0.01	0	0	0	0	0	0	0	0	0.26	0	0	0	0	0	0	0	0	0	0	0	0	0	0	0	0	0	0	0	0
0.000459496	0	0	0	0	0	0	0	0	0	0	0	0	0	0	0	1.	0	0	0	0	0	0	0	0	0	0	0	0	0	0	0	0	0	0	0	0
0.000875994	0	0	0	0	0	0.02	0.02	0	0	0	0	0	0	0	0	0.58	0	0	0	0	0.55	-1.	0.65	0	0.01	-0.01	0	0	0	0	0	0	0	0	0	0
0.00101243	0	0	0	0.01	0	-0.08	-0.09	0	0.06	-1.	0.68	-0.01	0	0	0.02	0	0	0	0	0	0	0	0	0	0	-0.01	0	0	0	0	0	0	0	0	0	0
0.00106021	0	0	0	0	0	0	0	0	0	0	0	0	0	0	0	0	0	0	0	0	0	0	0	0	0	-1.	0	0	0	0	0.01	0	0.12	0.4	0.01	0
0.00137355	0	0	0	-0.19	-0.01	0.79	1.	0	-0.04	0.01	0	0.08	-0.01	0	-0.18	-0.03	0	0	0	0	-0.03	-0.03	-0.03	0.02	-0.05	-0.01	0	0	0.02	0	0	0	0	0	0	0
0.00563773	0	0.17	0.14	-1.	-0.01	0.23	0.3	0	0.1	-0.23	-0.16	0.01	-0.02	0	-0.06	-0.12	0	0	0	0	-0.07	-0.06	-0.07	0.03	-0.09	0.08	0	0.33	-0.2	0.02	0.04	-0.18	0.06	0.05	0	-0.05
0.00713775	0	-0.19	-0.16	1.	0	0.04	0	0	0.01	-0.02	-0.01	0	0.01	0	0.03	0.08	-0.02	0	0	0	-0.01	-0.01	-0.01	0.02	-0.02	0	0	0	0	0	0	0	0	0	0	0
0.00766951	0	-0.2	-0.18	1.	-0.01	0.11	0.02	0	0.04	-0.06	-0.05	-0.01	0.03	0	0.09	0.05	-0.05	0	0	0	-0.04	-0.04	-0.04	0.04	-0.06	-0.02	0	-0.01	0	-0.01	-0.01	0.01	-0.02	-0.02	0	0
0.0083197	0	0	0	0.09	0	0.02	0.01	0	0.01	-0.01	-0.01	0	0	0	0.01	-0.48	-1.	-0.02	0.03	0	-0.01	-0.01	-0.01	0	-0.01	-0.01	0	0	0	0	0	-0.01	-0.01	0	0	
0.00908223	0	0.03	0.02	-0.09	0	-0.02	0.03	0	0.01	-0.01	-0.01	0	-0.02	0	-0.05	-0.02	0	0	0	0	-0.02	-0.02	-0.02	0	0.01	1.	0	0	-0.02	0	0.4	-0.07	1.	0.97	-0.01	0.17
0.00608922	0	0.19	0.19	0.17	0.04	-0.21	-0.57	0	-0.97	-0.42	-0.3	0.17	0.38	0	0.53	0.27	-0.06	-0.04	-0.02	0	0.75	0.73	0.75	-0.52	1.	-0.2	0.01	0.01	0.05	-0.01	0.01	-0.34	-0.22	-0.18	-0.04	-0.22
0.0141137	0	0	0	0.01	0	0	0.01	0	0.01	0	0	0	0	0	0	0	0	0	0	0	0	0	0	0	-0.01	0.07	0	0	0	0	-0.04	0	0.07	0.07	0	-1.
0.0154747	0	0.03	0.03	-0.03	0	-0.02	0.04	0	0.02	0.02	0.02	-0.03	-0.06	0	-0.09	-0.08	0.01	0.01	0.01	0	-0.14	-0.14	-0.14	0.08	-0.16	0.93	0	-0.05	-0.06	0.01	0.08	0.86	1.	0.99	0.01	-0.41
0.0266285	-0.01	1.	0.97	-0.66	0.18	-0.67	-0.67	0	-0.75	-0.26	-0.24	-0.09	-0.12	0	-0.1	-0.84	-0.01	0	0.17	0	-0.99	-0.97	-0.99	0.03	-0.04	0.05	0	-0.01	0	0.01	-0.01	-0.04	0.06	-0.05	0.11	-0.01
0.0299764	0	0.44	0.43	-0.23	0.08	-0.26	-0.27	0	-0.29	-0.12	-0.11	-0.05	-0.07	0	-0.04	-0.2	-0.06	-0.04	0.05	0	-0.04	-0.04	-0.04	0.04	-1.	-0.01	0	-0.01	0	0	0	-0.02	-0.01	-0.02	0.01	-0.01
0.0484216	-0.01	1.	0.99	0.29	-0.41	0.66	0.89	-0.01	0.94	0.6	0.57	0.37	0.44	0	0.15	-0.36	-0.22	-0.19	0.17	0	-0.03	-0.04	-0.03	-0.81	0.88	0.14	0.02	0.04	0.01	-0.01	-0.16	0.06	0.15	0.16	0.01	0.08
0.0626555	0	-0.06	-0.06	0	0.02	-0.02	-0.1	0	-0.13	-0.09	-0.08	-0.09	-0.11	0	-0.02	0.01	0.03	0.02	-0.01	0	-0.02	-0.03	-0.02	0.23	0.14	0.4	-0.01	-0.06	-0.02	0.02	-1.	-0.1	0.46	0.41	0.06	0.3
0.0628489	-0.02	0.69	0.69	0.5	0.56	-0.09	-0.68	0.02	-0.68	-0.73	-0.73	-0.24	-0.53	0	0.34	-0.23	-1.	-0.95	0	0	0.24	0.24	0.24	0.6	0.11	-0.12	-0.01	0.29	0.1	-0.07	-0.13	0.34	-0.2	0.52	-0.75	0.11
0.176416	0	-0.01	-0.01	0.22	0.16	0.05	0.17	0	0.17	0.17	0.16	0.06	0.13	0	-0.06	0.02	-1.	-0.97	0.04	0	-0.05	-0.05	-0.05	-0.15	0.01	0.05	0	-0.07	-0.04	-0.01	0.08	-0.07	0.07	-0.15	0.22	-0.04
0.21632	-0.01	0	0	-0.14	-0.09	-0.04	-0.01	0	0.14	0.13	0.13	0.01	0.28	0.26	-0.01	0.01	-0.11	-0.11	0.03	0	-0.04	-0.04	-0.04	-0.03	-0.03	-0.26	0.01	0.23	0.08	-0.08	-0.37	0.24	-0.35	0.63	-1.	0.16
0.276229	0	0.08	0.08	0.25	0.16	0.08	0.82	-0.04	0.87	0.89	0.88	0.1	0.7	0	-0.63	0.08	-0.08	-0.08	0.19	0	-0.14	-0.15	-0.14	-0.22	0.08	-0.66	0.01	-0.26	-0.09	0.06	-0.61	-0.28	-0.69	0.31	-1.	0.1
0.295868	0.01	0.58	0.58	0.51	0.34	0.15	0.23	-0.01	0.18	0.21	0.21	-0.32	0.08	0	-0.42	-0.34	0.94	0.93	-0.32	0	0.53	0.52	0.53	1.	0.41	0.1	-0.02	-0.22	-0.09	0.03	0.05	-0.24	0.16	-0.37	0.53	-0.08
2.01538	0.65	-0.16	-0.16	-0.19	-0.1	-0.09	-0.04	-0.01	-0.03	-0.03	-0.03	0.06	-0.01	0	0.07	-0.92	-0.09	-0.09	-1.	0	0	0	0	-0.03	-0.12	0.44	0.06	0.79	0.77	0.75	0.68	0.79	0.39	0.27	0.17	0.06
3.2126	0	0	0	0	0	0	0	0	0	0	0	0	0	0	0	-1.	0	0	-1.	0.02	0	0	0	0	0	0	0	0	0	0	0	0	0	0	0	0
5.62514	-0.15	-0.29	-0.29	-0.35	-0.17	-0.17	-0.12	-0.11	-0.06	-0.06	-0.06	0.13	-0.01	0	0.14	-0.96	-0.26	-0.26	-1.	0	-0.22	-0.21	-0.22	-0.29	-0.21	-0.2	0.06	-0.21	-0.27	-0.33	-0.14	-0.21	-0.21	0.05	-0.2	0.01

Figure 6.10: Metabolite Jacobian for the red cell mass action model.

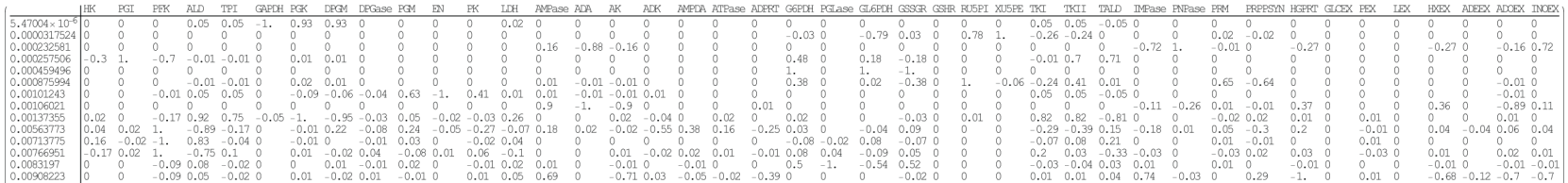

	HK	PGI	PFK	ALD	TPI	GAPDH	PGK	DPGM	DPGase	PGM	EN	PK	LDH	AMPase	ADA	AK	ADK	AMPDA	ATPase	ADPRT	G6PDH	PGLase	GL6PDH	GSSGR	GSHR	RU5PI	XU5PE	TKI	TKII	TALD	TMPase	PNPase	PRM	PRPPSYN	HGPRT	GLCEX	PEX	LEX	HXEX	ADEEX	ADOEX	INOEX
5.47004×10^{-6}	0	0	0	0.05	0.05	-1.	0.93	0.93	0	0	0	0	0.02	0	0	0	0	0	0	0	0	0	0	0	0	0	0.05	0.05	-0.05	0	0	0	0	0	0	0	0	0	0	0
0.0000317524	0	0	0	0	0	0	0	0	0	0	0	0	0	0	0	0	0	0	0	0	-0.03	0	-0.79	0.03	0	0.78	1.	-0.26	-0.24	0	0	0	0.02	-0.02	0	0	0	0	0	0	0
0.000232581	0	0	0	0	0	0	0	0	0	0	0	0	0	0.16	-0.88	-0.16	0	0	0	0	0	0	0	0	0	0	0	0	0	-0.72	1.	-0.01	0	-0.27	0	0	0	-0.27	0	-0.16	0.72
0.000257506	-0.3	1.	-0.7	-0.01	-0.01	0	0.01	0.01	0	0	0	0	0	0	0	0	0	0	0	0	0.48	0	0.18	-0.18	0	0	0	-0.01	0.7	0.71	0	0	0	0	0	0	0	0	0	0	0
0.000459496	0	0	0	0	0	0	0	0	0	0	0	0	0	0	0	0	0	0	0	0	1.	0	1.	-1.	0	0	0	0	0	0	0	0	0	0	0	0	0	0	0	0	0
0.000875994	0	0	0	-0.01	-0.01	0	0.02	0.01	0	0	0	0	0	0.01	-0.01	-0.01	0	0	0	0	0.38	0	0.02	-0.38	0	1.	-0.06	-0.24	0.41	0.01	0	0	0.65	-0.64	0	0	0	0	0	-0.01	0
0.00101243	0	0	-0.01	0.05	0.05	0	-0.09	-0.06	-0.04	0.63	-1.	0.41	0.01	0.01	-0.01	-0.01	0.01	0	0	0	0	0	0	0	0	0	0	0.05	0.05	-0.05	0	0	0	0	0	0	0	0	0	0	-0.01	0
0.00106021	0	0	0	0	0	0	0	0	0	0	0	0	0	0.9	-1.	-0.9	0	0	0	0.01	0	0	0	0	0	0	0	0	0	0	-0.11	-0.26	0.01	-0.01	0.37	0	0	0	0.36	0	-0.89	0.11
0.00137355	0.02	0	-0.17	0.92	0.75	-0.05	-1.	-0.95	-0.03	0.05	-0.02	-0.03	0.26	0	0	0.02	-0.04	0	0.02	0	0.02	0	0	-0.03	0	0.01	0	0.82	0.82	-0.81	0	0	-0.02	0.02	0.01	0	0.01	0	0	0	0.01	0
0.00563773	0.04	0.02	1.	-0.89	-0.17	0	-0.01	0.22	-0.08	0.24	-0.05	-0.27	-0.07	0.18	0.02	-0.02	-0.55	0.38	0.16	-0.25	0.03	0	-0.04	0.09	0	0	0	-0.29	-0.39	0.15	-0.18	0.01	0.05	-0.3	0.2	0	-0.01	0	0.04	-0.04	0.06	0.04
0.00713775	0.16	-0.02	-1.	0.83	-0.04	0	-0.01	0	-0.01	0.03	0	-0.02	0.04	0	0	0	0	0	0	0	-0.08	-0.02	0.08	-0.07	0	0	0	-0.07	0.08	0.21	0	0	0.01	-0.01	0	0	0.01	0	0	0	0	0
0.00766951	-0.17	0.02	1.	-0.75	0.1	0	0.01	-0.02	0.04	-0.08	0.01	0.06	-0.1	0	0	0.01	-0.02	0.02	0.01	-0.01	0.08	0.04	-0.09	0.05	0	0	0	0.2	0.03	-0.33	-0.03	0	-0.03	0.02	0.03	0	-0.03	0	0.01	0	0.02	0.01
0.0083197	0	0	-0.09	0.08	-0.02	0	0	0.01	-0.01	0.02	0	-0.01	0.02	0.01	0	-0.01	0	-0.01	0	0	0.5	-1.	-0.54	0.52	0	0	0	-0.03	-0.04	0.03	0.01	0	0.01	0	-0.01	0	0	-0.01	0	-0.01	-0.01
0.00908223	0	0	-0.09	0.05	-0.02	0	0.01	-0.02	0.01	-0.01	0	0.01	0.05	0.69	0	-0.71	0.03	-0.05	-0.02	-0.39	0	0	0	-0.02	0	0	0	0.01	0.01	0.04	0.74	-0.03	0	0.29	-1.	0	0.01	0	-0.68	-0.12	-0.7	-0.7
0.00608922	-0.01	0.01	0.67	-0.49	0.1	-0.01	-0.17	-0.07	-0.06	-0.57	0.11	0.68	-0.21	0.08	0	-0.04	-0.12	-0.06	0.04	0.01	-0.22	0	0.2	0.25	0	-0.01	0	-1.	-0.88	0.67	0.14	0	0.44	-0.43	-0.19	0	-0.17	0	-0.02	0.11	0	0
0.0141137	0	0	-0.01	0	0	0	0	0.01	-0.01	0.01	0	0	0	-0.07	0	0.07	0	0	0	-1.	0	0	0	0	0	0	0	-0.01	-0.01	0.02	-0.07	0	0	0.04	0.03	0	0	0	0.07	-0.96	0.07	0.07
0.0154747	-0.03	0	-0.12	0.01	-0.02	0	0.05	-0.04	0.02	-0.01	0	-0.01	0.12	0.93	0.07	-1.	0.08	0.87	-0.07	0.27	0.06	0	-0.05	-0.08	0	0	0	0.32	0.3	-0.18	0.14	0	-0.14	0.16	-0.21	0	0.06	0	-0.95	0.4	-0.89	-0.96
0.0266285	-0.61	0.02	1.	-0.1	0.52	0	0.05	-0.41	0.46	-0.3	-0.01	-0.07	-0.08	-0.04	-0.01	0.05	0	0.01	0.01	0	0	0	-0.02	0.61	0	-0.01	0	-0.8	-0.81	-0.96	-0.06	0	0.66	-0.57	-0.01	0	-0.08	0	-0.03	0	0.03	0.04
0.0299764	0.37	-0.01	-0.55	0.04	-0.28	0	-0.02	0.22	-0.25	0.14	0.01	0.04	0.05	-0.01	0	0	0	-0.01	-0.01	-0.01	-0.21	0.01	0.21	-0.2	0	-0.01	0	-0.12	1.	-0.29	0	0	-0.04	0.03	0	0	0.05	0	0.02	0.01	0.01	0.01
0.0484216	-0.51	0.01	0.34	0.02	-0.53	0	-0.02	0.45	-0.48	0.17	0.01	0.07	0.11	-0.06	0	0.04	-0.01	-0.01	-0.02	-0.08	0.35	-0.01	-0.34	0.26	0	0	0	0.04	-0.4	-1.	-0.06	0	0.03	0.04	-0.05	0.01	0.22	0	0.08	0.04	0.07	0.08
0.0626555	0.1	0	-0.02	0	0.04	0	-0.01	-0.09	0.13	-0.04	0	-0.02	-0.04	-0.44	-0.06	0.48	0	0.04	0.04	-0.6	-0.07	0	0.06	-0.02	0	0.01	0	-0.25	0.19	0.12	-0.54	-0.02	0.09	1.	-0.45	0	-0.1	0	0.4	0.28	0.38	0.44
0.0628489	0.47	0	-0.04	-0.02	-0.42	0	-0.15	0.76	-0.83	0.01	0.01	0.05	0.01	-0.31	-0.05	0.39	0.01	0.03	0.08	0.26	-0.98	0.03	0.96	0.01	0	0	0	0.08	-0.3	-0.34	-0.4	-0.02	1.	-0.41	-0.01	-0.01	0.63	0	-0.4	-0.1	0.12	0.18
0.176416	-0.04	0	0.2	-0.01	-0.12	0	0.03	-0.18	0.18	0	0	-0.01	0	0.12	0.02	-0.15	0	-0.01	-0.03	-0.11	-1.	0.03	0.97	-0.02	0	0	0	0	0.09	0.11	0.15	0.01	-0.29	0.07	0	0	-0.13	0	0.15	0.04	-0.05	-0.07
0.21632	0.17	0	0.02	0	0.06	0	0	0.01	0.17	-0.01	0	-0.01	0	-0.5	-0.09	0.67	-0.01	0.02	0.18	0.48	-0.09	0	0.09	-0.02	0	0	0	0.01	0.04	0.04	-0.61	-0.03	1.	-0.02	0	-0.01	-0.29	-0.27	-0.66	-0.17	0.27	0.37
0.276229	0.08	0	-0.03	0.01	0.08	0	-0.21	0.94	-1.	-0.02	0.01	0.04	-0.02	0.42	0.04	-0.28	0.04	0.02	0.15	-0.3	0.06	0	-0.05	0.12	0	0.01	0	-0.16	-0.24	-0.32	0.44	0.01	-0.93	0.85	-0.05	-0.01	0.77	0	0.33	0.1	-0.72	-0.76
0.295868	0.53	0	-0.09	-0.01	-0.13	0	0.06	-0.22	0.06	0.02	0	0	0	0.21	0.06	-0.43	0	-0.02	-0.22	-0.21	0.14	0	-0.14	-0.11	0	-0.01	0	0.16	0.03	0.1	0.29	0.02	0.2	-1.	0.05	-0.03	0.1	0	0.34	0.07	0.13	0.07
2.01538	1.	0	0.01	0	-0.01	0	0.01	-0.04	-0.05	0	0	0	0	0.36	0.06	-0.46	0.01	-0.01	-0.11	-0.22	0.01	0	-0.01	-0.1	0	-0.01	0	0.16	0.16	0.2	0.43	0.02	0.21	-0.91	0.04	-0.82	-0.01	0	0.35	0.07	0.57	0.5
3.2126	0	0	0	0	0	0	0	0	0	0	0	0	0	0	0	0	0	0	0	0	-0.01	0	0	-1.	0.5	0	0	0	0	0	0	0	0	0	0	0	0	0	0	0	0	0
5.62514	0.34	0	0	0	-0.01	0	0.07	-0.29	-0.09	0.03	0	0	0	-0.5	-0.01	0.05	-0.02	0	-0.44	0	0.01	0	-0.01	-0.09	0	0	0	0.06	0.06	0.07	-0.5	0	-0.02	-0.37	0	0.36	-0.01	0	-0.01	0	-1.	-0.99

Figure 6.11: Flux Jacobian for the red cell mass action model.

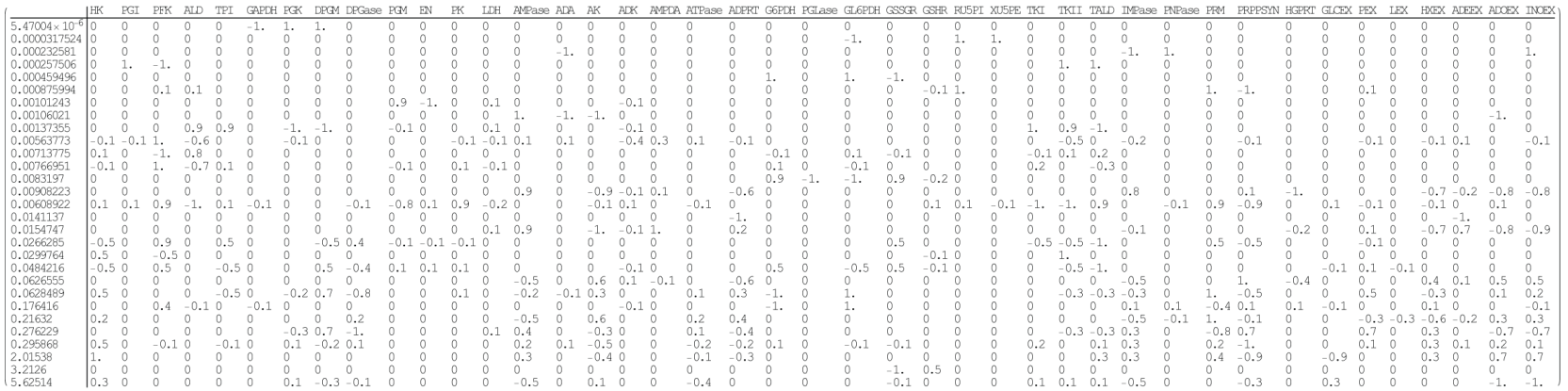

	HK	PGI	PFK	ALD	TPI	GAPDH	PGK	DPGM	DPGase	PGM	EN	PK	LDH	AMPase	ADA	AK	ADK	AMPDA	ATPase	ADPRT	G6PDH	PGLase	GL6PDH	GSSGR	GSHR	RU5PI	XU5PE	TKI	TKII	TALD	IMPase	PNPase	PRM	PRPPSYN	HGPRT	GLCEX	PEX	LEX	HXEX	ADEEX	ADOEX	INOEX
5.47004×10^{-6}	0	0	0	0	0	-1.	1.	1.	0	0	0	0	0	0	0	0	0	0	0	0	0	0	0	0	0	0	0	0	0	0	0	0	0	0	0	0	0	0	0	0	0
0.0000317524	0	0	0	0	0	0	0	0	0	0	0	0	0	0	0	0	0	0	0	0	0	0	-1.	0	0	1.	1.	0	0	0	0	0	0	0	0	0	0	0	0	0	0
0.000232581	0	0	0	0	0	0	0	0	0	0	0	0	0	0	-1.	0	0	0	0	0	0	0	0	0	0	0	0	0	0	0	-1.	1.	0	0	0	0	0	0	0	0	1.
0.000257506	0	1.	-1.	0	0	0	0	0	0	0	0	0	0	0	0	0	0	0	0	0	0	0	0	0	0	0	0	0	1.	1.	0	0	0	0	0	0	0	0	0	0	0
0.000459496	0	0	0	0	0	0	0	0	0	0	0	0	0	0	0	0	0	0	0	0	1.	0	1.	-1.	0	0	0	0	0	0	0	0	0	0	0	0	0	0	0	0	0
0.000875994	0	0	0.1	0.1	0	0	0	0	0	0	0	0	0	0	0	0	0	0	0	0	0	0	0	0	-0.1	1.	0	0	0	0	0	0	1.	-1.	0	0	0.1	0	0	0	0
0.00101243	0	0	0	0	0	0	0	0	0	0.9	-1.	0	0.1	0	0	0	-0.1	0	0	0	0	0	0	0	0	0	0	0	0	0	0	0	0	0	0	0	0	0	0	0	0
0.00106021	0	0	0	0	0	0	0	0	0	0	0	0	0	1.	-1.	-1.	0	0	0	0	0	0	0	0	0	0	0	0	0	0	0	0	0	0	0	0	0	0	0	-1.	0
0.00137355	0	0	0	0.9	0.9	0	-1.	-1.	0	-0.1	0	0	0.1	0	0	0	-0.1	0	0	0	0	0	0	0	0	0	0	1.	0.9	-1.	0	0	0	0	0	0	0	0	0	0	0
0.00563773	-0.1	-0.1	1.	-0.6	0	0	-0.1	0	0	0	0	-0.1	-0.1	0.1	0.1	0	-0.4	0.3	0.1	-0.1	0	0	0	0	0	0	0	0	-0.5	0	-0.2	0	0	-0.1	0	0	-0.1	0	-0.1	0.1	0	-0.1
0.00713775	0.1	0	-1.	0.8	0	0	0	0	0	0	0	0	0	0	0	0	0	0	0	0	-0.1	0	0.1	-0.1	0	0	0	-0.1	0.1	0.2	0	0	0	0	0	0	0	0	0	0	0
0.00766951	-0.1	0	1.	-0.7	0.1	0	0	0	0	-0.1	0	0.1	-0.1	0	0	0	0	0	0	0	0.1	0	-0.1	0	0	0	0	0.2	0	-0.3	0	0	0	0	0	0	0	0	0	0
0.0083197	0	0	0	0	0	0	0	0	0	0	0	0	0	0	0	0	0	0	0	0	0.9	-1.	-1.	0.9	-0.2	0	0	0	0	0	0	0	0	0	0	0	0	0	0	0	0
0.00908223	0	0	0	0	0	0	0	0	0	0	0	0	0	0.9	0	-0.9	-0.1	0.1	0	-0.6	0	0	0	0	0	0	0	0	0	0	0.8	0	0	0.1	-1.	0	0	0	-0.7	-0.2	-0.8	-0.8
0.00608922	0.1	0.1	0.9	-1.	0.1	-0.1	0	0	-0.1	-0.8	0.1	0.9	-0.2	0	0	-0.1	0.1	0	-0.1	0	0	0	0	0	0.1	0.1	-0.1	-1.	-1.	0.9	0	-0.1	0.9	-0.9	0	0.1	-0.1	0	-0.1	0	0.1	0
0.0141137	0	0	0	0	0	0	0	0	0	0	0	0	0	0	0	0	0	0	0	-1.	0	0	0	0	0	0	0	0	0	0	0	0	0	0	0	0	0	0	0	-1.	0	0
0.0154747	0	0	0	0	0	0	0	0	0	0	0	0	0.1	0.9	0	-1.	-0.1	1.	0	0.2	0	0	0	0	0	0	0	0	0	0	-0.1	0	0	0	-0.2	0	0.1	0	-0.7	0.7	-0.8	-0.9
0.0266285	-0.5	0	0.9	0	0.5	0	0	-0.5	0.4	-0.1	-0.1	-0.1	0	0	0	0	0	0	0	0	0	0	0	0.5	0	0	0	-0.5	-0.5	-1.	0	0	0.5	-0.5	0	0	-0.1	0	0	0	0	0
0.0299764	0.5	0	-0.5	0	0	0	0	0	0	0	0	0	0	0	0	0	0	0	0	0	0	0	0	0	-0.1	0	0	0	1.	0	0	0	0	0	0	0	0	0	0	0	0	0
0.0484216	-0.5	0	0.5	0	-0.5	0	0	0.5	-0.4	0.1	0.1	0.1	0	0	0	0	-0.1	0	0	0	0.5	0	-0.5	0.5	-0.1	0	0	0	-0.5	-1.	0	0	0	0	0	-0.1	0.1	-0.1	0	0	0	0
0.0626555	0	0	0	0	0	0	0	0	0	0	0	0	0	-0.5	0	0.6	0.1	-0.1	0	-0.6	0	0	0	0	0	0	0	0	0	0	-0.5	0	0	1.	-0.4	0	0	0	0.4	0.1	0.5	0.5
0.0628489	0.5	0	0	0	-0.5	0	-0.2	0.7	-0.8	0	0	0.1	0	-0.2	-0.1	0.3	0	0	0.1	0.3	-1.	0	1.	0	0	0	0	0	-0.3	-0.3	-0.3	0	1.	-0.5	0	0	0.5	0	-0.3	0	0.1	0.2
0.176416	0	0	0.4	-0.1	0	-0.1	0	0	0	0	0	0	0	0	0	0	-0.1	0	0	0	-1.	0	1.	0	0	0	0	0	0	0	0.1	0.1	-0.4	0.1	0.1	-0.1	0	0	0.1	0	0	-0.1
0.21632	0.2	0	0	0	0	0	0	0	0.2	0	0	0	0	-0.5	0	0.6	0	0	0.2	0.4	0	0	0	0	0	0	0	0	0	0	-0.5	-0.1	1.	-0.1	0	0	-0.3	-0.3	-0.6	-0.2	0.3	0.3
0.276229	0	0	0	0	0	0	-0.3	0.7	-1.	0	0	0	0.1	0.4	0	-0.3	0	0	0.1	-0.4	0	0	0	0	0	0	0	0	-0.3	-0.3	0.3	0	-0.8	0.7	0	0	0.7	0	0.3	0	-0.7	-0.7
0.295868	0.5	0	-0.1	0	-0.1	0	0.1	-0.2	0.1	0	0	0	0	0.2	0.1	-0.5	0	0	-0.2	-0.2	0.1	0	-0.1	-0.1	0	0	0	0.2	0	0.1	0.3	0	0.2	-1.	0	0	0.1	0	0.3	0.1	0.2	0.1
2.01538	1.	0	0	0	0	0	0	0	0	0	0	0	0	0.3	0	-0.4	0	0	-0.1	-0.3	0	0	0	0	0	0	0	0	0	0.3	0.3	0	0.4	-0.9	0	-0.9	0	0	0.3	0	0.7	0.7
3.2126	0	0	0	0	0	0	0	0	0	0	0	0	0	0	0	0	0	0	0	0	0	0	0	-1.	0.5	0	0	0	0	0	0	0	0	0	0	0	0	0	0	0	0	0
5.62514	0.3	0	0	0	0	0	0.1	-0.3	-0.1	0	0	0	0	-0.5	0	0.1	0	0	-0.4	0	0	0	0	-0.1	0	0	0	0.1	0.1	0.1	-0.5	0	0	-0.3	0	0.3	0	0	0	0	-1.	-1.

Figure 6.12: Flux Jacobian modal matrix of the mass action model of the red cell, rotated to minimize the number of zero entries.

leak channel that gave rise to the extremely slow motions in the red cell. The composition of the very fast motions are similar to those seen for the red cell (glycolytic intermediates, ribose sugars, etc). It is curious that the diphosphoglycerates move on the order of 4 minutes in this model, which is much faster than the expected motions (half a day to a day).

6.3 Incorporating Mechanistic Regulation

As noted in Chapter 2, fundamentally, all interactions between metabolites and enzymes are bilinear interactions, that is two components interact at a given time. The mass action model for the red blood cell was expanded in order in order to include an increased level of detail for the biochemical reactions, accounting for mechanistic regulation in the key regulatory enzymes of the red cell. Many of the association and dissociation constants for the steps involved in enzymatic catalysis for the enzymes in the red cell have been characterized. The five key regulatory enzymes in the red blood cell were described in terms of their mechanisms, these include hexokinase (HK), phosphofructokinase (PFK), diphosphoglyceromutate and diphosphoglycerate phosphatase (DPGM and DPGase carried out by the same enzyme), glucose-6-phosphate dehydrogenase (G6PDH), and adenosine kinase (AK). The mass action model discussed in the previous section was used as a basis for this model. The incorporation of the bilinear interactions reflecting small metabolite regulation of the enzymes increased the number of reactions significantly, however the network fluxes for each of the regulated reactions had already been determined. Hence each regulated enzyme was treated as a 'module', whose relevant parameters were calculated individually. After each individual enzymatic step was completed and test, they were integrated into the whole network model. A summary of the dimensions and sizes of the subspaces for the regulated model appear in Table 6.3.

Note that this network is significantly larger than the previous version (also, the reactions are net reactions, not the irreversible elementary steps). Enzyme catalyzed mechanisms were introduced in this model for 5 enzymes and the size of the left null space increased from 3 to 10. The size null space grew by 6 dimensions

Table 6.3: Dimensions of the regulated red cell model.
The dimensions of the stoichiometric and gradient matrices, along with their ranks and sizes of their null spaces for the regulated mass action model of red cell metabolism.

	Rows	Columns	Rank	Left Null	Right Null
Stoichiometric matrix	90	92	80	10	12
Gradient matrix	92	90	87	5	3

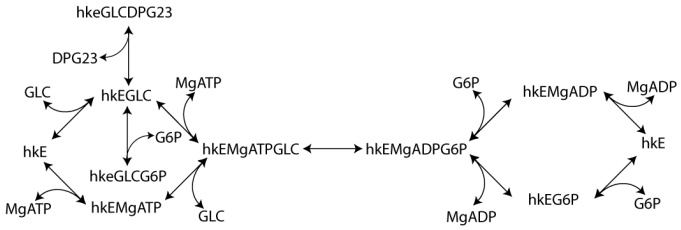

Figure 6.13: Hexokinase reaction scheme [61].

due to the addition of the 5 enzymes (note that PFK has an inactive and active form) plus the conservation of total magnesium. The right null space increased by 3 as a result of the non-sequential mechanism of some of the enzymes, such as HK.

The mechanism for unordered mechanism for hexokinase along with the association and dissociation constants were used as described in [61]. Figure 6.13 illustrates the individual steps; figure 6.14 more explicitly illustrates the conservation of the enzyme, hkE. The total amount of enzyme is conserved (appears in the left null space) and was fixed at 24nM as described by [61]. The net flux for the reaction was fixed according to the steady state flux for the mass action

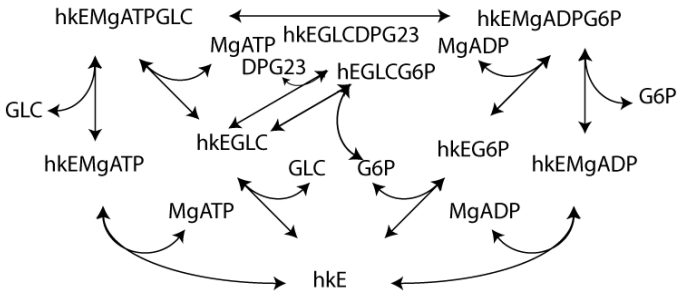

Figure 6.14: An alternative (but equivalent) rendering hexokinase reaction scheme.

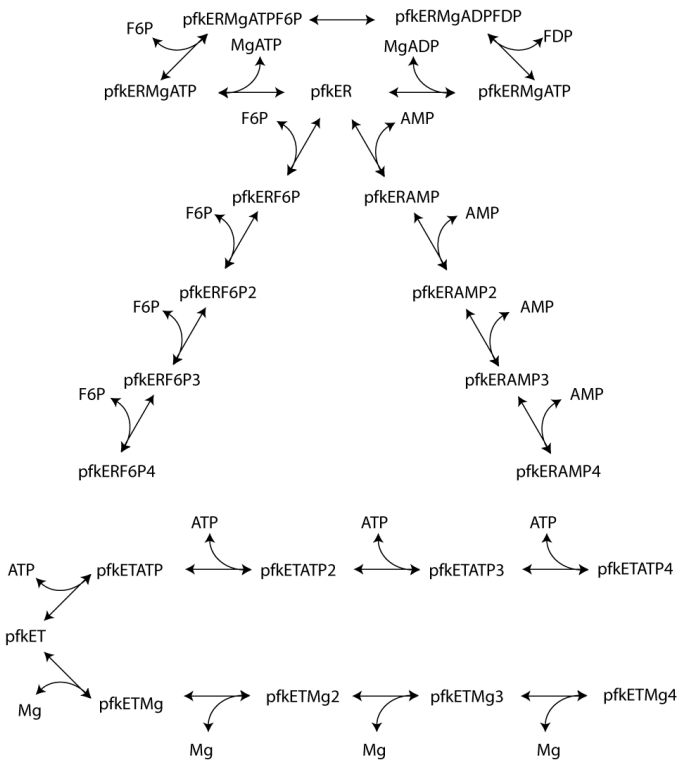

Figure 6.15: PFK reaction scheme including allosteric interactions.

model. The regulatory interactions by 2,3DPG and G6P do not carry net fluxes, so their equilibrium concentrations were calculated. The remaining set of intermediate concentrations were then calculated. Association and dissociation constants for the regulated steps for PFK in the red blood cell were not available, hence an approximation of 100,000 was made for most of the steps, for the exception of the catalytic transition, which was assumed to be much slower. The total concentration of enzyme was 0.033 μM according to [1]. PFK is a tetramer and as is apparent from the reaction diagram in Figure 6.15, it has four binding allosteric regulators. Although such interactions have been described using the well known Hill equation, they can be directly described as a set of sequential bilinear interactions. The diphosphoglyceromutase and diphosphoglycerol phosphatase reactions are both carried out by the same enzyme. The enzymatic steps were described according to [60]. As with HK, the majority of the association and dissociations steps were measured [60]. A similar procedure was carried out in order to calculated the concentrations of the enzyme-metabolite intermediates.

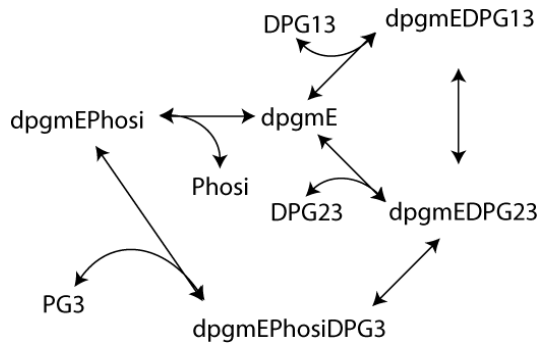

Figure 6.16: Rapoport-Leubering shunt reaction scheme [60].

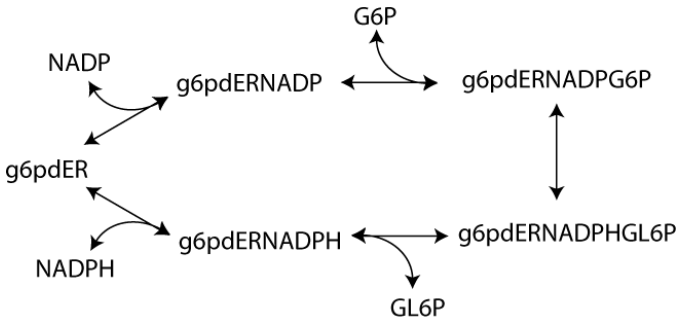

Figure 6.17: Glucose-6-Phosphate Dehydrogenase reaction scheme [61].

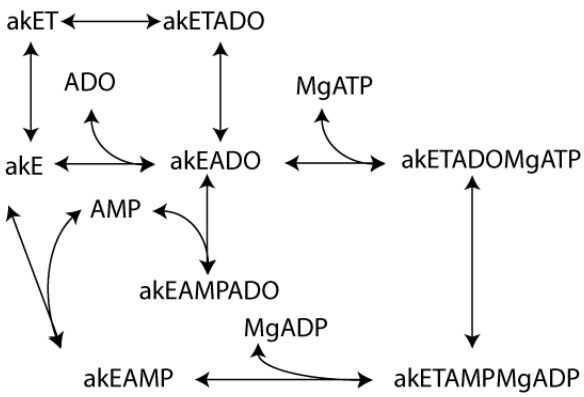

Figure 6.18: Adenosine Kinase reaction scheme [23].

akE represents the enzyme in the catalytic state and akET represents the tense or inactive form of the enzyme.

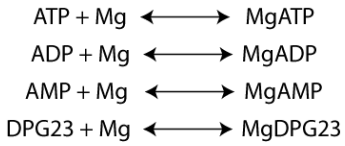

Figure 6.19: Magnesium equilibrium reactions for the adenosine phosphates and 2,3 bisphosphoglycerol.

The reactions for G6PDH were implemented as described by [61] and solved in an analogous manner as HK.

The reaction scheme for AK is outlined in Figure 6.18, as described by [23]. The magnesium equilibrium reactions with 2,3DPG and the adenosine phosphates were implemented as described in [41].

Unfortunately the dimensions of the network are such that it is no longer possible to display the stoichiometric, gradient, Jacobian, or modal matrices in a legible manner. In order to illustrate a point however, the product of the concentration modal matrix with with metabolites, ordered by time scale is shown in Figure 6.21. Although this figure is difficult to read, a few points should become clear,

- The time scale separation has improved ranging from less than microseconds (the fastest modes are actually $\sim$ zero) to ten hours.

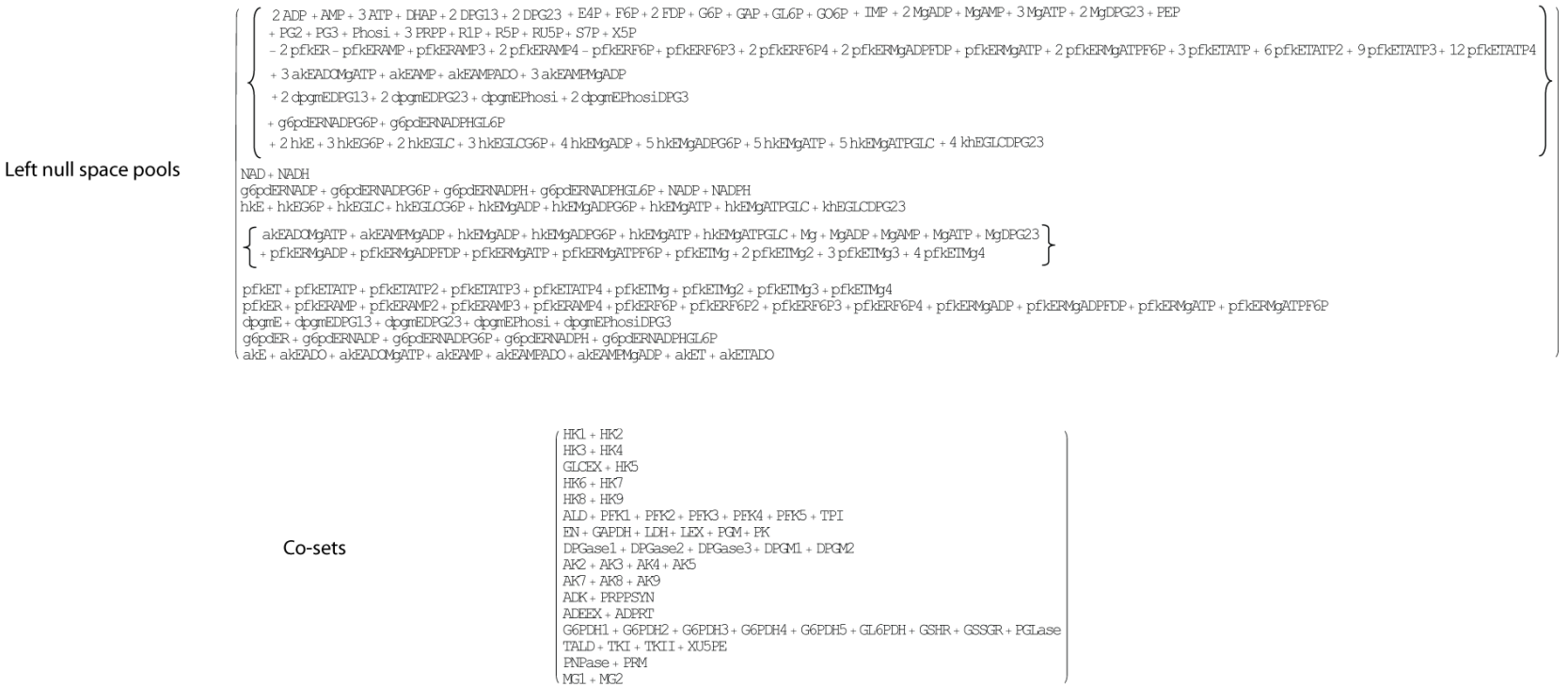

Figure 6.20: The left null conserved pools and the right null co-sets for the regulated mass action model.

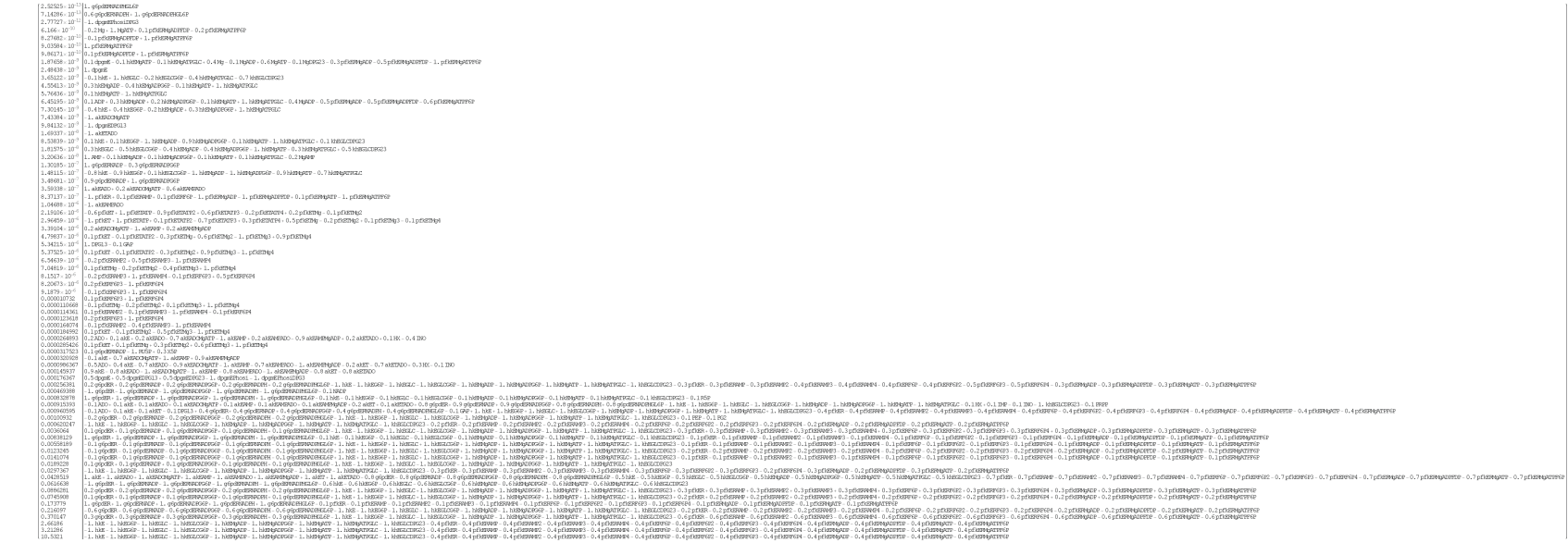

Figure 6.21: The product of the metabolite modal matrix with the metabolites for the for the regulated mass action model. Time scales in hours appear on the left.

- The slow modes are dominated by the reactions with enzymes. In particular the reactions that have a larger number of intermediate complexes play a more dominant role, especially at the slower time scales.

- The movement of 2,3DPG (enzyme bound forms) have moved to the slowest time scales.

In short the structure of the modal matrix more closely approximates the features in the full red cell kinetic model. This has encouraging and interesting implications, since the starting point was a basic model of glycolysis, expanded it to a model of red cell metabolism, and then incorporated regulatory interactions in a mechanistic manner. The results from the regulated model of red cell metabolism suggest that one manner in which regulatory enzymes exert their influence over the rest of the network is their ability to bind more than one substrate and to exist in multiple states (active and inactive).

6.3.1 Unregulated Versus Regulated Model Responses to Perturbations

In order to investigate the systemic responses to a pulsed energy and redox load, prolonged loads on ATP and NADPH were applied independently to the models. Comparing the responses of the unregulated versus regulated models in response to the same perturbation, it is immediately evident that the regulated model exhibits a significantly more damped response to the energy and redox loads than the unregulated model. This is particularly noticeable when comparing the changes in the Energy Charge (Figure 6.22, top panel) and NADPH Redox State (Figure 6.22 bottom panel) of the models.

Provided the changes in energy and redox states under these simulation conditions, we explored the enzyme states. Rather that considering only the bound versus unbound, one can calculate the fraction of activated and inactivated enzyme for some of the regulated reactions in the network. Enzymes are present in much smaller concentrations than the metabolites which they act upon, thus their absolute concentration is not as important as the fraction in different states, i.e.

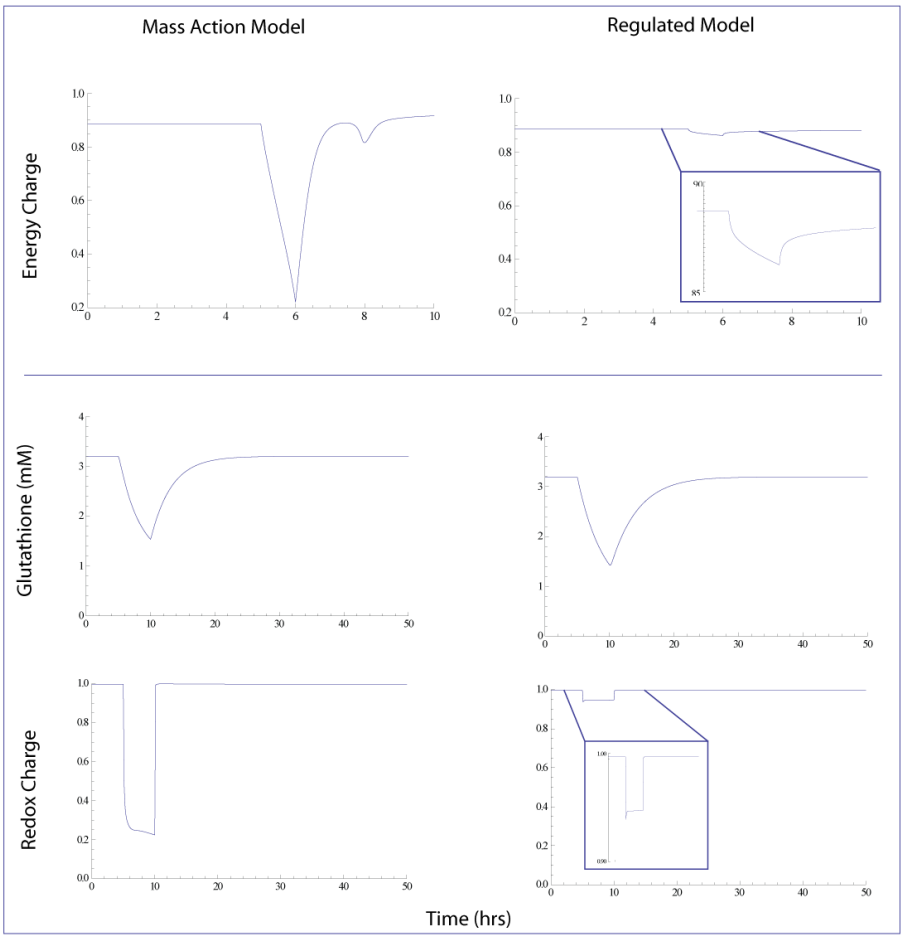

Figure 6.22: Network responses to pulsed energy loads.

The Energy Charge (ATP + 0.5*ADP/(ATP + ADP + AMP)) (36) as a function of time during a rectangular pulse load on ATP lasting from t=5 to t=6 hours (magnitude 4mM/hr). Network responses to pulsed redox loads. The changes in glutathione and NADPH/(NADPH + NADP) as a function of time when the cell is exposed to a first order load on NADPH (100*NADPH) from t=5 to t=10 hours.

percent phosphorylated versus unphosphorylated. Relatively small changes in enzyme states appear to influence larger changes in the flux dynamics. 3-dimensionsal enzyme state plots are shown for Hexokinase in Figure 6.23 for the pulsed energy and redox loads. The percent change over the course of the simulations from the activated state do not exceed about 2%, while the changes in the energy charge and redox charge were approximately 5%. In the network HK is before the split between the oxidative branch in the pentose phosphate pathway and glycolysis, hence it is not surprising that in response to energy or redox loads, the percent in the activated state increases, and the fraction of the enzyme in the inactivated state decreases. Although the changes in the fractional state in AK are small, there is a shift in the balance between the inactive/active fractions with respect to the total percent bound/unbound when the energy load is applied. Such changes are not seen with the redox load and reflects the difference between a direct demand/depletion of energy which drives the increased glycolytic flux (and decreased pentose pathway flux) as opposed to an increased redox load which also drives an opposite change (decreased glycolytic and increased pentose pathway flux). Hence these changes reflect the different types of responses of the network by different perturbations.

6.4 A core *E. coli* model

An updated version of the core *E. coli* metabolic network [64] was used to apply the same methodology for building kinetic networks. The contents of the model are the same as the core model described in [64] with the addition of reactions to enable glutamine, glutamate, and glycerol metabolism (see Appendix Tables .3 and .2). Unfortunately the size of the network causes similar problems for illustration and figures as the regulated red blood cell model. *E. coli* was grown on three different substrates, glucose, acetate, and glycerol. Measurements were made for 25 intracellular metabolites in the network [101]. The majority of the unmeasured metabolites were isomers of the measured metabolites and were assumed to be approximately the same concentration as the measured metabolites. Unfor-

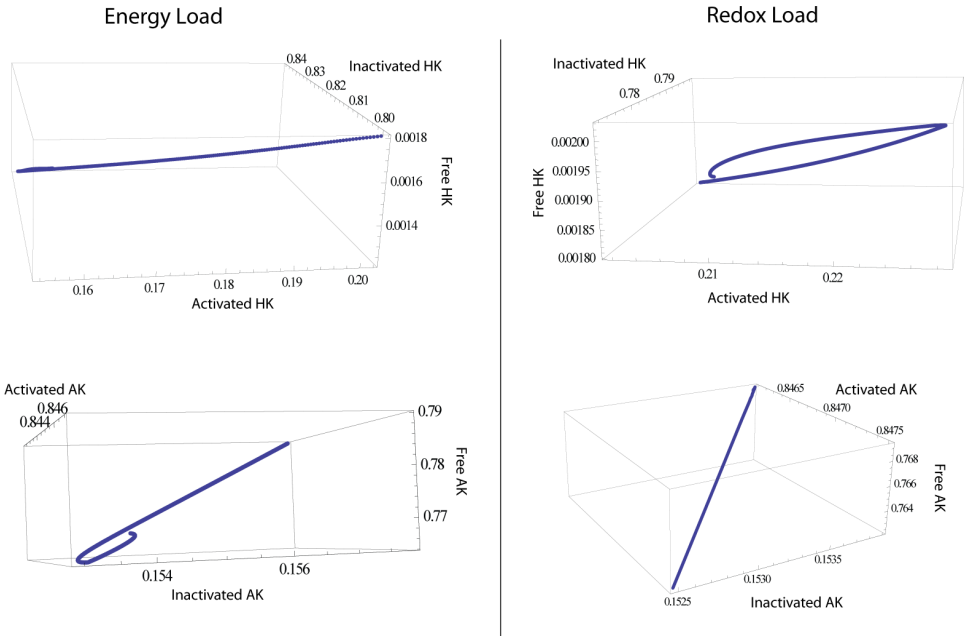

Figure 6.23: Enzyme State plots for HK and AK

Responses to an energy (left panel) and redox (right panel) perturbations from the simulations in Figure 6.22. The majority of the enzyme is in the inactivated state, however in response to either load, the amount in the inactivated state decreases and the amount in the activated state increases in order to increase the flux through glycolysis or the pentose pathway.

Table 6.4: Dimensions of steady state and kinetic *E. coli* networks. **S** refers to stoichiometric matrix. **G** refers to gradient matrix. Parantheses indicate growth media for each of the condition specific kinetic models.

	Rows	Columns	Rank	Left Null	Right Null
S	71	90	65	6	25
S (Glucose)	54	51	48	7	3
G (Glucose)	51	54	48	3	6
S (Acetate)	55	53	49	6	4
G (Acetate)	53	55	49	4	6
S (Glycerol)	52	47	46	6	1
G (Glycerol)	47	52	43	4	9

tunately extracellular concentrations were not known, so it was assumed that most of the secrete metabolites were at low (μM) concentrations and that salts and phosphate were at mM concentrations. The core *E. coli* network was then optimized for biomass under glucose, acetate, or glycerol uptake (10 mM/hr). The growth rates for the models were 0.9 mm/gDW/hr, 0.21 mM/gDW/hr, and 0.52 mM/gDW/hr for growth on glucose, acetate, and glycerol, respectively. An optimal flux distribution for each of these cases was chosen and the subsequent models were reduced (removal of any fluxes whose net value was zero at the steady state). Equilibrium constant approximations are available for the set of reactions, thus armed with steady state fluxes, and concentrations measurements, the same scheme in Figure 6.2 was implemented to solve for the forward rate constants and hence enable the definition of the gradient matrices. The dimensions of the resulting models and subspace sizes are listed in Table 6.4. The biomass function is involved in approximately every single every mode of *E. coli* under all three growth conditions. The maximum and minimum time scales do not correlate with the different growth rates. The slower time scales are dominated by transport reactions, with generally being the slowest, followed by ammonium (and glutamine/glutamate related fluxes), and pyruvate. Also, similar modes are moving on different time scales. For example for growth under glucose, a pyruvate transport mode moves on a time scale of about 150 milliseconds. A similar mode for growth on acetate takes place on 360 milliseconds. A more dramatic difference is observed when comparing the succinate transport mode between the glucose and acetate grown *E. coli*,

Table 6.5: The maximum and minimum time scales for *E. coli* grown on different media.

	Glucose	Acetate	Glycerol
Min Time Scale (ms)	0.04	0.57	2.9
Max Time Scale (hrs)	316	128	0.43

Table 6.6: Stoichiometric dimensions of the hepatocyte core mitochondria

	Rows	Columns	Rank	Left Null	Right Null
Stoichiometric matrix	274	290	251	23	29

with time scales of half an hour and 13 hours, respectively. Based on Table 6.5 one might be lead to believe that glucose grown cells are the slowest responders, however 1) note that it also has the fastest time scale and 2) the mode responsible for the exceedingly slow motion is dominated by orthophosphate, neither of the other strains have this mode.

6.5 A core hepatocyte mitochondria model

The global human metabolic network reconstruction, Recon 1 [11], was used to produce a central metabolism model of a hepatocyte mitochondria (see Appendix Tables .5 and .4). The main functions which were of interest were the ability to incorporate 20 amino acids, glucose, and fatty acids into central metabolism and to produce ATP. Certain pathways were intentionally not included, as they were outside of the scope of interest for the anticipated studies, these include porphoryin biosynthesis, and cardiolipin, phosphatidylcholine, and phosphatidylserine interconversions.

A map of the network can be seen in Figure 6.28. Table 6.6 lists the dimensions of the stoichiometric matrix. With 29 dimensions in the right null space, this model is still smaller than contemporary genome-scale models, however the right null space dependencies are already becoming dizzying, as highlighted by the 3-dimensional tree-plot in Figure 6.31, which as already reduced as much as possible to account for the co-sets. The lesson to note is that transporters alone aren't enough to uniquely specify the null space, there are key internal reactions,

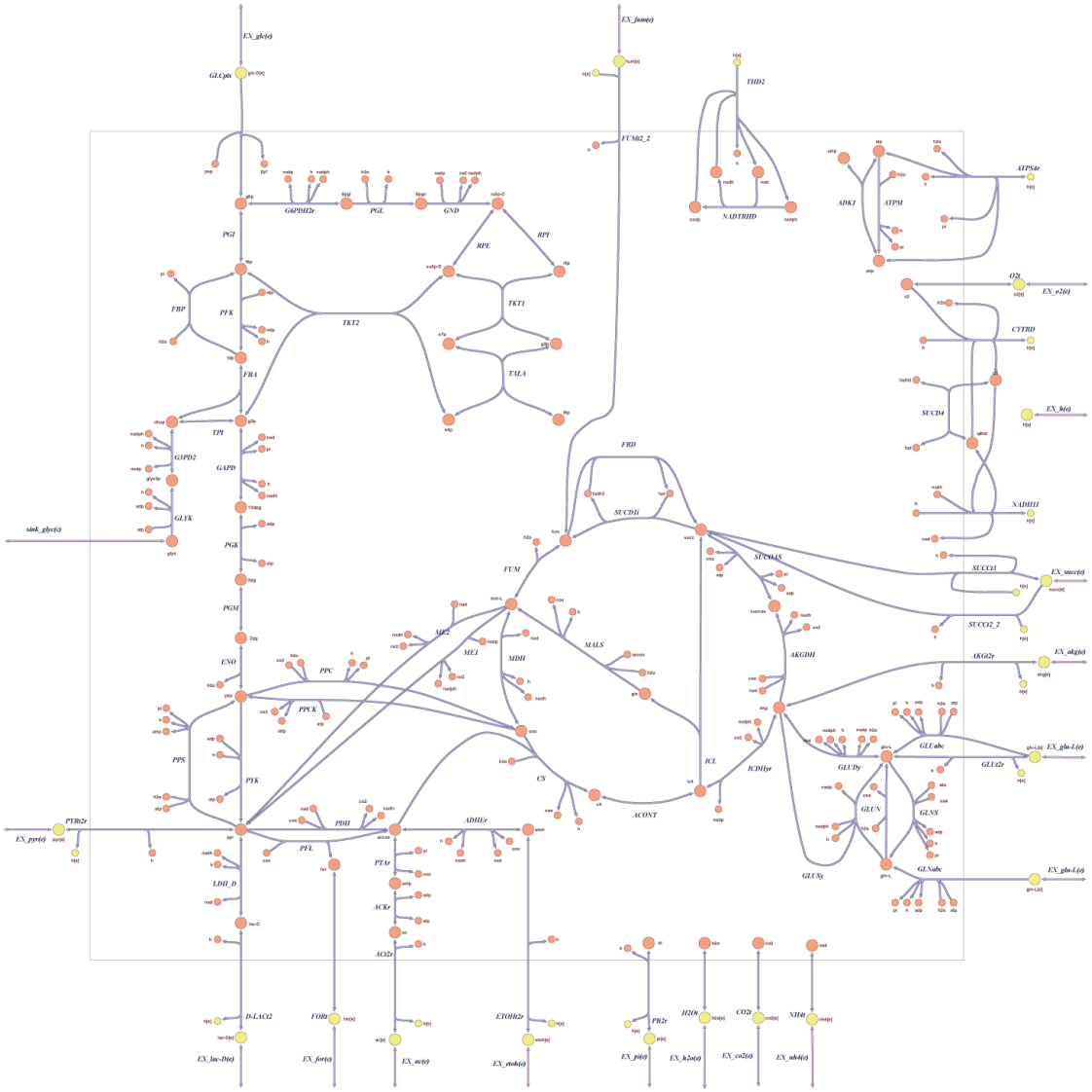

Figure 6.24: Core *E. coli* model network map.

Figure 6.25: The product of the metabolite modal matrix with the metabolites for the *E. coli* model grown on glucose. Time scales in hours appear on the left.

Figure 6.26: The product of the metabolite modal matrix with the metabolites for the *E. coli* model grown on acetate. Time scales in hours appear on the left.

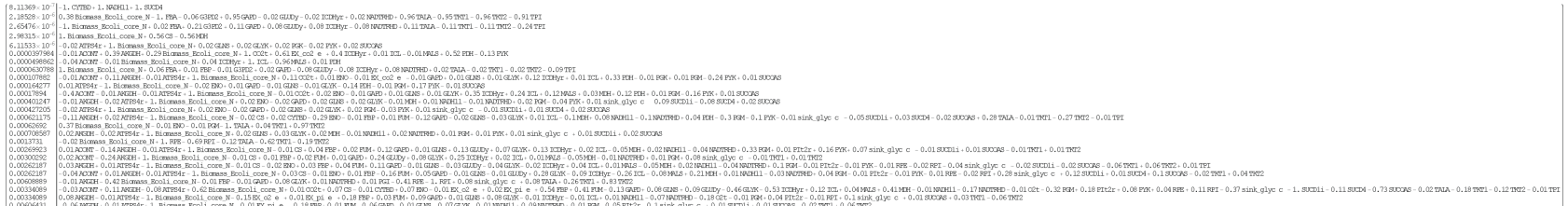

Figure 6.27: The product of the metabolite modal matrix with the metabolites for the *E. coli* model grown on glycerol. Time scales in hours appear on the left.

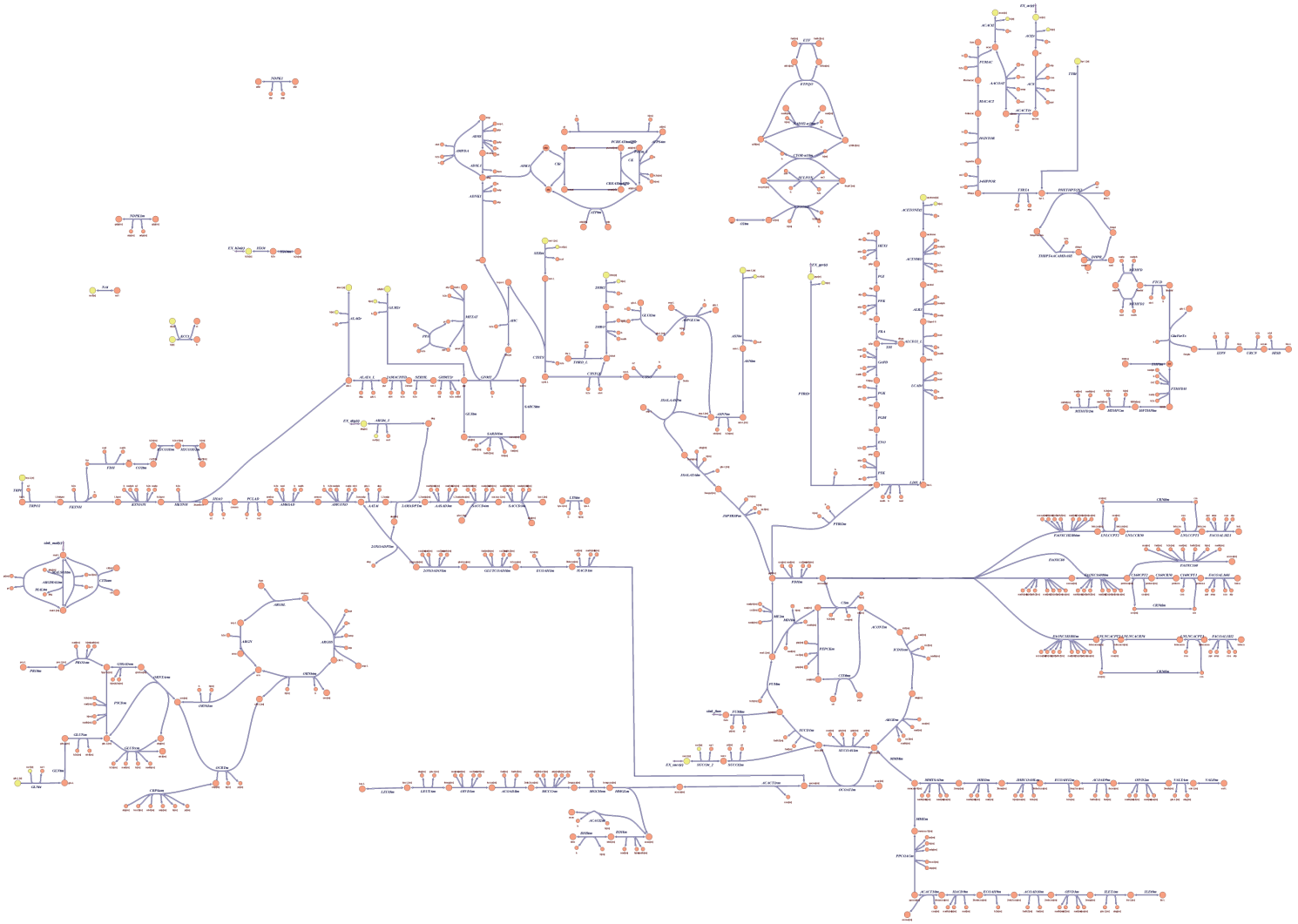

Figure 6.28: A map of the metabolic network for the 274x290 core hepatocyte mitochondria.

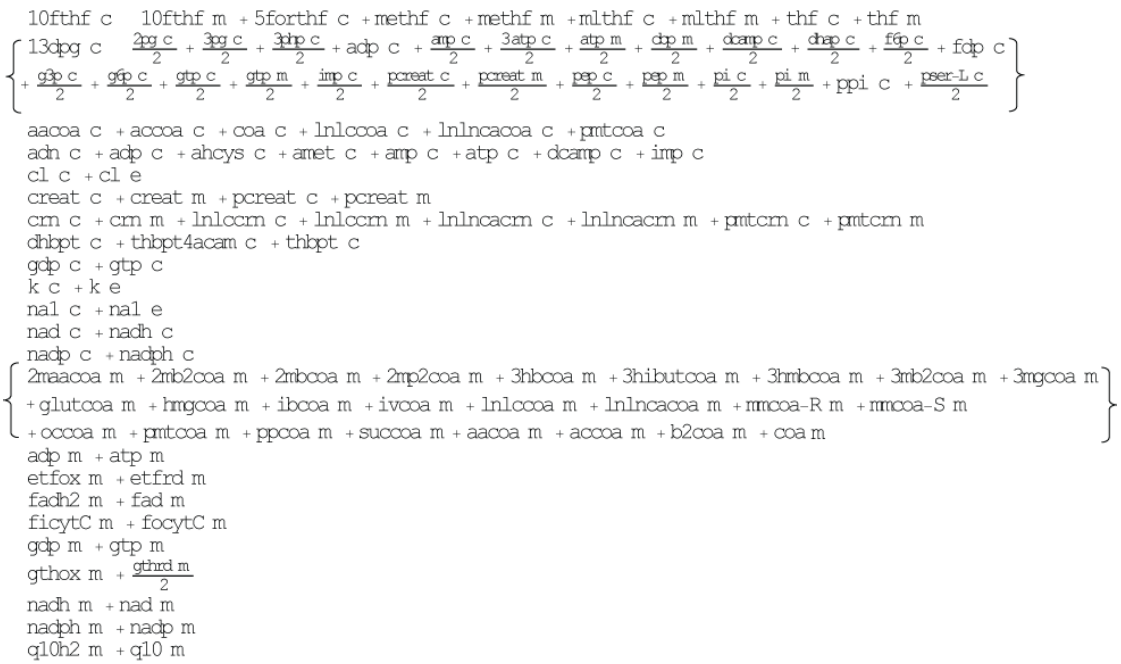

Figure 6.29: Left null space pools of the core hepatocyte mitochondria.

such as PDH that need to be specified as well.

The left null space (Figure 6.29) contains many of the expected quantities, nucleotide phosphate pools, redox pools, single carbon carrier (folate) pools, coenzyme-A pools etc. It is important to appreciate that many of the pools are compartmentalized, i.e. the cytosolic NAD + NADH pool is distinct from the corresponding intramitochondrial pool. These are important distinctions which likely have real biological relevance.

6.6 Quality control issues and potential challenges

Just as there are a number of quality control issues associated with constructing proper stoichiometric matrices (e.g. ensuring mass and charge balanced equations), there are quality control/quality assurance (QC/QA) issues with the development of kinetic models and the workflows described in Figures 6.1 and 6.2. This point was alluded to in Chapter 5.7 and came to bear light in during the construction and analysis of the *E. coli* network. I will begin by first noting the

```
2HBO + 2HBt2 + EX_2hb e
AACOAT + ACACT1r + ACS + ACt2r + EX_ac e
ACACt2 + EX_acac e
ACETONEt2 + ACTNMO + ALCD21_L + ALR3 + EX_acetone e + LCADi
AKGt4_3 + EX_akg e
ALAt2r + EX_ala-L e
ARGtiDF + EX_arg-L e + G5SADxm + ORNt3m + ORNTAxm
ASNNm + ASNt4 + ASNtm + EX_asn-L e
ASPt6 + EX_asp-L e
BDHm + BHBt + BHBtm + EX_bhb e
CO2t + EX_co2 e
CYStec + EX_cys-L e
EX_glc e + FBA + GAPD + GLCt1r + HEX1 + PFK + PGI + PGK + TPI
EX_gln-L e + GLNt4 + GLNtm + GLUNm
EX_glu-L e + GLUt6
AMPTASECG + CGLYt3_2 + EX_gluala e + GLUCYS + GTHS + GTMLTe
EX_gly e + EX_his-L e + FTCD + GHMT2r + GluForTx + HISD + HIStiDF + IZPN + URCN
EX_h2o e + H2Ot
C160CPT1 + C160CPT2 + C160CRNt + EX_hdca e + FACOAL160i + HDCAtr
ACACT10m + ACOAD10m + ECOAH9m + EX_ile-L e + HACD9m + ILEt5m + ILETAm + ILEtec + MMEm + OIVD3m + PPCOACm
EX_lac-L e + L-LACt2r
ACOAD8m + EX_leu-L e + HMGLm + LEUt5m + LEUTAm + LEUtec + MCCCrm + MGCHrm + OIVD1m
EX_lnlc e + FACOAL1821 + FAOXC182806m + LNLCCPT1 + LNLCCPT2 + LNLCCRNt + LNLCt
EX_lnlnca e + FACOAL1832 + FAOXC183803m + LNLNCACPT1 + LNLNCACPT2 + LNLNCACRNt + LNLNCAt
2AMADPTm + AASAD3m + AATAi + EX_lys-L e + LYStiDF + LYStm + SACCD3m + SACCD4m
10FTHFtm + ADNK1 + AHC + CYSTGL + CYSTS + EX_met-L e + FTHFDH + GLYtm + GNMT + METAT + METtec + MTHFCm + MTHFD2m + SARCStm + SARDHm + THFtm
EX_nh4 e + NH4t3r
EX_o2 e + O2t
DHPR + EX_phe-L e + PHEtec + PHETHPTOX2 + THBPT4ACAMDASE
EX_pro-L e + PRO1xm + PROt2r + PROtm
EX_pyr e + PYRt2r
EX_ser-L e + SERt4
3SALAASPm + 3SALATAim + 3SPYRSPm + CYSO + EX_so4 e + MALSO3tm + SULFOX
EX_succ e + SUCCt2m + SUCCt4_2
EX_thr-L e + THRD_L
3HAO + AM6SAD + AMCOXO + EX_trp-L e + FDH + FKYNH + HKYNH + KYN3OX + PCLAD + TRPO2 + TRPt
EX_tyr-L e + TYRt
ARGN + EX_urea e + UREAt
3HBCOAHLm + ACOAD9m + ECOAH12m + EX_val-L e + HIBDm + MMTSADm + OIVD2m + VALt5m + VALTAm + VALtec
2AMACHYD + SERHL
2OXOADOXm + 2OXOADPTm + ECOAH1m + GLUTCOADHm + HACD1m
34HPPOR + FUMAC + HGNTOR + MACACI + TYRTA
ACONTm + CSm + ICDHxm
ADK1 + PPA
ADSL1 + ADSS + AMPDA + NDPK1
ARGSL + ARGSS + CBPSam + OCBTm + ORNt4m
CITtam + CITtbm + PEPCKm
CK + CKc + CREATtmdiffir + PCREATtmdiffir
CytOxe- + GTHOm + GTHPm + ME2m + SOProd + SPODMm
ENO + PGM
ETF + ETFQO
H2CO3D2m + H2CO3Dm
KCCt + SO4CLtex2
PGCD + PSERT + PSP_L
```

Figure 6.30: Right null space co-sets for the core hepatocyte mitochondria.

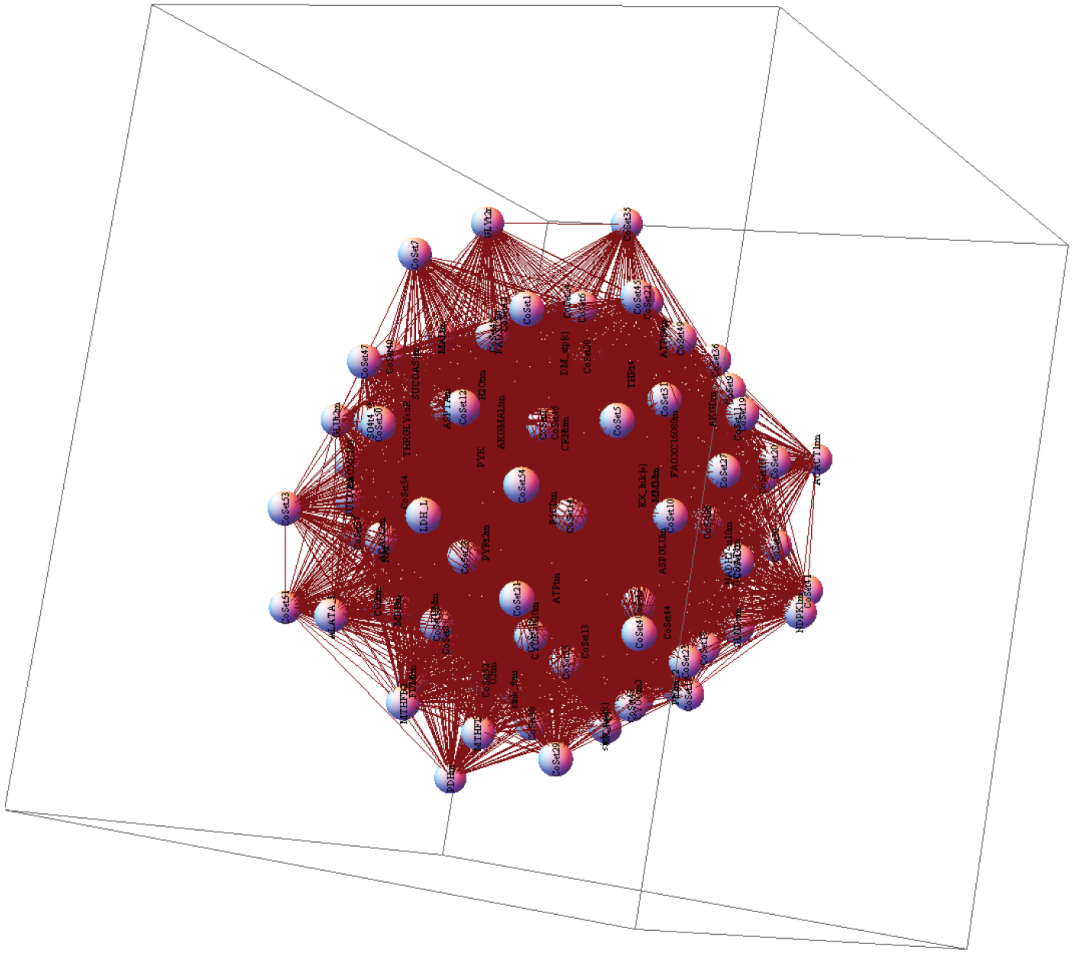

Figure 6.31: Mitochondria flux dependencies: anatomy of a hairball.

main QC/QA procedures that were enforced during the model construction process. The starting point for the workflow in Figure 6.2 was a mass and charge balanced, high quality stoichiometric network reconstruction. In carrying out this process, I will presumet that this network is already available and has fulfilled its own QC/QA checks. From the perspective of building kinetic models, for an mxn stoichiometric matrix, then it is also necessary to have the following,

1. m - r independent flux measurements (r is the rank of $\mathbf{S}$)
2. m metabolite measurements
3. n K_{eq} approximations
4. Rate constants must be positive when solving the mass and flux balance expressions

The most common failure mode for this process is step 4. When all of the rate constants are not positive, then the rate expressions need to be adjust in some manner, this can occur by adjustment of the flux measurements, metabolite measurements, or equilibrium constants. If there are experimental error bounds on the flux and metabolite measurements, then model refinement becomes an iterative trial and error process. Often times K_{eq} approximations are missing for some reactions, so the equilibrium constant values can be adjusted in these cases (this is the most direct and convenient approach for making sure the rate constants are all positive).

When the above process succeeds (which it did for the *E. coli* models), there is another failure mode. This is a data consistency challenge. When multiple measurements are made for an organism under different conditions and multiple metabolomic data sets are available (as was the case for *E. coli*, then the resulting models can serve as consistency checks among one another. For the case of *E. coli*, some of the equilibrium constants needed to be adjust in order to satisfy the positive rate constant condition. However, these adjustments led to different approximations for some of the reaction equilibrium constants. While it is possible that *E. coli* grown under different conditions has a different intracellular pH, it

is not expected that these differences would be very significant. Hence, there is a data consistency issue with respect to the equilibrium constant approximation that arises. One approach to dealing with this problem is to use the metabolomic data under different conditions to approximate the equilibrium constants (so one no longer needs K_{eq} approximations). This leads to the formulation of a variation on a theme of the model construction process. Consider measurements made under two different conditions ${}^1\mathbf{v}$ and ${}^1\mathbf{x}$ for fluxes and concentrations, respectively, under condition 1 and ${}^2\mathbf{v}$ and ${}^2\mathbf{x}$ for fluxes and concentrations, respectively, under condition 2. For rate expressions, we continue with the mass action rate law,

$$v_j = k_j^+ \prod_{j=1}^{n} x_i^{S_{ij}^-} - k_j^- \prod_{j=1}^{n} x_i^{S_{ij}^+} \tag{6.1}$$

So the constraint equations to be followed are,

$$\mathbf{S} \cdot {}^{\mathbf{1}}\mathbf{v} = \mathbf{0} \tag{6.2}$$

and

$$\mathbf{S} \cdot {}^{\mathbf{2}}\mathbf{v} = \mathbf{0} \tag{6.3}$$

Two more constraint equations for the set of fluxes that have been measured,

$${}^1v_j = {}^1\, k_j^+ \prod_{j=1}^{n} {}^1x_i^{S_{ij}^-} - {}^1\, k_j^- \prod_{j=1}^{n} {}^1x_i^{S_{ij}^+} \tag{6.4}$$

$${}^2v_j = {}^2\, k_j^+ \prod_{j=1}^{n} {}^2x_i^{S_{ij}^-} - {}^2\, k_j^- \prod_{j=1}^{n} {}^2x_i^{S_{ij}^+} \tag{6.5}$$

Finally, the optimization criteria to try to ensure as much consistency between the two models as possible,

$$\sum_{j=1}^{n} min(\frac{{}^2k_j^+}{{}^2k_j^-} - \frac{{}^1k_j^+}{{}^1k_j^-}) \tag{6.6}$$

If the experimental conditions are such that it is further expected that the individual rate constants will change very little, then the optimization criteria will change

leading to two new sets of equations,

$$\sum_{j=1}^{n} min({}^{2}k_j^{+} - {}^{1}k_j^{+}) \tag{6.7}$$

and

$$\sum_{j=1}^{n} min({}^{2}k_j^{-} - {}^{1}k_j^{-}) \tag{6.8}$$

So depending on the type of perturbation applied to the cells under the different conditions, the constraint equations are either equations 6.2, 6.3, 6.4, 6.5, and 6.6 or equations 6.2, 6.3, 6.4, 6.5, 6.7, and 6.8. This section in the chapter highlights some of the new challenges and reas of need for the development of optimization methods not only for construction of kinetic models but the utility of model construction as a means for interrogation of data consistency.

6.7 Summary

This chapter began with the glycolytic pathway and ended up with a core mitochondrial model, significant ground has been covered, however open gaps remain. The principle points to be made from this chapter are,

- With the appropriate data streams, kinetic models can in in practice be constructed with fluxomic and metabolomic data. This has been demonstrated with a model of glycolysis, a model of red cell metabolism, and a core model of *E. coli*.

- Models constructed through this **middle-out integration** approach reasonable biological interpretations, with the dynamic properties of the resulting models reflecting different functional capabilities of their respective organisms.

- Mechanistic regulation can be incorporated into the stoichiometric matrix through bilinear interactions.

- The changes in the time scales that develop with the incorporation of mechanistic steps are consistent with traditionally constructed kinetic models.
- It appears that one manner in which regulatory enzymes exert influence on metabolic pathways is driven by the fact that these enzymes can bind a larger number of metabolites.
- The ability of an enzyme to bind multiple substrates confers tighter control of the network to perturbations in substrate concentrations.
- Changes in the fractional state of bound enzymes are reflective of changes in network function, thus laboratory measurements of enzyme fractions in active versus inactive states (e.g. different phosphorylation states) may reflect flux activity through different pathways in the network. These simulations support the efforts to measure and characterize the phosphoproteome as a means for summarizing not just local, but global cellular functional states.
- A functional sub-model can be tailor made from Recon 1, allowing the left and right null spaces to be defined.
- The process of construction of these models have important QC/QA issues that must not be neglected
- The process of kinetic network construction can also serve the dual purpose as a means for data consistency checks
- These new methods bring to light the need for new optimization methods for the construction and analysis of dynamic networks
- While fluxomic and metabolomic data appear to be critical for kinetic network construction, K_{eq} approximations may not be necessary if there is ample metabolomic data measured under different conditions

Chapter 7

The environment, genetics, simulations, and perturbations

Computational models are increasingly being recognized as important investigational tools for the analysis of complex biological systems [62, 81, 96, 47] . There are now suggestions that even simulations of a whole human being may one day become possible; the virtual human [45]. While such statements and propositions are likely to conjure up misleading and unrealistically ambitious visions of the future, nevertheless, it is increasingly being recognized that models will play a progressively more important role in science and medicine. Such models are being used to accelerate discovery [76, 22], develop understanding of complex physiological processes [51], and for prospective biological design [8].

Some *in silico* whole cell models can now represent cellular functions with a reasonable degree of accuracy. Understanding and properly characterizing the function of a biological network includes characterization of how the network responds to different types of perturbations; environmental and/or genetic. Thus, single cell *in silico* models should be used to predict outcomes of dual perturbation experiments (that cross genetic and environmental perturbations) before they are performed in the laboratory. Just as for experimental models, relative predictions by *in silico* models may be more useful than absolute predictions. This use of *in silico* models can now be prototyped at the single cell level.

Analysis vs simulation Analytical approaches for the characterization of network properties, such as the hierarchical decomposition discussed in Chapter 4 are useful for identifying and generalizing network properties. However, individual simulations are often very helpful when the behavior of a system under specific conditions are of interest. Analytical methods are usually more powerful and the results for these can be justifiably generalized. However, there is also a place for simulation based studies, as will be discussed. Regardless of the type of approach however, perturbing a system is critical into gaining insight into its functional state.

7.1 Perturbational analysis of the red blood cell

A growing number of realistic *in silico* models of metabolic functions are being formulated. One of their uses is to serve as dry lab platforms to prototype and simulate experiments before they are performed. Dual perturbation experiments that vary both genetic and environmental parameters can readily be simulated *in silico*. The studies presented here yield two important conclusions: 1) that the functional states of transporters are informative about the internal functional states of a cell; and, 2) that genetic variations can disrupt the natural dynamic sequence of interactions between network components. The former arises from adjustments in the capacity term in the energy and redox charges, while the latter is a result of shifting time scales and alternation in the modal structure of the Jacobian matrix. These two concepts are illustrated for G6PD and PK in the human red blood cell.

The red blood cells primary physiological function is to deliver oxygen that enters the body through the lungs, to tissues and to return carbon dioxide back to the lungs, to be expelled from the body [17]. In order to carry out these functions, basic but critical metabolic functionality must be maintained, including maintaining adequate ATP levels to maintain cell shape and the preservation of reduced glutathione to counteract oxidative stresses. These capabilities are directly affected in varying degrees in patients with metabolic enzyme deficiencies. The

two most common of such deficiencies are in G6PD and PK. We will consider dual perturbations in silico where genetic variations in the properties of these two enzymes are crossed with changing environmental conditions.

Baseline responses of the normal red cell: the role of pooled variables and transporters The normal of nominal set of parameters in the dynamic model of red cell metabolism (abbreviated here as the nRBC) forms a reference case from which parameters can be perturbed. The dynamic responses nRBC (Figure 7.1, top) was analyzed under conditions of increased redox and energy loads to provide a baseline, or the normal response to such stresses. The nRBC under increased redox vs. increased energy loads resulted in different flux states, notably shifting between reliance on the glycolytic pathway versus the pentose phosphate pathway. The computed steady state concentrations and fluxes are given in supplementary tables.

The evaluation of the computed network responses and the resulting internal changes from the imposition of redox or energy loads led to the observation that changes in certain transport fluxes reflected changes in internal functional states:

1. As the redox load increases, flux through glycolysis decreases and flux through the pentose phosphate pathway increases. At very high redox loads, the flux through phosphoglucoisomerase (PGI) even reverses direction to achieve maximal total flux through the oxidative branch of the pentose phosphate pathway. These expected shifts in pathway uses are accompanied by some unexpected changes in transport fluxes. The flux through adenine phosphoribosyltransferase (ADPRT) and phosphoribosylpyrophosphate synthetase (PRPPSYN) increases significantly. There is a dramatic decrease in adenosine (ADO) uptake and with a moderate increase in the ADA flux. Hypoxanthine (HX) excretion increases and inosine (INO) uptake decreases.

2. As the energy load is increased, flux through the pentose phosphate pathway is decreased and increased through glycolysis. The adenosine kinase (AK) flux decreases, with a relatively small decrease in AMP deaminase (AMPDA), adenine phosphoribosyltransferase (ADPRT), IMP nucleotidase

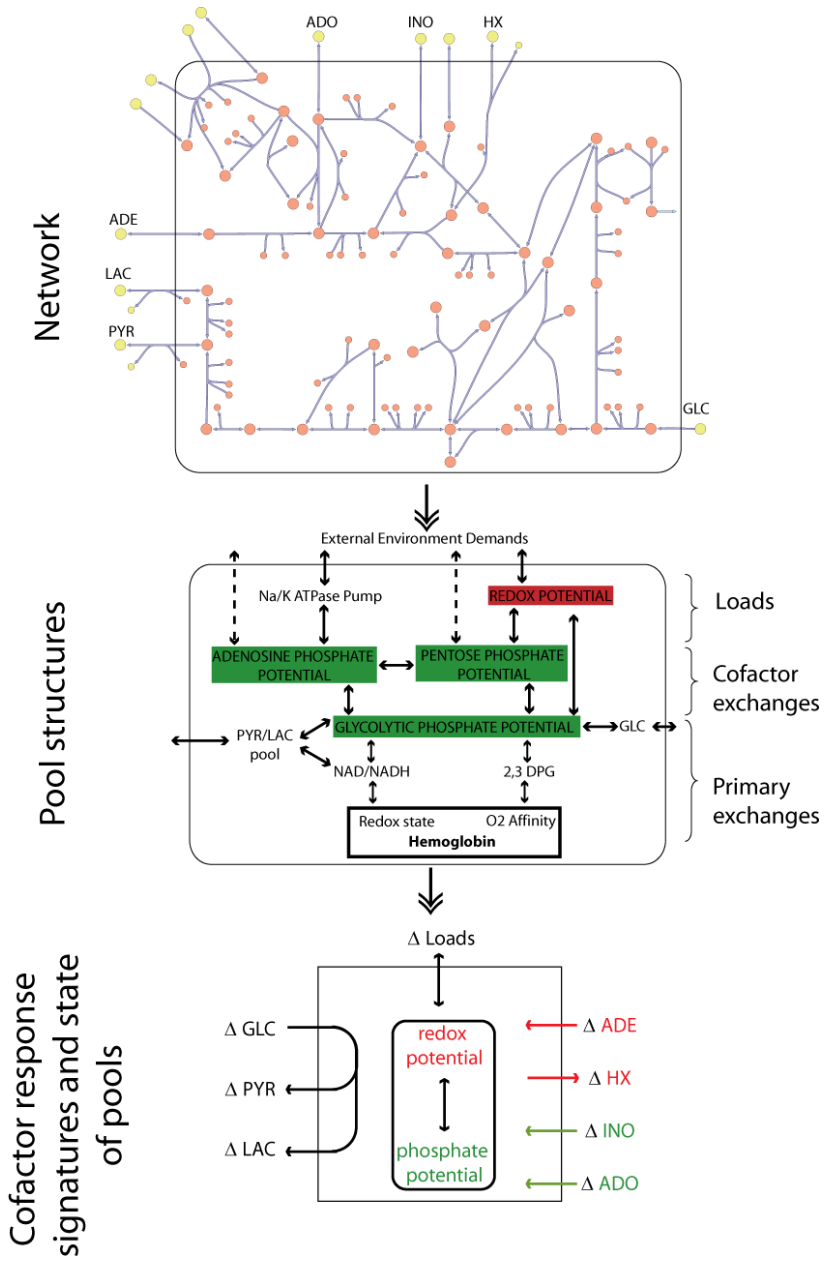

Figure 7.1: Cofactor driven simplification of kinetic red cell model.

Simplifying the kinetic model of red cell metabolism into biologically relevant pooled variables and metabolite ratios, such as cofactor pools. Further simplification will result in classification of the network functional states based on changes in transport fluxes. When the cell needs to increase its redox potential in order to counteract an oxidative stress, ADE uptake and HX secretion are increased, while ADO and INO uptake are decreased. The reverse trends occur with increased energy loads. The relative magnitudes of the changes tend to be larger with ADE and ADO than INO and HX.

(IMPase) and purine nucleoside phosphorylase (PNPase). The phosphoribosylpyrophosphate synthetase (PRPPSYN) flux decreases. HX excretion decreases and INO uptake increases slightly. There is a reduction in adenine (ADE) uptake and a parallel increase in adenosine (ADO) uptake. Thus, the ratio of the adenosine to adenine uptake reflected whether the cell was responding to an increased redox load or an energy load.

Red cell metabolic functions have previously been described [36, 44] in terms of pooled concentration variables and ratios thereof; such as redox and phosphate capacities and potentials (Figure 7.1, middle). This description represents a functional description of the state of red cell metabolism, rather than a detailed biochemical description. The computations of changes in fluxes and concentrations at varying redox and energy loads can be interpreted within this functional network description. The altered function state of the nRBC in response to environmental parameters can be reduced to changes in the states of transport fluxes (Figure 7.1, bottom). Increases in energy demands will shift the internal pathways to maintain the phosphate potential and ADO uptake will increase, while ADE uptake decreases and HX secretion decreases. Conversely, when increased oxidative stresses are experienced, the fluxes shift towards the redox potential with decrease in ADO uptake and an increase in ADE uptake and HX secretion.

These simulated responses provide the baseline case for the nRBC and they can be characterized in terms of a functional description of the state of nRTBC metabolism (Figure 7.1). The key results here are that the environmental loads shift the use of pathways and the redox/energy pools. The state of these pools (their charge = occupancy/capacity [36, 44]) is adjusted by alterations in key transport fluxes.

7.1.1 Dual perturbations *in silico*

Since the simulated flux uptake patterns reflect changes in the internal states of the nRBC to environmental perturbations, it suggests the possibility to characterize the responses different genetic variants (nRBC versus vRBC; v for variant) in the same fashion, and using the responses of the nRBC as a reference.

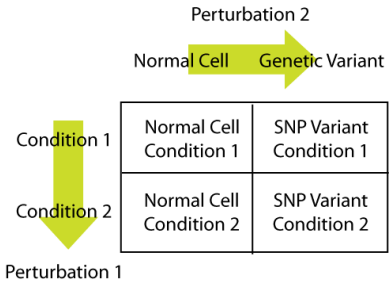

Figure 7.2: Dual perturbation design.

A schematic 2x2 table illustrating the *in silico* dual perturbation experiment. The condition change for the G6PD variant was an altered redox load and the condition change for the PK variant was an altered energy load.

This leads to the notion of a dual perturbation experiment *in silico* as a way to analyze and design experiments to determine the effects of genetic variation. Differences in functional capabilities would be assessed by comparisons between different states in two different environmental conditions for the nRBC vs. a vRBC (i.e. genetic variant), see Figure 7.2.

Calculating the differences between the rows in Figure 7.2 and then comparing the nRBC to the vRBC results in a dual perturbation comparison, in which the one perturbation reflects an environmental change and the other results from a genetic mutation. Such *in silico* studies were carried out for G6PD variants and PK variants whose altered kinetic parameters were measured from patients citefiorelli, beutler.

The steady state flux distributions for the nRBC along with the six G6PD variants (vRBC$_i$, i=1, 6) were calculated at a different redox loads. These loads were applied by increasing the rate constant for the first order load on glutathione (reduced form) (GSHR reaction). The maximum coefficient for the normal erythrocyte was 7.5/hr. Most of the variants could not tolerate a load this high, although some of the variants could tolerate an even higher load. The high and low redox loads between the normal cell and the G6PD variants for the comparative study were 2.5 and 0.5 mM /hr, respectively (the maximum applicable load was limited by some of the variants).

The comprehensive set of steady state fluxes and concentrations calculated

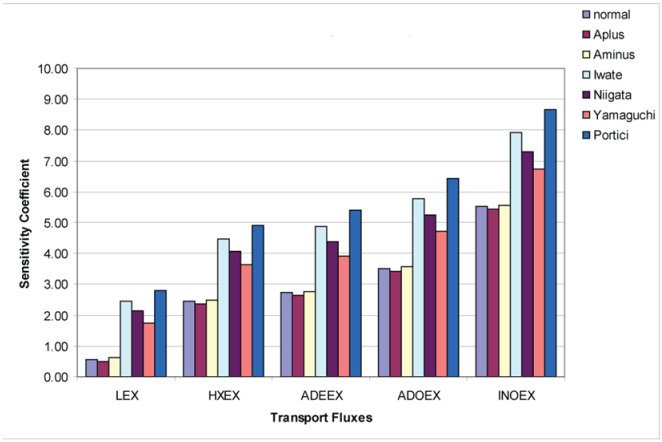

Figure 7.3: Intracellular sensitivity to transport fluxes.

Intracellular changes to cofactor pools are very sensitive to the related extracellular transporters. The sensitivity parameter is a logarithmic ratio between the change in redox potential between two states over the relative change in a particular transport flux between two states. Changes in the intracellular redox state can be reflected in the extracellular transport of related metabolites.

for the cell under different conditions led to the definition of a sensitivity parameter relating the intracellular redox state of the cell and extracellular transporters can be defined,

$$\log_{10}(|\frac{R_{\text{high}} - R_{\text{low}}}{R_{\text{low}}} / \frac{v_{\text{high}} - v_{\text{low}}}{v_{\text{low}}}|) \tag{7.1}$$

in which R_{high} and R_{low} reflect the redox state of the cell (R = NADPH/(NADP + NADPH) under high and low redox loads, respectively, and v is a corresponding transport flux. A logarithmic sensitivity measure is used since this proves to be sensitive relationship. The computational results illustrate how the change in the redox state of the cell (summarized as the relative size of the reduced NADP pool), an intracellular quantity, is tracked by transport fluxes, an extracellular quantity (see Figure 7.3). Hence, changes in the internal states of cells can be detected by measuring the exchange rates.

To further elaborate the relationship between the cofactor pools and trans-

port fluxes in the cell, the differences between the high and low exchange fluxes were calculated for each variant and then normalized to the corresponding flux difference in the nRBC. A value of 1 indicates no difference compared to the nRBC, whereas values greater than or less than one reflect differences between the vRBCs from the nRBC. Figure 7.4 illustrates that the transport fluxes alone are enough to distinguish between the less severe (A+ and A-, vRBC1 and vRBC2, respectively) and more severe (Iwate, Niigata, Yamaguchi, and Portici, vRBC3 through vRBC6, respectively) SNP variants. This finding suggests that changes in transport fluxes can be used to identify changes in internal functional states and differentiate between normal and pathophysiological situations. Interestingly, these changes were identified using relative (and not absolute) changes in the fluxes.

PK dual perturbation studies were carried out by applying different energy loads instead of redox loads (Figure 7.5). Energy loads were applied by increasing the rate constant for the first order load on ATP (ATPase reaction). The maximum coefficient was 1.6/hr, although many of the variants could not tolerate this high of a load. The high and low energy loads between the normal cell and the PK variants for the comparative study were 0.6 and 0.2 mM/hr, respectively. All of the vRBCs considered differed from the nRBC, but to varying degrees. Decreased lactate production by all of the variants reflects a decreased glycolytic flux due to the decreased activity of PK. The increased transport of the other metabolites is a result of the need to balance all carbon uptake and secretion. The Mantova variant would be predicted to be less severe than the other vRBCs. In these cases, the altered transport fluxes reflect a decreased total pool size of ATP internally.

7.1.2 Dynamic responses

In order to further characterize the differences that occur between the nRBC and the vRBCs, the dynamic states of the vRBCs were analyzed by comparing changes in the dynamic sequence of events that occur when they respond to a perturbation. Different biochemical inter-conversions, illustrated in Figure 7.1 (middle), occur on different time scales [44] when the nRBC is exposed to an environmental perturbation. This sequence of events can be different in a vRBC

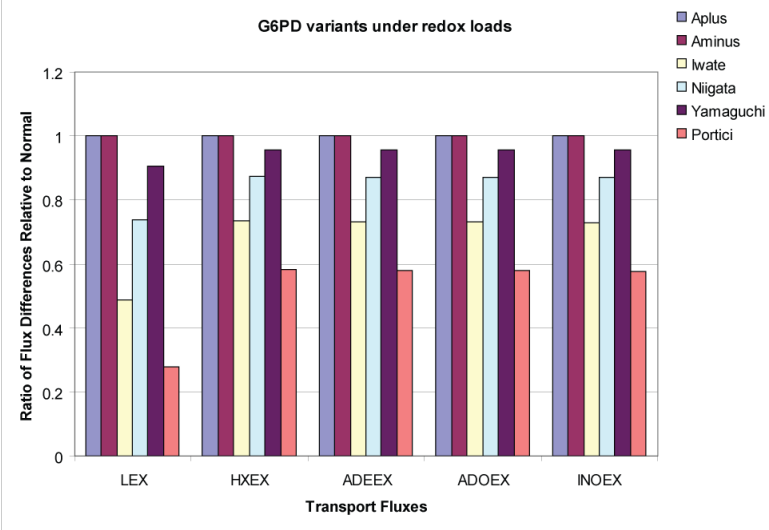

Figure 7.4: Red cell transport phenotypes: G6PD variants.

Characterization of different G6PD variants as functions of transport fluxes. The steady state flux differences were calculated for the nRBC and the vRBC variants considered at high and low redox loads for each case, respectively. The SNP variants were then normalized with respect to the flux differences for the normal case. The A minus and A plus variants exhibit a more mild phenotype with non-chronic hemolytic anemia. The transport fluxes for these cases are effectively the same as the normal erythrocyte. In contrast, the other variants, with more severe phenotypes, have altered steady state flux differences compared to the normal case. Abbreviations: LEX: lactate transport, HXEX: hypoxanthine transport, INOEX: inosine transport, ADEEX: adenine transport, ADO: adenosine transport.

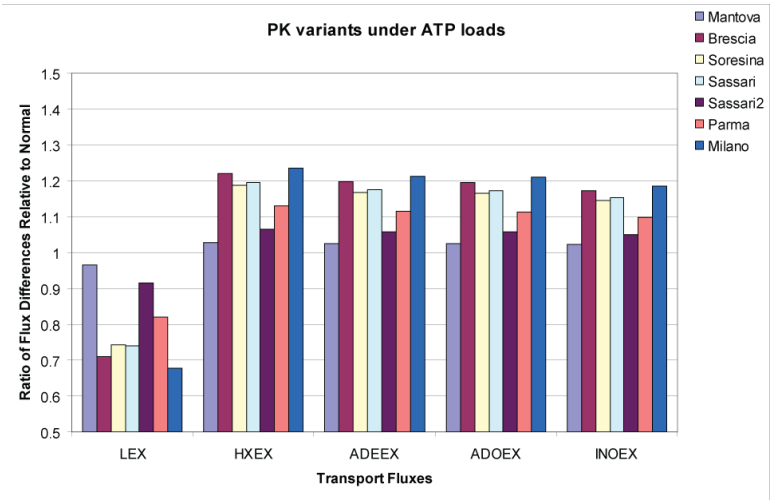

Figure 7.5: Red cell transport phenotypes: PK variants.

Characterization of different PK variants in terms of transport fluxes. A series of calculations analogous to those in Figure 2 were carried out for the PK variants with high and low energy loads. All of these variants showed altered uptake/secretion patterns for the transport fluxes compared to the normal red cell.

and how much they differ could be a measure of the pathological severity of the genetic variation.

One approach for the characterization of the dynamic response is to comprehensively identify the time-sequence of pool formation between all of the metabolites in a network [39]. This approach for determining the pooling structure in metabolic networks can be used to analyze how the cell responds to different fixed perturbations. As the nRBC responds to an increased redox load, the shift in flux from glycolysis to the pentose pathway is also reflected in changes in the time scales for pooling (see Appendix). The shifts in pooling time scales are observed throughout the network, however the most pronounced shifts involve the interactions between GL6P and the hexose-phosphates, the pentose phosphates and glutathione/NADPH, and the high energy phosphates (AMP, ADP, ATP) with the nucleotide precursor and degradation products. The pooling of metabolites over progressive time scales is a complex series of woven interactions. Pool formation on fast time scales generally reflect fast achievement of equilibrium between

isomers and other metabolites whose steady state concentration ratios are close to their equilibrium ratios [63, 66]. Pooling on slower time scales involve interactions between aggregate pools between different pathways in the network. These interactions are loosely illustrated in Figure 7.6, in order to highlight the distinction between pooling within pathways and interactions between pathways.

Dynamic response of the nRBC to energy loads

Similar computations of interactions among metabolites across all time scales can be characterized in response to energy loads for the nRBC. As discussed above, when the nRBC responds to an increased energy load, flux through glycolysis is increased at the cost of a reduced flux through the pentose pathway. When the dynamic pooling among metabolites for the nRBC at a normal versus an increased load are compared, there is a broad shifting of pooling between metabolites, with significant changes occurring between glycolytic intermediates and adenosine metabolites, and between nucleotide precursors and pentose phosphates.

Glucose-6-Phosphate Dehydrogenase Deficient Cases

The G6PD variants due to causal SNP mutations were analyzed in terms of their response to increased redox loads. Modal decomposition [68, 69] was carried out for each of these cases under low and high redox loads. The pooling between metabolites was then determined and compared for each of the cases under high redox loads (see Appendix) [39]. Changes in metabolite pooling over progressive time scales for the non-chronic variants (A+ and A-) are very similar to the normal cell, with the significant differences in pooling between metabolites occurring between members of the pentose phosphate pathway and some of the nucleotide precursors. The chronic hemolytic anemia variants in contrast, exhibit more pronounced changes in the dynamic sequence of interactions. The largest difference involve interactions between the oxidative branch of the pentose phosphate pathway and the first half of glycolysis, interactions among members within the non-oxidative branch of the pentose phosphate pathway, and the nucleotide

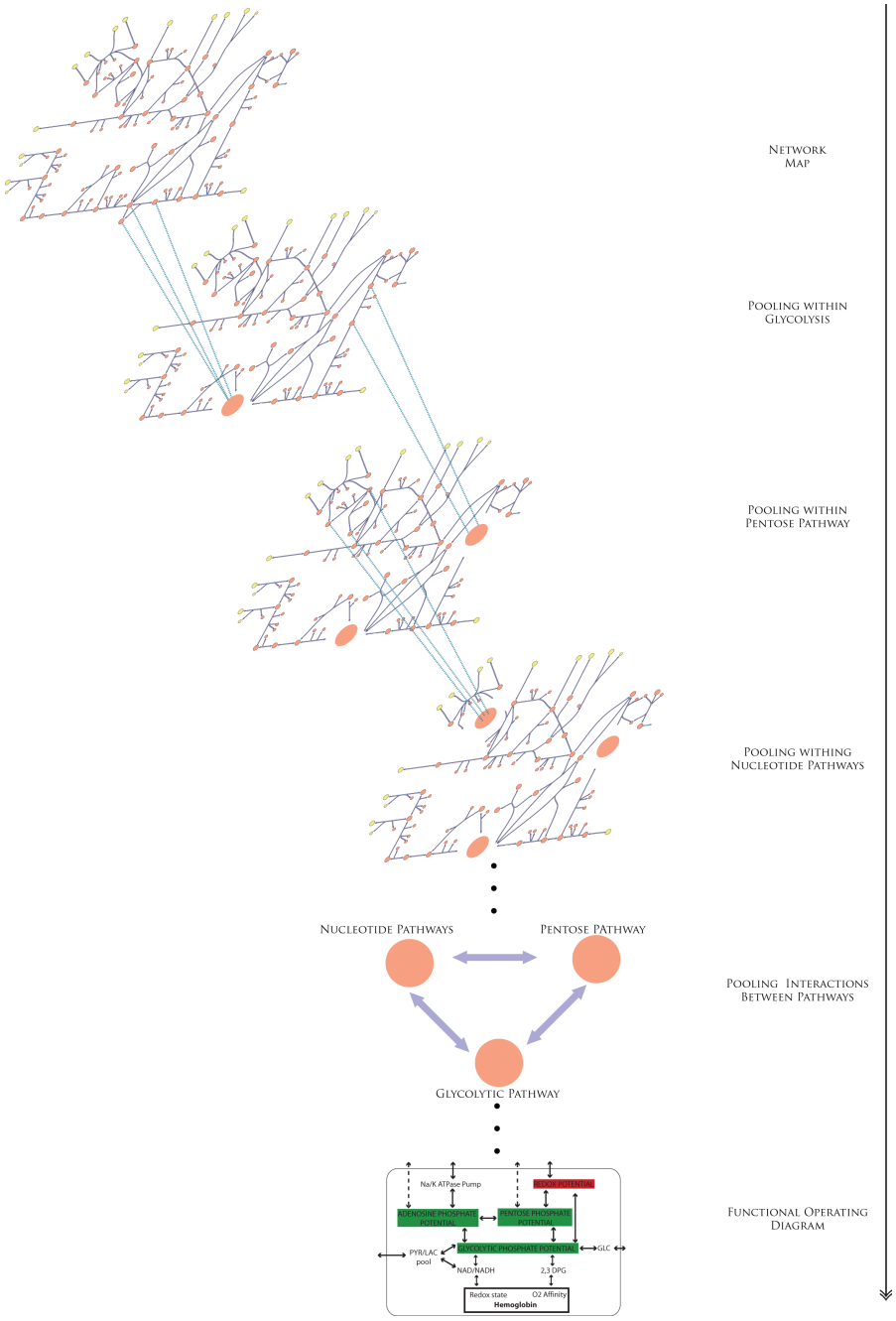

Figure 7.6: Dynamic pooling across multiple pathways.

A high-level schematic overview of the pooling interactions that occur over progressive time scales. Generally pooling occurs within particular pathways on the fast time scales and these pools of metabolites from the different pathways then interact with one another on the slower time scales. Changes in pooling time scales that occur within pathways can affect overall interactions between larger modules in the network.

salvage pathway metabolites. Referring to Figure 7.6, the alterations in dynamics of the oxidative branch in the pentose phosphate pathway resulted in disruptions of the interactions between the different pathways on slower time scales.

Considering the network in the context of the pools described in the middle panel in Figure 7.1, an macro summary of the alterations in metabolic states under increased redox loads of the six genetic variants considered are shown in Figure 7.7. The sizes of the boxes reflect the size of the respective metabolite pools at the steady state. It is immediately apparent that the chronic hemolytic variants have substantially reduced abilities to counteract oxidative stresses. Additionally there are changes in the dynamics of the chronic hemolytic variants, primarily among the metabolites that contribute to the adenosine phosphate potential and the pentose phosphate potential. The last four variants exhibited altered dynamic interactions among members of the nucleotide salvage pathways and the non-oxidative branch of the pentose phosphate pathway. These changes are highlighted, in a high level manner by the slanted arrows between the adenosine and phosphate pathway arrows in Figure 7.7.

Pyruvate Kinase Deficient Cases

In order to characterize the time hierarchical functionality of PK deficient variants, the dynamic pooling correlations were calculated for each vRBC under high-energy load conditions. Each vRBC was then compared to the nRBC under high-energy load conditions (see Appendix). The salient observations to be made from these computational results are: 1) the vRBCs all exhibit fairly similar patterns of variation from the responses of nRBC (unlike the G6PD variants considered above) and 2) the changes between high and low energy load in the variants are all similar to the changes observed for the nRBC. Since the energy charge remained fairly constant for all of the variants as well, the changes resulting from PK deficiency are reflected primarily as changes in the pool size of available ATP.

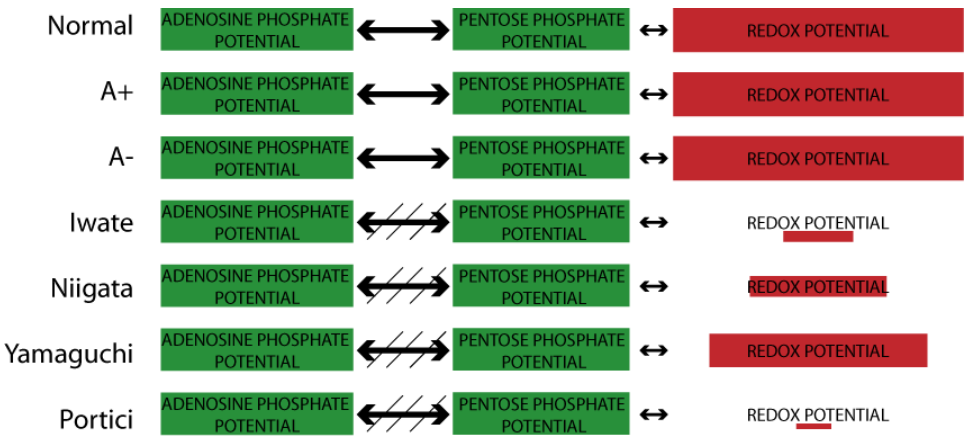

Figure 7.7: Phosphate and redox pool changes for G6PD variants.

A summary of the disruptions of the global pooling structure that occurs in the different G6PD variants. The size of the boxes reflects the size of the redox and phosphate potentials. The NADPH redox state (NADPH/(NADP + NADPH)) is used as the surrogate for the overall redox potential. The A+ and A- variants are almost identical to the normal cell. The chronic hemolytic variants however have significant changes in the size of their redox pools. Additionally, the dynamics of the interactions between the adenosine and pentose phosphate pathways are disrupted in the more severe variants (slanted lines through arrows).

7.1.3 Summary

Previous work has illustrated the utility of *in silico* models for elucidating the genotype-phenotype relationship through analysis of data from patients with two enzymopathies resulting from causal SNPs [35]. It has been established that intracellular cofactor ratios reflect intracellular functional states [3, 78]. Starting with an understanding of metabolic states in terms of a pooling structure (Figure 7.1), the present study focused on an in depth in silico investigation of the changes that occur in a normal and a genetically variant human erythrocyte. The chief results from the analysis herein are: 1) transport fluxes of bases can be used to characterize changes in the intracellular cofactor pools and dominant metabolic pathways, 2) internal charge ratios can be reflected in cofactor exchange rate response signatures, both of which are affected by genetic variants that have pathological consequences, and 3) the dynamic sequence of interactions that occur within a cell over time can be affected by pathological genetic variants.

Since the enzymopathies considered involved the redox and energy producing functions of the RBC, and these are two of its essential metabolic functions, the relevant perturbation conditions are altered redox and energy loads. When a cell changes from one steady state to another, there may be changes in the steady state concentrations, steady state fluxes, and/or the hierarchical interactions that occur over time. We investigated these changes in the red cell under various conditions, including clinically relevant disease states.

Calculation of the steady state concentrations and fluxes of the nRBC at various redox and energy loads illustrated that the two functional states can be distinguished according to the adenine, adenosine, hypoxanthine, and inosine transport fluxes. This observation can lead to a reduced and experimentally accessible view of the functional metabolic red cell (Figure 7.1) that maintains information about its functional metabolic state. An analysis comparing causal SNP variants and the normal erythrocyte (Figures 7.3, 7.4) demonstrates that the simplified view of the RBC can still be used to distinguish a range of pathophysiological states. The less severe G6PD variants could be differentiated from the more pathological chronic hemolytic patients based on changes in the transport fluxes, as depicted

in Figure 7.3.

In order to investigate the dynamic changes of the network under different conditions we calculated the time scales at which different metabolites pool together [39]. The resulting dynamic pooling plots allow a global assessment of the pooling structure of a network. Since we investigated dynamics near a region relatively close to a steady state, it is expected that the same cell may exhibit different dynamic properties when the external environmental conditions are varied. As such we proceeded to analyze the normal erythrocytes response to redox and energy loads in order to establish a reference point for comparison. The responses of the cell to each type of fixed perturbation resulted in different alterations in the resulting pooling structure of the network, however both types of perturbations resulted in changes in pooling of nucleotide salvage metabolites such as ADO, ADE, INO, HX, and R1P. The significance of this can be appreciated in consideration of the steady state changes (and the resulting distillation of the network shown in Figure 7.1 middle) and topological considerations. The two objectives, to produce ATP and to produce NADPH in order to maintain a reduced pool of GSH, compete for available G6P. Additionally, the nucleotide salvage pathway connects the two by virtue of the importance of ATP/ADP for glycolysis and the ribose phosphates in the non-oxidative branch of the pentose phosphate pathway. Thus although NADPH and ATP generation are linked at the top and bottom of their related pathways in the red cell, the dynamic response to an ATP load however will not be the direct opposite of a load on NADPH because the response times of enzymes in the different pathways differ significantly.

The non-chronic and chronic G6PD variants exhibited marked differences in the pooling of metabolites on progressively slower time scales. In general, the more severe, chronic G6PD variants exhibited a disrupted pooling structure of the network. The complex series of interactions and aggregate pool formation over progressive time scales are difficult to contemplate individually. As highlighted in Figure 7.6, pooling in general occurs between metabolites within pathways on faster time scales and between pathways on slower time scales. Analysis of the nRBC and vRBC dynamics under redox loads illustrated that disruptions that

shift the pooling behavior between metabolites within a pathway can subsequently result in disruption of interactions between pathways on the slower time scales. For the G6PD variants, this was reflected by changes in the interactions between the pentose phosphate pathway and the nucleotide salvage pathway. Thus, not all G6PD variants have the same metabolic disruptions in their pathways and furthermore, a red cell with G6PD deficiency is not the same as a red cell with a decreased ability to tolerate an oxidative load. These more severe changes result from the combined effect of significantly lowered Vmaxs and altered substrate binding constants.

It was observed that even PK variants were able to maintain their energy charge [3] in the 85-90% range [35], however it was not clear if the dynamics of the PK variants under higher energy loads were similar to that of the normal red cell. Investigations of the pooling structure suggest that indeed the dynamics of pool formation in PK variants, in contrast to the G6PD variants, are effectively the same as normal red cells, but with a diminished ability to respond to energy loads.

We carried out an analysis of a two different enzymopathies resulting from causal SNPs in human red cell using a kinetic model and investigating behavior at the steady state and dynamics close to steady state(s). While it was observed that the transport fluxes provided insight into the functional state of the cell, analysis of the dynamic structure and its variations under different conditions showed a more nuanced picture. Even for a normal cell, different conditions will result in different hierarchical dynamics between component variables. More interestingly, the dynamic behavior of PK deficient variants closely approximated the behavior of a normal cell in response to an energy load. A similar trend was observed for the less severe G6PD variants in response to redox loads. However chronic hemolytic G6PD deficient variants exhibited more pronounced and variable changes in the dynamic pooling hierarchy of metabolites.

Models can be used to simplify what appears complex and in some cases reveal complexity in areas that appeared to be simple. The use of kinetic models to assist in the characterization and understanding of the genotype-phenotype

relationship and disease states is likely to become a more valuable in the future, as models play a more active role in providing predictions and hypotheses to be tested experimentally. The predictions put forth can serve as hypotheses to be tested experimentally in future studies.

Ultimately such models can be used to simulate and compare normal (or nominal) and deviant behaviors based on genetic variation. Although whole body level simulations across temporal and spatial hierarchies are not achievable today, they are likely to become possible in the future. When this capability is at hand, diagnostic procedures and therapeutic interventions can be designed based on genetic variations.

7.2 Simulated perturbations of the example system

Linearized networks enable the analysis of the dynamic properties of networks, through the analysis of the Jacobian matrices, as discussed in detail throughout this work. The linearized network can also be used for the purpose of simulations, as alluded to in Chapter 2. In fact representation of the dual sets of equations describing network dynamics (Equations 2.8 and 2.10) lends themselves to analyzing networks in a biologically relevant manner since they are defined in terms of the deviations variables for concentrations and fluxes, $\mathbf{x}'$ and $\mathbf{v}'$, respectively. The panels in Figure 7.8 show the response of the example system when a 'cofactor load' is placed on the network. For the initial conditions, all of the metabolite concentrations were set to their steady state concentrations (i.e. deviation variables are 0), except for the metabolite X, which was set to one-tenth of its steady state value when t = 0. The response times for the v_1 and v_2 fluxes are much slower than those for v_3, v_9, and v_{10}. The charge state for X+Y returns to its original level (about 98%), however the C+D pool moves to a new steady state (Figure 7.8 D). Rather than simply plotting the responses from the system, one can adopt a more quantitative view and integrate the response of the system to a load. Figure 7.9 shows the integrated values for the set of metabolites and fluxes

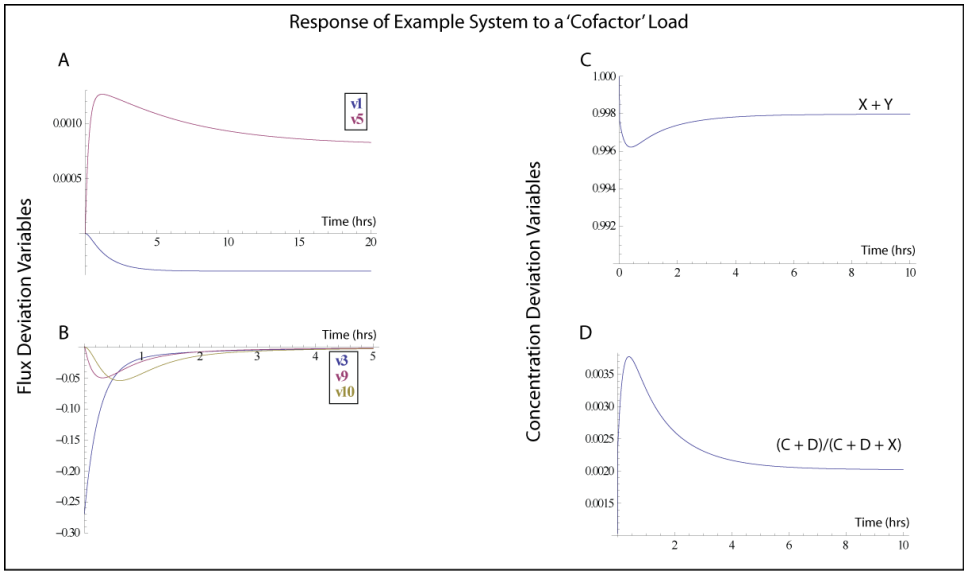

Figure 7.8: Response they toy network (Figure 2.4) to a cofactor load.

for the same system in response to the same load on X. Columns shown correspond to the 1, 5, 10, and 20 hour time points.

7.3 Simulated perturbations in the red blood cell

Perturbational analyses are most useful when there is a reference or base case to compare to. I return to the red cell model to compare the nRBC and vRBCs. The kinetic model of the red cell was linearized and a glutathione load of 90% from its steady state value (for each of the variants) was placed on the cell and the response of the system was plotted over time. Figure 7.10 shows the response of NADPH levels for nRBC and the 6 genetic variants over time. The response dynamics are clearly distinguishable for the different cases, with the non-chronic variants responding almost identically to the nRBC and the chronic variants showing various degrees of deviations from the nRBC. According to these plots, the Yamaguchi variant would be predicted to be less severe than the Portici, Niigata, or Iwate variants. In order to evaluate the validity of the linearization, the responses of the metabolites for the same set of initial conditions were integrated over an hour and compared to the non-linearized kinetic model (Figure 8.1). The

	1	5	10	20
metA	0.002	0.038	0.092	0.202
metB	0.051	0.332	0.689	1.403
metC	-0.039	-0.1	-0.114	-0.135
metD	0.036	0.09	0.096	0.102
metE	0.001	0.023	0.076	0.216
metF	-0.02	-0.033	-0.036	-0.039
metG	-0.014	-0.028	-0.031	-0.034
metX	0.003	0.01	0.018	0.033
metY	-0.003	-0.01	-0.018	-0.033

	1	5	10	20
v1	0	-0.001	-0.003	-0.006
v2	-0.005	-0.012	-0.014	-0.017
v3	0.191	1.244	2.579	5.253
v4	-0.038	-0.096	-0.108	-0.123
v5	0.001	0.006	0.011	0.019
v6	0	0.003	0.009	0.026
v7	-1.606	-7.752	-15.41	-30.72
v8	-0.027	-0.041	-0.045	-0.049
v9	-0.036	-0.06	-0.065	-0.071
v10	-0.039	-0.081	-0.089	-0.097

Figure 7.9: Response of toy network to a load on X.

The integrated response of the example system following a load on X. Column headings correspond to hours. Units of the metabolite table (top panel) are mM and in the flux table (bottom panel) are mM/hr.

magnitudes of the responses show clear differences, however the trends for each of the different models appear consistent between the linearized and non-linearized models.

7.4 Simulated perturbations with core *E. coli*

Simulations in response to perturbations can be carried out with the *E. coli* models constructed in Chapter 6. A series of simulations (with deviation variables so the baseline for all variables is 0) were carried out for the three different growth media conditions in response to a depletion of ATP (Figure 7.12. The predicted responses are surprisingly different for the same strain with different growth media. Cells grown in glucose respond by transiently decreasing the acetyl-coa and succinyl-coa pools, presumably to charge up the TCA cycle and increase ATP production. Consistent with this explanation is the spike in malate that occurs. Both of these changes occur on similar time scales (they relax to a new

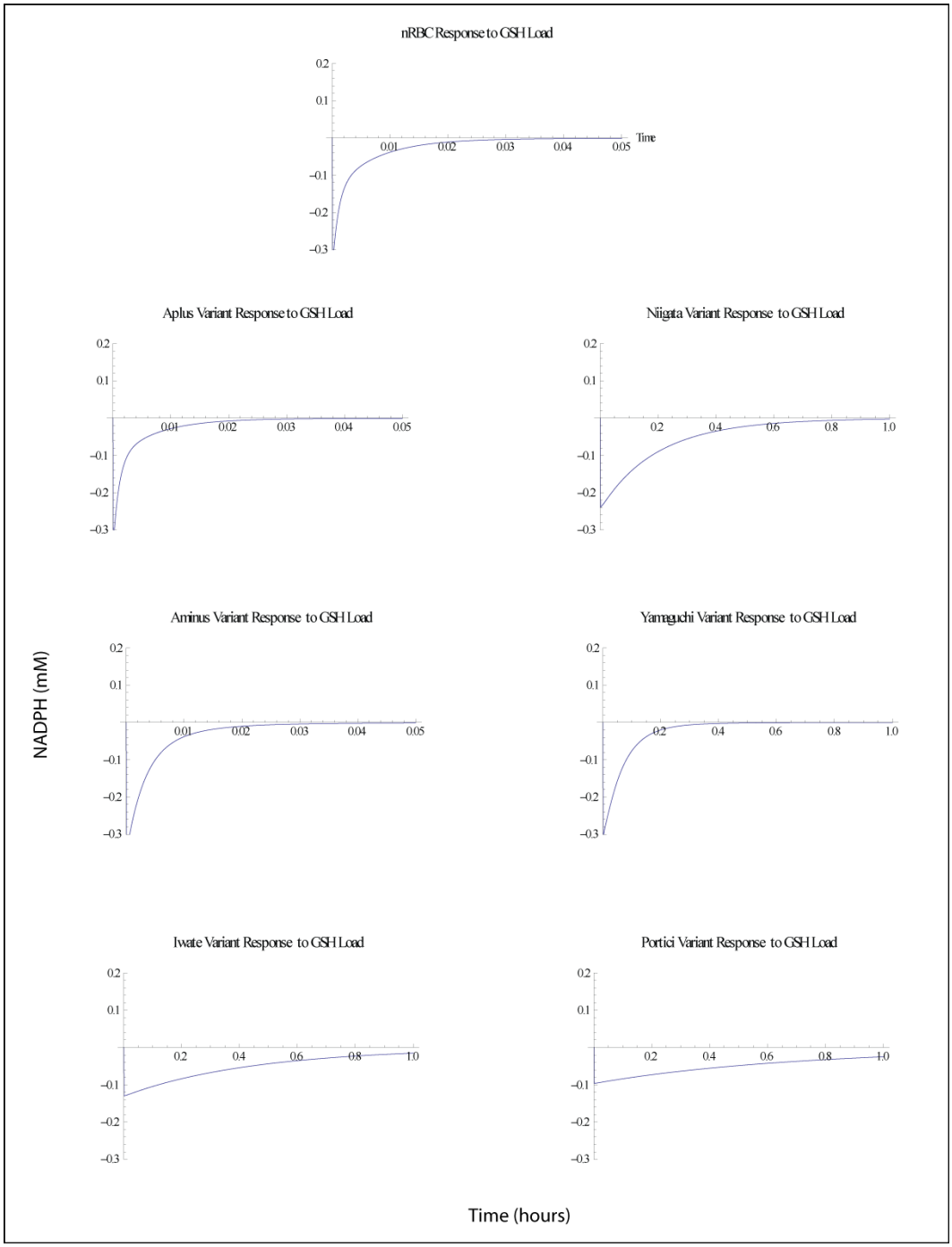

Figure 7.10: Redox laod on linearized red cell model.

NADPH response to a load on a series of linearized models of the red blood cell. Horizontal axis is time in hours. Note that the time course for the nRBC, Aplus Variant, and Aminus variant are only shown out to about 3 minutes since the response time is so fast. The other variants are shown out to 1 hour.

Integrated Response for Full Kinetic Model

	G6P	NADPH	GSH	ATP
Normal	-0.0325592	-0.0158051	2.63577	-0.0794545
Aplus	-0.0320633	-0.0152918	2.64604	-0.0771313
Aminus	-0.0329007	-0.0169943	2.60278	-0.0794759
Iwate	-0.0238788	-0.0223227	1.60959	-0.040167
Niigata	-0.0286104	-0.0320728	1.92427	-0.0513138
Yamaguchi	-0.0324575	-0.0268019	2.30772	-0.0660705
Portici	-0.0117884	-0.0226043	0.866509	-0.0174095

Integrated Response for Linearized Kinetic Model

	G6P	NADPH	GSH	ATP
Normal	-0.0331949	-0.00154318	2.97578	-0.0477571
Aplus	-0.0316343	-0.00125531	2.97806	-0.0450336
Aminus	-0.0350556	-0.00182245	2.97349	-0.0510104
Iwate	-0.0258975	-0.0530011	1.6746	-0.0369236
Niigata	-0.0349223	-0.0496549	2.3738	-0.0511497
Yamaguchi	-0.0380107	-0.0230819	2.77506	-0.0563935
Portici	-0.0186728	-0.052556	1.25689	-0.0262118

Figure 7.11: Kinetic versus linearized kinetic models.

A comparison between the full kinetic model and the linearized kinetic model in response to a significant glutathione load, integrated over one hour.

steady state after approximately 7.5 minutes). Cells grown on acetate have have a very slight and very fast dip in the charged coa pool and citrate levels increase significantly over a much slower time scale (relaxing back to a new steady state at about 4-5 minutes). The response by glycerol is different as well. Changes in the concentrations occur slightly slower than those observed with glucose. However the types of responses differ markedly, the charged coa pools actually increase, with a decrease in NADPH. At the same time, malate and citrate decrease while phosphoenolpyruvate and alpha-ketoglutarate increase.

These results are for linearized models and approximations to the kinetic structure of the networks, so the numerical values should be taken with a grain of salt. However, the qualitative differences are likely to reveal true differences. The summary point for these simulations is that core energy metabolism has different regulation and dynamics when the same strain of *E. coli* is grown under different conditions.

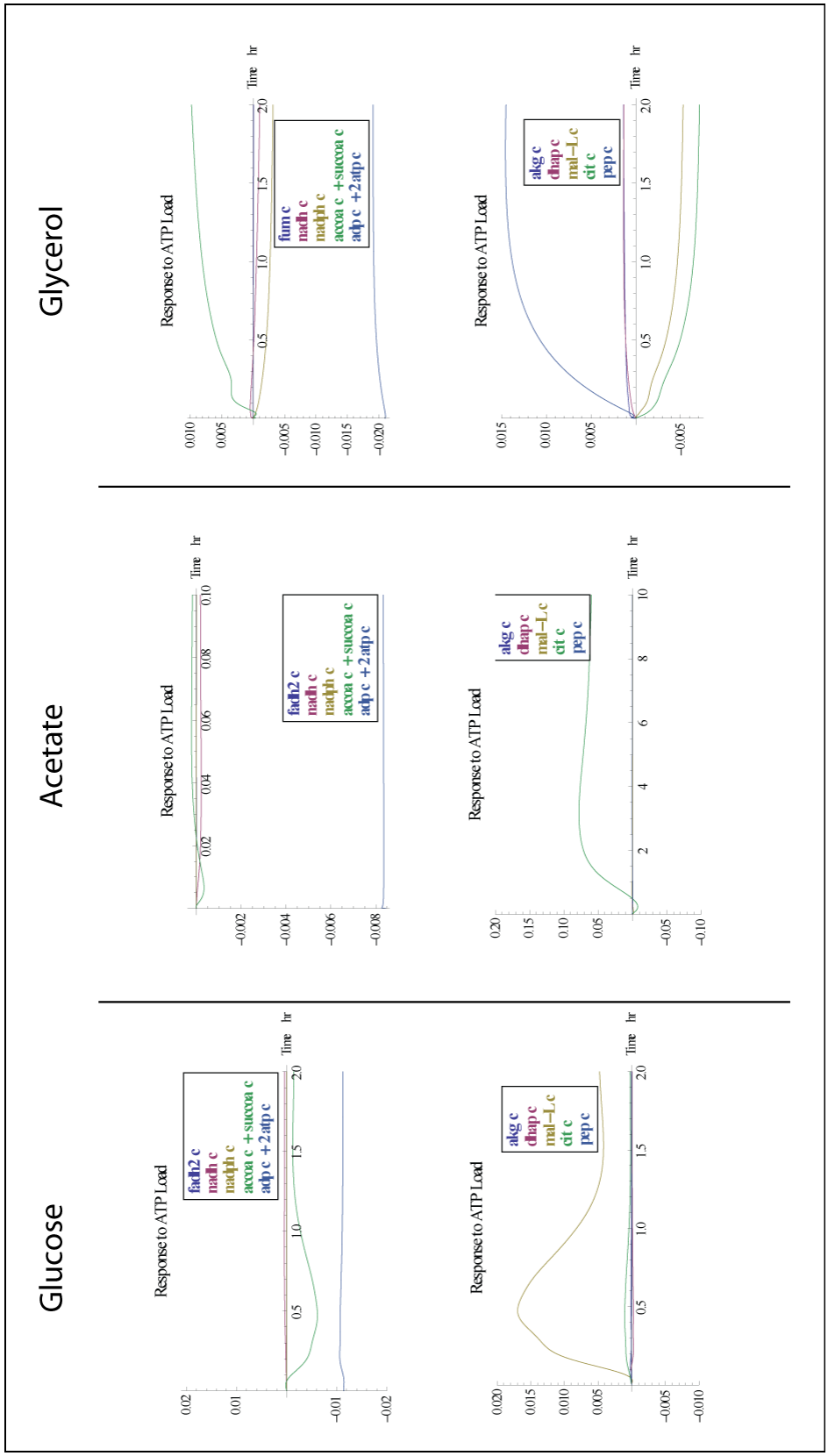

Figure 7.12: Response of *E. coli* grown on three different substrates responding to an energy load.

7.5 Summary

Biological systems are exceedingly complex across temporal and spatial hierarchies, it is thus very challenging to carry out comprehensive '-omics' measurements with absolute quantitation. The situation is not as bleak as this sounds however, because a great deal of information can be gained through the analysis of a system in response to perturbations. glucose tolerance test This concept is actually well known and accepted, and clinical tests often make use of this principal, for example the use of glucose tolerance tests for the diagnosis of diabetes mellitus. The main points to appreciate from the studies carried out in this chapter are,

- The best way to characterize different functional states (in the dry lab or wet lab) is to apply a stress to the system and to observe the response; perturbational studies are the key to describing and understanding function in biology.

- The transport fluxes can inform one about the intracellular metabolic state of a cell according to dry lab investigations and it would be worthwhile to test these hypotheses in the wet lab.

- The integrated response of a system (integrating fluxes and concentrations of interest) yield a 'response' parameter that is characteristic of that organism. Response parameters derived from the left null space will be informative about the general metabolic state (e.g. the redox state).

Chapter 8

Delta networks: It's all about changes and differences

Up until this point prominent topics in this work has involved the importance of changes, differences, and perturbations when analyzing metabolic networks in biology. This theme will be further advanced in this chapter. It may not be feasible or reasonable to expect to have comprehensive knowledge of biological systems and to be able to measure every metabolite quantitatively (or even to detect qualitatively). Hence there need to be methods for mechanistic modeling of networks in the absence of complete data sets. 'Delta modeling' approaches have been developed with this goal in mind.

8.1 The need, concept, and basic approach

Models are constructed with the goal of being comprehensive which allows for a systems based analysis. However, as the size of the models grows, so does the amount of data needed to carry out simulations or to apply the analytical approaches discussed herein, even for models that require none or very few parameters. Before getting wrapped up on the singular goal of building comprehensive models, with blinders on it is important to take a step back to consider what the general goals of models generally are, to test current understanding, to make predictions, to guide or direct future experiments, to test theories/hypotheses, and to

'find holes' where they haven't been seen before.

Often times for the above items the key information gained from models is to identify if changes occur and where they occur (or to at least present the most likely candidates responsible for the changes). With this in mind, it is often adequate to identify the change that occurs between two states, hence complete characterization of two models may not be necessary. It may in fact be adequate to characterize the change in the two networks, for example identifying the pathways that are more active in one condition as compared to another. The core idea is that when one has a reference data set to compare to the differences in the data sets can be evaluated under different 'hypothesis'. A comparison can be made against a constant genetic background, a constant environmental background, or a combination of the two.

I begin with the trivial consideration, that if two different flux distributions satisfy the non-trivial steady state condition for a specific $\mathbf{S}$ (Equations 8.1), then the difference of the fluxes, δ also satisfies the steady state conditions and Equation 8.4 must hold.

$$\begin{aligned} \mathbf{S} \cdot \mathbf{v}_1 &= \mathbf{0} \\ \mathbf{S} \cdot \mathbf{v}_2 &= \mathbf{0} \end{aligned} \tag{8.1}$$

$$\mathbf{S} \cdot (\mathbf{v}_1 - \mathbf{v}_2) = \mathbf{S} \cdot \delta = \mathbf{0} \tag{8.2}$$

This becomes an interesting discussion when one takes into consideration,

1. The different $\mathbf{v}$ may reflect changes in environmental or genetic factors.

2. The size of the null space does not change, thus even if one only knows the change in a handful of fluxes from one condition to another, then the changes in fluxes of the other reactions in the network may be predicted.

8.1.1 Illustrative example with the red blood cell

The simplest case carried out was for the normal versus the 6 G6PD variants using mass action rate laws,

$$\mathbf{v}_i(\mathbf{x}) - \mathbf{v}_1(\mathbf{x}) = \delta_{i-1} \tag{8.3}$$

for $i = 2 - 6$, for which δ was specified. Equation 8.3 was solved for a the reverse rate constants as functions of the forward rate constants. These equations were then solved for the forward rate constants, with the reverse rate constants held fixed. Since the same rate constant value was used for each of the variants, each of the values should be the same, if there are not differences between the variants. Differences in parts of the pathway that were perturbed appeared (e.g. different values for the rate constants). This was a comparison against an assumed constant environmental background, so the interpretation would be that the variants are due to altered genetics or an unknown regulatory influence. However, if a comparison were carried out against a constant genetic background, then the consistency of the equilibrium constant approximations could be evaluated.

8.2 δ mass balances

In the situation for which the changes in fluxes are not known (or partially known), then the set of mass balance equations can be solved for. Obviously, the sensitivity of detection of changes will decrease, since there is less data available.

$$\mathbf{S} \cdot (\mathbf{v}_1(\mathbf{x}) - \mathbf{v}_2(\mathbf{x})) = \mathbf{0} \tag{8.4}$$

The most obvious and direct application of this approach is for exometabolomic analyses [46], in which only measurements in the external media are made for cells grown in culture. When measurements are made under more than one condition, then delta constraints can be directly applied. The biofluid analogue (see Figure 8.3) extension for this approach can be carried out directly as well.

	Aplus	Aminus	Iwate	Niigata	Yamaguchi	Portici
HK	1.	1.	1.02	1.01	1.	1.03
PGI	1.	1.	0.99	1.	1.	0.99
PFK	1.	1.	0.99	1.	1.	0.98
ALD	1.	1.	0.99	1.	1.	0.99
TPI	1.	1.	0.99	1.	1.	0.99
GAPDH	1.	1.	0.86	0.95	0.98	0.81
PGK	1.	1.	0.87	0.95	0.99	0.82
DPGM	1.	1.	1.	1.	1.	1.
DPGase	1.	1.	1.	1.	1.	1.
PGM	1.27	1.27	1.07	1.2	1.25	1.
EN	1.27	1.27	1.07	1.2	1.25	1.
PK	1.3	1.3	1.08	1.22	1.27	1.
PEX	0.01	0.01	0.01	0.01	0.01	0.01
LDH	1.	1.	1.	1.	1.	1.
LEX	0.01	0.01	0.01	0.01	0.01	0.01
AMPase	1.	1.	1.	1.	1.	1.
ADA	1.	1.	1.	1.	1.	1.
AK	1.	1.	0.99	1.	1.	0.98
ADK	1.06	1.06	1.02	1.05	1.06	1.
AMPDA	1.	1.	1.	1.	1.	1.
ATPase	1.	1.	1.	1.	1.	1.
ADPRT	0.97	0.97	0.99	0.98	0.97	1.
G6PDH	1.01	1.01	1.	1.01	1.01	1.
PGLase	1.	1.	1.	1.	1.	1.
GL6PDH	0	0.01	0.74	0.27	0.09	1.
GSSGR	0.52	0.52	0.87	0.65	0.56	1.
GSHR	0.01	0.01	0.01	0.01	0.01	0.01
RU5PI	1.	1.	0.99	1.	1.	0.99
XU5PE	1.	1.	0.99	1.	1.	0.99
TKI	0.99	0.99	1.	0.99	0.99	1.
TKII	0.98	0.98	1.	0.99	0.98	1.
TALD	1.	1.	1.	1.	1.	0.99
IMPase	1.	1.	1.	1.	1.	1.
PNPase	1.	1.	1.	1.	1.	1.
PRM	1.	1.	1.	1.	1.	1.
PRPPSYN	1.	1.	1.	1.	1.	1.
HGPRT	0.95	0.95	0.99	0.96	0.95	1.
HXEX	0.01	0.01	0.01	0.01	0.01	0.01
ADEEX	0.01	0.01	0.01	0.01	0.01	0.01
ADOEX	0.01	0.01	0.01	0.01	0.01	0.01
INOEX	0.01	0.01	0.01	0.01	0.01	0.01
NALEAK	0.01	0.01	0.01	0.01	0.01	0.01
KLEAK	0.01	0.01	0.01	0.01	0.01	0.01
PUMP	1.	1.	1.	1.	1.	1.

Figure 8.1: δ network example in red blood cell.

An example of δ network analysis using the nRBC and vRBCs. Given a set of concentrations and differences in fluxes, the forward rate constants were solved for, assuming the for each enzyme the reverse rate constant did not change. The values for each enzyme were then scaled by the minimum rate constant.

0	−0.1 EN + 0.2 GAPDH − 0.3 LDH − 0.1 PEX + 0.3 PK
0.0000249936	0.1 EN − 0.2 GAPDH + 0.2 LDH + 0.1 PEX − 0.2 PK
-1.36457×10^{-6}	−0.2 ADA − 0.2 IMPase + 0.2 INOEX + 0.2 PNPase
−0.00226065	−0.1 DPGM − 0.1 EN + 0.1 GAPDH − 0.1 LDH − 0.1 PEX − 0.1 PGK + 0.1 PGM + 0.1 PK
−0.000650269	0.1 G6PDH + 0.1 GL6PDH − 0.1 PEX − 0.1 PGLase + 0.1 PGM − 0.1 RU5PI − 0.1 XU5PE
−0.0102857	0.1 DPGM + 0.1 G6PDH − 0.1 GL6PDH + 0.1 PEX − 0.1 PGM + 0.1 RU5PI + 0.1 XU5PE
0.0232575	−0.1 G6PDH + 0.2 PGLase − 0.1 RU5PI − 0.1 TALD + 0.1 TKII − 0.1 XU5PE
−0.00335449	−0.1 ALD − 0.1 DPGM − 0.1 EN + 0.1 GAPDH − 0.1 LDH − 0.1 PEX − 0.1 PGK + 0.1 PGM + 0.1 PK
−0.0134424	−0.1 DPGM − 0.1 HGPRT − 0.1 HXEX − 0.1 PEX + 0.1 PNPase + 0.1 TALD
−0.0468562	0.1 ADA + 0.1 ADOEX + 0.1 AK − 0.1 AMPase + 0.2 HGPRT + 0.2 HXEX − 0.2 PNPase
0.0838344	0.1 ADA + 0.1 ADOEX + 0.1 AK − 0.1 AMPase + 0.2 HGPRT + 0.2 HXEX − 0.2 PNPase
−0.190722	−0.1 ADA − 0.1 ADEEX − 0.1 ADOEX − 0.1 ADPRT − 0.1 AK + 0.1 AMPase − 0.1 HGPRT − 0.1 HXEX + 0.1 PNPase
0.150211	0.1 ADA + 0.1 ADOEX + 0.1 AK − 0.1 AMPase + 0.2 HGPRT + 0.2 HXEX − 0.2 PNPase
0.144826	−0.1 ADA + 0.1 ADEEX − 0.1 ADOEX − 0.1 AK + 0.1 AMPase − 0.2 HGPRT − 0.2 HXEX + 0.2 PNPase
0.186631	0.1 ADA + 0.1 HGPRT + 0.1 HXEX − 0.1 PNPase − 0.1 PRM
−0.286855	−0.1 ADA − 0.1 ADEEX − 0.1 ADOEX − 0.1 ADPRT − 0.1 AK + 0.1 AMPase − 0.1 HGPRT − 0.1 HXEX + 0.1 PNPase
−0.247335	0.2 DPGase − 0.2 DPGM − 0.2 PEX
−49.5727	0.1 ADEEX − 0.2 ADK + 0.1 ADOEX + 0.1 ADPRT + 0.1 HXEX + 0.1 INOEX − 0.1 PNPase + 0.1 PRM − 0.2 PRPPSYN
62.0662	−0.1 KLEAK − 0.3 NALEAK + 0.5 PUMP
−62.1601	−0.1 KLEAK + 0.2 NALEAK − 0.7 PUMP
136.369	−0.1 ADEEX − 0.1 ADOEX − 0.1 ADPRT − 0.2 AMPDA − 0.2 HGPRT + 0.2 IMPase + 0.1 PNPase − 0.1 PRM
−1141.64	0.3 AMPDA + 0.3 HGPRT − 0.3 IMPase

Figure 8.2: δ modal matrix.

The modal matrix for a δ approximation to the gradient matrix. Time scales appear to the left; any time scale with a negative entry reflects an unstable mode.

8.3 δ dynamics

As with analysis of dynamic networks, there are two approaches for the construction of δ networks: the analytical based and the simulation based.

8.3.1 Gradient approximations for analytical analyses

The dynamics, rather the dynamic changes in networks can be evaluated with this approach as well. Given measurements of fluxes and concentrations under two conditions, the elements of the gradient matrix can be grossly approximated as,

$$\mathbf{G} \approx \frac{\mathbf{v}_2 - \mathbf{v}_1}{\mathbf{x}_2 - \mathbf{x}_1} \tag{8.5}$$

Not surprisingly the Jacobian and modal matrices that result from these approximations exhibited unstable behavior. See for example 8.3, in which the eigenvalues are dominated by complex conjugate pairs and positive eigenvalues. While the interpretation of these modes is not presently apparent, there is clearly some structure in these modes (most of the reactions involved are from the pentose pathway and the nucleotide salvage pathways.

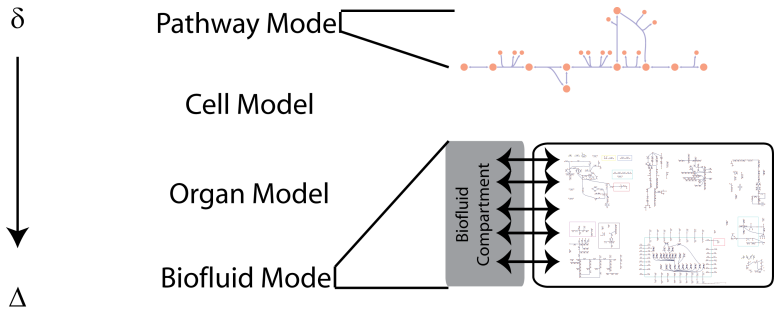

Figure 8.3: Delta Model Hierarchies.

The range of models, from 'little' delta (δ) to 'big' delta (Δ) models.

8.3.2 Rate law approximations for simulations

The concept of δ models can transgress spatial hierarchies as well. Figure 8.3 illustrates the progression from δ to Δ. The 'biofluid' model, is a concept in which one models the collective metabolism between all organ systems and a particular fluid compartment (plasma, CSF, or urine). The δ model approach (particularly Δ models) is focused on achieving the following goals,

- To allow the integration of *in vivo* data with stoichiometric models
- To support partial or 'incomplete' data sets
- To identify changes between different conditions

The approach explicitly discussed in this thesis to build kinetic models has been reduced to practice and shown to be feasible for core model of a prokaryote. These data may never be achievable for mitochondria, hence the δ model approach may set the stage to help characterize the row and column spaces of the mitochondria.

8.4 Summary

Given the fact that comprehensively complete data sets will never become available, the delta modeling approaches will likely be the framework for most analyses in the future. The type of model that is used is dependent on the type

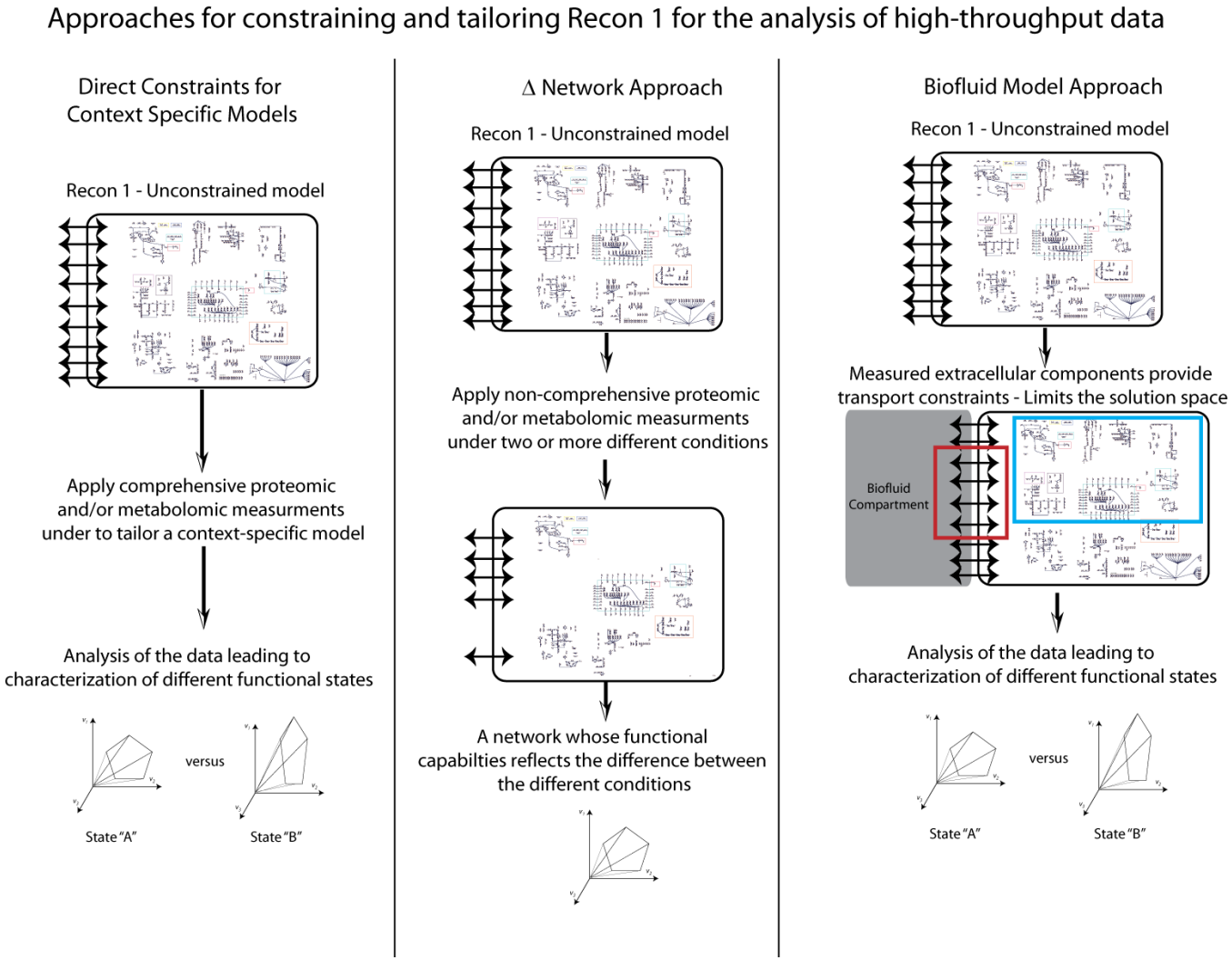

Figure 8.4: Approaches for constraining and analyzing biofluid models.

of question being asked the type of data that is available. The two questions that can stratify the type of model to be used are,

1. Does scientific question at hand require analytical or simulation based methods?

2. What type of concentration or flux data is available (intracellular versus exometabolomic/extracellular)?

Addressing these two questions will direct construction of the delta model. Growth and development of regulated, kinetic stoichiometric models are likely to be through the maturation of δ models. The initial conception with some simple, concrete illustrative cases are described herein in order to set the stage for future developments in this area.

Chapter 9

Conclusion

This thesis was introduced with an description of the four fundamental subspaces of biochemical reaction networks. In visiting each of these subspaces, it has become evident that the underlying mathematical restrictions imposed by the subspaces on another have biological implications and interpretations. Throughout this work there have been a number of lessons learned from the studies with the different models and the process of building these models. Along the way an effort has been made to highlight the key points and there is not a need to rehash what has already been summarized. I will only make mention of two very general statements, which will hopefully have very concrete interpretations after having read this thesis, interestingly the first stems from Chapter 2 and the second stems from Chapter 8,

- Structure determines function (The Fundamental Theorem of Linear Algebra and the physical/biological interpretations of $\frac{d\mathbf{x}}{dt} = \mathbf{S} \cdot \mathbf{v}$)
- It is response to a perturbations that truly informs a 'functional' state

Truly appreciating these statements, the findings that mechanistic regulation is should be represented as bilinear interactions, the potential and ability to approximate the dynamic structure of networks with the gradient matrix, the intracellular information that can be derived from knowledge about transporters, and all of the other observations and findings follow from above statements.

The approaches and methods described here can be applied to any almost any type of biological network (assuming that the components are at concentrations above the continuum limit; if stochastic effects begin to dominate, the governing equation must be revised). The work done during the course of this thesis and studies which have been done (in this work and outside of this work) have culminated to the recognition and appreciation of a particular concept and somewhat ironically, I am introducing this in the conclusion of this thesis.

9.1 Summary

Summaries and recapitulations are abound in this dissertation. In keeping with this trend, I will present a final broad recap of some of the main concepts described and realized in this thesis.

- Characterizing a network requires an understanding of all the major subspaces
- Structure determines function applies to steady states as well as dynamic states
- Mechanistic incorporation of regulation can be achieved with bilinear kinetics and can account for the robust behavior characteristic in many biological systems
- Kinetic models can be built in an integrated middle-out fashion using fluxomic and metabolomic data
- There is a duality between fluxes and concentrations fundamentally born out the relationship between enzyme turnover times (which span multiple orders of magnitude in biological systems) and compound concentrations (which span many orders of magnitude in biology)
- Perturbational analyses are critical in identifying and characterizing different ***functional*** states

- Transport fluxes can track and reflect internal states
- Data will never be as comprehensive as desired, hence delta models will be crucial for the characterization of model building and analysis
- Models can now be seen as means to understand biological systems from physical perspectives by serving as a means to integrate data as well as serving as a tool to evaluate data consistency

Taking a slightly different view of the components and divisions of the topics covered in this dissertation, Figure 9.1 considered the sub-topics related to model construction, the role of mathematics, and the conceptual motivation behind the analyses. All of these aspects serve a purpose in the construction of kinetic models and the characterization of metabolic networks. Furthermore all of these flow together and is centered around the data; the data drives theory and model development and the purpose of models is to analyze, integrate, and interrogate data. Briefly put, in the omics era, data is king ... in theory and practice.

9.2 The future

While many areas were covered in the course of the last 8 Chapters, this is still a drop in the bucket for the different fields and topics that were touched upon. For example models were discussed ranging from prokaryotes (*M. tb* and *E. coli*) to the most complex eukaryotes (*H. sapiens*). Clearly then the studies and methods described were not meant to be the last word in this area, but hopefully the first few words in an area that will grow and lead to a new generation of dynamic models. The most trivial direction forward is to increase the scope and complexity of the networks and the regulated enzymes. Incorporation of signaling networks to account for their interactions with metabolism for integrated dynamic signaling and metabolism models will be important in the application of models to pathophysiological cases. A topic that was not covered in detail, but has some relevance is that of traditional thermodynamics. While thermodynamics clearly plays a very important role in these models (see 5.2), there are still some large

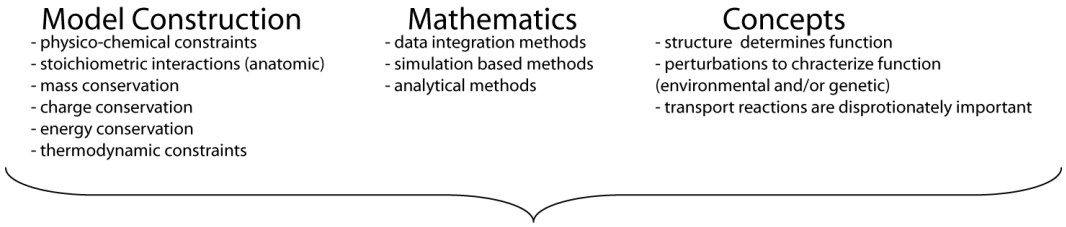

Figure 9.1: Models, math, and concepts.

gaps in need of substantial bridges in order to bring *in vivo* data measurements in line with current quantitative descriptions and approximations of thermodynamic parameters. A few examples of the present challenges are,

1. The semi-crystalline intracellular environment is markedly different than the aqueous environment found in the test tubes that measurements are often made.

2. Equilibrium thermodynamic interpretations are not regularly applicable for the analysis of living systems, which exist in non-equilibrium conditions.

3. In spite of many years of research in the area, there still appears to be some discussion in the community about what the value of the activity coefficients are for small metabolites.

These concerns call into question many of the assumptions and approximations that are used in thermodynamic analysis in the literature. Progress in science of course occurs through taking small steps forward and it is not the intent to criticize, but just to highlight an area that needs further effort, focus, and investigation by bright, motivated individuals.

9.3 On the conception and utility of models

There are likely to be many uses and applications of models that are not recognized today, that will be recognized in the future. Additionally, there are likely to be some uses which are believed to be of interest in the future that will simply not 'pan-out'. No attempt will be made here to try to classify, predict, and prognosticate all of the different fields which modeling and Systems Biology will influence and the potential impact on society as a whole. I will however make one general prediction that Systems Biology and medicine will affect one another significantly with the next 20-30 years.

9.3.1 Models and medicine

Two significant areas of focus in medical research are translational medicine, how to pave the most direct and efficient route from bench to bedside, and personalized medicine, how to treat a patient based on their individual genotype and lifestyle characteristics, not based upon general population statistics (the exception is when one is able to control for the genetic background). The goals and aims of Systems Biology can directly contribute to helping the medical field make this shift. The key is to develop models that have mechanistic components, yet can still be feasible to construct and can incorporate the types of data that are actually measured. Given the central role of metabolism in healthy and disease states, plus the ability to measure the metabolic phenotype directly from patients (i.e. the metabolome) in addition to the network structure which serves to integrate the data into a self consistent model, it appears clear to me that metabolism and Metabolic Systems Biology will be a key link in achieving the visions of personalized medicine and making translational medicine success stories in the process. Furthermore it will be the models ability to characterize and analyze changes within and individual and between individuals that will likely be of greatest utility.

9.3.2 Models as tools

The philosophy and conception of mathematical models and *in silico* modeling has been changing dramatically within the past decade. Models are being seen less as the irrelevant occupations of niche researchers and more as useful and in some budding cases, vital in the progress of biology. Out of the studies born from this dissertation, given the utility of models in generating as well as testing hypotheses and for the integration of data to enable the rational analysis of the data, this portends the use of Model Driven Analysis of Data (MoDAD) and the application of models in the field of medicine as Model Driven Diagnostics (MoDD). Thus there is a shift in the philosophy about why models are built and what they are used for. This new role for models views them as tools for evaluation (e.g. consistency checks), integration, and analysis of experimental data. It seems that during the past few centuries each decade has been brighter and brighter in

science and it appears that on the eve of the era of genome-scale kinetics, the future looks just even brighter.

Appendix A

Reference Material

HCR set	Reaction	Metabolic Subsystem
1	G3PAT190	Fatty Acid Metabolism
1	AGPAT190	Fatty Acid Metabolism
2	THDPS	Lysine Metabolism
2	DHDPRy	Lysine Metabolism
2	DHDPS	Lysine Metabolism
3	DHAD1	Valine, Leucine, and Isoleucine Metabolism
3	KARA1i	Valine, Leucine, and Isoleucine Metabolism
3	ACLS	Valine, Leucine, and Isoleucine Metabolism
4	KARA2i	Valine, Leucine, and Isoleucine Metabolism
4	DHAD2	Valine, Leucine, and Isoleucine Metabolism
4	ACHBS	Valine, Leucine, and Isoleucine Metabolism
5	ADSL2r	Purine Metabolism
5	PRASCS	Purine Metabolism
6	DHPPDA	Riboflavin Metabolism
6	GTPCII	Riboflavin Metabolism
7	GTPCII2	Cofactor Metabolism
7	DHPPDA2	Riboflavin Metabolism
8	SDPDS	Lysine Metabolism
8	DAPE	Lysine Metabolism
9	HPPK	Folate Metabolism
9	FOLD3	Folate Metabolism
9	DHNPA	Folate Metabolism
10	IGPS	Phenylalanine Tyrosine Tryptophan Metabolism
10	PRAIi	Histidine Metabolism
10	ANPRT	Phenylalanine Tyrosine Tryptophan Metabolism
10	ANS	Phenylalanine Tyrosine Tryptophan Metabolism
11	DHQS	Phenylalanine Tyrosine Tryptophan Metabolism
11	DDPA	Phenylalanine Tyrosine Tryptophan Metabolism
11	SHK3Dr	Phenylalanine Tyrosine Tryptophan Metabolism

11	DHQD	Phenylalanine Tyrosine Tryptophan Metabolism
12	PNTK	Pantothenate and CoA Metabolism
12	PANTS	Pantothenate and CoA Metabolism
12	DPR	Pantothenate and CoA Metabolism
12	MOHMT	Pantothenate and CoA Metabolism
13	AMMQT6	Ubiquinone Metabolism
13	DHNAOT2	Ubiquinone Metabolism
14	IPPMIb	Valine, Leucine, and Isoleucine Metabolism
14	IPPMIa	Valine, Leucine, and Isoleucine Metabolism
15	TMPKr	Thiamine Metabolism
15	TMPPP	Thiamine Metabolism
15	THZPSN	Sugar Metabolism
15	PMPK	Thiamine Metabolism
16	CDPMEK	Polyprenyl Metabolism
16	DXPRIi	Polyprenyl Metabolism
16	MEPCT	Polyprenyl Metabolism
16	MECDPDH	Polyprenyl Metabolism
16	MECDPS	Polyprenyl Metabolism
17	GUACYC	Purine Metabolism
17	PDE4	Purine Metabolism
18	OMCDC	Valine, Leucine, and Isoleucine Metabolism
18	IPMD	Valine, Leucine, and Isoleucine Metabolism
19	PSERT	Glycine, Serine, and Threonine Metabolism
19	PGCD	Glycine, Serine, and Threonine Metabolism
19	PSP_L	Glycine, Serine, and Threonine Metabolism
20	SHKK	Phenylalanine Tyrosine Tryptophan Metabolism
20	CHORS	Phenylalanine Tyrosine Tryptophan Metabolism
20	PSCVT	Phenylalanine Tyrosine Tryptophan Metabolism
21	GLUDC	Glutamate Metabolism
21	ABTA	Glutamate Metabolism
22	ADCL	Folate Metabolism

22	ADCS	Folate Metabolism
23	CHRPL	Membrane Metabolism
23	FASPHDCA	Membrane Metabolism
23	AACPS11	Membrane Metabolism
24	OHPBAT	Glycine, Serine, and Threonine Metabolism
24	E4PD	Cofactor Metabolism
24	4HTHRS	Cofactor Metabolism
24	PERD	Cofactor Metabolism
25	G1SATi	Porphyrin Metabolism
25	UPP3S	Porphyrin Metabolism
25	GLUTRR	Cofactor Metabolism
25	PPBNGS	Porphyrin Metabolism
25	HMBS	Porphyrin Metabolism
26	APRAUR	Riboflavin Metabolism
26	PMDPHT	Cofactor Metabolism
27	ADMDCr	Methionine Metabolism
27	MTAN	Methionine Metabolism
27	AGMT	Glutamate Metabolism
27	ARGDC	Glutamate Metabolism
27	SPMS	Urea Cycle
27	UREA	Purine Metabolism
28	METS	Methionine Metabolism
28	MTHFR2	Folate Metabolism
29	GGLUCT2	Membrane Metabolism
29	GTMLT	Other Amino Acid Metabolism
29	OPAH	Glutamate Metabolism
29	AMPTASECG	Other Amino Acid Metabolism
30	ACBIPGT	Cofactor Metabolism
30	NNDMBRT	Riboflavin Metabolism
30	ADOCBLS	Porphyrin Metabolism
30	RZ5PP	Cofactor Metabolism

31	HPPK2	Folate Metabolism
31	DHNPA2	Folate Metabolism
31	DHPS2	Folate Metabolism
32	G6PDH2	Pentose Phosphate Pathway
32	GND	Pentose Phosphate Pathway
32	PGL	Pentose Phosphate Pathway
33	DBTSr	Biotin Metabolism
33	AOXSr	Biotin Metabolism
33	AMAOTr	Biotin Metabolism
34	G16MTM2	Membrane Metabolism
34	MANAT1	Membrane Metabolism
35	G16MTM5	Membrane Metabolism
35	G16MTM4	Membrane Metabolism
36	G16MTM7	Membrane Metabolism
36	G16MTM9	Membrane Metabolism
36	G16MTM8	Membrane Metabolism
36	G16MTM10	Membrane Metabolism
37	ACOTA	Urea Cycle
37	AGPR	Urea Cycle
38	SERAT	Cysteine Metabolism
38	CYSS	Cysteine Metabolism
39	BMNMSHS	Redox Metabolism
39	MSHAMID	Redox Metabolism
39	ACYSBMNt	Transport
39	EX_acysbmn(e)	Transport
40	PC8XM	Cofactor Metabolism
40	R05219	Cofactor Metabolism
40	COCHL	Porphyrin Metabolism
40	ADCYRS	Porphyrin Metabolism
40	PC17M	Cofactor Metabolism
40	PC6YM	Cofactor Metabolism

40	PC20M	Cofactor Metabolism
40	R05217	Cofactor Metabolism
40	PC6AR	Cofactor Metabolism
40	PC11M	Cofactor Metabolism
40	CYRDAR	Cofactor Metabolism
40	CYRDAAT	Cofactor Metabolism
40	R05224	Cofactor Metabolism
41	PDHbr	Glycolysis
41	PDHa	Glycolysis
42	GLGC	Sugar Metabolism
42	GLCS1	Glycolysis
42	GLCP	Sugar Metabolism
43	UDPGALM	Peptidoglycan Metabolism
43	O16RHAT	Membrane Metabolism
43	HAS	Fatty Acid Metabolism
43	ACGAMT	Peptidoglycan Metabolism
43	TAS	Fatty Acid Metabolism
43	ARABF	Membrane Metabolism
43	GALFT	Membrane Metabolism
43	AFTA	Membrane Metabolism
43	AFE	Membrane Metabolism
43	GMT2	Membrane Metabolism
44	GTPCI	Folate Metabolism
44	DNMPPA	Folate Metabolism
44	DNTPPA	Folate Metabolism
45	GCCc	Methionine Metabolism
45	GCCb	Glycine, Serine, and Threonine Metabolism
45	GCCa	Glycine, Serine, and Threonine Metabolism
46	PREPTHS	Membrane Metabolism
46	ARACHTA	Membrane Metabolism
46	FACOAL200	Membrane Metabolism

47	ARGSL	Alanine and Aspartate Metabolism
47	ARGSS	Alanine and Aspartate Metabolism
48	BETALDHx	Other Amino Acid Metabolism
48	CHOLD	Other Amino Acid Metabolism
48	CHLabc	Transport
49	PDE1	Purine Metabolism
49	ADNCYC	Purine Metabolism
50	CIGAMS	Redox Metabolism
50	MSHS	Redox Metabolism
51	CPC6MT	Porphyrin Metabolism
51	CPC6R	Porphyrin Metabolism
51	CPC8MM	Porphyrin Metabolism
52	CPC3MT	Porphyrin Metabolism
52	CPC2MT	Porphyrin Metabolism
52	CPC4MT	Porphyrin Metabolism
53	UPPDC1	Porphyrin Metabolism
53	CPPPGO	Porphyrin Metabolism
53	PPPGO	Porphyrin Metabolism
54	Cut1	Transport
54	Cuabc	Transport
55	NTPP5	Nucleotide Sugar Metabolism
55	NDPK8	Pyrimidine Metabolism
56	RBFSa	Riboflavin Metabolism
56	DB4PS	Cofactor Metabolism
56	RBFSb	Riboflavin Metabolism
57	FAS100	Fatty Acid Metabolism
57	FAS140	Fatty Acid Metabolism
57	FAS120	Fatty Acid Metabolism
58	ADSL1r	Purine Metabolism
58	ADSS	Purine Metabolism
59	NTD3	Nucleotide Sugar Metabolism

59	DCYTD	Pyrimidine Metabolism
60	DPPS	Polyprenyl Metabolism
60	UDPDPS	Polyprenyl Metabolism
61	DCPT2	Membrane Metabolism
61	DCPDPP2	Membrane Metabolism
62	DCPE	Polyprenyl Metabolism
62	DCPT	Polyprenyl Metabolism
62	DCPDPP	Polyprenyl Metabolism
63	DADA	Nucleotide Sugar Metabolism
63	PUNP6	Purine Metabolism
64	FASm2401	Membrane Metabolism
64	FASm1801	Membrane Metabolism
64	FASm2001	Membrane Metabolism
64	FASm2601	Membrane Metabolism
64	FASm2201	Membrane Metabolism
64	FASm1601	Membrane Metabolism
64	FASm2801	Membrane Metabolism
65	FASm2002	Membrane Metabolism
65	FASm2402	Membrane Metabolism
65	FASm2202	Membrane Metabolism
66	FASm240	Membrane Metabolism
66	FASm260	Membrane Metabolism
66	FASm220	Membrane Metabolism
66	FASm280	Membrane Metabolism
67	NADS2	Glutamate Metabolism
67	NNAT	Pantothenate and CoA Metabolism
68	PPCDC	Pantothenate and CoA Metabolism
68	PTPATi	Pantothenate and CoA Metabolism
68	DPCOAK	Pantothenate and CoA Metabolism
69	TDPGDH	Nucleotide Sugar Metabolism
69	G1PTT	Nucleotide Sugar Metabolism

69	TDPDRR	Nucleotide Sugar Metabolism
69	TDPDRE	Nucleotide Sugar Metabolism
70	IGPDH	Histidine Metabolism
70	ATPPRT	Histidine Metabolism
70	HISTD	Histidine Metabolism
70	HSTPT	Histidine Metabolism
70	PRAMPC	Histidine Metabolism
70	IG3PS	Histidine Metabolism
70	PRATPP	Histidine Metabolism
70	HISTP	Histidine Metabolism
70	PRMICIi	Histidine Metabolism
71	MEOHt2	Transport
71	PRDX	Redox Metabolism
71	ALDD1	Redox Metabolism
72	CMCBTFU	Redox Metabolism
72	CMCBTFL	Redox Metabolism
73	GARFT	Purine Metabolism
73	PRFGS	Purine Metabolism
73	PRAIS	Purine Metabolism
73	GLUPRT	Purine Metabolism
73	PRAGSr	Purine Metabolism
74	RRPPDIMAS	Membrane Metabolism
74	RPPDIMAS	Membrane Metabolism
74	GFUCS	Sugar Metabolism
74	GMAND	Sugar Metabolism
74	PGLS	Membrane Metabolism
74	FRRPPDIMAS	Membrane Metabolism
75	GALT	Nucleotide Sugar Metabolism
75	GALKr	Sugar Metabolism
76	GLUCYS	Glutamate Metabolism
76	GTHS	Redox Metabolism

77	GRTT	Polyprenyl Metabolism
77	DMATT	Cofactor Metabolism
78	ACChex	Fatty Acid Metabolism
78	ACCC	Fatty Acid Metabolism
79	FASm2602	Membrane Metabolism
79	FASm340	Membrane Metabolism
79	FASm300	Membrane Metabolism
79	FASm320	Membrane Metabolism
79	FASm2802	Membrane Metabolism
80	IACGAMS	Redox Metabolism
80	IGAMD	Redox Metabolism
81	QULNS	Pantothenate and CoA Metabolism
81	ASPO5	Alanine and Aspartate Metabolism
81	NNDPR	Pantothenate and CoA Metabolism
82	EX_id3acald(e)	Transport
82	ID3ACALDt	Transport
82	TRPTA	Other Amino Acid Metabolism
82	INDPYRD	Pyruvate Metabolism
83	ADK4	Nucleotide Sugar Metabolism
83	NDPK9	Pyrimidine Metabolism
84	ILEt2r	Transport
84	ILETA	Valine, Leucine, and Isoleucine Metabolism
85	TRPS3	Phenylalanine Tyrosine Tryptophan Metabolism
85	TRPS2	Phenylalanine Tyrosine Tryptophan Metabolism
86	FAMPL3	Fatty Acid Metabolism
86	MYCON3	Fatty Acid Metabolism
86	MYC1CYC3	Fatty Acid Metabolism
86	MYC2CYC3	Fatty Acid Metabolism
87	LACZ	Sugar Metabolism
87	LCTSabc	Transport
88	LEUTA	Valine, Leucine, and Isoleucine Metabolism

88	LEUt2r	Transport
89	MOTH	Sugar Metabolism
89	MALTHPabc	Transport
89	MOTS	Sugar Metabolism
90	FAMPL1	Fatty Acid Metabolism
90	MYC1CYC1	Fatty Acid Metabolism
90	MYCON1	Fatty Acid Metabolism
90	MYCSacp50	Fatty Acid Metabolism
90	MYC2CYC1	Fatty Acid Metabolism
91	METSOXR2	Other Amino Acid Metabolism
91	METOX2s	Methionine Metabolism
92	METSOXR1	Other Amino Acid Metabolism
92	METOX1s	Methionine Metabolism
93	MYC1M2	Fatty Acid Metabolism
93	MYCON5	Fatty Acid Metabolism
93	FAMPL5	Fatty Acid Metabolism
93	MYC1CYC5	Fatty Acid Metabolism
94	MMM2r	Fatty Acid Metabolism
94	MME	Fatty Acid Metabolism
95	MYCON2	Fatty Acid Metabolism
95	MYC2CYC2	Fatty Acid Metabolism
95	MYC1CYC2	Fatty Acid Metabolism
95	FAMPL2	Fatty Acid Metabolism
96	MYC1M1	Fatty Acid Metabolism
96	FAMPL4	Fatty Acid Metabolism
96	MYCON4	Fatty Acid Metabolism
96	MYC1CYC4	Fatty Acid Metabolism
97	AACPS10	Fatty Acid Metabolism
97	FASm180	Membrane Metabolism
98	DHORD3	Pyrimidine Metabolism
98	FRD5	Citric Acid Cycle

99	APATr	Alanine and Aspartate Metabolism
99	MMSAD3	Sugar Metabolism
100	MSHOXH	Redox Metabolism
100	MDFDH	Redox Metabolism
101	NAt3_1	Transport
101	NAKtr	Transport
102	NO	Redox Metabolism
102	NOt	Transport
103	FACOAL80	Fatty Acid Metabolism
103	MCBTS3	Membrane Metabolism
104	OXCDC	Glyoxylate Metabolism
104	GLXO1	Glyoxylate Metabolism
104	OXACOAL	Glyoxylate Metabolism
105	PHYCBOXL	Phenylalanine Tyrosine Tryptophan Metabolism
105	ALDD19x	Phenylalanine Tyrosine Tryptophan Metabolism
105	PEAMNO	Phenylalanine Tyrosine Tryptophan Metabolism
106	PHTHS	Membrane Metabolism
106	PDIMAT	Transport
106	PHTHDLS	Membrane Metabolism
106	PDIMAS	Membrane Metabolism
106	EX_pdima(e)	Transport
107	CLPNS160190	Membrane Metabolism
107	PGSA160190	Membrane Metabolism
107	PGPP160190	Membrane Metabolism
108	PGSA160	Fatty Acid Metabolism
108	PGPP160	Membrane Metabolism
109	PGPP190	Membrane Metabolism
109	PGSA190	Membrane Metabolism
110	PHDCAt	Transport
110	PHDCATA	Fatty Acid Metabolism
110	FACOALPHDCA	Membrane Metabolism

111	HSK	Glycine, Serine, and Threonine Metabolism
111	THRS	Glycine, Serine, and Threonine Metabolism
112	PHTHS2	Membrane Metabolism
112	PREPPACPH	Membrane Metabolism
112	PPDIMAS	Membrane Metabolism
112	PHTHDLS2	Membrane Metabolism
112	PREPTHS2	Membrane Metabolism
113	PREPTTA	Membrane Metabolism
113	FACOALPREPH	Membrane Metabolism
114	PSSA160	Fatty Acid Metabolism
114	PSD160	Fatty Acid Metabolism
115	PSD180	Fatty Acid Metabolism
115	PSSA180	Fatty Acid Metabolism
116	PLCD	Fatty Acid Metabolism
116	CDPPT160	Membrane Metabolism
117	G16MTM1	Membrane Metabolism
117	CDPPT160190	Membrane Metabolism
118	PYDXNO	Cofactor Metabolism
118	PYDXO	Cofactor Metabolism
119	ARABI	Sugar Metabolism
119	RBK_Dr	Sugar Metabolism
120	ARAI	Sugar Metabolism
120	RBK_L1r	Sugar Metabolism
121	TKT1	Pentose Phosphate Pathway
121	TALA	Pentose Phosphate Pathway
122	SUCBZL	Ubiquinone Metabolism
122	NPHS	Ubiquinone Metabolism
122	SUCBZS	Ubiquinone Metabolism
123	SHCHD3	Cofactor Metabolism
123	SHCHF2	Cofactor Metabolism
124	DSERt2r	Transport

124	SERD_D	Glycine, Serine, and Threonine Metabolism
125	OXGDC2	Ubiquinone Metabolism
125	SHCHCS2	Other Amino Acid Metabolism
126	SADH	Arginine and Proline Metabolism
126	SGDS	Arginine and Proline Metabolism
126	AST	Arginine and Proline Metabolism
126	SOTA	Arginine and Proline Metabolism
126	SGSAD	Arginine and Proline Metabolism
127	TARTRt7	Transport
127	TARTD	Other Amino Acid Metabolism
128	FACOAE140	Fatty Acid Metabolism
128	FACOAL140	Fatty Acid Metabolism
129	TMN	Cofactor Metabolism
129	THMDP	Cofactor Metabolism
130	TRE6PP	Membrane Metabolism
130	TRE6PS	Membrane Metabolism
131	TRESULT	Membrane Metabolism
131	TATSO	Membrane Metabolism
132	FAS240_L	Fatty Acid Metabolism
132	FAS260	Fatty Acid Metabolism
133	UAAGLS1	Peptidoglycan Metabolism
133	PAPPT1	Peptidoglycan Metabolism
133	UGLDDS1	Peptidoglycan Metabolism
133	UAGPT1	Peptidoglycan Metabolism
134	UAAGLS2	Peptidoglycan Metabolism
134	UAGPT2	Peptidoglycan Metabolism
134	UGLDDS2	Peptidoglycan Metabolism
134	PAPPT2	Peptidoglycan Metabolism
135	UAGCVT	Sugar Metabolism
135	UAPGR	Sugar Metabolism
136	UGMDDS	Peptidoglycan Metabolism

136	PAPPT3	Peptidoglycan Metabolism
136	UAGPT3	Peptidoglycan Metabolism
136	UAAGDS	Peptidoglycan Metabolism
137	UAMAGS	Peptidoglycan Metabolism
137	UAMAS	Peptidoglycan Metabolism
138	UGAGDS	Peptidoglycan Metabolism
138	UGGPT3	Peptidoglycan Metabolism
138	UAMRH	Membrane Metabolism
138	UGMDDS2	Peptidoglycan Metabolism
138	PGPPT3	Peptidoglycan Metabolism
138	UGMAGS	Peptidoglycan Metabolism
138	UGMAS	Peptidoglycan Metabolism
139	VALt2r	Transport
139	VALTA	Valine, Leucine, and Isoleucine Metabolism
140	NTD10	Nucleotide Sugar Metabolism
140	PUNP7	Purine Metabolism
141	EX_bmn(e)	Transport
141	BMNt	Transport
142	EX_cobalt2(e)	Transport
142	COBALTt5	Transport
143	GLYCt	Transport
143	EX_glyc(e)	Transport
144	EX_h2(e)	Transport
144	H2td	Transport
145	EX_h2s(e)	Transport
145	H2St1	Transport
146	MGt5	Transport
146	EX_mg2(e)	Transport
147	EX_ppdima(e)	Transport
147	PPDIMAT	Transport

Table .1: The HCRs for *iNJ661* by grouped by number, along with the associated reaction and the metabolic subsystem

Abbreviation	Keq
EXac(e)	1
EXakg(e)	1
EXco2(e)	6000
EXetoh(e)	1
EXfor(e)	1
EXfum(e)	1
EXglc(e)	1
EXgln-L(e)	1
EXglu-L(e)	1
EXh(e)	0.9
EXh2o(e)	1.1
EXlac-D(e)	1
EXnh4(e)	0.5
EXo2(e)	1
EXpi(e)	1
EXpyr(e)	1100000
EXsucc(e)	10
sinkglyc(c)	1
ACKr	0.000712043
ACONT	0.118
ACt2r	1
ADHEr	14.831
ADK1	1.183579758
AKGDH	1189583.463
AKGt2r	1

ATPM	67769.91219
ATPS4r	0.000014756
BiomassEcolicoreN	1
CO2t	0.1
CS	1972365.992
CYTBD	1.7E+27
D-LACt2	1
ENO	4.558036118
ETOHt2r	1
FBA	0.00084276
FBP	112.0806951
FORt	1
FRD	0.0001849
FUM	2.749066052
FUMt22	1
G3PD2	0.000843
G6PDH2r	14.83065958
GAPD	1.183579758
GLCpts	4580000
GLNS	17.55326847
GLNabc	67770
GLUDy	1.55822E-07
GLUN	3860.814429
GLUSy	24777023756
GLUt2r	1
GLYK	605
GND	0.219392733
H2Ot	0.5
ICDHyr	0.003245518
ICL	0.000259013
LDHD	2.06708E-05

MALS	2334452.463
MDH	2.06708E-05
ME1	0.111797508
ME2	0.067427884
NADH11	5.45E+12
NADTRHD	1.658030775
NH4t	100
O2t	5
PDH	1189583.463
PFK	604.652854
PFL	5408.464531
PGI	3.851059539
PGK	0.008922143
PGL	5408.464531
PGM	1
PIt2r	10
PPC	94936.22993
PPCK	0.713846676
PPS	7.557364159
PTAr	0.001653842
PYK	7576.507268
PYRt2r	0.001
RPE	1
RPI	0.430538858
SUCCt22	5
SUCCt3	1
SUCD1i	34.447
SUCD4	34.447
SUCOAS	5.394799286
TALA	17.55326847
THD2	0.60313

TKT1	0.04066745
TKT2	17.55326847
TPI	0.094457097

Table .2: *E. coli* reactions and equilibrium constants

Abbreviation	Name
13dpg(c)	3-Phospho-D-glyceroyl phosphate
2pg(c)	D-Glycerate 2-phosphate
3pg(c)	3-Phospho-D-glycerate
6pgc(c)	6-Phospho-D-gluconate
6pgl(c)	6-phospho-D-glucono-1,5-lactone
ac(c)	Acetate
accoa(c)	Acetyl-CoA
actp(c)	Acetyl phosphate
adp(c)	ADP
akg(c)	2-Oxoglutarate
amp(c)	AMP
atp(c)	ATP
cit(c)	Citrate
co2(c)	CO2
coa(c)	Coenzyme A
dhap(c)	Dihydroxyacetone phosphate
e4p(c)	D-Erythrose 4-phosphate
etoh(c)	Ethanol
f6p(c)	D-Fructose 6-phosphate
fad(c)	Flavin adenine dinucleotide oxidized
fadh2(c)	Flavin adenine dinucleotide reduced
fdp(c)	D-Fructose 1,6-bisphosphate
for(c)	Formate

fum(c)	Fumarate
g3p(c)	Glyceraldehyde 3-phosphate
g6p(c)	D-Glucose 6-phosphate
gln-L(c)	L-Glutamine
glu-L(c)	L-Glutamate
glx(c)	Glyoxylate
glyc(c)	Glycerol
glyc3p(c)	Glycerol 3-phosphate
h(c)	H+
h2o(c)	H2O
icit(c)	Isocitrate
lac-D(c)	D-Lactate
mal-L(c)	L-Malate
nad(c)	Nicotinamide adenine dinucleotide
nadh(c)	Nicotinamide adenine dinucleotide - reduced
nadp(c)	Nicotinamide adenine dinucleotide phosphate
nadph(c)	Nicotinamide adenine dinucleotide phosphate - reduced
nh4(c)	Ammonium
o2(c)	O2
oaa(c)	Oxaloacetate
pep(c)	Phosphoenolpyruvate
pi(c)	Phosphate
pyr(c)	Pyruvate
q8(c)	Ubiquinone-8
q8h2(c)	Ubiquinol-8
r5p(c)	alpha-D-Ribose 5-phosphate
ru5p-D(c)	D-Ribulose 5-phosphate
s7p(c)	Sedoheptulose 7-phosphate
succ(c)	Succinate
succoa(c)	Succinyl-CoA
xu5p-D(c)	D-Xylulose 5-phosphate

ac(e)	Acetate
akg(e)	2-Oxoglutarate
co2(e)	CO2
etoh(e)	Ethanol
for(e)	Formate
fum(e)	Fumarate
glc-D(e)	D-Glucose
gln-L(e)	L-Glutamine
glu-L(e)	L-Glutamate
h(e)	H+
h2o(e)	H2O
lac-D(e)	D-Lactate
nh4(e)	Ammonium
o2(e)	O2
pi(e)	Phosphate
pyr(e)	Pyruvate
succ(e)	Succinate

Table .3: *E. coli* metabolites and abbreviations

Metabolite Abbreviation	Metabolite Name
10fthf	10-Formyltetrahydrofolate
12ppd-S	(S)-Propane-1,2-diol
13dpg	3-Phospho-D-glyceroyl phosphate
2amac	2-Aminoacrylate
2hb	2-Hydroxybutyrate
2obut	2-Oxobutanoate
2oxoadp	2-Oxoadipate
2pg	D-Glycerate 2-phosphate
34hpp	3-(4-Hydroxyphenyl)pyruvate

3hanthrn	3-Hydroxyanthranilate
3pg	3-Phospho-D-glycerate
3php	3-Phosphohydroxypyruvate
3sala	3-Sulfino-L-alanine
4fumacac	4-Fumarylacetoacetate
4izp	4-Imidazolone-5-propanoate
4mlacac	4-Maleylacetoacetate
5forthf	5-Formiminotetrahydrofolate
L2aadp	L-2-Aminoadipate
Lfmkynr	L-Formylkynurenine
Lkynr	L-Kynurenine
aacoa	Acetoacetyl-CoA
ac	Acetate
acac	Acetoacetate
accoa	Acetyl-CoA
acetol	Acetol
acetone	Acetone
adn	Adenosine
adp	ADP
ahcys	S-Adenosyl-L-homocysteine
akg	2-Oxoglutarate
ala-L	L-Alanine
am6sa	2-Aminomuconate 6-semialdehyde
amet	S-Adenosyl-L-methionine
amp	AMP
amuco	2-Aminomuconate
arg-L	L-Arginine
argsuc	N(omega)-(L-Arginino)succinate
asn-L	L-Asparagine
asp-L	L-Aspartate
atp	ATP

bhb	(R)-3-Hydroxybutanoate
cgly	Cys-Gly
cit	Citrate
citr-L	L-Citrulline
cl	Chloride
cmusa	2-Amino-3-carboxymuconate semialdehyde
co2	CO2
coa	Coenzyme A
creat	Creatine
crn	L-Carnitine
cys-L	L-Cysteine
cyst-L	L-Cystathionine
dcamp	N6-(1,2-Dicarboxyethyl)-AMP
dhap	Dihydroxyacetone phosphate
dhbpt	6,7-Dihydrobiopterin
f6p	D-Fructose 6-phosphate
fdp	D-Fructose 1,6-bisphosphate
for	Formate
forglu	N-Formimidoyl-L-glutamate
fum	Fumarate
g3p	Glyceraldehyde 3-phosphate
g6p	D-Glucose 6-phosphate
gdp	GDP
glc-D	D-Glucose
gln-L	L-Glutamine
glu-L	L-Glutamate
glucys	gamma-L-Glutamyl-L-cysteine
gly	Glycine
gthrd	Reduced glutathione
gtp	GTP
h	H+

h2o	H2O
hLkynr	3-Hydroxy-L-kynurenine
hcys-L	L-Homocysteine
hdca	Hexadecanoate (n-C16:0)
hgentis	Homogentisate
his-L	L-Histidine
ile-L	L-Isoleucine
imp	IMP
k	potassium
lac-L	L-Lactate
lald-L	L-Lactaldehyde
leu-L	L-Leucine
lnlc	linoleic acid (all cis C18:2) n-6
lnlccoa	linoleic coenzyme A
lnlccrn	Linoleyl carnitine
lnlnca	alpha-Linolenic acid, C18:3, n-3
lnlncacoa	alpha-Linolenoyl-CoA
lnlncacrn	alpha-linolenyl carnitine
lys-L	L-Lysine
mal-L	L-Malate
met-L	L-Methionine
methf	5,10-Methenyltetrahydrofolate
mlthf	5,10-Methylenetetrahydrofolate
na1	Sodium
nad	Nicotinamide adenine dinucleotide
nadh	Nicotinamide adenine dinucleotide - reduced
nadp	Nicotinamide adenine dinucleotide phosphate
nadph	Nicotinamide adenine dinucleotide phosphate - reduced
nh4	Ammonium
o2	O2

orn	Ornithine
pcreat	Phosphocreatine
pep	Phosphoenolpyruvate
phe-L	L-Phenylalanine
pi	Phosphate
pmtcoa	Palmitoyl-CoA (n-C16:0CoA)
pmtcrn	L-Palmitoylcarnitine
ppi	Diphosphate
pro-L	L-Proline
pser-L	O-Phospho-L-serine
pyr	Pyruvate
sarcs	Sarcosine
ser-L	L-Serine
so3	Sulfite
so4	Sulfate
succ	Succinate
thbpt	Tetrahydrobiopterin
thbpt4acam	Tetrahydrobiopterin-4a-carbinolamine
thf	5,6,7,8-Tetrahydrofolate
thr-L	L-Threonine
trp-L	L-Tryptophan
tyr-L	L-Tyrosine
urcan	Urocanate
urea	Urea
val-L	L-Valine
gluala	5-L-Glutamyl-L-alanine
10fthf	10-Formyltetrahydrofolate
1pyr5c	1-Pyrroline-5-carboxylate
2maacoa	2-Methyl-3-acetoacetyl-CoA
2mb2coa	trans-2-Methylbut-2-enoyl-CoA
2mbcoa	2-Methylbutanoyl-CoA

2mop	2-Methyl-3-oxopropanoate
2mp2coa	2-Methylprop-2-enoyl-CoA
3hbcoa	(S)-3-Hydroxybutanoyl-CoA
3hibutcoa	(S)-3-Hydroxyisobutyryl-CoA
3hmbcoa	(S)-3-Hydroxy-2-methylbutyryl-CoA
3hmp	3-Hydroxy-2-methylpropanoate
3mb2coa	3-Methylbut-2-enoyl-CoA
3mgcoa	3-Methylglutaconyl-CoA
3mob	3-Methyl-2-oxobutanoate
3mop	(S)-3-Methyl-2-oxopentanoate
3snpyr	3-Sulfinopyruvate
4mop	4-Methyl-2-oxopentanoate
L2aadp6sa	L-2-Aminoadipate 6-semialdehyde
b2coa	trans-But-2-enoyl-CoA
cbp	Carbamoyl phosphate
e-	electron
etfox	Electron transfer flavoprotein oxidized
etfrd	Electron transfer flavoprotein reduced
fad	Flavin adenine dinucleotide oxidized
fadh2	Flavin adenine dinucleotide reduced
ficytC	Ferricytochrome c
focytC	Ferrocytochrome C
glu5sa	L-Glutamate 5-semialdehyde
glutcoa	Glutaryl-CoA
gthox	Oxidized glutathione
h2co3	carbonic acid
h2o2	Hydrogen peroxide
hco3	Bicarbonate
hmgcoa	Hydroxymethylglutaryl-CoA
ibcoa	Isobutyryl-CoA
icit	Isocitrate

ivcoa	Isovaleryl-CoA
mmcoa-R	(R)-Methylmalonyl-CoA
mmcoa-S	(S)-Methylmalonyl-CoA
o2s	Superoxide
oaa	Oxaloacetate
occoa	Octanoyl-CoA (n-C8:0CoA)
ppcoa	Propanoyl-CoA
q10	Ubiquinone-10
q10h2	Ubiquinol-10
saccrp-L	L-Saccharopine
succoa	Succinyl-CoA

Table .4: Core hepatocyte mitochondria metabolites.

Reaction Abbreviation	Reaction
DMatp(c)	Exchange Reaction
EX2hb(e)	Exchange Reaction
EXac(e)	Exchange Reaction
EXacac(e)	Exchange Reaction
EXacetone(e)	Exchange Reaction
EXakg(e)	Exchange Reaction
EXala-L(e)	Exchange Reaction
EXarg-L(e)	Exchange Reaction
EXasn-L(e)	Exchange Reaction
EXasp-L(e)	Exchange Reaction
EXbhb(e)	Exchange Reaction
EXco2(e)	Exchange Reaction
EXcys-L(e)	Exchange Reaction
EXglc(e)	Exchange Reaction
EXgln-L(e)	Exchange Reaction

EXglu-L(e)	Exchange Reaction
EXgluala(e)	Exchange Reaction
EXgly(e)	Exchange Reaction
EXh(e)	Exchange Reaction
EXh2o(e)	Exchange Reaction
EXhdca(e)	Exchange Reaction
EXhis-L(e)	Exchange Reaction
EXile-L(e)	Exchange Reaction
EXlac-L(e)	Exchange Reaction
EXleu-L(e)	Exchange Reaction
EXlnlc(e)	Exchange Reaction
EXlnlc(e)	Exchange Reaction
EXlnlnca(e)	Exchange Reaction
EXlys-L(e)	Exchange Reaction
EXmet-L(e)	Exchange Reaction
EXnh4(e)	Exchange Reaction
EXo2(e)	Exchange Reaction
EXphe-L(e)	Exchange Reaction
EXpro-L(e)	Exchange Reaction
EXpyr(e)	Exchange Reaction
EXser-L(e)	Exchange Reaction
EXso4(e)	Exchange Reaction
EXsucc(e)	Exchange Reaction
EXthr-L(e)	Exchange Reaction
EXtrp-L(e)	Exchange Reaction
EXtyr-L(e)	Exchange Reaction
EXurea(e)	Exchange Reaction
EXval-L(e)	Exchange Reaction
sinkfum	Exchange Reaction
sinkmal(c)	Exchange Reaction
10FTHFtm	10-Formyltetrahydrofolate mitochondrial

	transport via diffusion
2AMACHYD	2-Aminoacrylate hydrolysis
2AMADPTm	L-2-aminoadipate shuttle (cytosol/mitochondria)
2HBO	2-Hydroxybutyrate:NAD+ oxidoreductase
2HBt2	2-hydroxybutyrate cotransport with proton
2OXOADOXm	2-Oxoadipate:lipoamde 2-oxidoreductase (mitochondria)
2OXOADPTm	2-oxoadipate shuttle (cytosol/mitochondria)
34HPPOR	4-Hydroxyphenylpyruvate:oxygen oxidoreductase
3HAO	3-hydroxyanthranilate 3,4-dioxygenase
3HBCOAHLm	3-hydroxyisobutyryl-CoA hydrolase, mitochondrial
3SALAASPm	cysteinesulfinate-aspartate mitochondrial shuttle
3SALATAim	3-sulfino-alanine transaminase (irreversible), mitochondrial
3SPYRSPm	3-sulfinopyruvate hydrolase (spotaneous reaction), mitochondrial
AACOAT	Acetoacetyl-CoA:acetate CoA-transferase
AASAD3m	L-aminoadipate-semialdehyde dehydrogenase (NADH), mitochondrial
AATAi	2-aminoadipate transaminase, irreversible
ACACT10m	acetyl-CoA C-acetyltransferase, mitochondrial
ACACT1r	acetyl-CoA C-acetyltransferase
ACACT1rm	acetyl-CoA C-acetyltransferase, mitochondrial
ACACt2	acetoacetate transport via proton symport
ACACt2m	Acetoacetate mitochondrial transport via H+ symport
ACETONEt2	acetone transport via proton symport
ACOAD10m	acyl-CoA dehydrogenase (2-methylbutanoyl-CoA), mitochondrial
ACOAD8m	acyl-CoA dehydrogenase (isovaleryl-CoA), mitochondrial

ACOAD9m	acyl-CoA dehydrogenase (isobutyryl-CoA), mitochondrial
ACONTm	Aconitate hydratase
ACS	acetyl-CoA synthetase
ACTNMO	acetone monooxygenase
ACt2r	acetate reversible transport via proton symport
ADK1	adenylate kinase
ADNK1	adenosine kinase
ADSL1	adenylosuccinate lyase
ADSS	adenylosuccinate synthase
AHC	adenosylhomocysteinase
AKGDm	2-oxoglutarate dehydrogenase
AKGMALtm	alpha-ketoglutarate/malate transporter
AKGt43	AKG transport via sodium symport
ALATAL	L-alanine transaminase
ALAt2r	L-alanine reversible transport via proton symport
ALCD21L	alcohol dehydrogenase (L-1,2-propanediol)
ALR3	aldose reductase (acetol)
AM6SAD	aminomuconate-semialdehyde dehydrogenase
AMCOXO	2-aminomuconate reductase
AMPDA	Adenosine monophosphate deaminase
AMPTASECG	alanyl aminopeptidase (cys-gly)
ARGN	arginase
ARGSL	argininosuccinate lyase
ARGSS	argininosuccinate synthase
ARGtiDF	L-arginine transport via diffusion (extracellular to cytosol)
ASNNm	L-asparaginase (mitochondrial)
ASNt4	L-asparagine transport in via sodium symport
ASNtm	L-asparagine transport, mitochondrial
ASPGLUm	aspartate-glutamate mitochondrial shuttle

ASPTAm	aspartate transaminase
ASPt6	L-aspartate transport via Na, H symport and K antiport
ATPS4m	ATP synthase (four protons for one ATP)
ATPtm	ADP/ATP transporter, mitochondrial
BDHm	(R)-3-Hydroxybutanoate:NAD+ oxidoreductase
BHBt	(R)-3-Hydroxybutanoate transport via H+ symport
BHBtm	(R)-3-Hydroxybutanoate mitochondrial transport via H+ symport
C160CPT1	carnitine O-palmitoyltransferase
C160CPT2	C160 transport into the mitochondria
C160CRNt	C160 transport into the mitochondria
CBPSam	carbamoyl-phosphate synthase (ammonia) (mitochondrial)
CGLYt3(2)	Cys-Gly transport in via proton symport
CITtam	citrate transport, mitochondrial
CITtbm	citrate transport, mitochondrial
CK	ATP Creatine kinase
CKc	ATP Creatine kinase (c)
CO2t	CO2 transporter via diffusion
CO2tm	CO2 transport (diffusion), mitochondrial
CREATtmdiffir	Creatine transport to/from mitochondria via diffusion
CRNtim	L-carnitine transport out of mitochondria via diffusion
CSm	citrate synthase
CYOOm2	CYOOm2
CYOR-u10m	ubiquinol-6 cytochrome c reductase, Complex III
CYSO	cysteine oxidase
CYSTGL	cystathionine g-lyase
CYSTS	cystathionine beta-synthase

CYStec	L-cysteine transport via diffusion (extracellular to cytosol)
CytOxe-	CytOxe-
DHPR	6,7-dihydropteridine reductase
ECOAH12m	3-hydroxyacyl-CoA dehydratase (3-hydroxyisobutyryl-CoA) (mitochondria)
ECOAH1m	3-hydroxyacyl-CoA dehydratase (3-hydroxybutanoyl-CoA) (mitochondria)
ECOAH9m	2-Methylprop-2-enoyl-CoA, mitochondrial
ENO	enolase
ETF	electron transfer flavoprotein
ETFQO	Electron transfer flavoprotein-ubiquinone oxidoreductase
FACOAL160i	C160 fatty acid activation
FACOAL1821	fatty-acid–CoA ligase
FACOAL1832	fatty-acid–CoA ligase
FAOXC160	Beta oxidation of long chain fatty acid
FAOXC16080m	Beta oxidation of long chain fatty acid
FAOXC182806m	Beta oxidation of fatty acid
FAOXC183803m	Beta oxidation of fatty acid
FAOXC80	Beta oxidation of med/long chain fatty acid
FBA	fructose-bisphosphate aldolase
FDH	formate dehydrogenase
FKYNH	N-Formyl-L-kynurenine amidohydrolase
FTCD	formimidoyltransferase cyclodeaminase
FTHFDH	formyltetrahydrofolate dehydrogenase
FUMAC	fumarylacetoacetase
FUMm	fumarase, mitochondrial
FUMtm	fumarate transport, mitochondrial
G5SADrm	L-glutamate 5-semialdehyde dehydratase, reversible, mitochondrial

GAPD	glyceraldehyde-3-phosphate dehydrogenase
GHMT2r	glycine hydroxymethyltransferase, reversible
GLCt1r	glucose transport (uniport)
GLNt4	L-glutamine reversible transport via sodium symport
GLNtm	L-glutamine transport via electroneutral transporter
GLUCYS	gamma-glutamylcysteine synthetase
GLUDxm	glutamate dehydrogenase (NAD) (mitochondrial)
GLUNm	glutaminase (mitochondrial)
GLUTCOADHm	glutaryl-CoA dehydrogenase (mitochondria)
GLUt2m	L-glutamate reversible transport via proton symport (mitochondrial)
GLUt6	Glutamate transport via Na, H symport and K antiport
GLYt2r	glycine reversible transport via proton symport
GLYtm	glycine passive transport to mitochondria
GNMT	glycine N-methyltransferase
GTHOm	glutathione oxidoreductase
GTHPm	glutathione peroxidase, mitochondria
GTHS	glutathione synthetase
GTMLTe	g-glutamyltransferase (e)
GluForTx	Glutamate formimidoyltransferase
H2CO3D2m	carboxylic acid dissociation, mitochondrial
H2CO3Dm	carboxylic acid dissociation
H2Ot	H2O transport via diffusion
H2Otm	H2O transport, mitochondrial
HACD1m	3-hydroxyacyl-CoA dehydrogenase (acetoacetyl-CoA), mitochondrial)
HACD9m	3-hydroxyacyl-CoA dehydrogenase (2-Methylacetoacetyl-CoA), mitochondrial
HDCAtr	fatty acid transport via diffusion
HEX1	hexokinase (D-glucose:ATP)

HGNTOR	Homogentisate:oxygen 1,2-oxidoreductase (decyclizing)
HIBDm	3-hydroxyisobutyrate dehydrogenase, mitochondrial
HISD	histidase
HIStiDF	L-histidine transport via diffusion (extracellular to cytosol)
HKYNH	3-Hydroxy-L-kynurenine hydrolase
HMGLm	hydroxymethylglutaryl-CoA lyase
ICDHxm	Isocitrate dehydrogenase (NAD+)
ILETAm	isoleucine transaminase, mitochondrial
ILEt5m	Isoleucine mitochondrial transport
ILEtec	L-isoleucine transport via diffusion (extracellular to cytosol)
IZPN	imidazolonepropionase
KCCt	K+-Cl- cotransport
KYN3OX	kynurenine 3-monooxygenase
L-LACt2r	L-lactate reversible transport via proton symport
LCADi	lactaldehyde dehydrogenase
LDHL	L-lactate dehydrogenase
LEUTAm	leucine transaminase, mitochondrial
LEUt5m	leucine mitochondrial transport
LEUtec	L-leucine transport via diffusion (extracellular to cytosol)
LNLCCPT1	carnitine O-palmitoyltransferase
LNLCCPT2	carnitine transferase
LNLCCRNt	transport into the mitochondria (carnitine)
LNLCt	Linoleic acid (n-C18:2) transport in via diffusion
LNLNCACPT1	carnitine O-palmitoyltransferase
LNLNCACPT2	carnitine transferase
LNLNCACRNt	transport into the mitochondria (carnitine)
LNLNCAt	fatty acid transport via diffusion
LYStiDF	L-lysine transport via diffusion

	(extracellular to cytosol)
LYStm	Lysine mitochondrial transport via ornithine carrier
MACACI	maleylacetoacetate isomerase
MALSO3tm	Malate:sulfite antiport, mitochondrial
MALtm	malate transport, mitochondrial
MCCCrm	methylcrotonoyl-CoA carboxylase, mitochondrial
MDHm	malate dehydrogenase, mitochondrial
ME2m	malic enzyme (NADP), mitochondrial
METAT	methionine adenosyltransferase
METtec	L-methionine transport via diffusion (extracellular to cytosol)
MGCHrm	methylglutaconyl-CoA hydratase (reversible), mitochondrial
MMEm	methylmalonyl-CoA epimerase/racemase
MMMm	methylmalonyl-CoA mutase
MMTSADm	malonate-semialdehyde dehydrogenase (acetylating), mitochondrial
MTHFCm	methenyltetrahydrifikate cyclohydrolase, mitochondrial
MTHFD	methylenetetrahydrofolate dehydrogenase (NADP)
MTHFD2	methylenetetrahydrofolate dehydrogenase (NAD)
MTHFD2m	methylenetetrahydrofolate dehydrogenase (NAD), mitochondrial
NADH2-u10m	NADH dehydrogenase, mitochondrial
NAt	sodium transport (uniport)
NDPK1	nucleoside-diphosphate kinase (ATP:GDP)
NDPK1m	nucleoside-diphosphate kinase (ATP:GDP), mitochondrial
NH4t3r	ammonia transport via proton antiport
O2t	o2 transport (diffusion)
O2tm	O2 transport (diffusion)
OCBTm	ornithine carbamoyltransferase, irreversible

OCOAT1m	3-oxoacid CoA-transferase
OIVD1m	2-oxoisovalerate dehydrogenase (acylating; 4-methyl-2-oxopentaoate), mitochondrial
OIVD2m	2-oxoisovalerate dehydrogenase (acylating; 3-methyl-2-oxobutanoate), mitochondrial
OIVD3m	2-oxoisovalerate dehydrogenase (acylating; 3-methyl-2-oxopentanoate), mitochondrial
ORNTArm	ornithine transaminase reversible (m)
ORNt3m	ornithine mitochondrial transport via proton antiport
ORNt4m	ornithine mitochondrial transport exchange with citruline
P5CDm	1-pyrroline-5-carboxylate dehydrogenase, mitochondrial
PCLAD	picolinic acid decarboxylase
PCREATtmdiffir	Phosphocreatine transport to/from mitochondria via diffusion
PDHm	pyruvate dehydrogenase
PEPCKm	Phosphoenolpyruvate carboxykinase (GTP)
PFK	phosphofructokinase
PGCD	phosphoglycerate dehydrogenase
PGI	glucose-6-phosphate isomerase
PGK	phosphoglycerate kinase
PGM	phosphoglycerate mutase
PHETHPTOX2	L-Phenylalanine,tetrahydrobiopterin:oxygen oxidoreductase (4-hydroxylating)
PHEtec	L-phenylalanine transport via diffusion (extracellular to cytosol)
PIt2m2	PIt2m2
PPA	inorganic diphosphatase
PPCOACm	Propionyl-CoA carboxylase, mitochondrial
PRO1xm	proline oxidase (NAD), mitochondrial

PROt2r	L-proline reversible transport via proton symport
PROtm	L-proline transport, mitochondrial
PSERT	phosphoserine transaminase
PSPL	phosphoserine phosphatase (L-serine)
PYK	pyruvate kinase
PYRt2m	pyruvate mitochondrial transport via proton symport
PYRt2r	pyruvate reversible transport via proton symport
SACCD3m	saccharopine dehydrogenase (NADP, L-lysine forming), mitochondrial
SACCD4m	saccharopine dehydrogenase (NAD, L-glutamate forming), mitochondrial
SARCStm	Sarcosine transport (mitochondrial)
SARDHm	Sarcosine dehydrogenase (m)
SERHL	L-Serine hydro-lyase
SERt4	L-serine via sodium symport
SO4CLtex2	sulfate transport via chloride countertransport (2:1)
SO4t42	sulfate transport via sodium symport
SOProd	SOProd
SPODMm	superoxide dismutase
SUCCt2m	succinate transport, mitochondrial
SUCCt42	succinate transport via sodium symport
SUCD1m	succinate dehydrogenase
SUCOAS1m	Succinate–CoA ligase (GDP-forming)
SULFOX	sulfite oxidase
THBPT4ACAMDASE	Tetrahydrobiopterin-4a-carbinolamine dehydratase
THFtm	5,6,7,8-Tetrahydrofolate transport, diffusion, mitochondrial
THRDL	L-threonine deaminase
THRGLYexR	L-threonine/glycine reversible exchange
THRt4	L-threonine via sodium symport
TPI	triose-phosphate isomerase

TRPO2	L-Tryptophan:oxygen 2,3-oxidoreductase (decyclizing)
TRPt	L-tryptophan transport
TYRTA	tyrosine transaminase
TYRt	L-tyrosine transport
URCN	urocanase
UREAt	Urea transport via facilitate diffusion
VALTAm	valine transaminase, mitochondiral
VALt5m	Valine reversible mitochondrial transport
VALtec	L-valine transport via diffusion (extracellular to cytosol)

Table .5: Core hepatocyte mitochondria reactions.

Abbreviation	Name
G6P	Glucose-6-phosphate
F6P	Fructose-6-phosphate
FDP	Fructose-1,6-bisphosphate
DHAP	Dihydroxyacetone phosphate
GAP	Glyceraldehyde-3-phosphate
DPG13	1,3-bisphosphoglycerate
DPG23	2,3-bisphosphoglycerate
PG3	3-phosphoglycerate
PG2	2-phosphoglycerate
PEP	Phosphoenolpyruvate
PYR	Pyruvate
LAC	Lactate
NADH	Nicotinamide adenine dinucleotide (reduced)
GL6P	6-Phospho-D-glucono-1,5-lactone
GO6P	6-Phospho-D-gluconate
NADPH	Nicotinamide adenine dinucleotide phosphate (reduced)
GSH	glutathione (reduced)
RU5P	Ribulose-5-phosphate
R5P	Ribose-5-phosphate
X5P	Xylulose-5-phosphate
S7P	Sedoheptulose-7-phosphate
E4P	Erythrose-4-phosphate
ADO	Adenosine
AMP	Adenosine monophosphate
ADP	Adenosine diphosphate
ATP	Adenosine triphohsphate
PRPP	5-Phospho-D-ribose 1-diphosphate
IMP	Inosine monophosphate
INO	Inosine
HX	Hypoxanthine
R1P	Ribose-1-phosphate
ADE	Adenine
NAI	Sodium
KI	Potassium

Figure .1: Abbreviations for the metabolites in the red blood cell.

	Steady State Metabolite Concentrations (mM)
GLC	5
G6P	0.038
F6P	0.016
FDP	0.0076
DHAP	0.14
GAP	0.0067
DPG13	0.0004
DPG23	4.5
PG3	0.045
PG2	0.014
PEP	0.017
NAD	0.0584008
PYR	0.077
LAC	1.1
NADH	0.0305992
NADP	0.0002
GL6P	0.00175427
GO6P	0.0374753
NADPH	0.0658
GSH	3.2
RU5P	0.00493679
R5P	0.0126689
X5P	0.0147842
S7P	0.023988
E4P	0.00507507
ADO	0.0012
Phosi	1.2
AMP	0.08
ADP	0.27
ATP	1.54
PRPP	0.005
IMP	0.01
INO	0.001
HX	0.002
R1P	0.06
ADE	0.00103474

	Steady State Fluxes (mM/hr)
HK	1.12
PGI	0.91
PFK	1.10657
ALD	1.10657
TPI	1.10657
GAPDH	2.31143
PGK	1.81143
DPGM	0.5
DPGase	0.5
PGM	2.31143
EN	2.31143
PK	2.31143
LDH	2.31143
AMPase	0.257481
ADA	0.149006
AK	0.12
ADK	-0.138147
AMPDA	-0.123481
ATPase	1.5
ADPRT	0.014
G6PDH	0.21
PGLase	0.21
GL6PDH	0.21
GSSGR	0.42
GSHR	0.84
RU5PI	0.0134263
XU5PE	0.196574
TKI	0.0982869
TKII	0.0982869
TALD	0.0982869
IMPase	0.000666035
PNPase	0.223008
PRM	0.223008
PRPPSYN	0.138147
HGPRT	0.124147
GLCEX	1.12
PEX	0.
LEX	2.31143
HXEX	0.0988606
ADEEX	-0.014
ADOEX	-0.0115245
INOEX	-0.0733361

	Equilibrium Constants
HK	1000
PGI	0.43
PFK	1000
ALD	123.457
TPI	17.5
GAPDH	0.027
PGK	1800
DPGM	50000
DPGase	1000
PGM	6.8
EN	1.69492
PK	1000
LDH	446.429
AMPase	1
ADA	1
AK	500
ADK	1.65
AMPDA	0.1
ATPase	1000
ADPRT	100000
G6PDH	1000
PGLase	1000
GL6PDH	1000
GSSGR	100
GSHR	2
RU5PI	2.57
XU5PE	3
TKI	1.2
TKII	10.3
TALD	1.05
IMPase	1000
PNPase	0.11
PRM	13.3
PRPPSYN	605
HGPRT	10000
GLCEX	1
PEX	1
LEX	2
HXEX	1
ADEEX	1
ADOEX	0.01
INOEX	0.01

Figure .2: Variable values and parameters for mass action red cell model.

The steady state concentrations, fluxes and equilibrium constants used to construct a middle-out mass action model of human red blood cell metabolism.

Bibliography

[1] K. R. Albe, M. H. Butler, and B. E. Wright. Cellular concentrations of enzymes and their substrates. *J Theor Biol*, 143(2):163–195, 1990.

[2] L. D. Altshuler, D.and Brooks, A. Chakravarti, F. S. Collins, M. J. Daly, and P. Donnelly. A haplotype map of the human genome. *Nature*, 437(7063):1299–1320, 2005.

[3] D. E. Atkinson. The energy charge of the adenylate pool as a regulatory parameter. interaction with feedback modifiers. *Biochemistry*, 7(11):4030–4034, 1968.

[4] J. E. Bailey. Mathematical modeling and analysis in biochemical engineering: past accomplishments and future opportunities. *Biotechnology progress*, 14:8–20, 1998.

[5] M. Bier, B. M. Bakker, and H. V. Westerhoff. How yeast cells synchronize their glycolytic oscillations: a perturbation analytic treatment. *Biophysical journal*, 78:1087–1093, 2000.

[6] G.E. Briggs and J.B. Haldane. A note on the kinetics of enzyme action. *Biochem J.*, 19(2):338339, 1925.

[7] A. P. Burgard, E. V. Nikolaev, C. H. Schilling, and C. D. Maranas. Flux coupling analysis of genome-scale metabolic network reconstructions. *Genome research*, 14(2):301–312, 2004.

[8] P. Maranas C. D. Burgard, A. P. Pharkya. Optknock: a bilevel programming framework for identifying gene knockout strategies for microbial strain optimization. *Biotechnol Bioeng*, 84(6):647–657, 2003.

[9] J. A. Camacho, N. Rioseco-Camacho, D. Andrade, J. Porter, and J. Kong. Cloning and characterization of human ornt2: a second mitochondrial ornithine transporter that can rescue a defective ornt1 in patients with the hyperornithinemia-hyperammonemia-homocitrullinuria syndrome, a urea cycle disorder. *Mol Genet Metab*, 79:257–271, 2003.

[10] S. T. Cole, R. Brosch, J. Parkhill, T. Garnier, C. Churcher, D. Harris, S. V. Gordon, K. Eiglmeier, S. Gas, 3rd Barry, C. E., F. Tekaia, K. Badcock, D. Basham, D. Brown, T. Chillingworth, R. Connor, R. Davies, K. Devlin, T. Feltwell, S. Gentles, N. Hamlin, S. Holroyd, T. Hornsby, K. Jagels, A. Krogh, J. McLean, S. Moule, L. Murphy, K. Oliver, J. Osborne, M. A. Quail, M. A. Rajandream, J. Rogers, S. Rutter, K. Seeger, J. Skelton, R. Squares, S. Squares, K. Sulston, J. E. an dTaylor, S. Whitehead, and B. G. Barrell. Deciphering the biology of mycobacterium tuberculosis from the complete genome sequence. *Nature*, 393(6685):537–544, 1998.

[11] N. C. Duarte, S. A. Becker, N. Jamshidi, I. Thiele, M. L. Mo, T. D. Vo, R. Srivas, and B. Ø. Palsson. Global reconstruction of the human metabolic network based on genomic and bibliomic data. *PNAS U S A*, 104:1777–1782, 2007.

[12] J. S. Edwards and B. Ø. Palsson. The escherichia coli mg1655 in silico metabolic genotype: its definition, characteristics, and capabilities. *Proceedings of the National Academy of Sciences of the United States of America*, 97:5528–5533, 2000.

[13] Ludwig von ertalanffy. *General system theory; foundations, development, applications.* Braziller, New York, 1965.

[14] I. Famili, R. Mahadevan, and B. Ø. Palsson. k-cone analysis: determining all candidate values for kinetic parameters on a network scale. *Biophys J*, 88(3):1616–1625, 2005.

[15] I. Famili and B. Ø. Palsson. The convex basis of the left null space of the stoichiometric matrix leads to the definition of metabolically meaningful pools. *Biophys J*, 85(1):16–26, 2003.

[16] E. Fischer. *Brr. Dl.uch. Chenr. Gc.s.*, 27:2985, 1894.

[17] A. C. Guyton. *Basic human physiology: normal function and mechanisms of disease.* Saunders, Philadelphia, 1971.

[18] A. C. Guyton, T. G. Coleman, and H. J. Granger. Circulation: overall regulation. *Annu Rev Physiol*, 34:13–46, 1972.

[19] Press W. H., Flannery B. P., Teukolsky S. A., and Vetterling W. T. *Numerical Recipes in C: The Art of Scientific Computing.* Cambridge University Press, New York, 1992.

[20] A. Hamosh, A. F. Scott, J. S. Amberger, C. A. Bocchini, and V. A. McKusick. Online mendelian inheritance in man (omim), a knowledgebase of human genes and genetic disorders. *Nucleic Acids Res*, 33:D514–517, 2005.

[21] H. H. Harman. *Modern factor analysis*. University of Chicago Press, 1976.

[22] R. Harrison, B. Papp, C. Pal, S. G. Oliver, and D. Delneri. Plasticity of genetic interactions in metabolic networks of yeast. *Proc Natl Acad Sci U S A*, 104(7):2307–2312, 2007.

[23] C. F. Hawkins and A. S. Bagnara. Adenosine kinase from human erythrocytes: Kinetic studies and characterization of adenosine binding sites. *Biochemistry*, 26:1982–1987, 1987.

[24] I. Heinrich, R. Sonntag. Dynamics of non-linear biochemical systems and the evolutionary significance of time hierarchy. *Biosystems*, 15(4):301–316, 1982.

[25] R. Heinrich. Mathematical models of metabolic systems: general principles and control of glycolysis and membrane transport in erythrocytes. *Biomedica biochimica acta*, 44:913–927, 1985.

[26] R. Heinrich, S.M. Rapaport, and T.A. Rapaport. Metabolic regulation and mathematical models. *Progress in Biophysics and Molecular Biology*, 32:1 – 82, 1977.

[27] V. Henri. The orie ge ne rale de laction de quelques diastases. *Hebd. Acad. Sci.*, 135:916919, 1902.

[28] C. S. Henry, M. D. Jankowski, L. J. Broadbelt, and V. Hatzimanikatis. Genome-scale thermodynamic analysis of *E. coli* metabolism. *Biophys J.*, 90(4):1453–61, 2005.

[29] G. Jacobasch Holzhutter, H. G. and Bisdorff A. Mathematical modelling of metabolic pathways affected by an enzyme deficiency. a mathematical model of glycolysis in normal and pyruvate-kinase-deficient red blood cells. *Eur J Biochem*, 149:101–111, 1985.

[30] H. G. Holzhutter. The principle of flux minimization and its application to estimate stationary fluxes in metabolic networks. *Eur J Biochem*, 271(14):2905–2922, 2004.

[31] N. Ishii, K. Nakahigashi, T. Baba, M. Robert, T. Soga, A. Kanai, T. Hirasawa, M. Naba, K. Hirai, A. Hoque, P. Y. Ho, Y. Kakazu, K. Sugawara, S. Igarashi, S. Harada, T. Masuda, N. Sugiyama, T. Togashi, M. Hasegawa, Y. Takai, K. Yugi, K. Arakawa, N. Iwata, Y. Toya, Y. Nakayama, T. Nishioka, K. Shimizu, H. Mori, and M. Tomita. Multiple high-throughput analyses monitor the response of e. coli to perturbations. *Science*, 316(5824):593–7, 2007.

[32] B.W. James, A. Williams, and P.D. Marsh. he physiology and pathogenicity of mycobacterium tuberculosis grown under controlled conditions in a defined medium. *Journal of applied microbiology*, 88(4):669–677, 2000.

[33] N. Jamshidi. *A model of the human red blood cell metabolism: the in silico erythrocyte*. University of California, San Diego, La Jolla, 2000.

[34] N. Jamshidi, J. S. Edwards, T. Fahland, G. M. Church, and B. Ø. Palsson. Dynamic simulation of the human red blood cell metabolic network. *Bioinformatics*, 17(3):286–287, 2001.

[35] N. Jamshidi and B. Ø. Palsson. Systems biology of snps. *Mol Syst Biol*, 2:38, 2006.

[36] N. Jamshidi and B. Ø. Palsson. Systems biology of the human red blood cell. *Blood Cells Mol Dis*, 36(2):239–247, 2006.

[37] N. Jamshidi and B. Ø. Palsson. Investigating the metabolic capabilities of mycobacterium tuberculosis h37rv using the in silico strain inj661 and proposing alternative drug targets. *BMC Systems Biology*, 1:26, 2007.

[38] N. Jamshidi and B. Ø. Palsson. Formulating genome-scale kinetic models in the post-genome era. *Mol Syst Biol*, 4:171, 2008.

[39] N. Jamshidi and B. Ø. Palsson. Top-down analysis of temporal hierarchy in biochemical reaction networks. *accepted*, 2008.

[40] A. Joshi and B. Ø. Palsson. Metabolic dynamics in the human red cell. part i-a comprehensive kinetic model. *J Theor Biol*, 141(4):515–528, 1989.

[41] A. Joshi and B. Ø. Palsson. Metabolic dynamics in the human red cell. part iii-metabolic reaction rates. *J Theor Biol*, 142(1):41–68, 1990.

[42] A. Joshi and B. Ø. Palsson. Metabolic dynamics in the human red cell. part iv–data prediction and some model computations. *J Theor Biol*, 142(1):69–85, 1990.

[43] D. Kasper, E. Braunwald, A. Fauci, S. Hauser, Longo D., and Jameson J. *Harrison's Principles of Internal Medicine*. McGraw-Hill Professional, 2004.

[44] K. J. Kauffman, J. D. Pajerowski, N. Jamshidi, B. Ø. Palsson, and J. S. Edwards. Description and analysis of metabolic connectivity and dynamics in the human red blood cell. *Biophys J*, 83(2):646–62, 2002.

[45] D. B. Kell. The virtual human: towards a global systems biology of multi-scale, distributed biochemical network models. *IUBMB Life*, 59(11):689–695, 2007.

[46] D. B. Kell, M. Brown, H. M. Davey, W. B. Dunn, Spasic, and S. G. Oliver. Metabolic footprinting and systems biology: the medium is the message. *Nat Rev Microbiol*, 3:557–565, 2005.

[47] E. Klipp, B. Nordlander, R. Kruger, P. Gennemark, and S. Hohmann. Integrative model of the response of yeast to osmotic shock. *Nat Biotechnol*, 23(8):975–982, 2005.

[48] D.E. Koshalnd. Application of a theory of enzyme specificity to protein synthesis. *Proc Natl Acad Sci U S A*, 44(2):98–104.

[49] B. Lin, J. T. White, W. Lu, T. Xie, A. G. Utleg, X. Yan, E. C. Yi, P. Shannon, I. Khrebtukova, P. H. Lange, D. R. Goodlett, D. Zhou, T. J. Vasicek, and L. Hood. Evidence for the presence of disease-perturbed networks in prostate cancer cells by genomic and proteomic analyses: a systems approach to disease. *Cancer Research*, 65(8):3081–3091, 2005.

[50] R. Mahadevan and C. H. Schilling. The effects of alternate optimal solutions in constraint-based genome-scale metabolic models. *Metabolic engineering*, 5(4):264–276, 2003.

[51] S. Mangan and U. Alon. Structure and function of the feed-forward loop network motif. *Proc Natl Acad Sci U S A*, 100(21):11980–11985, 2003.

[52] M. L. Mavrovouniotis. Estimation of standard gibbs energy changes of biotransformations. *J Biol Chem*, 266(22):14440–14445, 1991.

[53] E. Mayr. Cause and effect in biology. *Science*, 134:1501–1506, 1961.

[54] V.A. McKusick and J.S. Amberger. The morbid anatomy of the human genome: chromosomal location of mutations causing disease. *J Med Genet*, 30(1):1–26, 1993.

[55] K. Mdluli and M. Spigelman. Novel targets for tuberculosis drug discovery. *Curr Opin Pharmacol*, 6(5):459–467, 2006.

[56] L. Michaelis and M.L. Menten. Die kinetik der invertinwirkung. *Biochem. Z.*, 49:333369, 1913.

[57] G. Michal. *Biochemical Pathways: An Atlas of Biochemistry and Molecular Biology*. Wiley, New York, 1999.

[58] G. Middlebrook and M.L. Cohn. Bacteriology of tuberculosis: laboratory methods. *American journal of public health*, 48(7):844–853, 1958.

[59] WYMAN J. MONOD, J. and and J.P. CHANGEUX. On the nature of allosteric transitions: A plausible model. *J Mol Biol.*, 12:88–118, 1965.

[60] P.J. Mulquiney, Bubb W. A., and P. W. Kuchel. Model of 2,3-bisphosphoglycerate metabolism in the human erythrocyte based on detailed enzyme kinetic equations: *in vivo* kinetic characterization of 2,3-bisphosphoglycerate snthase/phosphatase using c13 and p31nmr. *Biochem J*, 342:567–80, 1999.

[61] P.J. Mulquiney and P. W. Kuchel. Model of 2,3-bisphosphoglycerate metabolism in the human erythrocyte based on detailed enzyme kinetic equations: equations and parameter refinement. *Biochem J*, 342:581–596, 1999.

[62] D. Noble. Modeling the heart–from genes to cells to the whole organ. *Science*, 295:1678–1682, 2002.

[63] M. S. Okino and M. L. Mavrovouniotis. Simplification of mathematical models of chemical reaction systems. *Chem Rev*, 98(2):391–408, 1998.

[64] B. Ø. Palsson. *Systems Biology: Properties of Reconstructed Networks*. Cambridge University Press, 2006.

[65] B. Ø. Palsson and E. N. Jamier, R. andLightfoot. Mathematical modelling of dynamics and control in metabolic networks. ii. simple dimeric enzymes. *Journal of theoretical biology*, 111:130:321, =1984,.

[66] B. Ø. Palsson, A. Joshi, and S. S. Ozturk. Reducing complexity in metabolic networks: making metabolic meshes manageable. *Fed Proc*, 46(8):2485–2489, 1987.

[67] B. Ø. Palsson and E. N. Lightfoot. Mathematical modelling of dynamics and control in metabolic networks. i. on michaelis-menten kinetics. *Journal of theoretical biology*, 111:273–302, 1984.

[68] B. Ø. Palsson and E. N. Lightfoot. Mathematical modelling of dynamics and control in metabolic networks. i. on michaelis-menten kinetics. *J Theor Biol*, 111(2):273–302, 1984.

[69] B. Ø. Palsson and E. N. Lightfoot. Mathematical modelling of dynamics and control in metabolic networks. ii. simple dimeric enzymes. *J Theor Biol*, 111(2):303–321, 1984.

[70] J. A. Papin, J. L. Reed, and B. Ø. Palsson. Hierarchical thinking in network biology: the unbiased modularization of biochemical networks. *Trends Biochem Sci*, 29(12):641–667, 2004.

[71] A. Payen and J.F. Persoz. *Ann. Chim. Phys.*, 53(73), 1833.

[72] T. Pfeiffer, I. Sanchez-Valdenebro, J.C. Nuno, F. Montero, and S. Schuster. Metatool: for studying metabolic networks. *Bioinformatics*, 15(3):251–257, 1999.

[73] N. D. Price and B. Ø. Reed, J. L.and Palsson. Genome-scale models of microbial cells: evaluating the consequences of constraints. *Nature Reviews Microbiology*, 2(11):886–897, 2004.

[74] N. D. Price, J. Schellenberger, and B. Ø. Palsson. Uniform sampling of steady state flux spaces: Means to design experiments and to interpret enzymopathies. *Biophysical Journal*, 87(4):2172–86, 2004.

[75] J. L. Reed, I. Famili, I. Thiele, and B. Ø. Palsson. Towards multidimensional genome annotation. *Nature Review Genetics*, 7(2):130–141, 2006.

[76] J. L. Reed, T. R. Patel, K. H. Chen, A. R. Joyce, M. K. Applebee, C. D. Herring, O. T. Bui, E. M. Knight, S. S. Fong, and B. Ø. Palsson. Systems approach to refining genome annotation. *Proc Natl Acad Sci U S A*, 103(46):17480–17484, 2006.

[77] M. C. Reed, H. F. Nijhout, M. L. Neuhouser, J. F. Gregory, B. Shane, S. J. James, A. Boynton, and C. M. Ulrich. A mathematical model gives insights into nutritional and genetic aspects of folate-mediated one-carbon metabolism. *J Nutr*, 136(10):2653–61, 2006.

[78] J. Reich and E. Selkov. *Energy metabolism of the cell: a theoretical treatise*. Academic Press, 1981.

[79] A. Reymond, V. Marigo, M. B. Yaylaoglu, A. Leoni, C. Ucla, N. Scamuffa, C. Caccioppoli, E. T. Dermitzakis, R. Lyle, S. Banfi, G. Eichele, S. E. Antonarakis, and A. Ballabio. Human chromosome 21 gene expression atlas in the mouse. *Nature*, 420(6915):582–586, 2002.

[80] P. Richard, J. A. Diderich, B. M. Bakker, B. Teusink, K. van Dam, and H. V. Westerhoff. Yeast cells with a specific cellular make-up and an environment that removes acetaldehyde are prone to sustained glycolytic oscillations. *FEBS Lett*, 341:223–226, 1994.

[81] J. J. Saucerman, L. L. Brunton, A. P. Michailova, and A. D. McCulloch. Modeling beta-adrenergic control of cardiac myocyte contractility in silico. *J Biol Chem*, 278(48):47997–8003, 2003.

[82] J. M. Savinell and B. Ø. Palsson. Network analysis of intermediary metabolism using linear optimization. i. development of mathematical formalism. *Journal of theoretical biology*, 154:421–454, 1992.

[83] J. M. Savinell and B. Ø. Palsson. Optimal selection of metabolic fluxes for in vivo measurement. i. development of mathematical methods. *Journal of theoretical biology*, 155:201–214, 1992.

[84] C. H. Schilling, D. Letscher, and B. Ø. Palsson. Theory for the systemic definition of metabolic pathways and their use in interpreting metabolic function from a pathway-oriented perspective. *J Theor Bio*, 203(3):229–248, 2000.

[85] E. Schneider, M. Moore, and K.G. Castro. Epidemiology of tuberculosis in the united states. *Clinics in chest medicine*, 26(3):183–195, 2005.

[86] S. Schuster, D. A. Fell, and T. Dandekar. A general definition of metabolic pathways useful for systematic organization and analysis of complex metabolic networks. *Nat Biotechnol*, 18(3):326–332, 2000.

[87] C.R. Scriver. *The metabolic and molecular bases of inherited disease*. McGraw-hill, New York, 1995.

[88] Irwin H. Segel. *Enzyme kinetics : behavior and analysis of rapid equilibrium and steady-state enzyme systems*. Wiley, New York, 1975.

[89] S.K. Sharma and A. Mohan. Multidrug-resistant tuberculosis: a menace that threatens to destabilize tuberculosis control. *Chest*, 130(1):261–272, 2006.

[90] R. Steuer, T. Gross, J. Selbig, and B. Blasius. Structural kinetic modeling of the metabolic networks. *PNAS*, 103(32):11868–11873, 2006.

[91] G. Strang. *Introduction to Linear Algebra*. Wellesley-Cambridge, 2003.

[92] S.H. Strogatz. *Nonlinear Dynamics and Chaos: With Applications to Physics, Biology, Chemistry, and Engineering.* Perseus, 1994.

[93] B. Teusink, J. Passarge, C. A. Reijenga, E. Esgalhado, C. C. van der Weijden, M. Schepper, M. C. Walsh, B. M. Bakker, K. van Dam, H. V. Westerhoff, and J. L. Snoep. Can yeast glycolysis be understood in terms of in vitro kinetics of the constituent enzymes? testing biochemistry. *Eur J Biochem*, 267(17):5313–29, 2000.

[94] I. Thiele, N. D. Price, T. D. Vo, and B. Ø. Palsson. Candidate metabolic network states in human mitochondria. impact of diabetes, ischemia, and diet. *J Biol Chem*, 280(12):11683–11695, 2005.

[95] A. Varma and B. Ø. Palsson. Metabolic flux balancing: basic concepts, scientific and practical use. *Biotechnology*, 12:994–998, 1994.

[96] T. D. Vo, H. J. Greenberg, and B. Ø. Palsson. Reconstruction and functional characterization of the human mitochondrial metabolic network based on proteomic and biochemical data. *J Biol Chem*, 279(38):39532–39540, 2004.

[97] L.G. Wayne and C.D. Sohaskey. Nonreplicating persistence of mycobacterium tuberculosis. *Annual review of microbiology*, 55:139–163, 2001.

[98] D. S. Wishart, D. Tzur, C. Knox, R. Eisner, A. C. Guo, N. Young, D. Cheng, K. Jewell, D. Arndt, S. Sawhney, C. Fung, L. Nikolai, M. Lewis, M. A. Coutouly, I. Forsythe, P. Tang, S. Shrivastava, K. Jeroncic, P. Stothard, G. Amegbey, D. Block, D. D. Hau, J. Wagner, J. Miniaci, M. Clements, M. Gebremedhin, N. Guo, Y. Zhang, G. E. Duggan, G. D. Macinnis, A. M. Weljie, R. Dowlatabadi, F. Bamforth, D. Clive, R. Greiner, L. Li, T. Marrie, B. D. Sykes, H. J. Vogel, and L. Querengesser. Hmdb: the human metabolome database. *Nucleic Acids Res*, 35(Database issue):D521–6, 2007.

[99] M. Yeung, I. Thiele, and B. Ø. Palsson. Estimation of the number of extreme pathways for metabolic networks. *BMC Bioinformatics*, 2007.

[100] Youmans and Karlson. 1947.

[101] J. Yuan and J. Rabinowitz. Unpublished data.